Publicly Accessible Penn Dissertations

Summer 8-14-2009

Mass Spectrometry-Based Proteomics Reveals Distinct Mechanisms of Astrocyte Protein Secretion

Todd M. Greco
University of Pennsylvania, tgreco@mail.med.upenn.edu

Mass Spectrometry-Based Proteomics Reveals Distinct Mechanisms of Astrocyte Protein Secretion

Abstract

The ability of astrocytes to secrete proteins subserves many of its known function, such as synapse formation during development and extracellular matrix remodeling after cellular injury. Protein secretion may also play an important, but less clear, role in the propagation of inflammatory responses and neurodegenerative disease pathogenesis. While potential astrocyte-secreted proteins may number in the thousands, known astrocyte-secreted proteins are less than 100. To address this fundamental deficiency, mass spectrometry-based proteomics and bioinformatic tools were utilized for global discovery, comparison, and quantification of astrocyte-secreted proteins. A primary mouse astrocyte cell culture model was used to generate a collection of astrocyte-secreted proteins termed the astrocyte secretome. A multidimensional protein and peptide separation approach paired with mass spectrometric analysis interrogated the astrocyte secretome under control and cytokine-exposed conditions, identifying cytokine-induced secreted proteins, while extending the depth of known astrocyte-secreted proteins to 169. Several of these proteins were likely secreted by non-conventional mechanisms. These non-conventional mechanisms were explored further using stable isotope labeling by amino acids in cell culture, revealing 12 putative non-conventionally secreted proteins. These qualitative and quantitative mass spectrometry approaches are broadly applicable for the study of cellular secretomes as well as for extension to in vivo secretomes.

Degree Type
Dissertation

Degree Name
Doctor of Philosophy (PhD)

Graduate Group
Neuroscience

First Advisor
Harry Ischiropoulos

Keywords
Mass Spectrometry, Proteomics, Astrocyte, Protein Secretion, Nitric Oxide, S-nitrosylation

Subject Categories
Cell Biology | Molecular and Cellular Neuroscience

MASS SPECTROMETRY-BASED PROTEOMICS REVEALS

DISTINCT MECHANISMS OF ASTROCYTE PROTEIN SECRETION

Todd Michael Greco

A DISSERTATION

in

Neuroscience
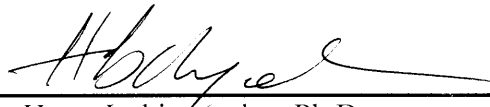
Presented to the Faculties of the University of Pennsylvania

in
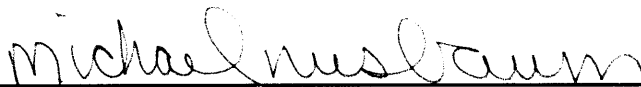
Partial Fulfillment of the Requirements for the

Degree of Doctor of Philosophy

2009

_____

Supervisor of Dissertation: Harry Ischiropoulos, Ph.D.

_____

Graduate Group Chairperson: Michael P. Nusbaum, Ph.D.

Dissertation Committee

Tom Parsons, Ph.D.

Matthew Dalva, Ph.D.

Ian Blair, Ph.D.

Steven Seeholzer, Ph.D.

Mass Spectrometry-based Proteomics Reveals Distinct Mechanisms of
Astrocyte Protein Secretion

COPYRIGHT

2009

Todd Michael Greco

To

My Parents

who have made my academic endeavours

and

life pursuits become reality with their unending support

ACKNOWLEDGEMENTS

short time we have been colleagues. Our computer programming sessions have benefited me tremendously by increasing the speed and efficiency with which I can analyze multiple sets of data. I would also like to thank Ethan Hughes, a fellow graduate student, whose enthuisiasm for astrocytes was so great I couldn't help but incorporate them into my dissertation work. His knowledge of astrocyte biology provided fruitful discussions for designing future experiments. I would like to give specific recognition to Dr. Sarah Keene for teaching me all about astrocyte isolation and cell culture and for joining our expertise in preparation of the astrocyte secretome manuscript. And last, but certainly not least, I would like to thank all the other members of the Ischiropoulos lab that I have worked with throughout the years; Dr. Roberto Hodara, Dr. Ioannis Parastatidis, Dr. Joseph Mazzulli, Dr. Leonor Thomson, Dr. Paschalis-Thomas Doulias, Dr. Margarita Tenopoulou, Dick Lightfoot, Elpida Tsika, Marissa Martinez, Kristin Malkus, Jennifer Greene, Dr. Lindsay Johnston, and Dr. Christie Burno; all your support and friendship, regardless of whether experiments were a success or failure, has carried me through the years.

ABSTRACT

MASS SPECTROMETRY-BASED PROTEOMICS REVEALS DISTINCT MECHANISMS OF ASTROCYTE PROTEIN SECRETION

Todd Michael Greco

Harry Ischiropoulos, Ph.D.

The ability of astrocytes to secrete proteins subserves many of its known function, such as synapse formation during development and extracellular matrix remodeling after cellular injury. Protein secretion may also play an important, but less clear, role in the propagation of inflammatory responses and neurodegenerative disease pathogenesis. While potential astrocyte-secreted proteins may number in the thousands, known astrocyte-secreted proteins are less than 100. To address this fundamental deficiency, mass spectrometry-based proteomics and bioinformatic tools were utilized for global discovery, comparison, and quantification of astrocyte-secreted proteins. A primary mouse astrocyte cell culture model was used to generate a collection of astrocyte-secreted proteins termed the astrocyte secretome. A multidimensional protein and peptide separation approach paired with mass spectrometric analysis interrogated the astrocyte secretome under control and cytokine-exposed conditions, identifying cytokine-induced secreted proteins, while extending the depth of known astrocyte-secreted proteins to 169. Several of these proteins were likely secreted by non-

conventional mechanisms. These non-conventional mechanisms were explored further using stable isotope labeling by amino acids in cell culture, revealing 12 putative non-conventionally secreted proteins. These qualitative and quantitative mass spectrometry approaches are broadly applicable for the study of cellular secretomes as well as for extension to *in vivo* secretomes.

TABLE OF CONTENTS

LIST OF TABLES

CHAPTER 2

CHAPTER 3

CHAPTER 4

LIST OF FIGURES

CHAPTER 1

CHAPTER 4

ABBREVIATIONS

DNIC: dinitrosyl iron complex

ER: endoplasmic reticulum

ESI: electrospray ionization

GFAP: glial fibrillary acidic protein

GSH: glutathione

GSNO: S-nitrosoglutathione

HPLC: high performance liquid chromatography

ICAT: isotope-coded affinity tagging

IL-1B: interleukin-1beta

INF-γ: interferon-gama

iNOS: inducible nitric oxide synthase

iTRAQ: amine-reactive isotope peptide labeling

MALDI: matrix-assisted laser desorption ionization

MS: mass spectrometry

MS-MS: tandem mass spectrometry

NGF: nerve growth factor

NO: nitric oxide

nNOS: neuronal nitric oxide synthase

sGC: soluble guanylate cyclase

TNF-α: tumor necrosis factor-alpha

CHAPTER 1

1.1 Introduction

One of the first roles of astrocytes to be appreciated was the maintenance of extracellular ion balance by inward and delayed rectifying K^+ channels (Ballanyi, Grafe & ten Bruggencate 1987) operating in concert with the Na^+/K^+ ATPase to clear extracellular K^+ (Sontheimer et al. 1994). Yet, in the last 15 years, the idea that astrocytes sole function was only as a support for neuronal function has been continually challenged (Volterra, Meldolesi 2005). An active role for astrocytes in many brain processes has been demonstrated, including nervous system development, neuronal survival, synaptic transmission, and neurogenesis (Christopherson et al. 2005, Haydon, Carmignoto 2006, Ihrie, Alvarez-Buylla 2008, Song, Stevens & Gage 2002). Importantly, not only uptake of biomolecules but their active release subserves these functions (Haydon, Carmignoto 2006).

An emerging field of astrocyte biology research seeks to understand astrocyte protein secretion under specific physiological and pathophysiological states. Thus far, studies have elegantly demonstrated secreted thrombospondins as regulators of synaptogenesis and angiogenesis during development and after recovery from stroke, respectively (Christopherson et al. 2005, Liauw et al. 2008). Astrocyte protein secretion may also play a fundamental role in the immune response as well as the pathogenesis of neurodegenerative diseases, such as amyotrophic lateral sclerosis (ALS) disease, where astrocyte protein secretion was linked to motor neuron cell death (Nagai et al. 2007, Cassina et al. 2005, Di Giorgio et al. 2007). Yet in many cases, the proteins that mediate

these effects have not been identified, and thus the potential molecular mechanisms of disease pathogenesis remain unclear.

Identification of unknown proteins that are important regulators of astrocyte function can be aided by unbiased, complementary proteomic and computational approaches. Previous studies have examined both the astrocyte intracellular proteome (Yang et al. 2005) as well as the secretome (Lafon-Cazal et al. 2003) by mass-spectrometry-based proteomics. However, current advances in both proteomic methodology and mass spectrometric instrumentation allow significantly increased depth of proteome analysis (Tang et al. 2005, Graumann et al. 2008). In addition, stable isotope labeling tools are now more widely available for conducting proteome-wide relative quantification of protein abundance by mass spectrometry. Applying these new technologies to the astrocyte secretome would permit the identification and quantification of previously unknown astrocyte-secreted proteins as well as provide robust methods to functionally evaluate cellular protein secretion under a variety of biological conditions.

Complementary to these functional proteomic studies of astrocyte protein secretion, this project also took a structural proteomics approach to explore consensus protein sequence motifs that may regulate the specificity of nitric oxide-mediated post-translational modification of cysteine residues, termed S-nitrosylation. S-nitrosylation has garnered significant attention as a mechanism by which nitric oxide confers its bioactivity, independent of soluble guanylate cyclase activation (Hess et al. 2005). An understanding of the protein targets as well as the selectivity of S-nitrosylation will aid in defining its role in cell signaling. To achieve these goals, development of improved mass spectrometry-based methods that facilitate sensitive and site-specific identification of the

2

modified cysteine residues are necessary. Additionally, by obtaining the identity of the protein targets along with the modified cysteine, current hypotheses regarding protein sequence motifs that govern S-nitrosylation specificity can be tested (Sun et al. 2001, Stamler et al. 1997).

1.2 Cellular pathways of protein secretion

The seminal discovery by Günter Blobel and colleagues (Lingappa, Lingappa & Blobel 1980) that newly synthesized proteins contain amino acid sequences that direct them to specific "zip codes" within the cell has paved the way for cell biologists to explore the mechanisms of protein sorting and secretion. The presence of an N-terminal signal peptide directs a protein for translocation across the endoplasmic reticulum (ER) in eukaryotes (von Heijne 1985). Proteins lacking an ER/Golgi retention signal (Davis, Tai 1980) are then secreted outside the cell, termed "classical" protein secretion. Although there is no strict consensus sequence for signal peptides, they often share common features (Figure 1.2-1). A comparison of signal peptides from human alpha-1-antichymotrypsin and *E. coli* class B acid phosphatase precursor shows both contain positively charged amino acids in the immediate N-terminus, a stretch of hydrophobic residues, and a C-terminal region of polar uncharged residues (Figure 1.2-1). As described in greater detail below (Chapter 1, Section 6), computational algorithms have been developed to effectively predict the presence of signal peptides, with at least 2,000 secreted proteins predicted for the mouse genome (Grimmond et al. 2003).

Human alpha-1-antichymotrypsin precursor signal peptide
N-term-ME**R**MLP**LLALGLLAAGFC**PAVL<u>**C**</u>HPNSPLDEEN…

Escherichia coli class B acid phosphatase precursor signal peptide
N-term-M**RK**ITQ**AISAVCLLFAL**NSSAVAL<u>**A**</u>SSPSPLNPGT…

Figure 1.2-1. Comparison of N-terminal signal peptides between human and *E.coli* proteins.
Across different species, most signal peptides share three distinct common features (underlined):
(1) an N-terminal region of positively charged residues (*orange*), (2) a hydrophobic region (*red*),
and (3) a C-terminal region of polar, uncharged residues around the cleavage site (*green*).

Using a genetic fusion of *Escherschia coli* beta-lactamase to cytoplasmic globulin, researchers were able to demonstrate that an N-terminal signal sequence is sufficient for translocation of a protein to the ER and ultimately allow its secretion (Lingappa et al. 1984). Yet, there are some secreted proteins, such as interleukins, galectins, and fibroblast growth factors that do not contain signal peptides (Nickel, Seedorf 2008). These non-classically or non-conventionally secreted proteins are not translocated to the ER but reach the outside of the cell by alternative mechanisms (Figure 1.2-2). While direct protein translocation or protein-assisted mechanisms have been proposed for transport of these substrates across the plasma membrane, the molecular details are not well understood (Nickel, Rabouille 2009).
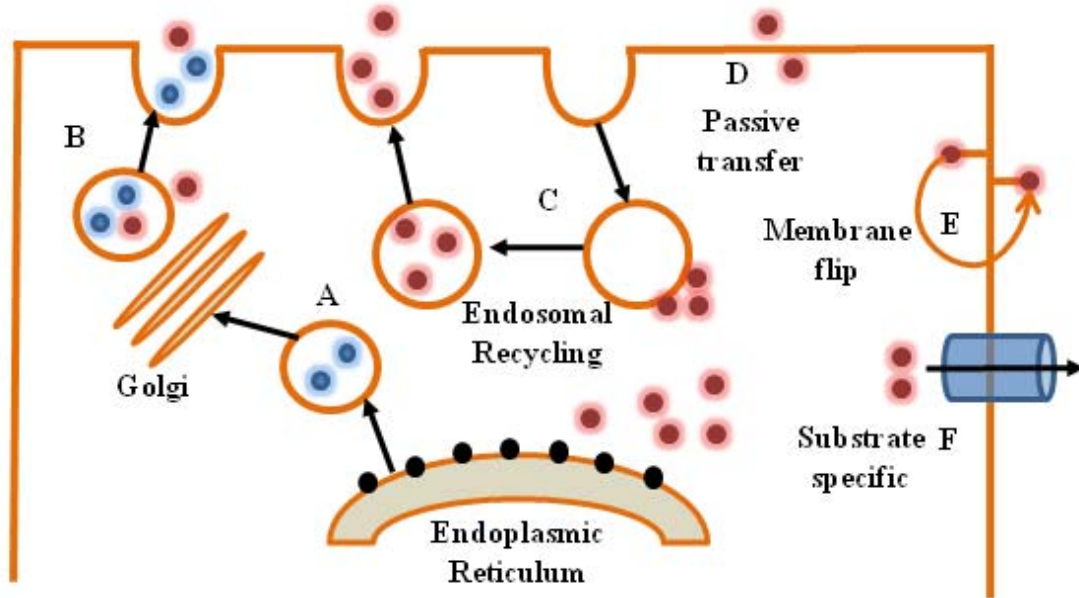
Figure 1.2-2. Potential secretion mechanisms for proteins that lack an N-terminal signal peptide. Diagram illustrates several potential mechanisms for secretion of non-conventional proteins (red balls), representing both passive and protein-assisted mechanisms (Nickel, Rabouille 2009). Although non-conventional proteins are produced in the cytoplasm and do not proceed via the canonical endoplasmic reticulum-Golgi pathway (A, blue balls), membrane affinity of some proteins could facilitate their entry into vesicles carrying classically secreted proteins (B, red and blue balls), or into vesicles recycled into the endosomal compartment (C). Alternatively, protein translocation could occur either through passive transfer (D) or membrane-associated flipping (E). In addition, yeast and mammalian systems suggest substrate-specific transporters may exist, for example, Nce102p-mediated galectin-1 secretion in yeast (Cleves et al. 1996).

In contrast, the mechanisms and pathways of classical protein secretion have been fairly well established. While classically secreted products are localized to the ER and Golgi compartments, there can be variation in the time (minutes to hours) and location (apical/basolateral) of secretion within the same cell (Kelly 1985). As illustrated in figure 1.2-3, the existence of two parallel protein sorting pathways is likely (Pfeffer, Rothman 1987). First, a "default" bulk-flow pathway exists where proteins are synthesized and secreted at a rate proportional to protein synthesis. In this pathway, no sorting or concentration of proteins occurs, with proteins reaching the surface in minutes. This mechanism would also support the flow of integral membrane proteins to the cell surface.
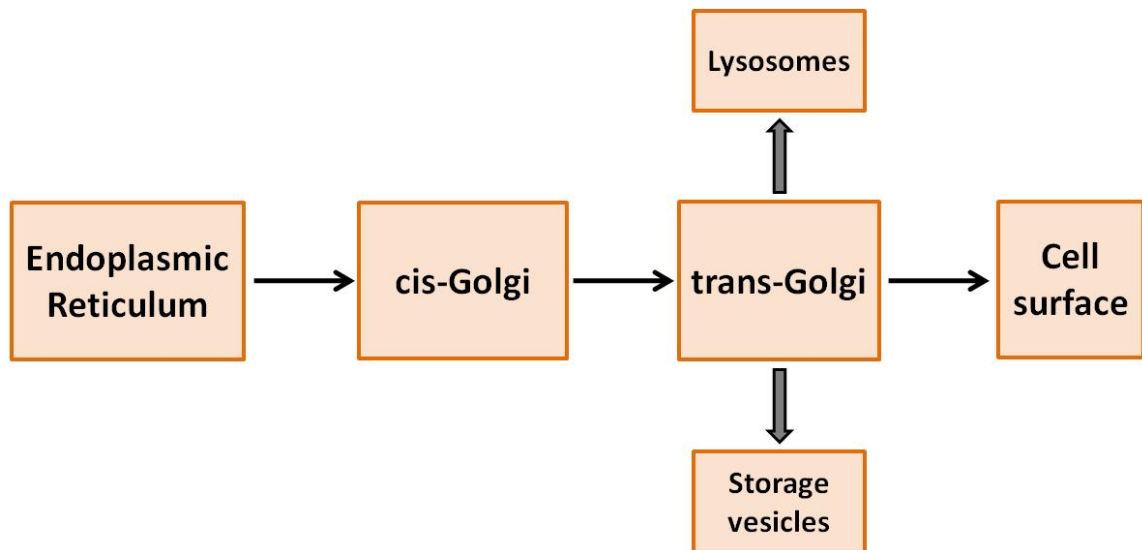
Figure 1.2-3. Protein sorting pathways. In the absence of an ER-Golgi retention sequence, many secreted proteins follow a "bulk-flow" pathway that results in their transport from the ER to the cell surface (*thin arrows*). Alternatively, proteins may possess motifs or signals, such as post-translational modifications (Pfeffer 1988), that result in their diversion from the bulk flow pathway at the level of the trans-Golgi (*thick arrows*). Two primary targets for these proteins are lysosomes and storage vesicles.

On the contrary, many proteins are diverted from bulk flow, entering a vesicular pool that can be released by stimulus-coupled or regulated secretion mechanisms (Kelly 1985). It is hypothesized that "molecular traps" facilitate the diversion of proteins from bulk flow. These molecular traps may be receptors that recognize specific cargo, thereby enriching proteins through sequestration from bulk flow (Pfeffer 1988, Gorr, Darling 1995, Chung et al. 1989). The identity of many of these receptors is unknown, but the molecular details for sequestration of lysosomal enzymes have been fairly well documented (Pfeffer 1988). Mannose-6-phosphate receptors, localized to Golgi, selectively bind proteins that have been tagged with asparagine-linked high mannose sugars, providing a molecular recognition system for removing proteins from bulk flow. Although the molecular mechanisms for sorting of secretory vesicle contents are not well understood, current evidence suggests secondary or tertiary structure in the N-terminal region may facilitate sorting (Gorr, Darling 1995). Further studies are needed to more clearly define these mechanisms, which include understanding the depth and diversity of secreted proteins, particularly with respect to regulated versus constitutive and classical versus non-classical secretion.

1.3 Astrocyte secretion of biomolecules

Astrocytes, a subtype of glia cell, were described by Ramon y Cajal in the early 20th century using Golgi stain, which enabled him to visualize the characteristic astrocyte-specific intermediate filaments, known today as glial fibrillary acidic protein (GFAP). While for many years the roles of astrocytes were limited to the support of neuronal networks, research in the past two decades has proven astrocytes hold a more

prominent, active role in the nervous system (Halassa, Fellin & Haydon 2007). The development of novel optical imaging techniques and fluorescent chemical probes has established astrocytes as active participants in synaptic signaling through the release and uptake of chemical transmitters such as glutamate, ATP, and D-serine (Volterra, Meldolesi 2005). Astrocytes release these transmitters by SNARE- and calcium-dependent mechanisms similar to neurons; but unlike neurons, exhibit graded potentials, where G-protein-coupled and Ins(1,4,5)P$_3$-induced calcium release drives vesicle fusion (Montana et al. 2006). In addition, astrocytes are known to synthesize and release eicosanoids in control of cerebral microvasculature (Mulligan, MacVicar 2004) and in response to microglia-derived pro-inflammatory cytokine mediators (Stella et al. 1997). These pro-inflammatory mediators, such as interleukin-1b and tumor necrosis factor-alpha, can also stimulate expression of inducible nitric oxide synthase (iNOS) and subsequent production of nitric oxide (NO) (Saha, Pahan 2006).

More recent studies have documented the ability to synthesize, package, and release peptide transmitters. Both secretogranin II and neuropeptide Y (NPY) were identified in dense-core granules similar in size to granules present in neuronal cells (Calegari et al. 1999, Kreft et al. 2009, Ramamoorthy, Whim 2008). Release of these peptide transmitters can be induced by specific stimuli, such as phorbol ester, in a calcium-dependent manner, consistent with regulated secretion. Yet the role of astrocyte-secreted peptides in modulating neuronal circuits has not been explored and is currently an active area of research.
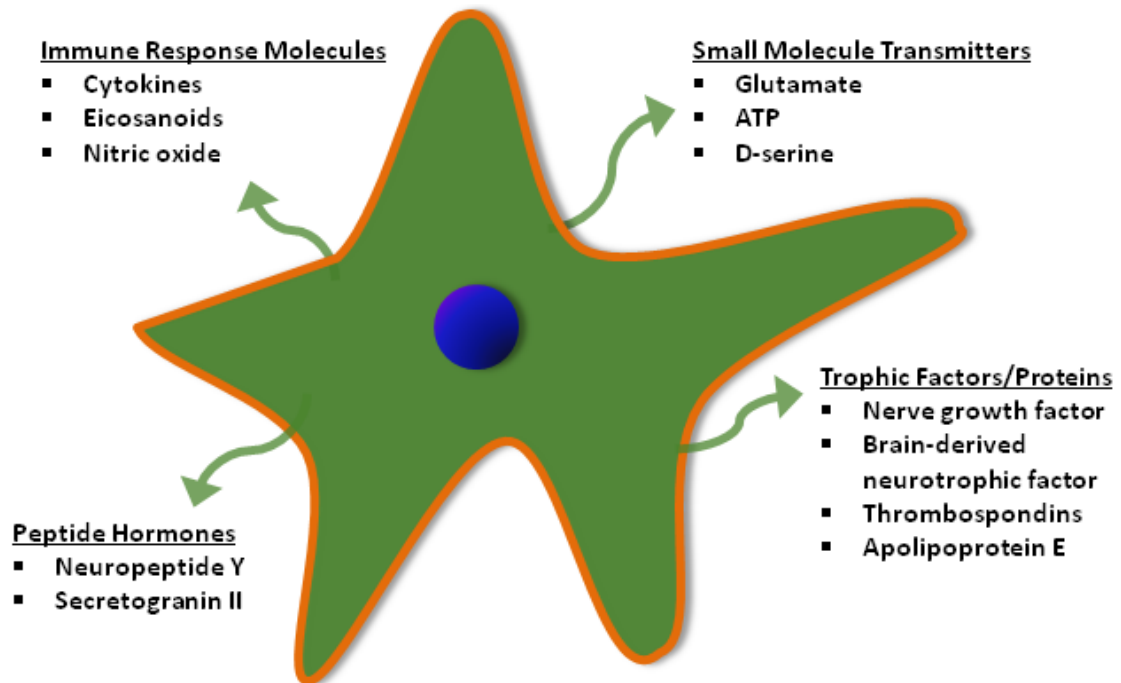
Figure 1.3-1. Astrocyte-secreted biomolecules. Active roles for astrocytes in neurotransmission, modulation of synaptic circuits, nervous system development, neurogenesis, and immune response are mediated by the secretion of several classes of signaling molecules from small molecule transmitters to proteins.

Astrocytes have been identified as key regulators of nervous system development with prominent roles in synapse formation and neuronal differentiation (Christopherson et al. 2005, Ihrie, Alvarez-Buylla 2008, Song, Stevens & Gage 2002, Seth, Koul 2008, Ullian, Christopherson & Barres 2004). The molecular mechanisms underlying these processes are an area of great interest as recent evidence suggests protein secretion may subserve these critical functions. In particular, *in vitro* and *in vivo* synapse formation was promoted by thrombospondins that were secreted by immature, but not mature astrocytes (Christopherson et al. 2005). Moreover, meteorin, a secreted protein localized to astrocyte endfeet, elicited the secretion of thrombospondin-1 and –2, which attenuated angiogenesis (Park et al. 2008). Astrocytes can also provide trophic support to neurons,

9

as evidenced by co-culture experiments demonstrating increased neuronal survival and neurite formation (Banker 1980). Although the identity and mechanisms of release of these factors are not completely characterized, the release of nerve growth factor (NGF), brain-derived neurotrophic factor (BDNF), and glial cell-derived neurotrophic factor (GDNF) in response to purinergic pathway activation has been observed (Seth, Koul 2008, Banker 1980, Ciccarelli et al. 1999, Sariola, Saarma 2003, Zafra et al. 1992) .

Under pathological conditions, astrocyte protein secretion may play an important role in etiology or disease progression. Aberrant astrocyte protein secretion has been linked to neurodegenerative disorders such as multiple sclerosis, amyotrophic lateral sclerosis (ALS), and Alzheimer's disease (Seth, Koul 2008). The neuroinflammatory components of multiple sclerosis implicate glia in disease pathogenesis as they are central to the generation of innate immune response in the nervous system. Specifically, astrocytes from patients with multiple sclerosis, but not those with other neurological impairments, were found to have increased expression of syncytin-1, an endogenous retroviral protein, which can modulate inflammatory cascades through the downstream production of cytokines (Antony et al. 2004, Antony et al. 2004, Antony et al. 2007). Moreover, during disease progression, the blood brain barrier breaks down, allowing CNS infiltration by somatic immune cells, including macrophages/monocyctes, which are attracted in part by chemokine production (Minagar, Alexander 2003, Krumbholz et al. 2006). Although microglia are a major source of secreted chemokines, evidence also indicates astrocyte-secreted chemokines may participate in this infiltration process (Krumbholz et al. 2006).

In addition, soluble factors released from astrocytes have a documented role in ALS. For instance, astrocytes that express familial ALS-causing mutant forms of superoxide dismutase 1 induced greater motor neuron death than the wild-type counterparts (Nagai et al. 2007). Independent studies have implicated fibroblast growth factor 1 (FGF1), a non-classically secreted protein, as a potential signaling molecule involved in the pathogenesis of ALS. Specifically, FGF1-induced activation of astrocytes was found to promote the expression and secretion of NGF, which increased motor neuron death (Cassina et al. 2005).

Also, Alzheimer's disease, a neurodegenerative condition characterized by amyloid-beta-containing plaques, has also been linked to astrocyte activation and altered signaling. Astrocytes highly express and secrete apolipoprotein E (ApoE), the most abundant lipoprotein in the central nervous system. A primary function of astrocytes is to process amyloid precursor protein (APP) to amyloid-beta peptides via an ApoE-dependent mechanism (Koistinaho et al. 2004). Since genetic isoforms of ApoE have been linked to increased risk of Alzheimer's disease (Huang et al. 2004), ApoE's role in astrocyte-derived APP processing may be particularly relevant to the development of Alzheimer's disease. Additionally, astrocyte-secreted proteins including butyrylcholinesterase (BchE) and S100β were found as components of neuritic plaques (Meda, Baron & Scarlato 2001). Collectively, these studies suggest astrocytes are an important component of neurodegenerative disease pathogenesis.

1.4 Analysis of complex biological protein mixtures by mass spectrometry

Comprehensive, whole cell biochemical and molecular approaches including RNA profiling arrays and mass spectrometry-based proteomics have the capacity to greatly accelerate progress in defining cell-specific secretomes. Genomic and computational approaches generate invaluable resources; comprehensive catalogs of potentially expressed and secreted proteins for many cells types within the mammalian CNS (Cahoy et al. 2008). Yet there is a need for global, unbiased protein-based methods that can directly document gene product expression and determine whether these expressed proteins are secreted under specific cellular conditions. While genomic and bioinformatic studies have predicted the number of secreted proteins into the thousands (Grimmond et al. 2003, Pickart et al. 2006), experimentally identified secreted proteins are currently in the hundreds for single cell types (Lafon-Cazal et al. 2003, Pellitteri-Hahn et al. 2006, Gronborg et al. 2006). Towards these goals, mass spectrometry serves as an important technology enabling the protein composition of complex biological samples to be determined with unmatched depth of analysis.

The first modern mass spectrometer was developed by Arthur Dempster in 1918 (Figure 1.4-1) (Dempester 1918). For efficient detection of analytes, most mass spectrometric analyses require the sample to exist as ionized molecules in the gas phase. In early spectrometers, ionization was accomplished directly by electron impact. However, this relatively high-energy ionization was ineffective for large macromolecules. A major advancement in ion sources was achieved by the development

of chemical ionization (Munson, M.S.B and Field, F.H. 1966), considered a "soft"
ionization technique. Later, the principles of chemical ionization were applied in the
development of laser desorption and electrospray ionization techniques (Fenn et al. 1989,
Nakanishi et al. 1994). The widespread use of these techniques, which were the basis for
the 2002 Nobel Prize in Chemistry, has ushered in a new era of mass spectrometric
analyses of larger biomolecules such as peptides and proteins.
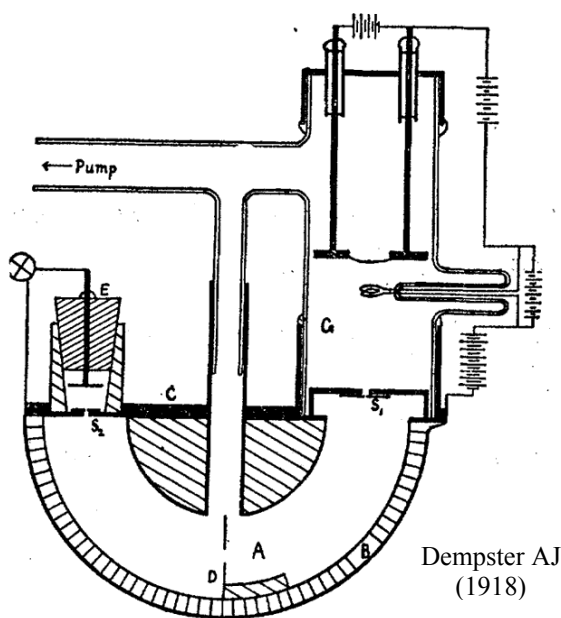
Dempster AJ
(1918)

Figure 1.4-1. First modern mass spectrometer. Arthur Dempster's mass spectrometer as originally published in *Phys. Rev.* 11(4), 316-25, 1918. This design is considered the first modern mass spectrometer as current mass spectrometers still utilize these design concepts. Analytes, e.g. salts in the initial experiments, were introduced into a glass tube (G) and ionized by electron bombardment from the electrometer (E). The analyte ions were accelerated through a slit (S_1) by a potential difference, entering into the analyzing chamber (A) where a strong magnetic field was applied. Using the potential difference, magnetic field strength, and radius of the curvature of the analyzing chamber, the charge to mass of the particles was determined.

These techniques permit peptide or protein ionization to occur without significant
in-source fragmentation. As shown in figure 1.4-2, peptides are ionized by a chemical-
assisted process in both matrix-assisted laster desorption ionization (MALDI) and
electrospray ionization (ESI) techniques. In MALDI (Figure 1.4-2A), analytes are mixed
with matrix compounds, evaporated on a target plate, and irradiated, usually with a UV
laser source. The laser primarily induces matrix ionization as it is designed to readily

absorb UV light and is more concentrated than the analyte. Some ionized matrix then reacts with the analyte, in this case the peptides, generating peptide ions in the gas phase.

Similarly, in electrospray ionization (Figure 1.4-2B) the analyte is mixed with solvent, often at low pH for peptide analysis. The solution is then infused through a capillary at high voltage, imparting charge to the molecules as they enter the evaporation chamber under nitrogen drying gas. These conditions facilitate progressive formation of smaller liquid droplets. As droplet size is decreased, positively charged species strongly repel, which causes a further decrease in droplet size until only a single ion species is present per droplet.
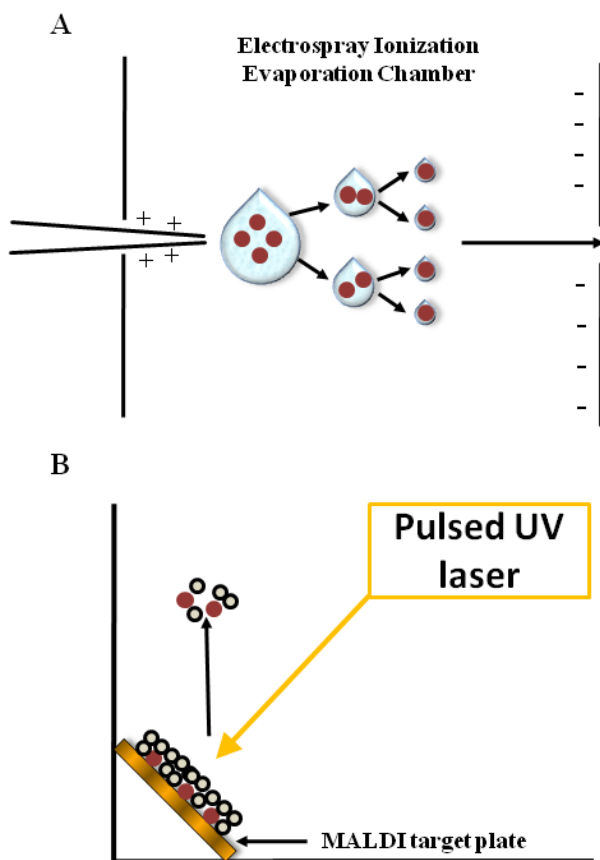
Figure 1.4-2. Soft ionization techniques for analysis of peptides and large macromolecules. (A) Matrix-assisted laser desorption ionization mass spectrometry (MALDI) induces ionization through irradiation of the target plate by laser pulses. Analytes (*red balls*) are applied to the target plate after mixing with various matrix compounds (*black circles*), such as α-cyano-4-hydroxycinnamic acid (CHCA). Matrix compounds more readily absorb UV energy, and therefore become the primary targets of direct ionization. Ionized matrix then reacts with the analyte to form molecular ions. (B) Electrospray introduces the sample in liquid phase through a heated capillary under a high potential difference. This favors the formation of solvent droplets containing the analyte (*red balls*). While in the evaporation chamber under low vacuum and nitrogen drying gas the analyte-containing droplets shrink, facilitated by the coulombic forces that repel positively charged analytes. This process continues until a single ion is present per droplet.

For MALDI, ionization conditions favor the addition of a single proton (H^+), usually to the N-terminal amino group, forming the molecular ion $[M+H]^+$. In contrast, electrospray ionization predominantly generates multiply protonated molecular ions, resulting in charge states greater than one $(M+H)^{n+}$. Higher charge states are observed for peptides containing amino acids with side chains that have high pK_a values, such as lysine, arginine, and histidine, as the side-chain nitrogen is largely protonated under acidic pH (Fig 1.4-3).
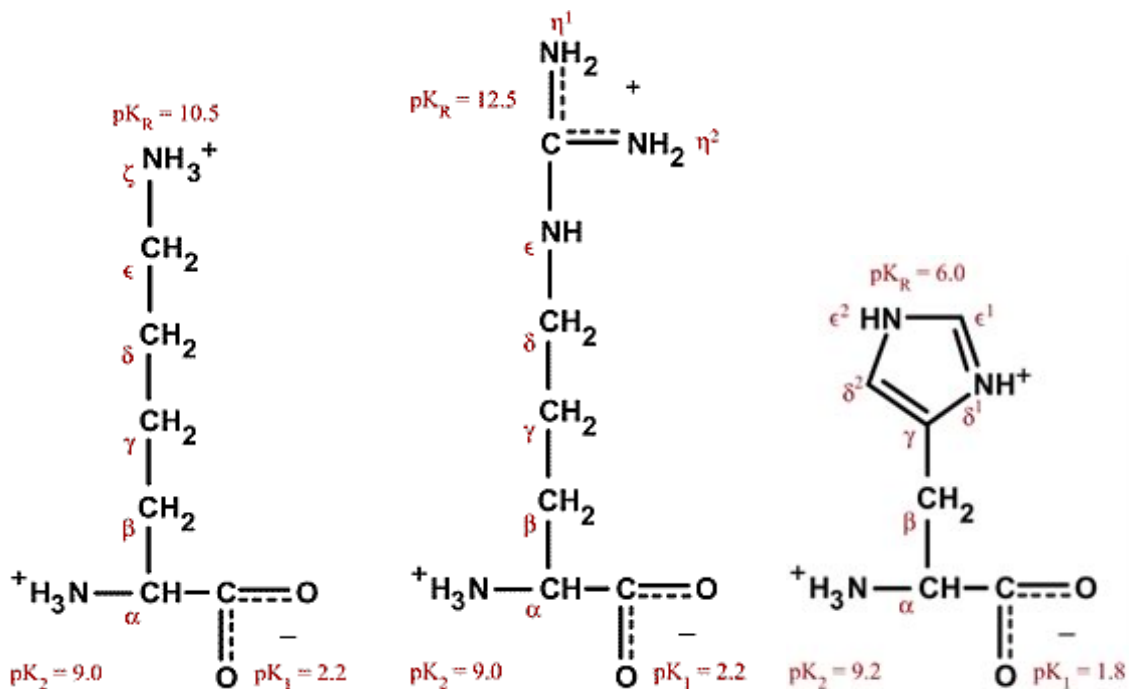
Figure 1.4-3. Chemical structures of basic amino acids. Amino acids lysine, arginine, and histidine exist as protonated species in aqueous solution at acidic pH due to the relatively high pK_a of their side chain nitrogens, denoted above as pK_R. This chemical property combined with their high occurrence in proteins makes the selection of trypsin an ideal protease for peptide mass spectrometric analysis.

Importantly, mass spectrometers measure the mass-to-charge ratio (m/z) of the peptide ion and not directly their mass. Therefore, in electrospray ionization, peptide ions that carry multiple charges (2+, 3+, 4+, etc) may exist in several distinct ionic species up to the maximum charge state. While multiple charge states result in increased spectral complexity, it does allow peptides with higher mass, which normally would be outside the suitable mass range for detection, to be observed as higher order charge states reduce the peptide's observed mass-to-charge. Commonly, these positively charged peptides are generated from complex protein mixtures by enzymatic digestion with trypsin, as it cleaves at the C-terminus of lysine and arginine, often referred to as tryptic peptides (Olsen, Ong & Mann 2004).

In summary, these "soft" ionization techniques are suitable for protein and peptide ionization as they provide efficient ionization with limited in-source fragmentation of the peptide backbone. Performed under acidic conditions, ionization of tryptic peptides can be extremely efficient due to positively-charged amino groups at the N- and C-terminus. As discussed in more detail below, electrospray ionization is more amendable than MALDI for direct coupling to multidimensional chromatographic separations, in particular liquid-based chromatrographies.

1.4.1 Protein and peptide separation by multidimensional chromatography

The importance of effective protein and peptide separation of complex biological mixtures with respect to depth of analysis has been demonstrated on a theoretical

(Eriksson, Fenyo 2007) as well as experimental basis (Tang et al. 2005, Graumann et al. 2008, Washburn, Wolters & Yates 2001). A core issue that protein and peptide separation techniques address is the issue of undersampling, where complexity (number of distinct proteins) and dynamic range (protein abundance) of biological samples limits the ability of the mass spectrometer to detect all peptides/proteins contained within the sample. Ideally, a sample should be fractionated and separated sufficiently so that the reduction in complexity eliminates undersampling. Practically, undersampling can occur despite multi-dimensional separation of complex cellular proteomes, as demonstrated by the need to analyze a single sample as many as ten times to identify greater than 95% of the proteins within the detectable range (Liu, Sadygov & Yates 2004). Moreover, experiments that involve whole cell proteomes and compare multiple biological conditions have become impractical for extensive fractionation and multiple technical replicates. Therefore, the experiment should always be designed to reduce complexity sufficiently such that the achieved sensitivity allows the biological question(s) to be answered.

Fundamentally, methods should (1) use orthogonal chromatographic separations that maximize separation efficiency and (2) when possible, perform depletion/separation of known high abundance species to reduce dynamic range. An exemplary example of this strategy was performed by Tang and co-workers (2005), whose multidimensional strategy was employed for mass spectrometric analysis of the plasma proteome. This work clearly demonstrated the utility of performing protein depletion and orthogonal separations of both proteins and peptides. First, the top six most abundant plasma proteins, which comprise at least 80% of the total plasma proteins were depleted by

immunoaffinity chromatography (Tang et al. 2005). Next, proteins were separated by apparent molecular weight using SDS-PAGE, with the resolving distance optimized for the proteome of interest. Then, the entire gel lane was cut into equal 1-2 mm slices. Each slice was individually processed by in-gel trypsin digestion to yield tryptic peptides. Each fraction of tryptic peptides was then separated by pI using in-solution isoelectric focusing. Finally, the peptides contained within each pI range were separated by their hydrophobicity using reverse phase C_{18} liquid chromatography, which was directly coupled to the electrospray mass spectrometer (ESI-LC-MS/MS). This four-dimensional strategy resulted in the detection of plasma and serum proteins that differ in abundance by nine orders of magnitude (10 mg/mL to 10 pg/mL) (Tang et al. 2005).

Although this study was performed with plasma and serum proteomes, these concepts are amenable to cellular secretomes as well. Conditioned media is one of the primary biological samples used for analysis of cellular secretomes, which traditionally contains extensive contamination by highly abundant serum proteins. One study documented that culturing smooth muscle cells in reduced serum media enabled significant improvement in depth of analysis of the secreted proteins (Pellitteri-Hahn et al. 2006). Since astrocytes can be cultured in serum-free media for up to 14 days without adverse effects on cell survival, a significant reduction in serum protein contamination prior to multidimensional chromatography and mass spectrometric analysis can be achieved.

1.4.2 Acquisition of mass spectra and automated sequence-to-spectrum database searching

Most modern mass spectrometers are capable of performing at least two successive "rounds" of mass analysis, referred to as tandem mass spectrometry (MS/MS or MS^2) (Figure 1.4.2-1). The first round determines the mass-to-charge (m/z) of the intact peptide ions, also known as the precursor ions. In liquid chromatography-mass spectrometry, a single mass spectrum represents the parents ions detected at a specific time during chromatographic separation. The second round of analysis involves selection and fragmentation of specific precursor ions within the mass spectrum, generating characteristic daughter or product ions. The collection of detected fragment ions derived from parent ion dissociation is stored within a single MS/MS spectrum. Acquisition of MS/MS spectra is often performed in a data-dependent fashion, which selects the most abundant parent ions contained within the MS spectrum for fragmentation. For instance, from a single MS spectrum, the top five most intense peptide ions can be selected for MS/MS analysis (Figure 1.4.2-1). This cycle is repeated over the entire chromatographic peptide separation. While the total MS/MS spectra collected during a single run can depend on LC gradient, sample abundance, and complexity, a typical gradient of 90 minutes on a linear ion trap mass spectrometer can generate approximately 12,000 MS/MS spectra.
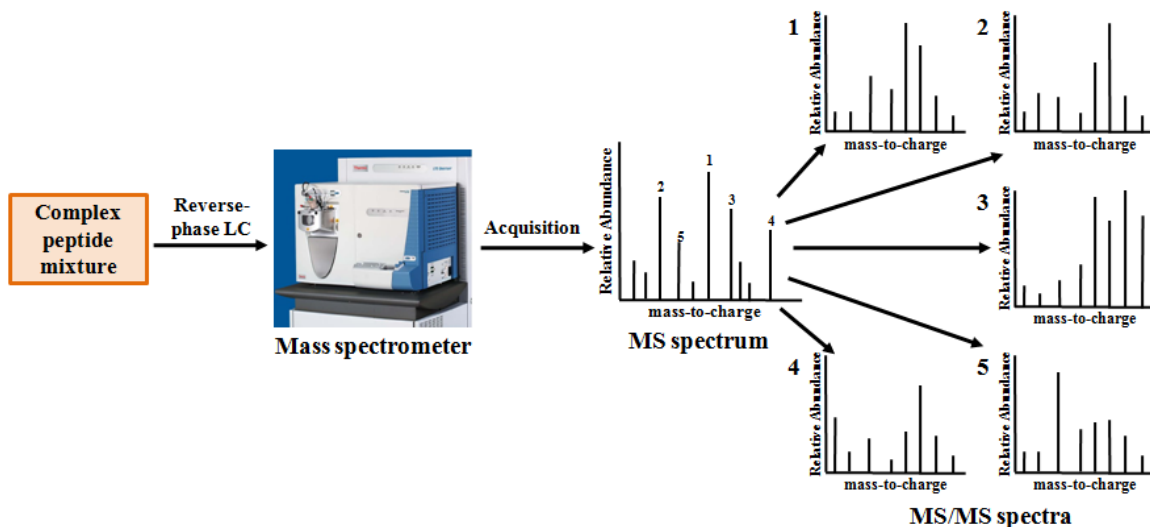
Figure 1.4.2-1. Typical data acquisition workflow for liquid chromatography tandem mass spectrometry. Complex peptide mixtures are separated by reverse-phase liquid chromatography and introduced inline to the mass spectrometer, above pictured with an electrospray ionization source. Throughout the reverse-phase separation of peptides, the mass spectrometer acquires a single mass (MS) spectrum, determines the top 5 most abundant peptide ions, and individually fragments by collision-induced dissocation (CID; figure 1.4.2-2) each peptide ion to generate 5 tandem (MS/MS) spectra.

The sequence information contained with an MS/MS spectrum depends on the type of peptide fragmentation employed. One fragmentation method, collision-induced dissociation (CID), induces cleavage of the parent ion along the C-N amide bonds of the peptide backbone (Figure 1.4.2-2). This cleavage generates complementary N-terminal and C-terminal daughter ions, referred to as b-ions and y-ions, respectively. With significant backbone cleavage, a nearly complete peptide sequence can be determined by manual inspection of the MS/MS spectrum (Shevchenko et al. 1997). However, given that thousands of MS/MS spectra can be generated from a single sample, manual assignment of the sequence to each spectrum (sequence-to-spectrum assignments) is not feasible.

20
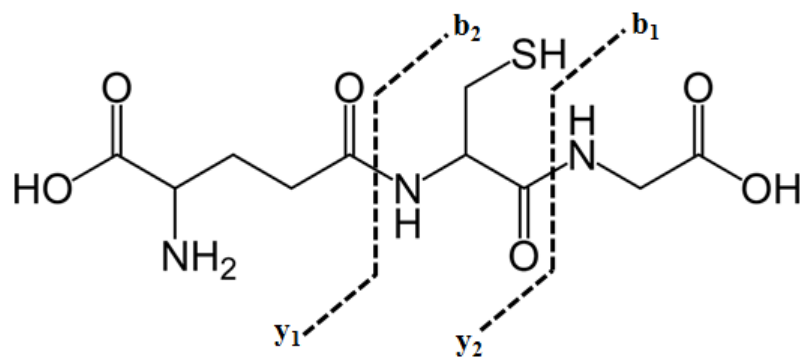
Figure 1.4.2-2. Collision-induced dissociation of peptide amide bonds. Shown are two amide bond cleavage sites of the tripeptide glutathione. These are the predominant cleavages produced by collision-induced dissociation (CID) fragmentation. CID is performed by selecting an intact peptide (precursor) ion, accumulating it in the mass analyzer, and then colliding it with an inert gas, often helium. These collisions impart kinetic energy to the peptide ion, and in CID, this kinetic energy is translated to internal energy that primarily breaks peptide amide (N-C) bonds. By convention, the fragment ions resulting from this cleavage are referred to as y- and b- ions, corresponding to the N- and C-terminal fragments, respectively. Usually for each collision only a single cleavage is generated, producing two complementary fragment ions, e.g. y_1 and b_2.

As a result, several software algorithms have been designed to generate sequence-to-spectrum assignments, including SEQUEST (Ducret et al. 1998), MASCOT (Perkins et al. 1999), and X!Tandem (Craig, Beavis 2004). Although each algorithm has been implemented differently, a shared concept of all the algorithms is to compare each experimental MS/MS spectrum to all the theoretical MS/MS spectra within a specified mass tolerance, generated from *in silico* tryptic digests of protein sequence databases. For each comparison the algorithm assigns a score and then returns the sequence-to-spectrum assignment that received the top score. This is performed for all experimental MS/MS spectra collected. From data acquisition to sequence assignment, this analysis workflow is often referred to as "shotgun" peptide sequencing (Wolters, Washburn & Yates 2001).

1.4.3 Probabilistic validation of sequence-to-spectrum assignments

Sequence-to-spectrum assignments for most database search algorithms return the top scoring hit, but this is not necessarily a measure of quality. It is necessary to apply score cutoff thresholds to retain the high quality (correct) assignments and eliminate poor quality (incorrect) assignments. The scoring parameters of the SEQUEST algorithm (Ducret et al. 1998) will be used for discussion as it was the primary algorithm used in in this work. SEQUEST's primary score output is a cross correlation score (X_c). While the X_c score can be a useful measurement of assignment quality, it is dependent upon several factors that may not be constant between experimental samples, such as peptide length, protein sequence database size, and number of input spectra (Keller et al. 2002a). Therefore, selecting an absolute X_c score threshold that defines correct-incorrect spectra is not optimal.

Much effort has been placed on developing new algorithms that do not rely on single scoring thresholds (Searle, Turner & Nesvizhskii 2008). For example, two widely utilized algorithms are PeptideProphet and ProteinProphet (Keller et al. 2002a, Nesvizhskii et al. 2003). Conceptually, these algorithms take multiple scoring parameters as input, and then based on these parameters generate two score distributions, reflecting incorrect and correct peptide assignments (Figure 1.4.3-1A). Using this two population model, a probabilistic value of being correct is calculated for each sequence-to-spectrum assignment depending on its normalized score within the distributions. Then, peptide assignment probabilities can be used as scoring thresholds, which allows the global error rate (at a defined scoring threshold) to be estimated. Peptide assignment probability thresholds are usually selected, which control global error rate to a desired value, for

instance, less than 1%. In addition, the ProteinProphet algorithm (Keller et al. 2002a) was developed to use individual peptide probabilities generated from PeptideProphet (Nesvizhskii et al. 2003) to calculate protein probabilities, allowing error rate control at the protein level.
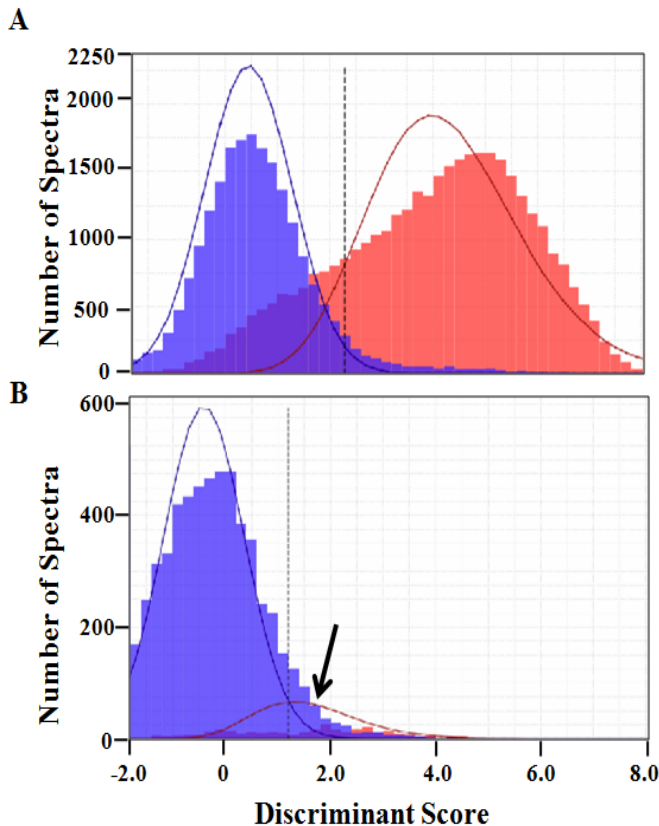
Figure 1.4.3-1. Probabilistic modeling of SEQUEST sequence-to-spectrum assignments. Sequence-to-spectrum scoring parameters are used to calculate a discriminant score. PeptideProphet uses an expectation maximization algorithm to model the distribution of discriminant scores as a function of the number of spectra (A) PeptideProphet modeling of 120,000 spectra (14 LC-MS runs) generated from in-gel digest of 60 ug of protein. This dataset contains many high quality MS/MS spectra that received excellent discriminant scores. This is reflected by the efficient separation of incorrect and correct distributions. (B) PeptideProphet modeling of 16,000 spectra from a single LC-MS/MS run examining low abundance post-translationally modified peptides. Most MS/MS spectra receive lower discriminant scores, causing poor separation (*arrow*) of correct and incorrect peptides.

An important caveat of these algorithms is their predictive ability depends on how well the statistical modeling fits the experimental dataset. For example, poorer quality MS/MS data or small datasets can invalidate the assumptions made by these algorithms during the modeling procedure. An example is shown in figure 1.4.3-1B that results in poor distribution modeling of incorrect and correct assignments. While the poor modeling

shown in figure 1.4.3-1B is apparent, subtle deviations that affect the goodness-of-fit may not be immediately recognized without careful manual inspection of MS/MS spectra and evaluation of peptide assignment probabilities (Greco TM and Seeholzer SH, personal observations). These deviations often result in the underestimation of peptide assignment error rates. Therefore, a combination of error rate control strategies can be used as a more reliable measure of the true error rate.

Another useful method for error rate control is to generate a sequence database that contains proteins not occurring in nature but that retains the same amino acid frequency, protein length, and overall size as the original database. A facile approach to generate this modified database is to reverse each of the protein sequences in the database of interest (Peng et al. 2003). This reverse sequence database is then appended to the forward sequence database, and sequence-to-spectrum assignments are generated as described in chapter 1, section 4.2. Since experimental spectra have equal opportunity to match forward (correct) and reverse (incorrect) sequences, sequence-to-spectrum assignments derived from reverse peptide sequences are considered false-positive assignments. These false-positive assignments can be used to rationally set scoring thresholds such that global error rate is controlled at a desired level (Peng et al. 2003).

Alternatively, DTASelect (Cociorva, L Tabb & Yates 2007), an extensively developed open-source software package, uses reverse (incorrect) database assignments as the primary determinant for the statistical modeling. This improves the ability of the algorithm to distinguish between incorrect and correct peptides, thereby providing more robust prediction of the correct peptide assignment. A similar concept has also been recently integrated into the PeptideProphet algorithm (Choi, Nesvizhskii 2008)). The

statistical methods and computational algorithms described above will be utilized to validate SEQUEST sequence-to-spectrum assignments, providing a controlled error rate (< 1%) at both the peptide and protein level.

1.5 Quantitative mass spectrometry-based proteomics

Currently, many methodologies for proteome-wide quantification of protein abundance have been developed, providing both relative and absolute quantification. The application of quantitative mass spectrometry to proteomic workflows can be divided into two broad categories: (1) label-free and (2) stable isotope labeling (Figure 1.5-1). Stable isotope labeling techniques use stable isotope-containing peptides/proteins as standards. These isotope standards do not significantly differ in their inherent physicochemical properties compared to the endogenously present peptides/proteins, but generate predictable shifts in mass-to-charge, which can be easily differentiated in mass spectrometric analyses. Therefore, the direct addition of a known amount of isotope-labeled reference to the experimental sample, referred to as stable isotope dilution, provides a means to correct for systematic and random errors that are introduced during subsequent processing steps, including affinity enrichments, analytical separations, and mass spectrometric analysis.

Depending on the experimental model and design, an appropriate stable isotope labeling method can be selected that incorporates the isotope label into the proteome at three different steps during sample preparation (Figure 1.5-1A, B, C). Figure 1.5-1 illustrates three parallel experimental workflows where isotope labels are incorporated for analysis of a cellular proteome, either during (A) the cell culture phase, (B) at the level of

protein extracts, or (C) at the peptide level. Techniques which accomplish (A) include stable isotope labeling by amino acids in cell culture (SILAC) (Ong et al. 2002) and stable atom metabolic enrichment strategies (e.g. ^{15}N) (Washburn et al. 2002, Oda et al. 1999), (B) isotope-coded protein labeling (ICPL) (Schmidt, Kellermann & Lottspeich 2005), and (C) isotope-coded affinity tagging (ICAT) (Gygi et al. 1999), O_{18} water (Yao et al. 2001), and amine-reactive stable isotope peptide labeling (iTRAQ). SILAC labeling is the most attractive as it incorporates the isotope label at the earliest stage of the workflow and therefore facilitates accurate quantification with relatively high reproducibility; although it may not be feasible for all experimental model systems. Overall, stable isotope labeling strategies enable higher precision for low abundance proteins, allowing even small changes in relative protein abundance to be detected.

As the name implies, label-free analysis is performed without the introduction of isotope label during sample preparation (Figure 1.5-1D, E), and therefore relies on mass spectrometric spectral data as an index of protein abundance. Although easier to implement and less costly than stable isotope labeling experiments, label-free analysis has reduced precision and often smaller dynamic range (Old et al. 2005). For this reason, most label-free methods are considered semi-quantitative. There are two main approaches for conducting label-free semi-quantitative analysis. The first method (Figure 1.5-1E) relies on the detection of spectral features in the precursor (MS^1) spectra. These spectral features are extracted by comparing mass (MS^1) spectra collected as a function of time across different biological samples. If inter-sample variability is high due to extensive sample preparation, then many technical (5 – 10) replicates per biological condition are

26

often required. This method of feature detection is also computationally intensive, requiring isotopic envelope modeling and retention time correction.

An alternative label-free approach is spectral counting (Figure 1.5-1D). This method uses the total number of MS/MS spectra assigned to a particular protein as the basis for calculating relative protein abundance. Early work using spectral counting analysis demonstrated that in complex protein mixtures spectral counts correlated linearly with protein abundance for two orders of magnitude (Liu, Sadygov & Yates 2004). Further work has extended this range using corrective factors, such as total number of MS/MS spectra collected, protein molecular weight, and propensity to generate ionizable peptides (Old et al. 2005, Zybailov, Florens & Washburn 2007, Lu et al. 2007). Label-free analyses benefit from direct incorporation into most standard proteomic workflows.

Isotope-labeling Strategies

A
Control Experimental

B
Control Experimental

C
Control Experimental

Label-free Strategies

Control Experimental

Harvest Proteins

Harvest Proteins

Harvest Proteins

Harvest Proteins

+Protein Labeling

Mix

Mix

Protein digestion

+Peptide Labeling

Protein digestion

Protein digestion

Protein digestion

Mix

LC-MS/MS analysis

E

Control Peak Areas

MS¹ feature extraction

Experimental Peak Areas

LC-MS/MS analysis

LC-MS/MS analysis

LC-MS/MS analysis

D

Peptide assignments

Control Spectral Counts

Experimental Spectral Counts

Peptide assignments

Peptide assignments

Peptide assignments

Computational Software

Computational Software

Computational Software

Figure 1.5-1. General workflows of quantitative mass spectrometric strategies. Strategies for performing quantitative analysis using mass spectrometry can be divided into isotope-labeling and label-free categories. The diagram illustrates these strategies applied to a cell culture model where comparison of relative protein expression between control and experimental groups is desired. For labeling approaches, the experimental sample has been illustrated to contain the stable isotope, but in practice the reverse can be performed as well. For label-free analyses, the two samples are analyzed in parallel with no mixing. (A) Stable isotope labeling by amino acids in cell culture (SILAC) incorporates isotope-coded amino acids, such as $^{13}C_6$-lysine, for several cell divisions before the experiment is performed. (B) Post-harvest labeling of protein extracts. Often performed using amino group-reactive compounds that have been synthesized with either ^{13}C or ^2H, such as d4-N-nicotinoyloxy-succinimide. The corresponding control protein extract would be labeled with light compound. (C) Peptide labeling is performed either during protein digestion or post-digestion. Enzymatic digestion of proteins in O_{18} water incorporates a single heavy oxygen atom into the carboxyl group of the C-terminal amino acid. Post-digestion labeling of peptides can be performed, often using commercially available reagents: isotope-coded affinity tags (ICAT) (Gygi et al. 1999) or amine-reactive stable isotope peptide labeling (iTRAQ), that contain ^{12}C or ^{13}C reagents for light and heavy labeling, respectively. (D) Spectral counting analysis can be performed with most traditional LC-MS/MS workflows. Total spectra are calculated for proteins within each sample independently. After normalization, spectral counts for the same protein can be compared between the samples to determine relative abundance. (E) Raw spectral (MS¹) data is compared over multiple (3 or more) LC-MS/MS technical replicates to identify common spectral features. Each feature is associated with either a peak height or area. Common spectral features between biological groups are then compared in terms of relative peak height or area. Significant features are then analyzed by database search algorithms to determine peptide and protein identity.

1.5.1 Spectral counting analysis for the quantification of relative protein abundance.

Since the initial development of spectral counting for data-dependent MS acquisition methods (Liu, Sadygov & Yates 2004), several studies have been performed to further define the technique's limit of detection, as well as improve linear range and accuracy in calculating relative protein abundance. In a study performed by Old et al (Old et al. 2005), the highest reproducibility was attained when the protein was identified with at least 4 spectra, as assessed by technical replicates within 95% confidence limits. They also noted the tendency for spectral counts to exhibit non-linearity above 30; however, this was likely due to specific instrument data acquisition parameters and limited chromatographic separations that reduced sampling depth.

An important advancement in spectral counting analysis was the creation of a spectral abundance factor (SAF), which corrected a protein's spectral counts by its length (Zybailov, Florens & Washburn 2007, Rappsilber et al. 2002). This reflects the concept that larger proteins have the potential to generate more spectra. Additionally, each SAF is normalized to the sum of all SAFs calculated from a single experiment. This normalized spectral abundance factor (NSAF) accounts for differences in depth of analysis between different experiments. NASF values can also be averaged allowing statistical significance to be assessed. Using this approach, Zybailov and colleague (Zybailov, Florens & Washburn 2007)) demonstrated that changes in relative protein abundance as small as 1.4-fold and across approximately 3 orders of magnitude could be detected for membrane proteins of yeast grown in minimal media versus rich media.

Undoubtedly, correction of spectral counts by protein length resulted in improved power of analysis, yet work from the Aebersold lab and others (Craig, Cortens & Beavis 2005, Mallick et al. 2007, Kuster et al. 2005) suggested that a protein's length may not always be a determinant for its ability to "produce" spectral counts. Specifically, proteotypic peptides, defined as peptides most readily detected during a mass spectrometric analysis, were observed, suggesting that the inherent physicochemical properties of peptides may be an even better measure to correct raw spectral counts. Comparing experimentally-derived proteotypic peptides between different experimental designs, biological samples, and proteins, an algorithm was developed that used 36 physicochemical peptide properties to predict the proteotypic nature of a peptide; its likelihood to be observed in an experiment (Mallick et al. 2007).

Using this strategy for proteotypic peptide prediction, a novel correction for spectral counts was developed which incorporated an individual protein's propensity to "generate" observable peptides (Lu et al. 2007). This factor, termed an observability index (O_i) value, was determined empirically and extended the dynamic range of spectral counting to four orders of magnitude, supported by comparison of protein abundance measured workflow to protein concentration determined by Western and flow cytometry analysis of GFP-tagged fusion proteins in yeast. Due to improvements in reproducibility of the method as well as depth of analysis afforded by multidimensional chromatography, this algorithm, called APEX, provided a measure of absolute protein abundance (Lu et al. 2007).

In summary, semi-quantitative mass spectrometric analysis by spectral counting provides a rapid, cost-effective strategy to measure protein abundances from complex

biological samples. Strategies that correct raw spectral counts by sampling depth achieve the best accuracy and linear range (Zybailov, Florens & Washburn 2007, Lu et al. 2007). The benefits of multidimensional chromatography for increased sample depth have been well-established (Tang et al. 2005, Washburn, Wolters & Yates 2001), but include the drawbacks of increased time and cost of analysis, and potentially additional sample losses. Currently, a greater proportion of proteomic studies are performing single, comprehensive proteome analysis, which has created new challenges for the determination of statistical significance between multiple biological samples when only a single replicate is available (Choi, Fermin & Nesvizhskii 2008, Carvalho et al. 2008).

1.5.2 Stable isotope labeling by amino acids in cell culture

Currently, stable isotope labeling by amino acids in cell culture (SILAC) can be implemented without issue in many different cell lines (refs). Initial development of this approach demonstrated that culturing NIH 3T3 fibroblasts for five population doublings in media depleted of natural abundance leucine and replaced with deuterium-labeled leucine (d_3-leucine) resulted in at least 97% incorporation of stable isotope label for most proteins (Ong et al. 2002). These conditions had no measureable effect on cell viability or proliferation rate. The authors selected d_3-leucine as it is the most frequently occurring amino acid; about half of the tryptic peptides detected were leucine-containing. Also, it enables the distinction between leucine and isoleucine and at the time was the most commercially accessible isotope-labeled amino acid.

Subsequent work by the Mann group and others (Ong, Kratchmarova & Mann 2003) has shown the benefit of using different combinations of amino acids with alternate

isotopic labels. Notably, carbon-13 and nitrogen-15-labeled amino acids, available in leucine, lysine, and arginine, are currently the preferred SILAC reagents for several reasons. First, the C_{18} reverse-phase separation of protium (^1H) versus deuterium (^2H)-labeled peptides is not identical, resulting in shorter retention times for deuterium-labeled peptides (Ong et al. 2002). Peptides with carbon or nitrogen isotopes do not show these isotope effects. Second, enrichment of 13-carbon-lysine and arginine generates a mass difference between the unlabeled and labeled amino acid of 6 mass units (daltons), which often prevents the occurrence of overlapping isotope envelopes between the unlabeled and labeled peptides. The lack of spectral overlap simplifies the calculation of abundance ratios between SILAC peptide pairs (Ong, Kratchmarova & Mann 2003).

The decreasing cost of these reagents has allowed multiple isotopic amino acids to be utilized in a single experiment. In particular, the simultaneous use of isotopic arginine and lysine offers the potential to quantify all fully tryptic peptides. However, several studies have confirmed that some cells such as HeLa, HEK293, and embryonic stem cells have significant metabolic conversion of arginine to proline under traditional culture conditions where arginine is present in excess (Ong, Kratchmarova & Mann 2003). It is possible to reduce this conversion through arginine starvation (Ong, Mann 2006), proline supplementation (Bendall et al. 2008), or by computational approaches that account for isotopic proline-containing peptides (Park et al. 2008b, Park et al. 2009). Alternatively, utilizing isotope-labeled leucine in place of arginine obviates these workarounds while importantly maintaining a high occurrence of isotope-containing peptides available for quantification (Yocum et al. 2006).

Over 10,000 unique peptides are often identified in large-scale proteomic analyses. Therefore, a vital element of the SILAC workflow is automated extraction and quantification of SILAC peptide ratios. In addition, evaluation of the accuracy of SILAC peptide ratios and selection of appropriate filters to retain high quality (high signal-to-noise) SILAC pairs is critical. Recently, two open source software tools, Census (Park et al. 2008a) and MaxQuant (Cox, Mann 2008), have been written to perform these functions using sequence-to-spectrum assignments generated by the SEQUEST and Mascot database search algorithms, respectively. As SEQUEST was used to generate all sequence-to-spectrum assignments, the functionality of Census is discussed.

Census is a robust quantitative software tool that supports many labeling strategies (isotope and label-free) implemented at the level of single-stage (MS^1) or tandem (MS^2) mass spectrometry, using either low- or high-resolution instrumentation (Park et al. 2008a). To provide robust quantification accuracy over a broad dynamic range, Census uses multiple algorithms, including weighted peptide measurements, dynamic peak finding and post-analysis statistical filters. For isotope labeling experiments, raw MS^1 spectra and unique sequence-to-spectrum assignments are used as input, as well as the specific isotope-labeled amino acids used in the experiment. From these data, Census computes the extracted ion chromatograms (XIC) for light (natural abundance) and heavy (labeled) peptide pairs, also called isopeptides. For high-resolution instruments, these XICs are constructed from each calculated isotope within the distribution using a narrow mass tolerance, usually 30ppm (Figure 1.5.2-1). This method increases signal-to-noise as a result of eliminating signal from nearly isobaric, co-eluting peptides.

Yet, for complex samples, signal from interfering species cannot be completely eliminated. For these cases, Census relies on a correlation factor (R^2) calculated for each pair of XICs. If XICs are accurate, that is each isopeptide chromatogram is composed of one ion, then the correlation between the two extracted ion chromatograms is usually high (Figure 1.5.2-1A). In some cases, interfering signals differ by less than the specified mass tolerance. This occurrence is especially problematic for lower signal to noise XICs. However, since most of these signals are not entirely coincident in time with the identified peptide, the correlation coefficient between the XIC pair would be low (Figure 1.5.2-1B). This correlation factor can be used to filter most incorrect SILAC peptide ratios. However, post-translational modifications occurring under one biological condition, but not the other would generate a highly correlated, but incorrect, XIC pair. In this case, the calculated XIC ratio would not be representative of the actual relative protein abundance. Therefore, Census applies statistical outlier testing to all peptide ratios belonging to the same protein group. Also, Census can detect singleton peptides, occurring when one isopeptide signal is at the detection limit, extending the dynamic range of peptide ratio calculation.

After these post-analysis filters, Census computes the intensity-weighted average of peptide ratios belonging the same protein. Census can perform extracted ion chromatograms and ratio calculation for thousands of proteins in several hours on a modern, dual-core Pentium 4 processor.
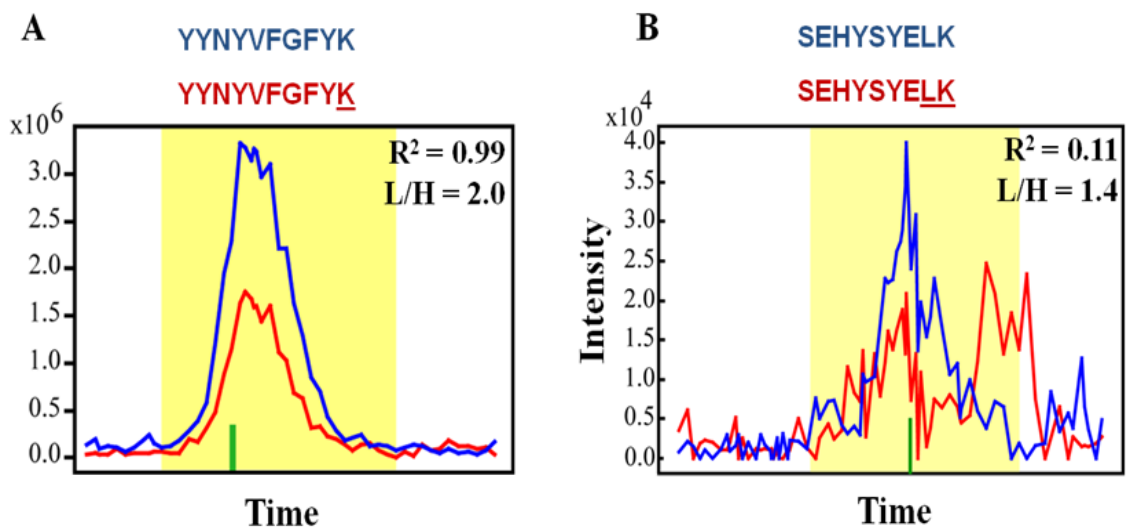
Figure 1.5.2-1. Automatic evaluation of extracted ion chromatograms by Census. Extracted ion chromatograms (XICs) are constructed from raw spectral data using the calculated m/z isotope values for each light and heavy isopeptide (SILAC pair) within a mass window of 30ppm. XICs shown were generated from two different peptides identified from beta-hexoaminidase B. In both cases, the MS/MS spectrum identified the heavy isopeptide, with the software performing the calculation of the corresponding light isopeptide mass. The green bar indicates where the highest scoring MS/MS spectrum was acquired (A) XICs for the SILAC pair corresponding to the peptide sequence YYNYVFGFYK. Census calculation of the correlation coefficient between the light (*blue*) and heavy (*red*) XIC was extremely good ($R^2 = 0.99$). The corresponding light/heavy (L/H) ratio calculated from the best-fit curve was 2.0. (B) XICs for the SILAC pair corresponding to the peptide sequence SEHYSYELK. For this pair of XICs, the correlation coefficient was poor ($R^2 = 0.11$). Although the main peaks are likely composed only of the identified peptide (green bar), the relatively low signal-to-noise contributes to an overall poor correlation and therefore a less accurate L/H ratio determination. Given the correlation coefficient of 0.11, this ratio would be removed and would not contribute to the overall protein abundance ratio.

1.6 Computational tools for the analysis of cellular secretomes

In large-scale mass spectrometry-based proteomics experiments, the initial characterization of a proteome is usually performed in an unbiased manner and often serves to generate novel hypotheses. These experiments generate extensive datasets that demand the use of bioinformatics and computational tools to distill the data into manageable sets that can uncover biological relevance. For the analysis of cellular secretomes obtained by mass spectrometry-based proteomics, bioinformatic tools that predict signal peptides and subcellular localization are invaluable (Bendtsen et al. 2004b, Emanuelsson et al. 2007).

In particular, N-terminal signal peptide prediction algorithms, such as SignalP (Bendtsen et al. 2004b) and ProteinProwler (Hawkins, Boden 2006), are of great utility for predicting proteins that are classically secreted. The use of machine-learning algorithms, such as neural networks, has improved their predictive ability substantially over weight matrix approaches. For instance, SignalP 3.0 can routinely predict the presence of a signal peptide at a sensitivity of 0.99 and specificity of 0.85 (Bendtsen et al. 2004b). This algorithm is publicly available for use at the Center for Biological Sequence Analysis (http://www.cbs.dtu.dk/services/).

The presence of a signal peptide only assures that the protein enters the secretory pathway via the classical mechanism, but does not guarantee a protein is secreted, as N-terminal signal peptides can direct proteins to membrane compartments other than the ER, such as mitochondria or lysosomes. Therefore, protein sequences predicted to have a signal peptide by SignalP should be analyzed by TargetP (Emanuelsson et al. 2000) to predict subcellular localization. Alternatively, for proteins that may be secreted by means

other than the classical pathway (Chapter 1, Section 2), the SecretomeP algorithm can be used to predict non-conventional or leaderless secretion (Bendtsen et al. 2004a). This algorithm utilizes protein features not contained within the protein N-terminus as predictive metrics, such as number of atoms, positively charged residues and propetide cleavage site. Utilizing the six features with highest discriminatory capacity, SecretomeP was able to perform at a sensitivity of 0.40 with less than 5% false positive rate. Reduced sensitivity could be attributed to the relatively small number of known nonconventionally secreted proteins available for the training dataset. Notwithstanding, this algorithm provides a useful tool to evaluate cellular secretomes and generate testable hypotheses regarding non-conventionally secreted proteins.

As an adjunct to bioinformatic algorithms, gene ontology and functional analysis tools, such as FatiGO (Al-Shahrour, Diaz-Uriarte & Dopazo 2004) and Ingenuity Pathways analysis, which were originally developed for genome-wide datasets, are now commonly utilized for proteomic datasets. These tools enable rapid classification of proteins by annotated gene ontology and functional groups and provide methods for determining enrichment of functional groups relative to the whole genome. Statistical comparisons of proteomic datasets are routinely performed by approaches similar to gene array analyses, determining statistical significance by t-tests followed by p-value correction for multiple comparisons using the Benjamini and Hochberg method. While comparison to a specific tissue/cell proteome of interest would be ideal, these proteome-centric datasets are rather incomplete.

Evaluation of cellular secretomes by bioinformatics approaches assists with functional comparison of secretomes from multiple biological states. Also, it may

identify extracellular proteins that were predicted as false negatives by signal peptide prediction. Moreover, functional pathway tools, such as Ingenuity, incorporate relative expression/abundance measurements obtained by quantitative analysis, providing a way to identify molecular signaling pathways that may be perturbed between biological conditions (Liu et al. 2008).

1.7 Nitric oxide signaling as a modulator of protein function

Nitric oxide (NO$^{\bullet}$), a gaseous, free radical, serves as an important cellular signaling molecule (refs). The production of nitric oxide is tightly regulated by nitric oxide synthase (NOS) enzymes (Moncada, Higgs 1993), which catalyze the five-electron oxidation of the guanidino group of L-arginine (Figure 1.7-1). Nitric oxide was first identified as one of the endogenous sources of endothelium-derived relaxing factor (EDRF) released from vascular endothelium, which then diffuses to smooth muscle, activates soluble guanylate cyclase (sGC) and initiates the downstream signaling that results in smooth muscle relaxation (Ignarro et al. 1986, Furchgott, Zawadzki 1980, Katsuki et al. 1977) . The elucidation of this signaling pathway, which was awarded the 1999 Nobel Prize in Physiology and Medicine, currently reflects approximately 80,000 publications referencing nitric oxide's involvement in diverse physiological and pathophysiological processes such as neurotransmission, immune defense, cancer, and stroke.
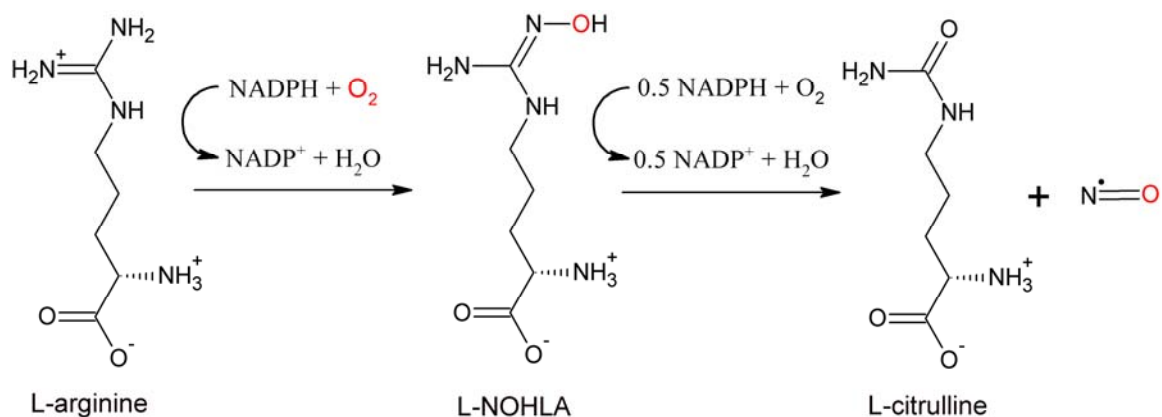
Figure 1.7.1. Reaction scheme for enzymatic production of nitric oxide. The above two-step reaction is catalyzed by a family of nitric oxide synthase enzymes (NOS I, II, and III). Overall, the reaction is a five-electron oxidation of the guanidino group of arginine, producing citrulline as a by-product and nitric oxide. The reaction consumes 1.5 mols of NADPH and 2 mols of oxygen. In addition, all NOS enzymes require cofactors: FAD, FMN, Ca^{2+}-calmodulin, heme, and tetrahydrobiopterin for full catalytic activity.

At the molecular level, nitric oxide bioactivity is conveyed through reaction with several classes of targets. Broadly, these targets can be grouped into iron-heme proteins, metalloproteins, protein and low molecular weight cysteine residues, as well as protein tyrosine residues. Nitric oxide reacts with the iron-heme moiety of soluble guanylate cyclase by forming a hexacoordinate iron-nitrosyl complex after cleavage of the axial histidine bond, which increases the enzyme activity of sGC by several hundred-fold (Stone, Marletta 1996). In contrast, reaction of nitric oxide with the metalloprotein aconitase, an Fe-S cluster protein, causes near complete enzyme inhibition, likely through the formation of a dinitrosyl iron complex (DNIC) (Duan et al. 2009).

Lastly, a major target of nitric oxide is amino acids in proteins, predominantly the side chains of cysteine and tyrosine (Hess et al. 2005, Radi 2004), though also protein amines (Hansen, Croisy & Keefer 1982). In comparison to metal centers, reaction of NO with these residues does not occur by a direct mechanism. The mechanisms of NO-

39

mediated tyrosine nitration to form 3-nitrotyrosine have been well documented (Radi 2004, Ischiropoulos et al. 1992). Formation of this post-translational modification can occur through the reaction of nitric oxide with reactive oxygen species, such as superoxide anion (O_2^-), to form peroxynitrite (Koppenol et al. 1992). Or under certain biological conditions, tyrosine nitration can be catalyzed by either superoxide dismutase (Ischiropoulos et al. 1992) or by myeloperoxidase if a source of nitrite and hydrogen peroxide (H_2O_2) is available (Sampson et al. 1998). In contrast, the intermediate reactive nitrogen/oxygen species, which may mediate S-nitrosocysteine formation, at least *in vivo*, have not been conclusively identified. Nonetheless, the existence of both low molecular weight cysteine-NO carriers, such as S-nitrosoglutathione, and protein S-nitrosocysteine residues have been clearly documented (Jaffrey, Snyder 2001, Gow et al. 2004). These issues will be discussed further in the following section.

1.7.1 S-nitrosylation as a mediator of nitric oxide bioactivity

NO-mediated formation of protein S-nitrosocysteine, termed S-nitrosylation, has received significant interest as the modification of critical protein cysteine residues has been demonstrated as a regulator of enzyme activity (Choi, Lipton 2000, Whalen et al. 2007), subcellular localization (Hara et al. 2005), and protein-protein interaction (Hara et al. 2005, Kim, Huri & Snyder 2005). These studies provided key evidence in support of the hypothesis that S-nitrosylation functions as a ubiquitous signaling system, akin to protein phosphorylation (Hess et al. 2005). Importantly, S-nitrosylation was stimulus-coupled, that is dependent upon NOS activation and NO production, and was shown to occur on a physiologically relevant timescale (Kim, Huri & Snyder 2005, Choi et al.

40

2000). Yet there are several remaining issues that deserve attention before establishing S-nitrosylation as a ubiquitous signaling event.

One issue is the lack of knowledge regarding the proximal species that mediate S-nitrosylation and denitrosylation *in vivo*. Although nitric oxide is a prerequisite for S-nitrosylation, it cannot react with reduced cysteine to form the S-nitroso species directly. Based on *in vitro* studies, several potential mechanisms have been proposed (Figure 1.7.1-1). Conceptually, the simplest reaction (Figure 1.7.1-1; Eq. 1) proposes reduced cysteine is not the primary target, but rather a thiyl radical, which reacts rapidly with nitric oxide to produce S-nitrosocysteine (Heo et al. 2005). This reaction is unlikely to participate in cell signaling, as there is little precedent for temporal and site-specific control of radical-radical recombination reactions in cell signaling. A more plausible mechanism (Figure 1.7.1-1; Eq. 2) could occur by the formation of an S-nitroso-radical intermediate, which is then immediately oxidized in the presence of an electron acceptor, such as oxygen or a transition metal (Gow, Buerk & Ischiropoulos 1997). Specificity may be achieved by the nature of the electron acceptor, for instance catalysis by a metalloprotein. Although physiologically relevant, evidence has not been advanced to define this mechanism *in vivo*.

Third, the reaction of nitric oxide with oxygen in the presence of nitric oxide, leads to the formation of dinitrogen trioxide (N_2O_3) (Figure 1.7.1-1; Eq. 3). In aqueous solution, N_2O_3 is rapidly converted to nitrous acid (HNO_2), a potent nitrosating (NO^+) agent. Chemically, nitrosonium (NO^+) equivalents are attractive mediators of S-nitrosylation *in vivo* as nitrosonium can react directly with reduced cysteine. Yet in this mechanism, the rate-limiting step in N_2O_3 formation is NO autoxidation, the reaction

between nitric oxide and oxygen, which has an overall third-order rate constant of 1.5 - 3 $\times 10^6$ M^{-2} s^{-1} (Czapski, Goldstein 1995). Given that the reaction is second-order in nitric oxide concentration and that physiological nitric oxide concentration is in the nanomolar range, NO autoxidation would proceed slowly *in vivo*. However, an alternative mechanism of nitrosonium formation may occur under conditions of low pH and excess nitrite anion (NO$_2^-$), where a sufficient concentration of nitrous acid may exist to facilitate nitrosation chemistries. Therefore, under specific conditions, nitrous acid can be a biologically relevant source of S-nitrosylation (Darwin et al. 2003).

$$R-S^\bullet + N{=}O \longrightarrow R-S-N{=}O \qquad \text{(Eq. 1)}$$

$$R-SH + N{\dot{=}}O \longrightarrow R-S-\overset{\bullet}{N}-OH + O_2 \longrightarrow R-S-N{=}O + \overset{\bullet}{O}_2 \qquad \text{(Eq. 2)}$$

$$\overset{\bullet}{N}{=}O + 1/2\,O_2 \longrightarrow N\overset{\bullet}{O}_2 + \overset{\bullet}{N}{=}O \rightleftharpoons N_2O_3 + R-SH \longrightarrow R-S-N{=}O + HNO_2 \qquad \text{(Eq. 3)}$$

$$R^1-S-N{=}O + R^2-SH \rightleftharpoons R^1-SH + R^2-S-N{=}O \qquad \text{(Eq. 4)}$$
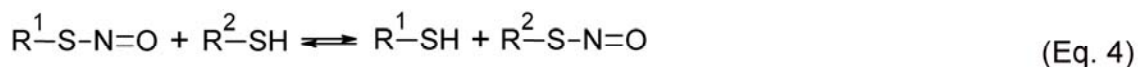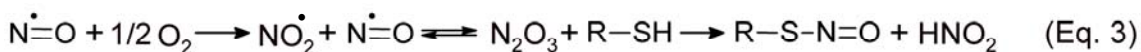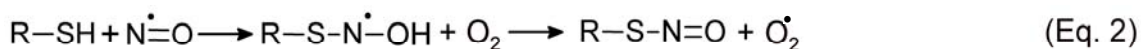
Figure 1.7.1-1. Potential mechanisms for S-nitrosocysteine formation *in vivo*. Each of the reactions has been demonstrated *in vitro*, but none has been shown *in vivo* to directly participate in S-nitrosylation. (Eq. 1) Radical-radical recombination of nitric oxide and protein thiol or cysteine thiyl radical form S-nitrosocysteine. (Eq. 2) Reaction of nitric oxide and reduced cysteine forms an S-nitroso-radical intermediate, which is oxidized by an electron acceptor, shown here as oxygen, to yield S-nitrosocysteine and superoxide. (Eq. 3) Overall third-order reaction between nitric oxide and oxygen, forming dinitrogen trioxide, a potent S-nitrosating agent that reacts with reduced cysteine to form S-nitrosocysteine and nitrous acid. (Eq. 4) A specific form of S-nitrosation, transnitrosation, which occurs by the transfer of nitrosonium from a low molecular weight or protein S-nitrosocysteine (R^1) to a reduced cysteine (R^2).

Finally, low molecular weight cysteines, such as L-cysteine and glutathione (GSH), may serve as more stable carriers of nitric oxide equivalents as well as provide

42

specificity for protein S-nitrosylation (Hess et al. 2005). The S-nitroso derivative of GSH, S-nitrosoglutathione (GSNO), is a capable S-nitrosating agent (Tannenbaum, White 2006, Padgett, Whorton 1995, Zhang, Hogg 2005). S-nitrosation occurs through a transnitrosation reaction (Figure 1.7.1-1; Eq. 4), the transfer of nitrosonium from S-nitrosocysteine to reduced cysteine on proteins or other low molecular weight cysteines. Current evidence suggests this is a plausible mechanism for S-nitrosocysteine formation *in vivo* as a physiological role for GSNO as an NO carrier has been demonstrated (de Belder et al. 1994, Radomski et al. 1992). And moreover, GSNO reductase, an enzyme that metabolizes GSNO and can indirectly regulate the steady-state levels of protein S-nitrosylation, provides strong evidence that a GSH/GSNO/protein-SNO equilibrium may regulate cellular S-nitrosylation (Liu et al. 2001). Also, protein S-nitrosocysteine residues, such as cysteine 73 of thioredoxin (Trx) can perform transnitrosation of caspase-3 (Cys163) in a site-specific fashion (Mitchell, Marletta 2005, Mitchell et al. 2007). Admittedly, this mechanism still leaves open the question of how *de novo* S-nitrosocysteine residues are formed, but given the relatively high intracellular concentration of GSH (5 mM), these conditions are favorable for overcoming kinetic barriers of S-nitrosocysteine formation through nitrosation chemistries. These hypotheses warrant further exploration into the potential *in vivo* mechanisms of GSNO-mediated S-nitrosylation.

While proteomics has been used extensively for identifying proteins and specific residues that may be S-nitrosylated (see discussion below), a complementary effort has been made to discover S-nitrosylation motifs that would predict potential cysteines susceptible to S-nitrosylation. These studies have focused on examining structural

elements in proteins that surround the modified cysteine residue. Ideally, these motifs are derived from known three-dimensional protein structures, but primary amino acidic sequences are also a viable alternative as post-translational modifications such as phosphorylation have been shown to possess consensus primary sequence motifs (Pearson, Kemp 1991).

Collectively, evidence at both primary amino acid and tertiary structure level has suggested two potential motifs (Hess et al. 2005); an acid/base motif and a hydrophobic motif. The acid/base motif was initially proposed based on data that Cys93 in the β-chain of hemoglobin can be S-nitrosylated and was flanked by acidic and basic residues (Stamler et al. 1997). This motif involves acidic (D, E) and basic (K, H, R) amino acids surrounding the modified residue in close apposition, within approximately 6 angstroms. Functionally, this structural motif would alter the nucleophilicity (pK_a) of the reduced cysteine and potentially modulate S-nitrosylation/denitrosylation. A hydrophobic motif has also been proposed based in part on the identification that a single cysteine, Cys3635, out of approximately 50 in the skeletal muscle calcium release channel (RyR1) is S-nitrosylated *in vivo* (Sun et al. 2001). This residue is localized to a hydrophobic pocket based on primary amino acid sequence hydropathy calculations. This motif could increase the rate of NO autoxidation (Figure 1.7.1-1; Eq. 3) through partitioning of NO and O_2 into the hydrophobic pocket, overcoming kinetic barriers by increasing their effective concentration (Liu et al. 1998, Moller et al. 2005). Despite these motifs, predictive algorithms have been unable to define consensus S-nitrosylation motifs. This may be due to the known datasets containing mostly *in vitro* identified S-nitrosocysteine residues or biased towards sites within peptides that are readily detected by mass

spectrometry (Hao et al. 2006a). This suggests that predictive capabilities could be improved using complementary approaches that increase depth and coverage of the S-nitrosocysteine proteome.

1.7.2 Mass spectrometry-based proteomic methods for identification of S-nitrosylated proteins

To enable *in vivo* studies, sensitive biochemical and analytical methods for detecting S-nitrosylated proteins are of critical importance. Hypothesis-generating proteomic methodologies are useful for identifying proteins that are targets of modification without *a priori* knowledge of which proteins may be modified. Additionally, tandem mass spectrometric methods can be employed to localize the sites of post-translational modification.

The first proteomic method developed for the identification of S-nitrosylated proteins was the biotin switch method (Jaffrey, Snyder 2001). Given the labile nature of some S-nitrosocysteine bonds, direct detection greatly limits sensitivity. The biotin switch method resolved this issue by replacing the cysteine-bound NO group with a cysteine-bound biotinylated linker. As shown in figure 1.7.2-1, the biotin switch is carried out by blocking reduced cysteine with methyl methane thiosulfonate (MMTS), then selectively reducing S-nitrosocysteine by ascorbate while concomitantly labeling the newly generated reduced cysteines with *N*-[6-(biotinamido)hexyl]-3′-(2′-pyridyldithio)propionamide (biotin-HPDP). Biotinylated proteins can then be resolved by SDS-PAGE for detection by anti-biotin Western blot analysis or enriched by avidin

affinity chromatography followed by mass spectrometry analysis. Using this approach, the original study identified 12 proteins endogenously S-nitrosylated in the mouse brain, which were absent from brains of nNOS$^{-/-}$ knockout mice (Jaffrey, Snyder 2001).

Many proteomic studies have used this method to identify more than 100 S-nitrosylated proteins, though usually lacking confirmation of the specific modified cysteine (Jaffrey, Snyder 2001, Kuncewicz et al. 2003, Yang, Loscalzo 2005, Zhang, Hogg 2004a). Moreover, apart from the original biotin switch work by Jaffrey and colleagues conducted in 2001 (Jaffrey, Snyder 2001), only one other publication has successfully identified endogenously S-nitrosylated proteins using a proteome-wide approach (Hao et al. 2006b).
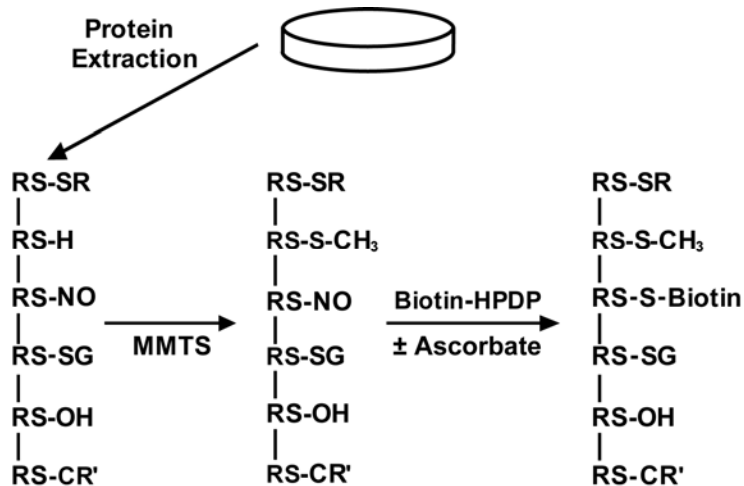
Figure 1.7.2-1. Biotin switch method diagram. Adapted from (Jaffrey, Snyder 2001). this diagram illustrates the original biotin switch methodology. Using complex protein mixtures, this method "switches" labile S-nitrosocyteine groups for more stable disulfide-linked biotinylated probes. The switch is accomplished by first blocking reduced cysteine residues with MMTS in the presence of SDS. After removal of excess MMTS, ascorbate is added to reduce S-nitrosocysteine residues and not other oxidation products of cysteine (see below), while concurrently labeling with biotin-HPDP. Omission of ascorbate would serve as a negative control accounting for artifactual biotin-HPDP labeling. Biotinylated proteins can then be enriched by streptavidin affinity capture and detected by Western blot or identified by mass spectrometric analysis. Abbreviations: RS-H, reduced cysteine; RS-SR, disulfide; RS-S-CH$_3$, S-methylthiol; RS-NO, S-nitrosocysteine; RS-S-Biotin, S-biotinylated cysteine; RS-SG, S-glutathionylated cysteine; RS-OH, sulfinic acid; RS-CR', S-alkylated cysteine.

1.8 Rationale and Objectives

1.8.1 The astrocyte secretome (Aims 1 and 2)

While significant progress has been made in understanding the functional roles of astrocyte signaling at the molecular level, the contribution of astrocyte protein secretion to paracrine and autocrine signaling in the nervous system has not been fully elucidated. For the mouse genome, at least 2000 proteins are predicted to be secreted by classical pathways (Grimmond et al. 2003), whereas the number of identified astrocyte-secreted proteins is an order of magnitude less. This suggests that improved techniques to identify additional astrocyte-secreted proteins would expedite progress in determining the roles of protein secretion in astrocyte biology and in disease. Although transcriptional profiling of neurons, astrocytes, and oligodendrocytes has provided relative expression levels for more than 20,000 genes (Cahoy et al. 2008); ultimately proteomic approaches are necessary to determine which transcripts give rise to expressed proteins and then which subset of proteins are present in the seretome.

Methodological advances in the analysis of complex proteomes and technological developments in mass spectrometry has increased depth of proteome coverage and allowed robust, proteome-wide quantitative capabilities (Tang et al. 2005, Gilchrist et al. 2006). Therefore, the overall goal of this project is to develop improved mass spectrometry-based proteomic approaches for evaluating cellular secretomes that enable (1) reproducible characterization and comparison under different cellular states, (2) secretome and proteome-wide relative quantification of protein abundance, and (3) evaluation of astrocyte protein secretion mechanisms. As outlined in figure 1.8.1, these

goals will be accomplished by using fundamental principles of protein and peptide separation, "shotgun" mass spectrometry paired with quantitative analysis, and automated computational/bioinformatics tools.

Experiments will utilize well-established procedures to isolate enriched astrocytes at greater than 95% purity from postnatal day one mouse brain cortex. The ability to characterize and compare secretomes under multiple cellular states will be established using astrocyte-conditioned media (ACM) from cells exposed to inflammatory mediators or vehicle for either an acute, 1 day exposure, or a sustained, 7 day exposure. Previous studies have documented stereotypical astrocyte responses to cytokine exposure and therefore should be an ideal model to develop comparative mass spectrometry-based proteomic methods. Current secretome analyses lack robust, proteome-wide quantitative approaches; therefore, stable isotope labeling quantitative mass spectrometry, often employed in cell lines for determining relative protein abundance, will be developed in primary astrocyte cultures. This approach will permit the relative abundance of proteins to be calculated between intracellular and extracellular compartments, providing a means to quantify secretion independent of secretion pathway, e.g. classical and non-conventional secretion. In addition, quantitative analysis will facilitate the classification of non-secreted proteins present in medium due to mechanisms independent of protein secretion. Overall, this work will provide an expanded, quantitative knowledgebase of the astrocyte secretome, identifying potentially novel astrocyte-secreted proteins that participate in intercellular signaling and/or disease pathogenesis. These potentially novel astrocyte-secreted factors can generate new, testable hypotheses concerning *in vivo* significance of astrocyte protein secretion in the nervous system.
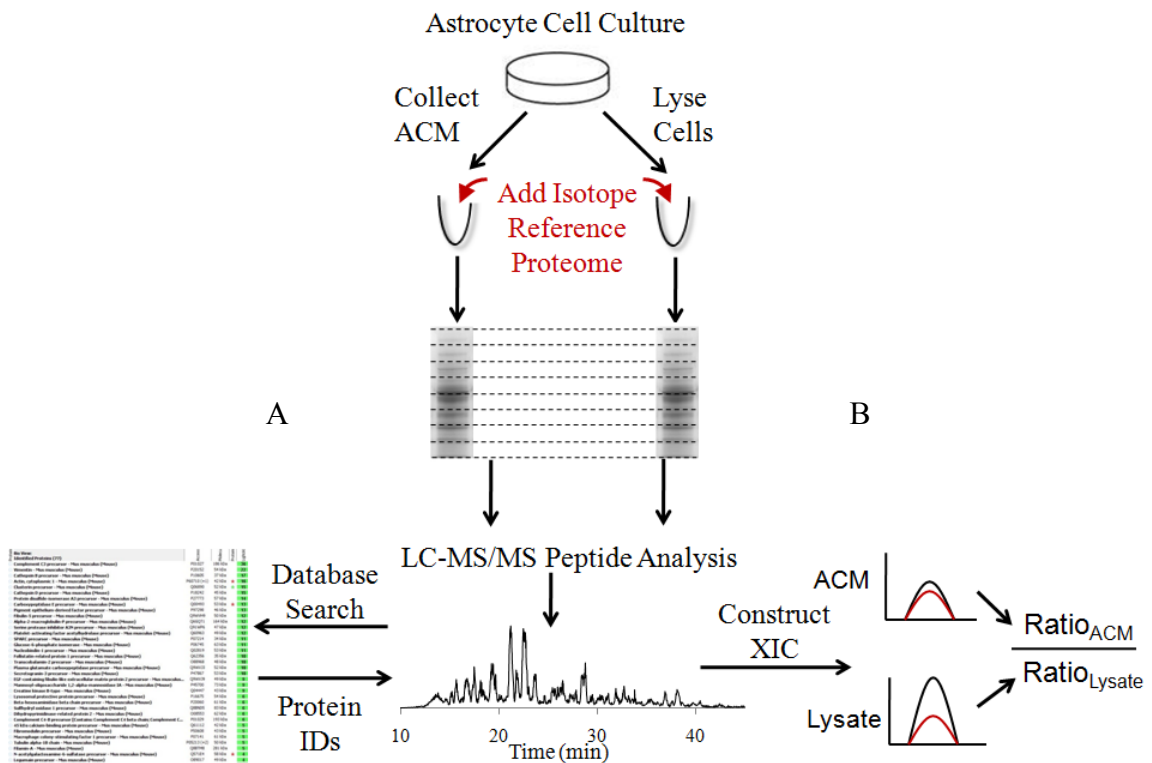
Figure 1.8.1-1. Proposed workflow for the characterization and quantification of the astrocyte secretome by mass spectrometry. Primary murine astrocytes isolated from P1 neonatal mice will be cultured to greater than 95% purity during a twelve day period, after which enriched astrocyte cultures will be placed in serum-free media. Then, the necessary cell treatments and controls will be performed while conditioning the media for between one and seven days after which media and cells are collected. For characterization of the astrocyte secretome, no isotope reference proteome will be added and only the flowchart to the left (A) will be performed. The protein fraction of the secretome will be separated by 1D SDS-PAGE, cut into equal gel slices, digested to peptides, and analyzed by reverse phase ESI-LC-MS/MS. MS/MS spectra will be subjected to protein sequence database searches, generating sequence-to-spectrum assignments that will be evaluated by probabilistic validation algorithms. Assignments meeting 1 % false positive criteria will be assembled into protein groups, requiring at least two unique peptides. For quantitative experiments, an isotope reference proteome (IRP) is spiked into samples to be analyzed. The IRP is prepared in separate experiments using SILAC. The mixed samples are then analyzed as above, but with addition of Census quantitative analysis by XIC (B).

50

1.8.2 The S-nitrosocysteine proteome (Aim 3)

The formation of S-nitrosocysteine residues in proteins, termed S-nitrosylation, is an NO-mediated post-translational modification that can alter protein function, subcellular localization, and protein-protein interactions (Hara et al. 2005, Kim, Huri & Snyder 2005, Choi et al. 2000). Although over 100 proteins have been identified, largely by *in vitro* global proteomic methods, the most widely used method (Jaffrey, Snyder 2001) does not provide the modified cysteine residue. This precludes the structural basis for S-nitrosylation selectivity from being investigated and requires additional validation experiments, such as mutagenesis. In addition, the low abundance of endogenous S-nitrosylated proteins creates enormous challenges for *in vivo* detection. Since the biotin switch method was published (see Chapter 1, section 7) it has mainly been used to identify endogenous S-nitrosylated proteins through coupling to Western blot detection. Identification of endogenous S-nitrosylated proteins on a proteome-wide scale with mass spectrometry-based detection has been largely unsuccessful, suggesting improvements in sensitivity are necessary.

Based on previous work investigating the selectivity of cysteine modification by reactive electrophiles (Dennehy et al. 2006), this project will incorporate two additional steps into the biotin switch method following biotin-HPDP labeling (Figure 1.8.2-1) These steps generate biotinylated peptides by trypsin digestion, which are then subjected to avidin affinity enrichment of peptides, as opposed to proteins. A revised biotin switch method incorporating peptide affinity capture will afford greater sensitivity through a reducing in sample complexity and provide both identification of the S-nitrosylated protein and the site of modification in a single experiment.

51
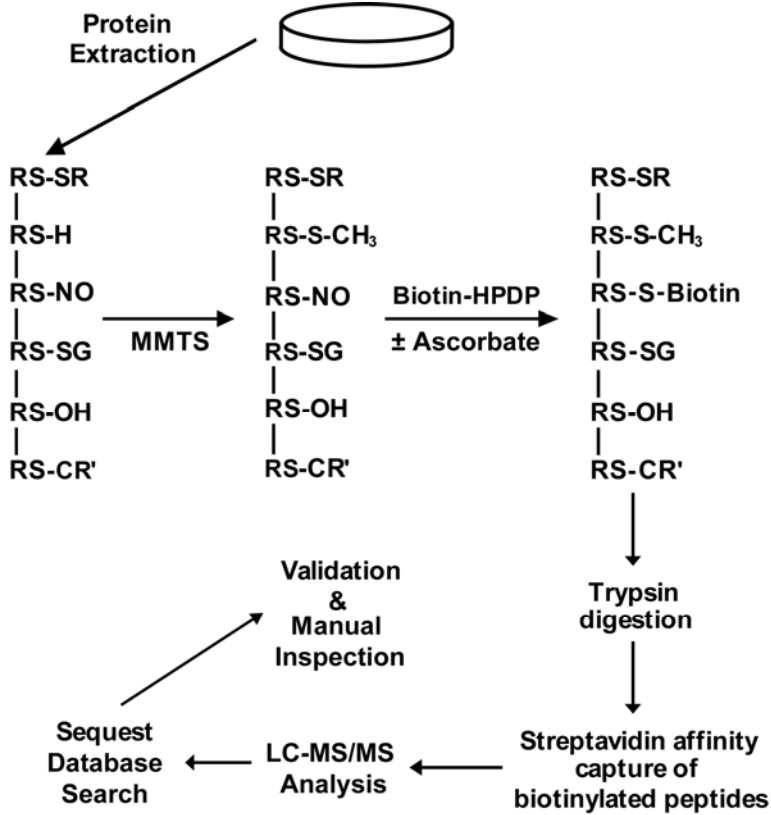
Figure 1.8.2-1. Modification of biotin switch method for site-specific identification of S-nitrosocysteine. Adapted from Jaffrey et. al. (Jaffrey et al. 2001), this diagram illustrates a modified biotin switch methodology (see Figure 1.7.2-1). As previously, the biotin switch is performed whereby labile S-nitrosocysteine groups in complex protein mixtures are exchanged for more stable disulfide-linked biotinylated probes. First, blocking of reduced cysteine residues is performed with MMTS in the presence of SDS. After removal of excess MMTS, ascorbate is added to reduce S-nitrosocysteine residues and not other oxidation products of cysteine (see below), while concurrently labeling with biotin-HPDP. Omission of ascorbate would serve as a negative control accounting for artifactual biotin-HPDP labeling. After biotin-HPDP labeling, rather than performing streptavidin affinity capture, biotinylated proteins are digested with trypsin. Then, the mixture of biotinylated and non-biotinylated peptides is enriched by streptavidin affinity capture. The bound fraction of peptides is then analyzed by LC-MS/MS. The resulting MS/MS spectra are analyzed by database search algorithms and manually reviewed to confirm both the residue of modification and the protein. Abbreviations: RS-H, reduced cysteine; RS-SR, disulfide; RS-S-CH$_3$, S-methylthiol; RS-NO, S-nitrosocysteine; RS-S-Biotin, S-biotinylated cysteine; RS-SG, S-glutathionylated cysteine; RS-OH, sulfinic acid; RS-CR', S-alkylated cysteine; LC-MS/MS, liquid chromatography-tandem mass spectrometry.

1.9 Specific Aims

Aim 1: Utilize mass spectrometry-based proteomic methods to characterize the effects of acute and sustained cytokine exposure on astrocyte protein secretion.

Hypothesis for Aim 1: Development of a sensitive and reproducible proteomic method will expand the current catalogue of known astrocyte-secreted proteins and identify time-dependent, cytokine-induced secreted proteins from primary mouse astrocyte cells.

Previous studies have begun to characterize the astrocyte secretome by proteomic approaches, resulting in the identification of about 30 proteins. Based on computational predictions, a secretome could contain thousands of proteins (Grimmond et al. 2003), suggesting a more rigorous proteomic approach is necessary to improve detection of lower abundance proteins. In addition, comparative proteomic analyses are critical for identification of differentially secreted proteins across multiple biological conditions. Towards these goals, fundamental principles in chromatographic separation and the latest mass spectrometric instrumentation will be utilized to compare and contrast the astrocyte secretome under control and cytokine-exposed conditions with greatly improved depth of analysis and reproducibility.

Aim 2: Develop quantitative mass spectrometry-based proteomic methods to distinguish between (1) secreted and non-secreted/intracellular proteins and (2) classically and non-conventionally secreted proteins in astrocyte-conditioned media.

Hypothesis for Aim 2: Quantitative mass spectrometric analysis of protein abundance in astrocyte conditioned media, normalized to intracellular protein abundance, will show high abundance ratios for secreted proteins, while abundance ratios from non-secreted protein, intracellular proteins will be less than unity. Of

the proteins determined to be secreted by quantitative MS analysis, 10 to 20 percent may lack an N-terminal signal peptide.

Quantitative mass spectrometry-based proteomics employing stable isotope labeling by amino acids in cell culture (SILAC) has become an important technique to assess differential intracellular protein expression (Ong et al. 2002). Though SILAC has been demonstrated in primary neuron cultures (Spellman et al. 2008), its feasibility has not been directly assessed in primary astrocyte cultures. In addition, SILAC has not been demonstrated for differential analysis of cellular secretomes. Therefore, incorporation of isotope-labeled amino acids into the astrocyte proteome and secretome will be evaluated. Using the proteomic techniques developed in aim 1 and high-resolution mass spectrometry, isotope-labeled astrocyte proteomes will be used as internal standards to quantify secreted protein abundance, relative to the corresponding abundance of intracellular protein expression. As a result, the classification of secreted versus non-secreted proteins will be made primarily by quantitative mass spectrometry analysis. The subset of proteins that are identified as secreted by quantitative MS analysis will be analyzed by N-terminal signal peptide prediction algorithms. Those proteins lacking an N-terminal signal peptide are putative non-conventionally secreted proteins.

Aim 3: Investigate protein structure motifs that govern S-nitrosylation selectivity in human vascular smooth muscle cells using affinity enrichment of S-nitrosocysteine-containing peptides paired with site-specific identification by tandem mass spectrometry.

Hypothesis for aim 3: Modification of the biotin switch method for site-specific identification of S-nitrosocysteine residues will improve assay sensitivity and permit examination of structural motifs that may govern S-nitrosylation.

The biotin switch method (Jaffrey, Snyder 2001) has provided a valuable tool for researchers investigating the effects of S-nitrosylation on cellular function, which addressed the inability to assess the S-nitrosylation status of a particular protein or an entire proteome. Application of this method revealed many proteins that were S-nitrosylated, but lacked confirmation of the specific modified cysteine residue. Identification of the modified cysteine residues is crucial to understanding the site specificity of S-nitrosylation, important both from a mechanistic as well as functional perspective. To address these issues, the biotin switch approach will be modified to allow identification of the S-nitrosylated cysteine residue as well as provide confidence in the corresponding protein identification. Based on previous work investigating cysteine reactivity towards reactive electrophiles (Dennehy et al. 2006), biotinylated (previously S-nitrosylated) proteins will be enzymatically digested to peptides, and enriched for biotinylated peptides. These biotinylated peptides will be analyzed by a linear ion trap tandem mass spectrometer to confirm the site of biotinylation, corresponding to the site of S-nitrosylation. This approach will be applied to S-nitrosocysteine- and NO donor-treated human aortic smooth muscle cells, which will augment intracellular protein S-nitrosocysteine. The identified S-nitrosylated cysteine residues will be evaluated for structural motifs that may govern S-nitrosylation selectivity.

CHAPTER 2

MASS SPECTROMETRIC AND COMPUTATIONAL ANALYSIS OF CYTOKINE-INDUCED ALTERATIONS IN THE ASTROCYTE SECRETOME

By

Todd M. Greco[1*], Sarah Dunn Keene [1*], Ioannis Parastatidis[1], Seon-Hwa Lee[2], Ethan G. Hughes[3], Rita J. Balice-Gordon[3], David W. Speicher[4] and Harry Ischiropoulos[1,2]

[1]Stokes Research Institute and Department of Pediatrics, Children's Hospital of Philadelphia, Philadelphia, PA 19104
[2]Department of Pharmacology, University of Pennsylvania School of Medicine, Philadelphia, PA 19104
[3]Department of Neuroscience, University of Pennsylvania School of Medicine, Philadelphia, PA 19104
[4]The Wistar Institute, Philadelphia, PA 19104
*These authors contributed equally to this work

Running title: Characterization of the astrocyte secretome

Address correspondence to: Harry Ischiropoulos, Stokes Research Institute, Children's Hospital of Philadelphia, 416D Abramson Research Center, 3517 Civic Center Boulevard, Philadelphia, Pennsylvania, 19104-4318, USA. Phone: (215) 590-5320; Fax: (215) 590-4267; E-mail: ischirop@mail.med.upenn.edu.

2.1 Abstract

The roles of astrocytes in the central nervous system (CNS) have been expanding beyond the long held view of providing passive, supportive functions. Recent evidence has identified roles in neuronal development, extracellular matrix maintenance, and response to inflammatory challenges. Therefore, insights into astrocyte secretion are critically important for understanding physiological responses and pathological mechanisms in CNS diseases. Primary astrocyte cultures were treated with inflammatory cytokines for either a short (1 day) or sustained (7 days) exposure. Increased interleukin-6 secretion, nitric oxide production, cyclooxygenase-2 activation, and nerve growth factor secretion confirmed the astrocytic response to cytokine treatment. Tandem mass spectrometry, computational prediction algorithms, and functional classification were used to compare the astrocyte protein secretome from control and cytokine-exposed cultures. In total, 169 secreted proteins were identified, including both classically and non-conventionally secreted proteins that comprised components of the extracellular matrix and enzymes involved in processing of glycoproteins and glycosaminoglycans. Twelve proteins were detected exclusively in the secretome from cytokine-treated astrocytes, including matrix metalloproteinase-3 and members of the chemokine ligand family. This compilation of secreted proteins provides a framework for identifying factors that influence the biochemical environment of the nervous system, regulate development, construct extracellular matrices, and coordinate the nervous system response to inflammation.

57

2.2 Introduction

Appreciation for the function of astrocytes in the central nervous system has been growing with the identification of integral roles in neurogenesis and synaptogenesis (Garcia et al. 2004, Mauch et al. 2001). Specifically, astrocytic secretion of glutamate, ATP, and D-serine serve as paracrine and autocrine factors regulating synaptic plasticity and the coordination of synaptic networks (Volterra, Meldolesi 2005, Pascual et al. 2005). Astrocytes are also important components of the blood brain barrier, providing dynamic regulation of the microvasculature through the release of nitric oxide and lipid metabolites (Mulligan, MacVicar 2004, Zonta et al. 2003), as well as modulating brain energy metabolism through the coordination of glutamate homeostasis between neurons and astrocytes (Bernardinelli, Magistretti & Chatton 2004, Escartin et al. 2006).

In contrast, the release of proteins by astrocytes under non-disease states has not been extensively explored. Proteins released by astrocytes include thrombospondin-1 and apolipoprotein E, which were found to mediate synaptogenesis and processing of amyloid-β peptides, respectively (Christopherson et al. 2005, Koistinaho et al. 2004). The advent of mass spectrometry-based proteomics has allowed for the global interrogation of astrocyte proteomes, including intracellularly expressed proteins as well as secreted proteins (Yang et al. 2005, Lafon-Cazal et al. 2003, Delcourt et al. 2005, Egnaczyk et al. 2003). However, only a limited number of proteins have been detected in the astrocyte secretome. Therefore, an expanded proteome of astrocyte-secreted proteins employing recent advances in proteomic methodology, instrumentation, and computational analyses is warranted. A more comprehensive astrocyte secretome would

provide new insights into astrocyte function and uncover novel mediators that can influence the extracellular biochemical environment in the central nervous system.

Astrocytes play a critical role in regulating the type and extent of central nervous system immune response by responding to inflammatory mediators such as IFN-γ and TNF-alpha and by producing additional cytokines and chemokines (Dong, Benveniste 2001). While an inflammatory response is necessary following tissue and cellular injury, it is also seen as a central process in the development and progression of disease states. Under certain pathological conditions, recent studies provide evidence that astrocytes secrete factors that are toxic to other cells in the central nervous system. For example, in patients with multiple sclerosis, astrocytes expressing syncytin released factors that were toxic to oligodendrocytes (Antony et al. 2004). Recently, soluble factors released from astrocytes that expressed familial amyotrophic lateral sclerosis (ALS)-causing mutant forms of superoxide dismutase 1 induced motor neuron death (Nagai et al. 2007, Cassina et al. 2005, Di Giorgio et al. 2007, Vargas et al. 2005). Collectively, these data emphasize that astrocytes under pathological conditions are capable of unleashing toxic, but in many cases unidentified factors. Insights into the factors secreted by astrocytes after treatment with inflammatory mediators may identify disease mediators and reveal targets for therapy.

2.3 Materials and Methods

Chemicals and Materials. The following primary antibodies were used to for Western blot validation experiments: anti-ApoE (1:1000, Biodesign, Saco, ME), anti-C3 complement (1:500, Cedarlane, Burlington, NC), anti-ceruloplasmin (1:500, BD Biosciences, San Jose, CA), and anti-CXCL1 (1:2500, Abcam, Cambridge, MA). 9-Oxo-10E,12Z-octadecadienoic acid (9-oxo-ODE), 13-oxo-9Z,11E-octadecadienoic acid (13-oxo-ODE), 15-oxo-5Z,8Z,11Z,13E-eicosatetraenoic acid (15-oxo-ETE), 9(R)-hydroxy-10E,12Z-octadecadienoic acid (9(R)-HODE), 9(S)-hydroxy-10E,12Z-octadecadienoic acid (9(S)-HODE), 13(R)-hydroxy-9Z,11E-octadecadienoic acid (13(R)-HODE), 13(S)-hydroxy-9Z,11E-octadecadienoic acid (13(S)-HODE), 11(R)-hydroxy-5Z,8Z,12E,14Z-eicosatetraenoic acid (11(R)-HETE), 11(S)-hydroxy-5Z,8Z,12E,14Z-eicosatetraenoic acid (11(S)-HETE), 12(R)-hydroxy-5Z,8Z,10E,14Z-eicosatetraenoic acid (12(R)-HETE), 12(S)-hydroxy-5Z,8Z,10E,14Z-eicosatetraenoic acid (12(S)-HETE), 15(R)-hydroxy-5Z,8Z,11Z,13E-eicosatetraenoic acid (15(R)-HETE), 15(S)-hydroxy-5Z,8Z,11Z,13E-eicosatetraenoic acid (15(S)-HETE), 9-oxo-11α,15S-dihydroxy-prosta-5Z,13E-dien-1-oic acid (PGE$_2$), 9-oxo-11β,15S-dihydroxy-prosta-5Z,13E-dien-1-oic acid (11β-PGE$_2$), 9-oxo-11α,15S-dihydroxy-(8β)-prosta-5Z,13E-dien-1-oic acid (8-iso-PGE$_2$), 9α,15S-dihydroxy-11-oxo-prosta-5Z,13E-dien-1-oic acid (PGD$_2$), 9α,11α,15S-trihydroxy-prosta-5Z,13E-dien-1-oic acid (PGF$_{2\alpha}$), 9α,11β,15S-trihydroxy-prosta-5Z,13E-dien-1-oic acid (11β-PGF$_2$), 9α,11α,15S-trihydroxy-(8β)-prosta-5Z,13E-dien-1-oic acid (8-iso-PGF$_{2\alpha}$), 9-oxo-11α,15S-dihydroxy-prosta-5Z,13E-dien-1-oic-3,3,4,4-^{2}H$_4$ acid ([^{2}H$_4$]-PGE$_2$), 9α,11α,15S-trihydroxy-prosta-5Z,13E-dien-1-oic-3,3,4,4-^{2}H$_4$ acid ([^{2}H$_4$]-PGF$_{2\alpha}$), [^{2}H$_4$]-

13(S)-hydroxy-9Z,11E-octadecadienoic acid ($[^2H_4]$-13(S)-HODE), and $[^2H_8]$-15(S)-hydroxy-5Z,8Z,11Z,13E-eicosatetraenoic acid ($[^2H_8]$-15(S)-HETE), and NS-398, (N-[2-cyclohexyloyl-4-nitrophenyl] methane-sulfonamide) were purchased from Cayman Chemical Co. (Ann Arbor, MI). Diisopropylethylamine (DIPE), 2,3,4,5,6-pentafluorobenzyl bromide (PFB-Br) was purchased from Sigma-Aldrich (St. Louis, MO). HPLC grade hexane, methanol and isopropanol were obtained from Fisher Scientific Co. (Fair Lawn, NJ). Gases were supplied by BOC Gases (Lebanon, NJ).

Astrocyte culture and cytokine treatment. All mouse studies were reviewed and approved by the Institutional Animal Care and Use Committee of the Stokes Research Institute, Children's Hospital of Philadelphia. Cortical astrocyte cultures were prepared from neonatal CD-1 mice (Charles River, Wilmington, MA) on DOL 1-2. Briefly, the animals were anesthetized, the brain removed and cortex dissected free. Cortices were washed twice with Earle's Balanced Salt Solution (EBSS; Invitrogen, Carlsbad, CA) and trypsinized (0.05 %) for 12 min at 37°C. Cortices were then titruated in Minimal Essential Media (Invitrogen, Carlsbad, CA) supplemented with 10% fetal bovine serum (Hyclone), sodium pyruvate (1 mM), L-glutamine (2 mM), D-glucose (42 mM), sodium bicarbonate (14 mM), penicillin (100 U/ml), streptomycin (100μg/ml), fungizone (2.5 μg/ml) and plated at one cortex per T-25 vent-cap flask (Corning, Corning, NY). Mixed cortical cultures were raised for 14 days in 37°C and 5% CO_2 with media change every 3-4 days. Cultures were then washed with cold EBSS and separated from neurons and microglia by shaking overnight at 37°C. Adherent cells were trypsinized (0.25%) and seeded in 100 mm Petri dishes (Corning) at 5 x 10^6 cells/plate (6 ml). Forty-eight hours after plating, cells were washed with EBSS, and serum-free media was added containing

IL-1β (0.2 ng/ml), IFN-γ (1 ng/ml), and TNF-α (10 ng/ml) (Roche Pharmaceuticals, Switzerland). Control astrocytes were cultured in serum-free media alone. Astrocyte-conditioned media (ACM) was either collected after 24 hours (1D ACM) or were either left untreated or treated with the cytokine cocktail (see above) every 48 hrs for an additional 6 days (3 total exposures) with no media change. ACM was again collected (7D ACM). For each collection, ACM was combined from two plates and centrifuged at 200 x g for 5 min to remove cell debris. The protein fraction (> 3 kDa) was obtained by ultrafiltration of ACM using CentriPrep Ultracel YM-3 filters (Millipore, Billerica, MA). The protein retentate (final vol. = 0.8 to1.0 ml) was aliquoted and stored at -80 °C for future use. Filtrates were reserved for lipid and small molecule analyses. To assess cell viability, astrocytes were trypsinized and combined with cell pellets obtained from the low speed centrifugation of ACM. Cell death was quantified either by flow cytometry using Vybrant Apoptosis Assay Kit #3 according to the manufacturer's instructions (Invitrogen, Carlsbad, CA) or by trypan blue exclusion. For flow cytometry, a minimum of 20,000 events was required for each analysis performed in quadruplicate.

Nitric oxide metabolite analysis. Nitric oxide-derived products (nitrate, nitrite, S-nitrosothiols, N-nitroso-, and iron nitrosyl) were quantified by chemical reduction to nitric oxide followed by ozone-based chemiluminescent detection using Nitric Oxide Analyzer 280 (Sievers, Boulder, CO). Briefly, helium gas was bubbled through an acidified (1 N) vanadium (III) chloride solution (50 mM) maintained at 90 °C in a jacketed glass purge vessel. Aliquots (20 μL) of ACM, serum-free media, or nitrite standards were injected into the glass purge vessel. Concentrations of nitric oxide

products were calculated using linear best-fit curves constructed against nitrite standards and were reported after correcting for the content of nitric oxide products quantified in serum-free media.

Immunofluorescence and cell morphology analysis. Astrocyte cultures were fixed with cold methanol for 20 min at –20 °C, followed by 50:50 methanol:acetone for 5 min at –20 °C. Immunodetection of GFAP or Cd11b were performed using a mouse anti-GFAP antibody (1:250, BD Pharmingen, San Jose, CA) or a rat anti-CD11b antibody (1:100, AbD Serotec, Raleigh, NC), respectively. Antigens were visualized with goat anti-mouse secondary antibodies conjugated to either Alexa Fluor 488 or 546 (Invitrogen, Carlsbad, CA). The nuclei were visualized by DAPI staining (1:10,000). Morphological analyses were performed by counting GFAP-positive cells with and without processes from 3-6 fields from at least 3 independent experiments.

Gel/LC-MS/MS Analysis of Conditioned Media. The protein fraction obtained from ACM was analyzed by Gel/LC-MS/MS as described previously (Tang et al. 2005). For each treatment condition described above, the concentrated protein fraction was mixed with 6X Laemmli sample buffer and equal volumes (30 µL) were loaded on NuPAGE 10% Bis-Tris gels (Invitrogen, Carlsbad, CA) and electrophoresed in MOPS running buffer for approximately 2 cm. For experiments that assessed reproducibility, ACM was collected and proteins were separated by electrophoresis from independent astrocyte cultures (biological duplicates) treated for 7D with and without cytokines. Proteins were visualized by Colloidal Blue (Invitrogen, Carlsbad, CA) and each lane was cut into uniform slices using a MEF-1.5 Gel Cutter (The Gel Company, San Francisco, CA). Gel slices were digested in-gel with trypsin as previously described (Speicher et al. 2000).

Tryptic digests were analyzed on an LTQ linear IT mass spectrometer (Thermo Electron, San Jose, CA) coupled with a NanoLC pump (Eksigent Technologies, Livermore, CA) and autosampler. Tryptic peptides were separated by RP-HPLC on a nanocapillary column, 75 µm id x 20 cm PicoFrit (New Objective, Woburn, MA, USA), packed with MAGIC C_{18} resin, 5 µm particle size (Michrom BioResources, Auburn, CA). Solvent A was 0.58% acetic acid in Milli-Q water, and solvent B was 0.58 % acetic acid in acetonitrile (ACN). Peptides were eluted into the mass spectrometer at 200 nL/min using an ACN gradient. Each RP-LC run consisted of a 10 min sample load at 1 % B; a 75 min total gradient consisting of 1–28 % B over 50 min, 28–50 % B over 14 min, 50–80 % B over 5 min, 80 % B for 5 min before returning to 1 % B in 1 min. To minimize carryover, a 36 min blank cycle was run between each sample. Hence, the total sample-to-sample cycle time was 121 min. The mass spectrometer was set to repetitively scan m/z from 375 to 1600 followed by data-dependent MS/MS scans on the ten most abundant ions with dynamic exclusion enabled.

Protein Identification and Validation. DTA files were generated from MS/MS spectra extracted from the RAW data file (intensity threshold of 5000; minimum ion count of 30) and processed by the ZSA, CorrectIon, and IonQuest algorithms of the SEQUEST Browser program. Database searching was performed by TurboSEQUEST v.27 (rev. 14) against the NCBI non-redundant protein database (4,379,558 proteins; 1/2007), which had been indexed with the following parameters: average mass range of 500-3500, length of 6-100, tryptic cleavages with 1 internal missed cleavage sites, static modification of Cys by carboxyamidomethylation (+57 amu), and variable modification of methionine (+16 amu). The DTA files were searched with a 2.5 amu peptide mass tolerance and 1.0

amu fragment ion mass tolerance. Potential sequence-to-spectrum peptide assignments generated by SEQUEST were loaded into Scaffold (version Scaffold-01_06_17, Proteome Software Inc., Portland, OR) to validate MS/MS peptide and protein identifications as well as to compare protein identifications across experimental conditions. Peptide and protein probabilities were calculated by the Peptide and Protein Prophet algorithms (Nesvizhskii et al. 2003, Keller et al. 2002b), respectively. A protein was identified if it received $\geq$ 99.0% protein confidence with $\geq$ 3 unique peptides at $\geq$ 95% confidence. A protein that received $\geq$ 99.0% protein confidence with 2 peptides at $\geq$ 50% probability was considered identified only if the same protein had been identified by the above criteria in another treatment group. If either of these criteria were not satisfied, the protein was considered to be low confidence and was scored as not detected. Proteins identifications not assigned to the *Mus musculus* taxonomy were manually inspected. These proteins were either contaminants and were removed in the final analysis, or contained identified peptides identical to the mouse sequence and therefore, based on rules of parsimony, were considered to be of mouse origin.

Computational and functional gene ontology analysis. NCBI database protein identifiers (gi) were matched to equivalent entries (accession) in the Uniprot database (www.uniprot.org), and if known, were reported as unprocessed precursors. Protein Prowler (http://pprowler.imb.uq.edu.au/) was used to identify proteins that possess a secretory pathway (SP) signal peptide (SP score > mTP/Other). Cytoscape/BiNGO was used to perform gene ontology (GO) assignments and determine significantly under- and over-represented functional GO categories. Cytoscape network visualization platform (ver 2.5; 7/23/2007; http://www.cytoscape.org/) implementing the latest release of the

65

BiNGO plugin (ver 2.0; 1/17/2007; http://www.psb.ugent.be/cbd/papers/BiNGO/) (Maere, Heymans & Kuiper 2005) was used to identify proteins that were annotated to the extracellular space (GO:5576) and cell surface (GO: 9986). Analyses were performed using the default BiNGO mouse annotation containing 19224 members (1/12/2007; ftp://ftp.ncbi.nlm.nih.gov/gene/DATA/) and either the GOSlim_GOA or GO_Full ontology (12/18/2006; http://www.geneontology.org). Statistical significance was determined by hypergeomtric analysis followed by Benjamini and Hochberg false discovery rate (FDR) correction (p < 0.001). SecretomeP 2.0 (http://www.cbs.dtu.dk/services/SecretomeP/) was used to evaluate proteins that may be non-classically secreted (p>0.5) in conjunction with prior experimental evidence. The proteins designated as secretory/extracellular were assigned to broad functional categories relevant to extracellular functions. SledgeHMMER (Chukkapalli, Guda & Subramaniam 2004) was used to perform batch searching of the Pfam database, followed by conversion of Pfam entries to their equivalent InterPro domain (release 14.1; http://www.ebi.ac.uk/interpro/).

Targeted lipid profiling of conditioned media. Astrocytes were cultured and treated for 7 days as described above. A portion of the ACM filtrate (3 ml) was transferred into a borosilicate glass tube. Tubes containing cell culture media alone (3 ml) were spiked with the following amounts of authentic lipid standards: 20, 50, 100, 200, 500, 1000, 2000 pg. A mixture of internal standards ($[^2H_8]$-5(S)-HETE, $[^2H_8]$-12(S)-HETE, $[^2H_8]$-15(S)-HETE, $[^2H_4]$-9(S)-HODE, $[^2H_4]$-13(S)-HODE, $[^2H_4]$-PGE$_2$, $[^2H_4]$-PGD$_2$, $[^2H_4]$-11β-PGF$_2$, $[^2H_4]$-PGF$_{2α}$, $[^2H_4]$-8-*iso*-PGF$_{2α}$-PFB, 1 ng each) was added to each analytical sample and standard solution. The analytical samples and standard solutions were

adjusted to pH 3 with 2.5 N hydrochloric acid. Lipids were extracted with diethyl ether (4 ml × 2) and the organic layer was then evaporated to dryness under nitrogen. The residue was dissolved in 100 μL of acetonitrile and treated with 100 μL of PFB-Br in acetonitrile (1:19, v/v) followed by 100 μL of DIPE in acetonitrile (1:9, v/v). The solution was heated at 60 °C for 60 min, allowed to cool, evaporated to dryness under nitrogen at room temperature, and re-dissolved in 100 μL of hexane/ethanol (97:3, v/v). Analysis of the PFB derivatives by normal phase chiral LC-electron capture APCI/MRM/MS analysis was conducted on a 20 μL aliquot of this solution along with PFB derivatives of 24 authentic lipids and 10 heavy isotope analog internal standards as described below.

A Waters Alliance 2690 HPLC system (Waters Corp., Milford, MA) was used for separation of lipids. For the normal phase chiral LC-APCI/MS analysis, a Chiralpak AD-H column (250 × 4.6 mm i.d., 5 μm; Chiral Technologies, Inc., West Chester, PA) was employed with a flow rate of 1.0 mL/min. Separations were performed at 30 °C using a linear gradient. Solvent A was hexane and solvent B was methanol/isopropanol (1:1, v/v). The mobile phase gradient was as follows: 2 % B at 0 min, 2 % B at 3 min, 3.6 % B at 11 min, 8 % B at 15 min, 8 % B at 27 min, 50 % B at 30 min, 50 % B at 35 min, and 2 % B at 37 min.

Liquid separation and mass spectrometric analysis of lipids. A Finnigan TSQ Quantum Ultra AM mass spectrometer (Thermo Fisher, San Jose, CA) was used for the detection of targeted lipids. The instrument was equipped with an APCI source and operated in the negative ion mode maintaining unit resolution for both parent and product ions during

MRM analyses. Operating conditions were as follows: vaporizer temperature was 450 ^{o}C, heated capillary temperature was 250 ^{o}C, with a discharge current of 30 μA applied to the corona needle. Nitrogen was used for the sheath gas, auxiliary gas and ion sweep gas set at 25, 3 and 3 (in arbitrary units), respectively. Collision-induced dissociation (CID) was performed using argon as the collision gas at 1.5 mTorr in the second (rf-only) quadrupole. An additional dc offset voltage was applied to the region of the second multipole ion guide (Q_0) at 10 V to impart enough translational kinetic energy to the ions so that solvent adduct ions dissociate to form sample ions.

Targeted chiral LC-electron capture APCI/MRM/MS analysis was conducted using PFB derivatives of 24 lipids and 10 heavy isotope analog internal standards using the following MRM transitions: 9- and 13-oxo-ODE-PFB, *m/z* 293 → 113 (collision energy, 21 eV); 15-oxo-ETE-PFB, *m/z* 317 → 273 (collision energy, 14 eV); 9(*R*)- and 9(*S*)-HODE-PFB, *m/z* 295 → 171 (collision energy, 18 eV); [^{2}H$_4$]-9(*S*)-HODE-PFB, *m/z* 299 → 172 (collision energy, 18 eV); 13(*R*)- and 13(*S*)-HODE-PFB, *m/z* 295 → 195 (collision energy, 18 eV); [^{2}H$_4$]-13(*S*)-HODE-PFB, *m/z* 299 → 198 (collision energy, 18 eV); 5(*R*)- and 5(*S*)-HETE-PFB, *m/z* 319 → 115 (collision energy, 15 eV); [^{2}H$_8$]-5(*S*)-HETE-PFB, *m/z* 327 → 116 (collision energy, 15 eV); 8(*R*)- and 8(*S*)-HETE-PFB, *m/z* 319 → 155 (collision energy, 16 eV); 11(*R*)- and 11(*S*)-HETE-PFB, *m/z* 319 → 167 (collision energy, 16 eV); 12(*R*)- and 12(*S*)-HETE-PFB, *m/z* 319 → 179 (collision energy, 14 eV); [^{2}H$_8$]-12(*S*)-HETE-PFB, *m/z* 327 → 184 (collision energy, 14 eV); 15(*R*)- and 15(*S*)-HETE-PFB, *m/z* 319 → 219 (collision energy, 13 eV); [^{2}H$_8$]-15(*S*)-HETE-PFB, *m/z* 327 → 226 (collision energy, 13 eV); PGE$_2$-PFB, PGD$_2$-PFB, 11β-

PGE$_2$-PFB, 8-*iso*-PGE$_2$-PFB, *m/z* 351 → 271 (collision energy, 18 eV); [^{2}H$_4$]-PGE$_2$-PFB, [^{2}H$_4$]-PGD$_2$-PFB, *m/z* 355 → 275 (collision energy, 18 eV); 11β-PGF$_2$-PFB, PGF$_{2\alpha}$-PFB, 8-*iso*-PGF$_{2\alpha}$-PFB, *m/z* 353 → 309 (collision energy, 18 eV); [^{2}H$_4$]-11β-PGF$_2$-PFB, [^{2}H$_4$]-PGF$_{2\alpha}$-PFB, [^{2}H$_4$]-8-*iso*-PGF$_{2\alpha}$-PFB, *m/z* 357 → 313 (collision energy, 18 eV).

Enzyme-Linked ImmunoSorbent Assay (ELISA). The levels of IL-6 were deterimined by a colorimetric ELISA kit (Pierce, Rockford, IL), and the levels of NGF were measured by Chemikine Sandwich ELISA kit (Chemicon, Billerica, MA), following the manufacturer's instructions. Serum-free media was used for dilution of the standards and unknowns.

Western blot analysis. Protein concentration was measured using the Bradford reagent (Bio-rad, Hercules, CA). ACM protein samples were boiled in Laemmli sample buffer and then separated by either 10 % 1-D SDS-PAGE or 10 % NuPAGE gels. Unless otherwise stated, Western blot detection was performed on identical biological samples and protein amounts as was performed in mass spectrometry analysis. Following electrophoresis, proteins were transferred to PVDF membranes (Millipore, Billerica, MA) and blocked in TBS containing 0.5% tween (TBS-t) and 5 % milk. Membranes were then incubated in TBS-t containing 5% milk and primary antibody (see Chemicals and Materials). Membranes were then washed in TBS-t, incubated with appropriate secondary antibodies conjugated to Alexa Fluor 680 (1:5000, Invitrogen, Carlsbad, CA) for 1 hour in TBS-t containing 1% milk, and visualized using the Odyssey Infrared Imaging system (Licor Biosciences, Lincoln, NE).

Statistical analyses. Graphs were constructed and statistical analyses were performed using GraphPad Prism 5 (GraphPad Software, Inc., San Diego, CA). Unless otherwise stated, statistical significance was performed by two-tailed unpaired t-test. For data that did not conform to Gaussian distributions, the non-parametric Mann-Whitney test was performed.

2.4 Results

Enriched neonatal cortical astrocyte cultures were prepared as described in the Materials and Methods and were treated under serum-free conditions with either vehicle (control) or TNF-alpha (10 ng/ml), interleukin (IL)-1β (0.2 ng/ml), and interferon (IFN)-γ (1 ng/ml) for either an acute (1D) or sustained (7D) exposure interval. Cell viability evaluated by flow cytometry after 1D or 7D did not significantly differ between control and cytokine-exposed cells (Figure 2-1B). Astrocyte activation by inflammatory mediators induced stereotypical morphological changes such as process formation and elongation (Figure 2-1A). These changes were quantified by counting the number of cells with processes, which revealed that 1D and 7D cytokine treatment significantly increased the percent of cells with processes compared to untreated cultures (Figure 2-2A). In addition, the percent of cells with processes was also significantly increased from 1D to 7D of cytokine treatment (Figure 2-2A).
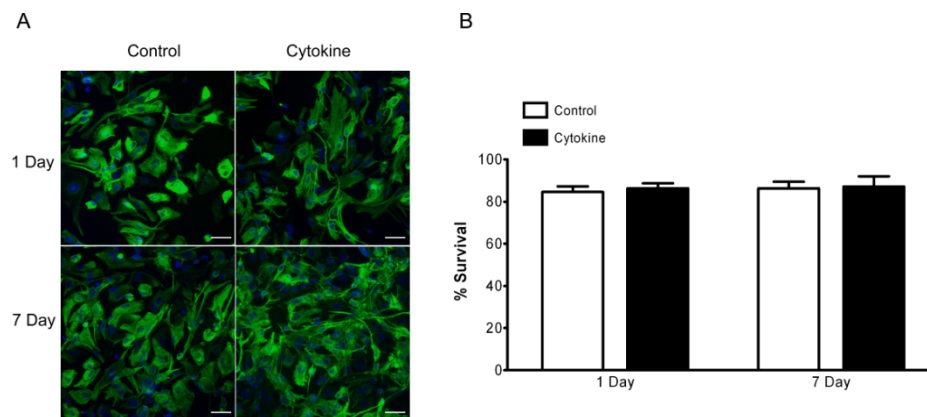
Figure 2-1. Characterization of primary murine astrocyte cell cultures. (A) Immunofluorescence staining for glial fibrillary acidic protein (GFAP, green). Nuclei were visualized with DAPI. (B) Cell viability as measured by flow cytometry (see Materials and Methods). Minimum event count 20,000 cells per condition (N = 4).
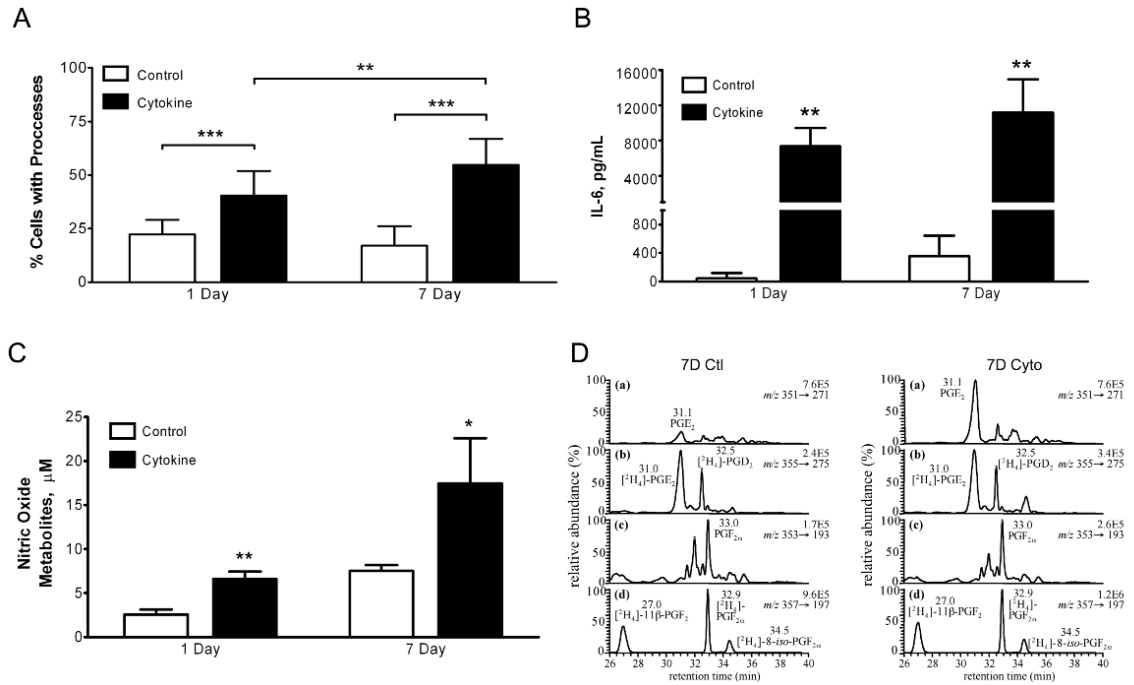
Figure 2-2. Morphological and biochemical responses of murine astrocytes to cytokine exposure. (A) Quantification of percent GFAP-positive cells with processes. The percent of cells with processes were calculated from 3-6 fields/condition taken from three independent experiments. **$p < 0.01$, ***$p < 0.001$ by unpaired, two-tailed t-test. (B) IL-6 production measured by ELISA in ACM. Data are reported as the mean ± SD. **$p < 0.01$ by unpaired, two-tailed t-test (n = 3-6). (C) Nitric oxide synthase (NOS) activity measured by nitric oxide metabolite accumulation in ACM. Metabolites were measured by reductive chemistries coupled to chemiluminescence. Data are reported as the mean ± SD. *$p < 0.05$, **$p < 0.01$ by unpaired, two-tailed t-test (n = 3-6). (D) LC-electron capture APCI/MRM/MS analysis of PGE_2 (a) and $PGF_{2\alpha}$ (c) in ACM from 7D control-treated (left) and 7D cytokine-treated (right) astrocytes. Concentrations of PGE_2 (retention time (rt) = 31.0 min) and $PGF_{2\alpha}$ (rt = 33.0 min) were calculated by interpolation of linear regression curves constructed from authentic lipid standards. Variation due to sample processing and mass spectrometry analysis was accounted for by addition of $[^2H_4]$-PGE_2 (b) and $[^2H_4]$-$PGF_{2\alpha}$ (d) internal standards.

72

Astrocytic responses to cytokine treatment were further characterized for each exposure interval by quantifying well-characterized markers of inflammation, namely IL-6, nitric oxide, and prostaglandin E_2 (PGE_2) in astrocyte-conditioned media (ACM) (See Materials and Methods). After 1D and 7D treatment with inflammatory mediators, robust production of IL-6 was detected in ACM compared to the control conditions (Figure 2-2B). The concentration of nitric oxide metabolites measured by reductive chemistries coupled to chemiluminescence detection was significantly increased in ACM compared to controls following 1D and 7D inflammatory mediator treatment (Figure 2-2C). Astrocytic responses to inflammatory mediators are also characterized by increased production of prostaglandins, such as prostaglandin E_2 (PGE_2), which is the most abundant prostanoid in the central nervous system. A lipidomic profile of 24 lipids was carried out on ACM using LC-electron capture atmospheric pressure chemical ionization/multiple reaction monitoring (APCI/MRM) MS analysis. Absolute quantification was performed against standard curves constructed using authentic lipids and normalized to deuterated lipid internal standards (Figure 2-2D). These analyses revealed a selective increase of PGE_2 (retention time (rt) = 31.0 min) after 7D cytokine treatment (0.49 ± 0.03 pmol/10^6 cells to 1.50 ± 0.12 pmol/10^6 cells; Figure 2-2D). In contrast, there was no difference in the levels of $PGF_{2\alpha}$ (rt = 33.0 min) detected in ACM from control (0.12 ± 0.01 pmol/10^6 cells) and cytokine-treated (0.13 ± 0.01 pmol/10^6 cells) astrocytes (Figure 2-2D).

While controlled inflammation is critical for innate immune defense as well as cellular remodeling and tissue repair, unregulated inflammation would clearly be detrimental. Therefore, glia, one of the primary immune cells in the central nervous

system, possesses compensatory, anti-inflammatory mechanisms to limit the scope of inflammation. In particular, trophic factors such as nerve growth factor (NGF) have been identified as initiators of signaling cascades that promote anti-inflammatory processes following pro-inflammatory events (Villoslada, Genain 2004). Consistent with this mechanism, we detected significantly elevated levels of NGF only after 7D cytokine treatment compared to 7D control (203.2 ± 158.4 pg/ml vs 964.2 ± 433.7 pg/ml; $P = 0.0025$). Collectively, morphological evaluation, flow cytometry analysis, and quantification of IL-6, nitric oxide, and lipid markers of inflammatory responses established the secretory capacity, viability and stereotypical responses to inflammatory mediators.

Extracellular and secretory proteins play a fundamental role in transforming the extracellular space and facilitating cell-cell contacts, such as during development or after synaptic remodeling following brain injury (Lukes et al. 1999). While neuron-neuron communication has been an area of intense study during synaptogenesis, the capacity of astrocytes to influence this process, specifically through secreted proteins, is not completely understood. Towards this goal, we employed a proteomic approach to identify soluble proteins secreted by murine astrocytes under control and cytokine-treated conditions. The protein fraction of ACM from control or cytokine-treated cultures was obtained by ultrafiltration and was subjected to Gel/LC-MS/MS analysis. Briefly, proteins were separated by 1D SDS-PAGE for approximately 2 cm and visualized by Colloidal blue (Figure 2-3A). Each lane was cut into 12 equal slices and digested in-gel with trypsin (Speicher et al. 2000). Tryptic digests were then analyzed by nanocapillary reverse phase liquid chromatography (LC) interfaced directly with a linear ion trap mass

spectrometer (Thermo LTQ) operated in data dependent mode (Tang et al. 2005). MS/MS sequence-to-spectrum assignments were generated using the SEQUEST algorithm searching against the NCBI nr database. SEQUEST search results from the 12 LC-MS/MS runs that comprised a complete proteome, i.e, a complete gel lane, were combined into a single biological sample within Scaffold (Proteome Software, Portland, OR). Scaffold served as a validation tool, employing the PeptideProphet and ProteinProphet algorithms, which provide statistical evaluation of the SEQUEST results by expressing potential sequence-to-spectrum assignments as confidence scores (Nesvizhskii et al. 2003, Keller et al. 2002b). A protein was identified if it received $\geq$ 99.0% protein confidence with $\geq$ 3 unique peptides at $\geq$ 95% confidence. A protein that received $\geq$ 99.0% protein confidence with 2 peptides at $\geq$ 50% probability was considered identified only if the same protein had been identified by the criteria listed above in another treatment group. If either of these criteria were not satisfied, the protein was considered to be low confidence and was scored as not detected. In total, 290 proteins were identified across all treatment groups (Table 2-1 and 2-2).

A
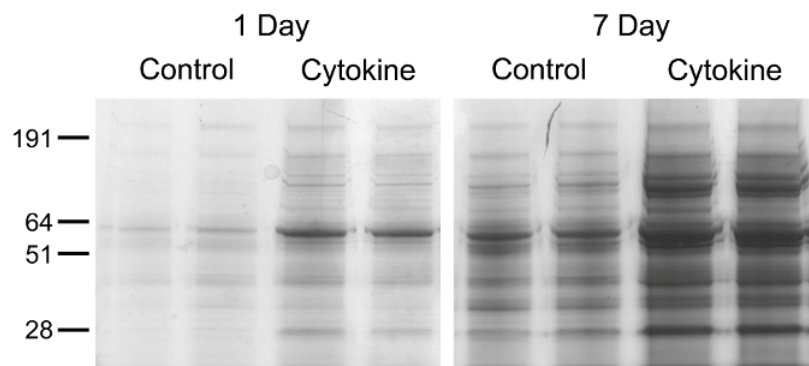
B
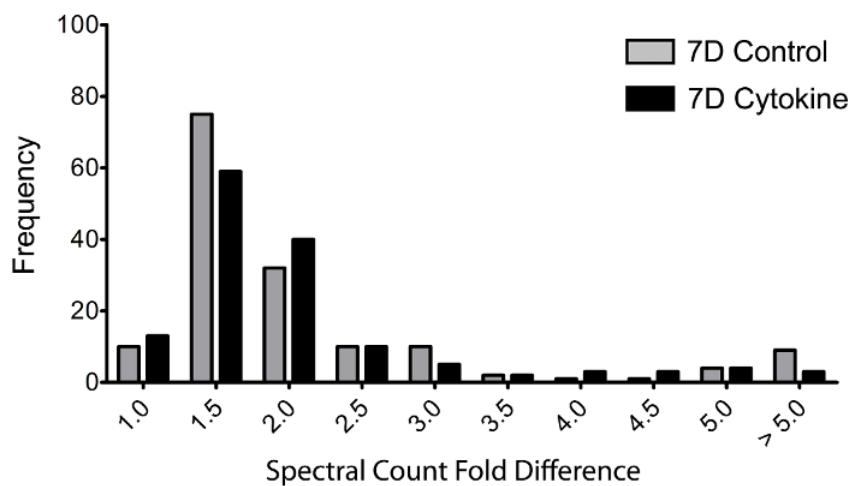
Figure 2-3. Reproducibility of Gel/LC-MS/MS. (A) ACM protein fraction from biological duplicates were resolved 1D-SDS-PAGE and visualized with Colloidal Blue. Biological duplicates show similar protein staining patterns. Increased total protein in ACM is observed after cytokine stimulation and after 7 days. (B) Frequency versus spectral count fold difference calculated for secreted proteins identified in biological duplicates from 7D control (gray bars) and 7D cytokine (black bars). Spectral counts between biological duplicates differed by less than 2.5-fold for about ninety percent of proteins.

The ability to compare and contrast protein identifications across several conditions is highly dependent upon the reproducibility of the treatment conditions and the proteomic approach. Gel/LC-MS/MS analysis of 7D ACM biological duplicates from control and cytokine-treated conditions showed 96% protein identity. As an additional measure of technical reproducibility, frequency versus fold difference in spectral counts (redundant peptides) between biological duplicates for each confirmed protein was calculated (Figure 2-3B). Both 7D control and cytokine-treated conditions showed similar reproducibility, with > 85 % of the confirmed proteins varying by ≤ 2.5 fold between biological duplicates. Importantly, slicing and analyzing the entire gel lane enabled identification of substantially more proteins than single protein band excision while not compromising depth of analysis or reproducibility as 90% of the proteins identified by a single band excision were confirmed by the Gel/LC-MS/MS method (data not shown). The high reproducibility of the experimental design and proteomic method paired with rigorous selection criteria permitted us to compare and contrast proteins identified between control and cytokine-treated conditions.

Previous studies have investigated mouse astrocyte intracellular proteomes (Yang et al. 2005, Egnaczyk et al. 2003), but only two studies have explored the secreteome, identifying a total of 40 unique proteins by 2-D SDS-PAGE and MALDI-TOF-MS (Lafon-Cazal et al. 2003, Delcourt et al. 2005). The current study found 38 of these proteins while identifying an additional 252. Since previous studies identified primarily the most abundant proteins contained within the secreteome, a rigorous analysis to distinguish between secreted/extracellular proteins and other non-secreted/intracellular proteins, which may be present due to cell death, was not necessary. In the current study,

cell death was unchanged (~15%) and cytokine-independent across all treatment conditions as quantified by flow cytometry (Figure 2-1A) and trypan blue exclusion (data not shown). Yet given the increased sensitivity of the current approach it was critical that the potential contribution of differences in depth of analysis be considered.

We addressed these potential differences in depth of analysis by evaluating the protein identifications using a multistep computational workflow. For the human proteome, cellular localization for only about 30% of all proteins has been determined experimentally (Nair, Rost 2005), making *in silico* localization prediction algorithms valuable computational tools for the analysis of secreted proteomes (Klee, Sosa 2007). Since the majority of soluble proteins destined for secretion into the extracellular space contain an N-terminal signal peptide, many computational algorithms utilize this feature for subcellular localization prediction. The use of trained neural networks and support vector machines has improved the overall performance of these algorithms. In particular, we utilized Protein Prowler (Hawkins, Boden 2006) for its excellent specificity (0.99) and sensitivity (0.91; Non-membrane) (Klee, Sosa 2007). Protein Prowler analysis predicted 149 proteins to contain an N-terminal signal peptide (Table 2-3), yet recent studies have clearly documented that not all extracellular/secreted proteins adhere to the N-terminal rule (Nickel 2005). To maximize inclusion of secreted proteins that may lack an N-terminal signal, we utilized two complementary approaches. First, gene ontology (GO) analysis was performed using Cytoscape network visualization software implementing the BiNGO plug-in. An additional 14 proteins were classified that lacked an identifiable signal peptide, but had been annotated to the extracellular region (GO:5576) or the cell surface (GO: 9986). Second, a sequence-based prediction

algorithm for non-classical secretion, SecretomeP (Bendtsen et al. 2004a), was employed in conjunction with existing experimental evidence. An additional 6 proteins that likely proceed via non-classical secretion were included as a result of this analysis, including vimentin, an intermediate filament protein secreted by activated macrophages (Mor-Vaknin et al. 2003), as well as annexin A2 (Zhao et al. 2003)and cyclophilin A (Suzuki et al. 2006).

Given that the majority of secreted proteins should become enriched in conditioned media between 1D and 7D compared to non-secreted proteins, the average fold change in relative protein abundance for proteins classified as secreted should be significantly greater than the changes in relative protein abundance of non-secreted proteins, which are largely identified due to uniform cell death (Figure 2-1A). To test this hypothesis, semi-quantitative mass spectrometry based on label-free spectral counting was employed. This method has been previously used as an effective means to estimate relative protein abundance (Liu, Sadygov & Yates 2004, Old et al. 2005, Rappsilber et al. 2002, Schmidt et al. 2007, Liu et al. 2007, Ishihama et al. 2005). While semi-quantitative MS based on spectral counting can be used to compare the relative abundance between different proteins, for example by normalizing spectral counts by either the protein molecular weight or by the number of observable tryptic peptides, our goal was to compare relative changes of the same protein across experimental conditions. Therefore, we simply compared the number of redundant peptides, i.e. spectral counts, for each protein between experimental conditions (Table 2-4 and 2-5). Supporting this hypothesis, the average, absolute fold change of protein abundance from 1D to 7D was significantly different ($P < 0.0001$) for the proteins classified in the secretome (3.9 ± 0.4,

mean ± SEM, N = 79) (Table 2-4) than for the proteins that were assigned as "non-secretory" (2.1 ± 0.1, mean ± SEM, N = 84) (Table 2-5).

While post-hoc analyses cannot achieve complete sensitivity for the classification of secretory proteins, by utilizing multiple complementary analyses, namely *in silico* cellular localization prediction algorithms, functional GO classification, and published experimental evidence, we generated a list of 169 high confidence secretory proteins, which could be assigned to seven broad functional categories (Figure 2-4A). The list included expected extracellular matrix proteins, such as laminins and collagens, proteins involved in processing and proteolysis, such as matrix metalloproteinase-3 (MMP-3) and cathepsins, as well as proteins that play critical roles in the immune response, such as the complement components and chemokine ligands. A complete list of these proteins and their corresponding numbers of unique peptides are reported in Table 2-1. InterPro domain analysis of these proteins was consistent with the InterPro domains of 2033 proteins that were computationally predicted to be soluble, secreted proteins from the mouse genome (Grimmond et al. 2003). Significantly, the EGF-like domain (IPR000561) was the most common domain in both the theoretical (Grimmond et al. 2003) and experimental mouse secretomes (Figure 2-4B). To ascertain specific molecular and biological processes that were represented among the proteins identified in the astrocyte secretome (Table 2-1), we used GO classification to assign proteins into molecular, biological, and cellular subcategories, followed by functional network analysis using hypergeometric statistics paired with multiple testing correction (p < 0.001) (see Materials and Methods). As shown in figure 2-4C, proteins with molecular functions assigned to protein binding (P = 2.6E-5) as well as enzyme regulator (P = 1.5E-7),

hydrolase (P = 4.9E-7), isomerase (P = 6.4E-7), and oxidoreductase (P = 1.8E-4) activities were over-represented. The biological process ontology contained proteins significantly over-represented in development (P = 4.1E-8) and response to stimulus (P = 2.6E-5). The proteins that remained unclassified (Table 2-2) were significantly over-represented in catabolism (P = 1.5E-26) and macromolecule metabolism (P = 3.3E-5) (data not shown), further supporting the computational and functional analysis workflow employed was largely successful in classifying extracellular and secretory proteins.
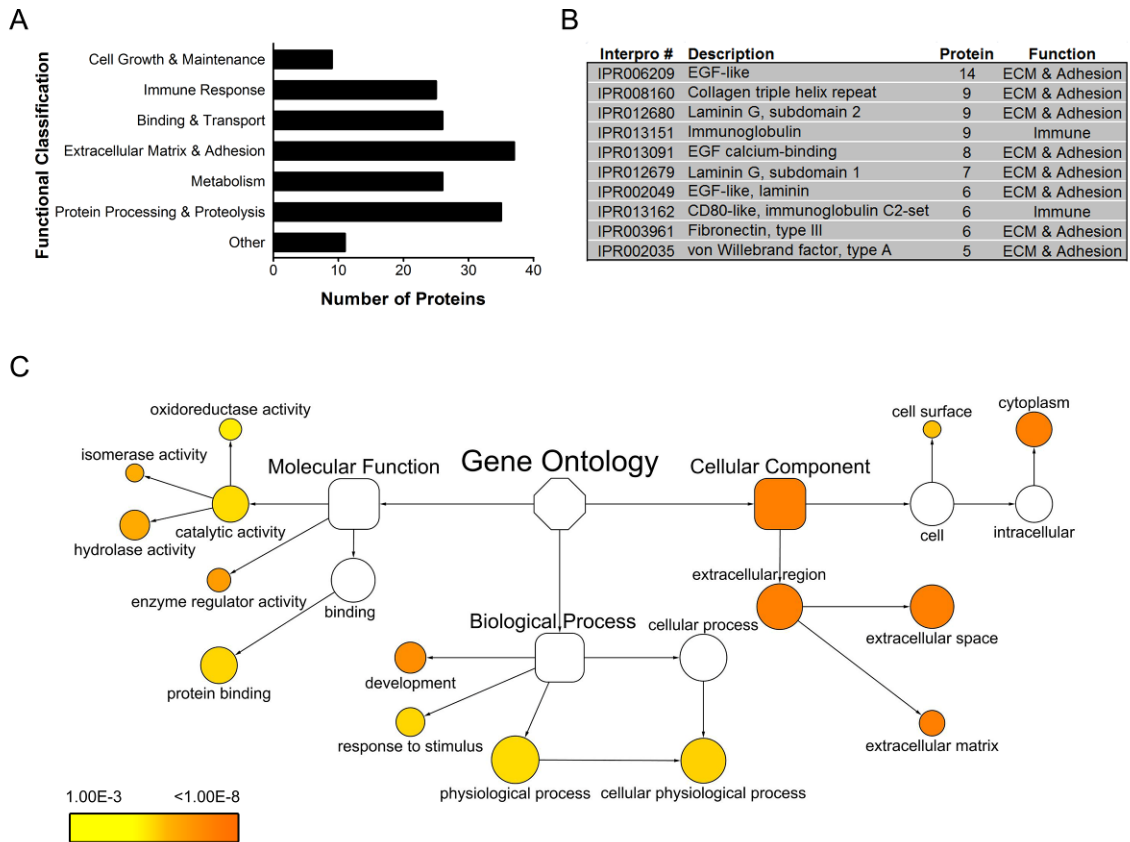
Figure 2-4. Functional gene ontology (GO) analysis of the astrocyte protein secretome. (A) Astrocyte protein secretome containing 169 proteins classified into broad functional categories. (B) InterPro domains (Top 10) represented by the astrocyte protein secretome. (C) Over-represented GO terms of the astrocyte protein secretome. Network visualization and statistical analysis was performed using BiNGO 2.0 implemented in the Cytoscape platform. Over-representation was determined for each GO term individually by comparing the proportion of genes assigned to each term from the astrocyte secretome to the proportion of genes assigned to that same term from the annotated mouse genome. Statistically significant over-representation was calculated by hypergeometric analysis and Benjamini & Hochberg false discovery rate (FDR) correction (p<0.001). Key represents range of p-values for significantly over-represented GO terms. To maintain hierarchical accuracy, parental GO terms that were not significantly over-represented are illustrated (white shapes). Relative sizes of shapes correspond to the number of members within that term.

The effects of pro-inflammatory cytokines on the astrocyte secretome (Table 2-1) were compared after 1D and 7D of conditioning. Under control conditions, 80 proteins were identified from 1D ACM, which subsequently increased to 109 upon cytokine stimulation (Figure 2-4A). In contrast, the total and unique numbers of proteins identified in 7D ACM between control and cytokine conditions were more similar (Figure 2-4B). The relative decrease in unique proteins at 7D versus 1D cytokine exposure can be partially attributed to the substantial basal protein secretion, as evidenced by the 77 proteins that were unique to 7D control versus 1D control (Figure 2-4C) and by the related increase in total secreted protein in 7D ACM as visualized by SDS-PAGE (Figure 2-3A). Importantly, this did not preclude identification of proteins which were unique to 1D or 7D conditions. Overall, 15 proteins were exclusively detected in control ACM ("c" in Table 2-1), while 12 proteins were exclusively detected in ACM only after cytokine treatment ("d" in Table 2-1). These cytokine-specific proteins included MMP-3 and four members of the chemokine ligand family, consistent with their roles in propagating immune response. Interestingly, three of the chemokine ligands, chemokine (C-C motif) ligand 7, chemokine (C-C motif) ligand 8, and chemokine (C-X3-C motif) ligand 1, were detected only after 7D cytokine treatment, while chemokine, (C-X-C motif) ligand 1 was also identified under the 1D exposure condition.
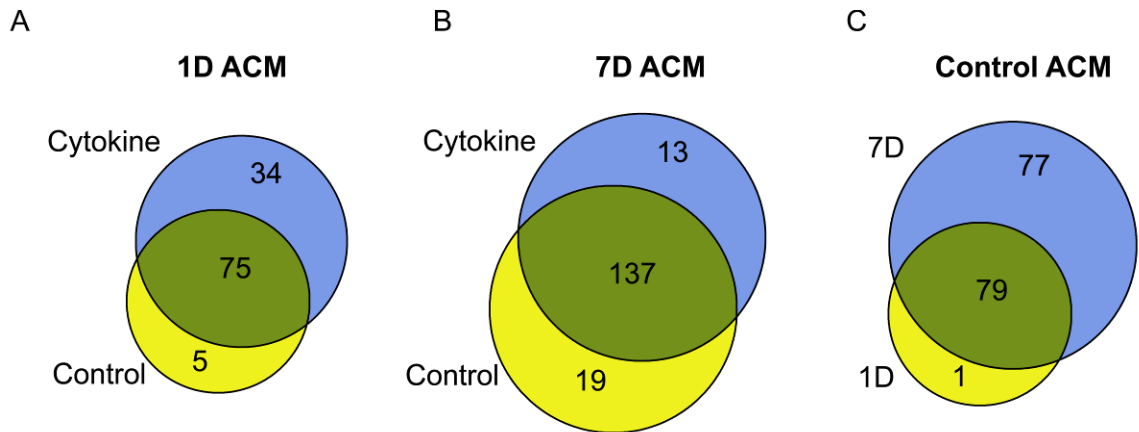
Figure 2-5. Basal and cytokine-induced protein identifications in the astrocyte protein secretome. (A) Comparison of 1D ACM between control and cytokine-treated astrocytes. (B) Comparison of 7D ACM between control and cytokine-treated astrocytes. (C) Evaluation of control ACM between 1D and 7D cultured astrocytes.
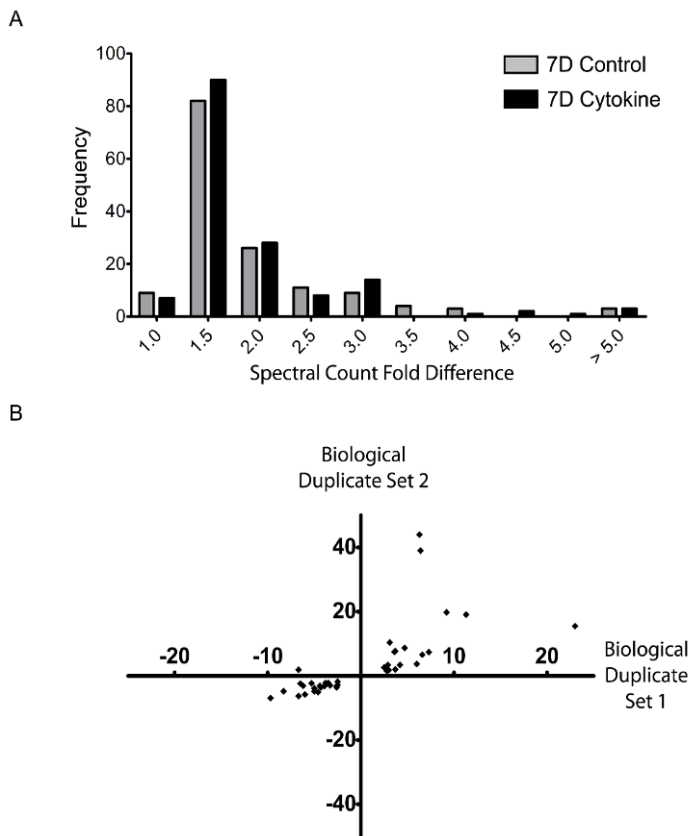
Figure 2-6. Technical and biological reproducibility of spectral counting.

(A) Histogram plotting frequency (number of proteins) versus fold difference in spectral counts between 7D control (gray bars) and 7D cytokine (black bars) biological duplicates. Data represents reproducibility of spectral count fold difference of a different set of biological duplicates (Set 2) from figure 2-3 (Set 1).(B) Scatterplot comparing fold-change in relative protein abundance (RPA) between two sets of biological duplicates from cytokine exposure. Values plotted are for proteins $\geq \pm2.5$-fold change relative to control. With one exception (quadrant I), proteins with increased (quadrant II) and decreased (quadrant IV) RPA were consistent between biological duplicates.

To reveal potential

functional alterations in the population of secretory proteins resulting from 7D cytokine, changes in relative protein abundance (RPA) were examined with respect to functional category. As previously described, spectral counting analysis can be used to calculate fold changes in relative protein abundance. The spectral count fold difference between 7D control and cytokine samples that could be considered significant was determined empirically. For this purpose, the achieved reproducibility of two sets of biological duplicates for both 7D control and 7D cytokine was examined (Figure 2-3A vs Figure 2-6). The first set, as shown in figure 2-3A, corresponds well with spectral count fold difference from independent experiments of two additional biological replicates (Figure 2-6A). Overall, technical reproducibility is demonstrated by the fact that the spectral count fold difference across both sets of biological duplicates was less than 2.5-fold for nearly 90% of proteins (Figure 2-3A and Figure 2-6A). Defining a 2.5-fold significance threshold, 7D cytokine-induced changes in RPA were consistent in magnitude between set 1 and set 2 of biological duplicates for all proteins (76) except one (Figure 2-6B). Although the absolute fold changes calculated was not always consistent between the two sets of biological duplicates, especially for positive values, this was expected as spectral counting analysis often provides a semi-quantitative measure of relative protein abundance. Importantly, these data support our selection of a 2.5-fold significance threshold for evaluating changes in RPA after cytokine exposure.

Based on these data, a protein was considered increased relative to control if it (1) was exclusively detected in 7D cytokine samples or (2) had a $\geq$ 2.5-fold increase in relative protein abundance (RPA) as assessed by the number of redundant peptides (spectral counts) (Table 2-4). A protein was considered significantly decreased relative

to control if it (1) was exclusively detected in 7D control samples or (2) had a $\geq$ 2.5-fold decrease in RPA (Table 2-4). RPA changes were calculated for the shared protein IDs between 7D control and 7D cytokine conditions (Figure 2-5B, circle overlap). Using these criteria, a total of 36 proteins (13 proteins unique to 7D cytokine ACM plus 23 proteins with increased RPA) identified after 7D cytokine treatment were considered significantly increased relative to 7D control. Of these, 28% and 33% were associated with immune response and extracellular matrix and adhesion, respectively (Figure 2-7A). In contrast, 40 proteins (19 proteins unique to 7D control ACM plus 21 proteins with decreased RPA) were considered significantly decreased after 7D cytokine stimulation. Interestingly, compared to the group of protein with increased RPA, proteins with decreased RPA comprised a smaller portion of immune response (8%) and extracellular matrix and adhesion (15 %), whereas those associated with metabolism (23%) were now the most prominent (Figure 2-7B). Notably, there were no significant decreases in RPA under control conditions from 1D to 7D suggesting that the observed decreases in RPA of metabolic enzymes after 7D cytokine treatment was due to the cytokine exposure and not to a decreased secretion over time. A similar analysis was not performed at the 1D time point, as there were too few proteins with significant decreases in RPA to perform functional comparisons.
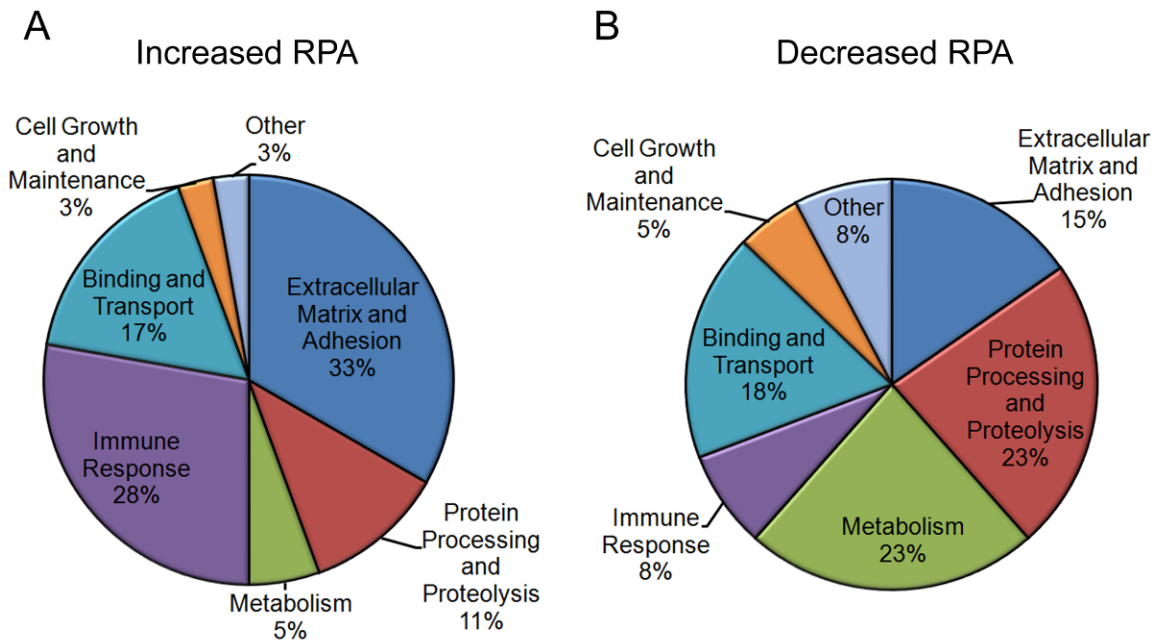
Figure 2-7. Functional comparison of proteins with relative protein abundance (RPA) changes after 7D cytokine treatment. (A) Functional classification of proteins with increased RPA. Thirty-six proteins were classified, composed of 23 proteins with ≥ 2.5-fold increase in redundant peptides and 13 proteins that were unique to 7D cytokine ACM. (B) Functional classification of proteins with decreased RPA. A total of 40 proteins were classified, composed of 21 proteins with ≥ 2.5-fold decrease in redundant peptides and 19 proteins that were unique to 7D control ACM.
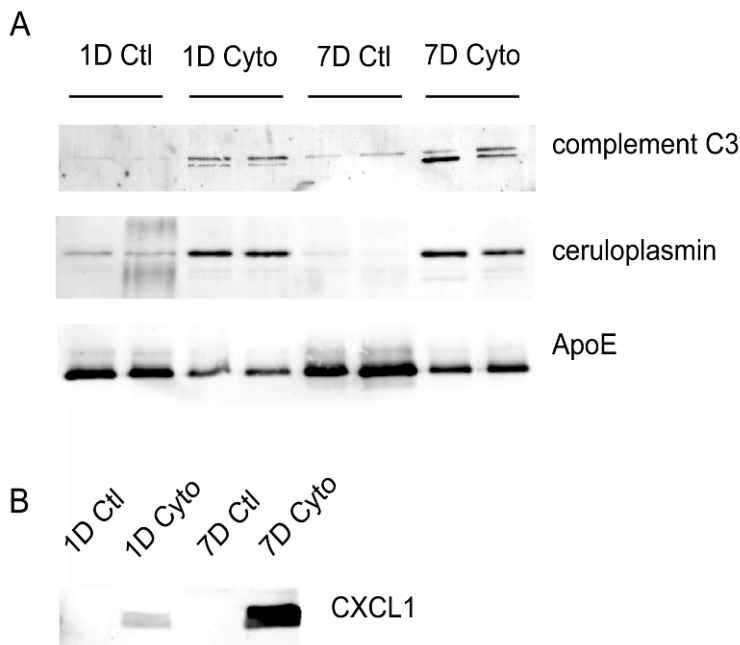
Figure 2-8. Western blot validation of Gel/LC-MS/MS analysis. (A) Western blots for proteins predicted to have increased (complement C3, ceruloplasmin) or decreased (ApoE) relative protein abundance (RPA) based on spectral count analysis. For each treatment condition, equal volumes of biological duplicates were loaded, identical to the conditions under which the mass spectrometry analysis was performed. (B) Western blot for chemokine ligand 1 (CXCL1) showed detection only after cytokine stimulation. Equal protein (25 ug) was loaded per lane.

Western blot analysis was performed for several of the proteins identified in the astrocyte secretome to (1) confirm their identification by mass spectrometry and (2) corroborate the spectral counting analysis. Consistent with the increase in spectral counts, complement C3 and ceruloplasmin show an increase upon cytokine treatment, while the cytokine-induced decrease in ApoE protein levels support the observed decrease in spectral counts (Figure 2-8A). Importantly, chemokine ligand 1, which was exclusively identified by mass spectrometry under cytokine-treated conditions (Table 2-1), was also only detected by Western analysis under these conditions (Figure 2-8B).

2.5 Discussion

The astrocyte secretome represents a relatively unexplored proteome but one with increasing interest and importance as astrocytes play vital roles in central nervous system development and synaptic communication. While activated astrocytes are a hallmark of many central nervous system pathologies, and as such their responses to inflammatory mediators have been studied extensively (Pekny, Nilsson 2005), a broad characterization of astrocyte-secreted biomolecules had not been performed. Here, we report a systematic secretome analysis from murine astrocytes under control and cytokine-treated conditions, which mimicked both acute (1D) and more sustained (7D) exposure to inflammatory mediators. Using validated proteomic approaches coupled with stringent selection criteria and a multistep bioinformatic workflow, 169 extracellular/secreted proteins were identified from astrocyte-conditioned media. This study confirmed a majority of known astrocyte-secreted proteins (Christopherson et al. 2005, Lafon-Cazal et al. 2003, Koistinaho et al. 2004, Delcourt et al. 2005), while identifying more than 100 proteins not previously ascribed to astrocyte protein secretion. Proteins identified in the secretome included components of the extracellular matrix and proteins involved in extracellular protein processing and metabolism, which are consistent with known functions of astrocytes in the maintenance and restructuring of the extracellular scaffolding. The secretome also included members of the insulin-like growth factor binding proteins and cystatin C, known to provide growth support for stem cells, neurons and astrocytes. In addition, we identified many lesser-known or studied components of the astrocyte ECM such as nidogen-2, cathepsins, proteinase inhibitors, and glucosamine transferases, which may not only regulate the composition of the ECM, but also serve as signaling molecules

89

in a paracrine or autocrine fashion. Interestingly, one of the largest functional categories containing protein with decreased RPA was metabolism (Figure 2-7B). This included several enzymes, such as hexosaminidase B and beta-glucuronidase, involved in protein glycosylation as well as the processing of glycosaminoglycans (GAGs). Deficiencies in these classes of proteins are associated with various lysosomal storage diseases, such as Sandhoff's disease and the mucopolysaccharidosis disorders, which can exhibit a diversity of central nervous system deficits (Donsante et al. 2007, Denny et al. 2007).

The study also found the secretion of four ligands from the C-C, C-X-C and C-X3-C chemokine ligand families upon cytokine stimulation. These low molecular weight proteins have diverse biological function in the central nervous system, including the regulation of inflammation (Bezzi et al. 2001, Babcock et al. 2003) and the migration of oligondendrocyte precursors (Tsai et al. 2002) and neural stem cells (Imitola et al. 2004). The C-X-C ligand 1, which was the only chemokine identified 1 day after inflammatory stimulation, is expressed in reactive astrocytes in mice models of multiple sclerosis (Glabinski et al. 1997) and although not toxic to oligodendrocytes may prevent their migration into demyelinated regions. The secretion of these chemokines may also have autocrine functions resulting in the elaboration of other inflammatory mediators such as products of the cyclooxygenase pathway and nitric oxide synthases. Quantitative lipidomics determined that PGE_2, and $PGF_{2\alpha}$, but not other lipid mediators of arachidonic acid metabolism were selectively secreted by astrocytes, and that only PGE_2 is significantly elevated upon cytokine treatment. Interestingly, elevated levels of PGE_2 have been documented in the cerebrospinal fluid (CSF) of patients with neurodegenerative diseases (Combrinck et al. 2006).

While the majority of classically secreted proteins are produced as unprocessed precursors that contain signal sequences, directing them through the traditional ER/Golgi secretion pathway, a limited number of proteins have been identified that do not contain signal sequences, but yet are still actively secreted (Nickel 2005). Of the 169 proteins reported in the astrocyte secretome, 12% did not contain an N-terminal signal sequence. Many of these proteins have been documented as proceeding through non-classical secretory pathways including macrophage inhibitory factor (MIF), galectin-3, phosphatidylethanolamine-binding protein 1 (PEBP-1), vimentin, meteorin, and acyl CoA-binding protein (ACBP) (Nickel 2005, Mor-Vaknin et al. 2003, Flieger et al. 2003, Guidotti et al. 1983, Hengst et al. 2001). Interestingly, the secretion of ACBP, also known as diazepam binding inhibitor (DBI), was originally described as a glial derived factor (Guidotti et al. 1983), and recent findings suggest that its secretion may require the Golgi-associated protein GRASP secretory pathway (Kinseth et al. 2007). Another protein of potential interest, meteorin, has been previously identified as a developmentally secreted protein that facilitates astrocyte formation and glial cell differentiation and can support neuron axonal extension (Nishino et al. 2004).

Global proteomic analyses of conditioned cellular media resulted in the identification of secreted and extracellular proteins as well as non-secreted proteins, which in part can be ascribed to cellular death. Given the depth of analysis afforded by current proteomic approaches, computational means are necessary for rapid, unbiased evaluation of protein secretomes. The current approach provides a computational workflow that can be applied in a systematic fashion to analyze protein identifications from any biological secretome. Importantly, the identification of secreted proteins with

distinct export mechanisms highlights the utility of this model system for elucidating the molecular mechanisms that govern the regulation and functionality of protein secretion. Overall, this systematic proteomic analysis provides a comprehensive profile of the astrocyte secretome that can be used as a reference for evaluating the impact of individual or multiple components on central nervous system physiology.

Table 2-1. Basal and cytokine-induced astrocyte secretome

Protein Name (Synonym)	Accession[a]	MW (kDa)	1D Control	1D Cyto	7D Control	7D Cyto
			Unique Peptides[b]			
Extracellular Matrix and Adhesion						
Agrin	A2ASQ0	205.0	6	26	8	27
Basement membrane-specific heparan sulfate proteoglycan core protein	Q05793	398.3	3	18	17	46
Cadherin-2 precursor (Neural-cadherin)	P15116	99.8	7	6	11	11
Calsyntenin 1	Q9EPL2	108.9	7	6	10	6
Collagen alpha-1(I) chain precursor	P11087	138.0	3	5	9	6
Collagen alpha-1(IV) chain precursor	P02463	160.7	-	-	2	3
[d]Collagen alpha-1(VI) chain precursor	Q04857	108.5	-	2	-	3
[c]Collagen alpha-1(XI) chain precursor	Q61245	181.0	-	-	2	-
Collagen alpha-1(XII) chain precursor	Q60847	340.2	3	13	41	27
Collagen alpha-2(I) chain precursor	Q01149	129.6	-	2	6	4
Collagen alpha-2(V) chain precursor	Q3U962	145.0	4	12	9	7
EGF-containing fibulin-like extracellular matrix protein 2	Q9WVJ9	49.4	3	4	11	4
Extracellular matrix protein	Q61508	62.8	-	-	7	4
Fat 1 cadherin	Q9QXA3	506.0	-	-	8	4
Fibromodulin precursor (FM)	P50608	43.1	4	5	6	6
Fibronectin 1	Q3UGY5	262.8	54	59	65	65
Fibulin-5 precursor (FIBL-5)	Q9WVH9	50.2	4	2	8	3
Galectin-3 (Galactose-specific lectin 3)	P16110	27.5	-	2	3	2
Glypican-4 precursor (K-glypican)	P51655	62.6	-	3	6	6
[d]Intercellular adhesion molecule (Icam1)	Q922B3	58.9	-	-	-	4
[d]Laminin subunit alpha-4 precursor	P97927	201.8	-	-	-	7
Laminin subunit alpha-5 precursor	Q61001	404.0	-	7	2	23
[d]Laminin subunit beta-2 precursor (S-laminin)	Q61292	196.4	-	8	-	19
Laminin subunit gamma-1 precursor (Laminin B2 chain)	P02468	177.3	-	11	4	25
Legumain	A2RTI3	49.4	2	6	6	6
Lysyl oxidase-like 3	Q91VN8	83.7	-	-	3	2
Mammalian ependymin related protein-2	Q99M71	25.5	7	7	8	7
Mimecan precursor (Osteoglycin)	Q62000	34.0	-	4	6	3
Mini-agrin	Q5EBX5	103.4	2	2	2	3
Neurocan core protein precursor (Chondroitin sulfate proteoglycan 3)	P55066	137.2	7	8	6	5
Nidogen 2 protein	Q8R5G0	153.9	3	-	7	2
SPARC-like protein 1 precursor (Matrix glycoprotein Sc1)	P70663	72.3	-	4	6	5
Tenascin precursor (TN-C)	Q80YX1	231.8	3	14	7	24
Tenascin-N precursor (TN-N)	Q80Z71	173.1	-	-	5	14
Thrombospondin 1	P35441	129.7	-	2	5	14
Vascular cell adhesion protein 1 precursor (CD106 antigen)	P29533	81.3	5	4	13	19
Vitamin K-dependent protein S precursor	Q08761	74.9	-	-	4	5
Protein Processing and Proteolysis						
78 kDa glucose-regulated protein precursor	P20029	72.4	8	8	9	5
Alpha-2-macroglobulin-P precursor (Alpha-2-macroglobulin)	Q6GQT1	164.3	38	48	51	47
Bone morphogenetic protein 1	P98063	111.7	2	4	3	4
Calreticulin precursor	P14211	48.0	3	2	3	-
Carboxypeptidase E precursor	Q00493	53.3	11	10	14	14

Cathepsin B precursor	P10605	37.3	13	11	13	13
Cathepsin D precursor	P18242	45.0	7	8	13	12
Cathepsin L1 precursor	P06797	37.5	7	3	7	7
Cathepsin S precursor	O70370	38.4	-	-	7	6
Cathepsin Z precursor	Q9WUU7	34.0	4	2	6	8
Cystatin-C precursor (Cystatin-3)	P21460	15.5	9	10	9	12
Dipeptidyl-peptidase 1 precursor (Cathepsin C)	P97821	52.4	-	2	2	3
Dipeptidyl-peptidase 2 precursor	Q9ET22	56.3	2	3	-	2
[c]Endoplasmic reticulum protein ERp29 precursor	P57759	28.8	-	-	3	-
Endoplasmin precursor (GRP94)	P08113	92.5	2	2	3	2
Glia-derived nexin precursor (Serpine 2)	Q07235	44.2	-	8	9	9
[c]Inter-alpha-trypsin inhibitor heavy chain H3	Q61704	99.0	-	-	7	-
Inter-alpha-trypsin inhibitor heavy chain H5	Q8BJD1	106.7	-	-	3	6
Lysosomal protective protein precursor	P16675	53.8	-	6	7	9
Metalloproteinase inhibitor 2 precursor (TIMP-2)	P25785	24.3	4	5	8	7
Peptidyl-prolyl cis-trans isomerase A	P17742	18.0	4	3	7	6
Peptidyl-prolyl cis-trans isomerase B	P24369	22.7	5	6	7	4
Plasma glutamate carboxypeptidase precursor	Q9WVJ3	51.8	6	6	7	5
Plasma protease C1 inhibitor	P97290	55.6	2	3	12	14
Plasminogen activator inhibitor 1	P22777	45.0	-	7	3	9
Pigment epithelium-derived factor (PEDF)	P97298	46.2	13	14	15	13
Protein disulfide-isomerase A3 precursor	P27773	56.7	10	11	13	6
Protein disulfide-isomerase A4 precursor	P08003	72.0	-	3	7	2
[c]Protein disulfide-isomerase A6 precursor	Q922R8	48.1	-	-	3	-
Protein disulfide-isomerase precursor (PDI)	P09103	57.1	3	3	5	-
Puromycin-sensitive aminopeptidase	Q11011	103.3	2	6	3	-
Serine protease inhibitor A3N precursor (Serpin A3N)	Q91WP6	46.7	5	11	11	10
[d]Stromelysin-1 precursor (MMP-3)	P28862	53.8	-	3	-	8
Sulfhydryl oxidase 1 precursor (Quiescin Q6)	Q8BND5	82.8	-	-	9	5
Tripeptidyl-peptidase 1 precursor	O89023	61.3	-	-	2	4

Metabolism

Acid ceramidase precursor (Acylsphingosine deacylase)	Q9WV54	44.7	-	-	4	5
Alpha-N-acetylglucosaminidase	O88325	82.6	-	-	3	3
Aspartate aminotransferase	P05202	47.4	3	4	4	2
[c]Beta-1,3-N-acetylglucosaminyltransferase lunatic fringe	O09010	42.0	-	-	3	-
[c]Beta-glucuronidase precursor	P12265	74.2	-	-	5	-
Beta-hexosaminidase alpha chain precursor (Hexosaminidase A)	P29416	60.6	-	-	4	2
Beta-hexosaminidase beta chain precursor (Hexosaminidase B)	P20060	61.1	4	3	13	4
[c]Bifunctional heparan sulfate N-deacetylase/N-sulfotransferase 1	Q3UHN9	100.7	-	-	3	-
Chitinase-3-like protein 1 precursor (Cartilage glycoprotein 39)	Q61362	43.0	5	16	14	15
Epididymis-specific alpha-mannosidase precursor	O54782	115.6	2	10	7	6
Exostosin-2	P70428	82.1	-	-	5	2
Galactocerebrosidase precursor (GALCERase)	P54818	75.5	-	-	3	2
Gamma-glutamyl hydrolase precursor	Q9Z0L8	35.4	2	2	5	4
Ganglioside GM2 activator precursor	Q60648	20.8	3	3	3	2
Glucose-6-phosphate isomerase (GPI)	P06745	62.8	7	5	7	4
[d]Lysosomal alpha-glucosidase precursor (Acid maltase)	P70699	106.2	-	-	-	4
N-acetylglucosamine-6-sulfatase precursor (G6S)	Q8BFR4	61.2	-	3	4	4
[c]N-acetyllactosaminide beta-1,3-N-acetylglucosaminyltransferase	Q8BWP8	47.4	-	-	4	-

Protein	Accession	MW				
N(4)-(beta-N-acetylglucosaminyl)-L-asparaginase precursor	Q64191	37.0	-	3	3	4
Palmitoyl-protein thioesterase 1 precursor (PPT-1)	O88531	34.5	-	-	5	5
Platelet-activating factor acetylhydrolase	Q60963	49.2	-	2	8	2
Procollagen-lysine, 2-oxoglutarate 5-dioxygenase 1 (Lysyl hydroxylase 1)	Q9R0E2	83.6	3	4	14	7
Procollagen-lysine, 2-oxoglutarate 5-dioxygenase 2 (Lysyl hydroxylase 2)	Q9R0B9	84.5	-	3	5	3
Procollagen-lysine, 2-oxoglutarate 5-dioxygenase 3 (Lysyl hydroxylase 3)	Q9R0E1	84.9	-	-	7	6
Putative phospholipase B-like 2 precursor	Q3TCN2	66.7	-	2	2	5
Ribonuclease T2 isoform 1	Q9CQ01	29.6	2	-	3	5

Immune

Protein	Accession	MW				
Beta-2-microglobulin precursor	P01887	13.8	2	2	3	5
[c]Cell adhesion molecule 4 precursor	Q8R464	42.7	-	-	4	-
[d]Chemokine (C-C motif) ligand 7	Q03366	11.0	-	-	-	3
[d]Chemokine (C-C motif) ligand 8	Q9Z121	11.0	-	-	-	3
[d]Chemokine (C-X3-C motif) ligand 1 (Fractalkine)	O35188	42.1	-	-	-	4
[d]Chemokine (C-X-C motif) ligand 1 (Growth-regulated alpha protein)	P12850	10.3	-	3	-	3
Complement C1q subcomponent subunit B precursor	P14106	26.7	-	-	2	3
Complement C1q tumor necrosis factor-related protein 5 precursor	Q8K479	25.4	3	5	3	4
Complement C3 precursor	P01027	186.5	33	72	66	89
Complement C4-B precursor	P01029	192.9	12	7	40	39
Complement C1q subcomponent subunit C precursor	Q02105	26.0	-	-	3	3
Complement C1r-A subcomponent	Q8CG16	80.1	-	4	9	15
Complement C1s-A subcomponent	Q8CG14	77.4	-	-	7	19
Complement factor B precursor	P04186	85.0	-	-	4	18
Cyclophilin C-associated protein	O35649	64.1	4	-	8	12
H-2 class I histocompatibility antigen, D-B alpha chain precursor	P01899	40.8	-	2	4	4
H-2 class I histocompatibility antigen, Q8 alpha chain	P14430	37.5	-	5	3	4
Immunoglobulin superfamily containing leucine-rich repeat	Q6GU68	45.6	2	4	3	2
Lysozyme C type M precursor	P08905	16.7	-	-	4	3
Macrophage colony-stimulating factor 1 precursor (CSF-1)	P07141	60.6	2	5	4	8
[c]Macrophage colony-stimulating factor 1 receptor	P09581	109.3	-	-	3	-
Macrophage migration inhibitory factor (MIF)	P34884	12.5	3	2	2	3
Monocyte differentiation antigen CD14 precursor	P10810	39.2	-	2	9	6
Pentraxin-related protein PTX3 precursor	P48759	41.8	5	10	3	11
Platelet-derived growth factor receptor-like protein precursor	Q6PE55	41.9	-	2	2	3

Binding and Transport

Protein	Accession	MW				
45 kDa calcium-binding protein precursor (SDF-4)	Q61112	42.1	2	2	4	5
[c]Acyl-CoA-binding protein (ACBP)	P31786	10.0	-	-	3	-
[d]Adipocyte enhancer-binding protein	Q640N1	128.4	-	-	-	6
Annexin A2	P07356	38.7	6	2	8	-
Apolipoprotein E precursor (Apo-E)	P08226	35.9	10	3	14	13
[c]Biotinidase precursor	Q8CIF4	58.6	-	-	3	-
Ceruloplasmin	Q61147	121.2	12	34	24	47
Dystroglycan precursor (Dystrophin-associated glycoprotein 1)	Q62165	96.9	5	4	10	7
Follistatin-related protein 1 precursor	Q62356	34.6	5	9	7	12
Gelsolin precursor (Actin-depolymerizing factor)	P13020	85.9	2	-	8	3
Lipopolysaccharide binding protein	Q61805	53.1	-	5	5	6
[d]Lysosomal-associated membrane glycoprotein 1 (LAMP1)	P11438	43.9	-	-	-	3

95

Protein	Accession	MW				
Neutrophil gelatinase-associated lipocalin precursor (Lipocalin 2)	P11672	22.9	-	6	5	7
Nucleobindin-1 precursor (CALNUC)	Q02819	53.4	2	9	7	7
Phosphatidylethanolamine-binding protein 1 (PEBP-1)	P70296	20.8	4	5	6	4
Phospholipid transfer protein precursor (Lipid transfer protein II)	P55065	54.5	3	-	16	13
Rab GDP dissociation inhibitor beta	Q61598	50.5	4	5	9	3
Renin receptor precursor	Q9CYN9	39.1	-	-	2	3
SPARC precursor	P07214	34.3	11	11	12	11
Serotransferrin precursor (Transferrin)	Q921I1	76.7	-	-	12	3
[c]Sortilin-related receptor, LDLR class A repeats-containing	O88307	247.1	-	-	3	-
Sulfated glycoprotein 1 precursor (Prosaposin)	Q61207	61.4	2	4	12	13
Superoxide dismutase, extracellular	O09164	27.4	-	-	5	6
Transcobalamin-2 precursor	O88968	47.6	7	7	8	9
Vacuolar ATP synthase subunit S1 precursor	Q9R1Q9	51.0	-	4	5	5
Vesicular integral-membrane protein VIP36 precursor	Q9DBH5	40.4	-	-	3	4

Cell Growth & Maintenance

Protein	Accession	MW				
Epididymal secretory protein E1 precursor	Q9Z0J0	16.4	4	5	5	5
Growth-arrest-specific protein 6 precursor (GAS-6)	Q61592	74.6	-	-	6	4
Insulin-like growth factor-binding protein 2	P47877	32.8	8	4	13	13
Insulin-like growth factor-binding protein 3	P47878	31.7	-	2	3	3
Insulin-like growth factor-binding protein 5	Q07079	30.4	3	4	4	6
Insulin-like growth factor-binding protein 7	Q61581	28.9	-	2	5	12
[c]Plexin domain-containing protein 2 precursor	Q9DC11	59.6	-	-	3	-
Prolow-density lipoprotein receptor-related protein 1 precursor (A2MR)	Q91ZX7	504.7	-	-	4	5
Ptprz1 protein (DSD-1 Proteoglycan)	B2RXS8	164.4	3	3	6	5

Other

Protein	Accession	MW				
4632419I22Rik protein	Q6NXM5	31.9	-	-	4	3
Acid sphingomyelinase-like phosphodiesterase 3a precursor	P70158	49.9	-	-	3	2
Amyloid beta A4 protein precursor (APP)	P12023	86.7	2	5	8	8
CD109 antigen precursor	Q8R422	161.7	-	5	10	3
Clusterin precursor (Apolipoprotein J)	Q06890	51.7	10	4	15	18
[c]Meteorin-like protein	Q8VE43	34.5	-	-	3	-
Profilin 1	P62962	11.8	6	6	6	5
Retinoic acid receptor responder protein 2 precursor	Q9DD06	18.4	-	-	3	4
Secretogranin 3	P47867	53.3	2	2	14	4
Thioredoxin-dependent peroxide reductase	P20108	28.1	-	-	2	3
Vimentin	P20152	53.7	18	20	23	20

Proteins are organized by functional category and reported with their corresponding Uniprot accession number, molecular weight (MW), and unique peptides identified for each treatment condition.

a) Accession numbers are reported from the Uniprot database (www.uniprot.org) and, when available, refer to the unprocessed precursor protein.

b) The average number of unique peptides identified is reported for protein identifications that passed the selection criteria as detailed in the Materials and Methods. A null value indicates the protein did not meet the minimum criteria for identification.

c) Protein was exclusively detected under control conditions.

d) Protein was exclusively detected under cytokine-treated conditions.

Table 2-2. Unique peptides from unclassified proteins.

Protein Name (Synonym)	Accession[a]	MW (kDa)	1D Control	1D Cyto	7D Control	7D Cyto
			Unique Peptides[b]			
14-3-3 protein beta	Q9CQV8	28,086	4	4	6	5
14-3-3 protein epsilon	P62259	29,174	11	8	12	8
14-3-3 protein eta	P68510	28,212	3	2	-	2
14-3-3 protein gamma	P61982	28,303	4	4	6	3
14-3-3 protein theta	P68254	27,778	3	4	8	4
14-3-3 protein zeta	P63101	27,771	7	8	8	6
Actin related protein 2/3 complex, subunit 2	Q9CVB6	34,357	2	4	2	3
Actinin, alpha 1	Q7TPR4	103,068	24	24	39	8
Actinin, alpha 4	P57780	104,977	6	32	17	17
Aldehyde dehydrogenase 1 family, member L1	Q8R0Y6	98,709	-	3	4	-
Aldo-keto reductase family 1, member A4	Q9JII6	36,587	4	2	2	3
Aldolase 1, isoform A	Q5FWB7	39,356	4	8	11	6
Aldolase 3, isoform C	Q5SYM1	39,395	2	10	2	4
Annexin A3	O35639	36,371	2	-	6	-
Annexin A5	P48036	35,752	5	3	6	2
Asparaginase like 1	Q8C0M9	33,950	3	4	4	-
Astrocytic phosphoprotein PEA-15	Q62048	15,054	-	4	3	3
Brain glycogen phosphorylase	Q8CI94	96,730	-	2	5	-
Calponin 3, acidic	Q9DAW9	36,429	-	-	2	2
Clathrin, heavy polypeptide (Hc)	Q68FD5	191,557	3	14	6	4
Cofilin 1, non-muscle	P18760	18,560	-	5	5	4
Creatine kinase, brain	Q04447	42,713	9	10	11	9
Cytochrome c	P62897	11,605	3	2	2	2
Dihydropyrimidinase-like 2	O08553	62,278	13	12	12	5
Dimethylarginine dimethylaminohydrolase 1	Q9CWS0	31,381	3	5	3	2
DJ-1 protein	Q99LX0	20,021	2	3	3	3
Enolase 1, alpha non-neuron	P17182	47,141	7	9	8	7
Eukaryotic initiation factor 4AII	P10630	46,402	-	2	5	3
Eukaryotic translation elongation factor 2	P58252	95,314	4	4	5	3
Eukaryotic translation initiation factor 5A	P63242	16,303	-	2	2	3
Fatty acid binding protein 7, brain	P51880	14,893	3	4	4	2
Fatty acid synthase	P19096	272,428	-	5	3	2
Ferritin heavy chain 1	P09528	21,067	-	2	4	4
Ferritin light chain 1	P29391	20,802	4	2	5	6
Filamin-A	Q8BTM8	281,194	9	23	26	15
Filamin-B	Q80X90	277,753	22	29	27	25
Filamin-C	Q8VHX6	291,119	-	-	8	2
Gelsolin-like capping protein	Q99LB4	38,769	-	-	2	4
Glial fibrillary acidic protein (GFAP)	P03995	46,492	11	9	12	12
Glutathione S-transferase, alpha 4	P24472	25,564	3	2	3	2
Glutathione S-transferase, mu 1	A2AE90	25,970	11	10	12	10
Glutathione S-transferase, mu 5	P48774	26,635	-	3	3	-
Glutathione S-transferase, pi 2	P46425	23,537	-	-	5	4

97

Protein	Accession	Mass				
Glyceraldehyde-3-phosphate dehydrogenase (GAPDH)	P16858	35,810	-	-	2	4
Glyoxalase domain containing 4	Q9CPV4	33,317	-	-	4	-
Guanosine diphosphate (GDP) dissociation inhibitor 1	P50396	50,522	2	3	5	-
H4 histone family, member A	P62806	11,367	3	5	2	3
Heat shock 70kDa protein 8 isoform 1	P63017	70,871	7	16	13	5
Heat shock protein 4	Q5NCS5	94,209	5	6	7	
Heat shock protein 90kDa alpha (cytosolic), class A member 1	P07901	84,788	6	6	13	9
Heat shock protein 90kDa alpha (cytosolic), class B member 1	Q71LX8	83,281	6	16	4	5
Heterogeneous nuclear ribonucleoprotein A2/B1	O88569	37,403	-	3	2	3
Hypoxanthine guanine phosphoribosyl transferase 1	P00493	24,570	-	-	3	-
Inositol monophosphatase	O55023	30,436	3	2	3	-
Isocitrate dehydrogenase [NADP] cytoplasmic	O88844	46,660	2	2	4	-
Lactate dehydrogenase 1, A chain	P06151	36,499	5	4	5	5
Lactate dehydrogenase 2, B chain	P16125	36,572	12	10	11	7
Lactoylglutathione lyase	Q9CPU0	20,810	-	3	2	2
Lamin A isoform A	P48678	74,238	-	-	3	2
Leukotriene A4 hydrolase	Q3UY71	69,051	2	-	6	-
Lysosomal alpha-mannosidase precursor (Mannosidase, alpha B)	O09159	114,604	3	5	11	6
Malate dehydrogenase 2, NAD (mitochondrial)	P08249	35,611	11	9	8	5
Malate dehydrogenase, cytoplasmic	P14152	36,511	7	3	6	5
Malic enzyme 1, supernatant	P06801	63,999	-	-	2	2
Mannosidase alpha, class 1A, member 1	Q544T7	73,276	2	2	10	5
Myosin, heavy polypeptide 9, non-muscle isoform 1	Q8VDD5	226,357	-	-	3	-
Myosin, light polypeptide 6, alkali, smooth muscle and non-muscle	Q60605	16,930	-	3	5	2
Nestin	Q6P5H2	202,011	-	7	4	-
Nit protein 2	Q9JHW2	30,502	-	-	2	-
Nucleoside-diphosphate kinase 1	P15532	17,208	3	-	4	4
Nucleoside-diphosphate kinase 2	Q01768	17,363	2	4	2	2
Ornithine aminotransferase	P29758	48,355	-	-	3	3
Peroxiredoxin 1	A2AP16	22,176	4	6	7	6
Peroxiredoxin 2 (Thioredoxin peroxidase 1)	Q61171	21,779	3	5	5	4
Peroxiredoxin 5 precursor	P99029	21,897	9	12	8	8
Peroxiredoxin 6 (Acidic calcium-independent phospholipase A2)	O08709	24,871	-	2	4	7
Phosphogluconate dehydrogenase	Q91V28	53,261	4	4	5	2
Phosphoglycerate kinase 1	P09411	44,536	9	11	8	8
Phosphoglycerate mutase 1 (brain)	Q9DBJ1	28,832	3	3	7	5
Phosphoserine aminotransferase 1	Q99K85	40,473	7	-	2	-
Plectin 1	Q9QXS1	534,216	-	-	6	-
Proteasome activator PA28 alpha subunit	P97371	28,673	-	-	3	4
Proteasome subunit, alpha type 1	Q9R1P4	29,547	3	2	3	-
Proteasome subunit, alpha type 2	P49722	25,926	-	2	3	-
Proteasome subunit, alpha type 3	Q9DCD8	28,490	4	2	2	-
Proteasome subunit, alpha type 5	Q3UPK6	26,411	3	2	4	-
Proteasome subunit, alpha type 6	Q9QUM9	27,372	2	3	3	3
Proteasome subunit, alpha type 7	Q9Z2U0	27,855	6	4	5	4
Proteasome subunit, beta type 1	O09061	26,372	4	-	4	-
Proteasome subunit, beta type 3	Q545G0	22,965	2	3	4	-
Proteasome subunit, beta type 5	Q3UZI1	28,532	3	7	4	-

Protein	Accession	MW				
Proteasome subunit, beta type 8	P28063	30,260	2	3	3	-
Purine-nucleoside phosphorylase	P23492	32,277	4	-	5	4
Pyruvate kinase isozyme M2	P52480	57,887	3	5	12	7
Rho GDP dissociation inhibitor (GDI) alpha	Q99PT1	23,407	3	2	5	3
Ribonuclease/angiogenesis inhibitor	Q91VI7	49,816	5	-	3	3
S-adenosylhomocysteine hydrolase	Q5M9P0	47,674	2	-	2	-
SH3-binding domain glutamic acid-rich protein like	Q9JJU8	12,811	2	3	4	4
Soluble calcium-activated nucleotidase 1	Q8VCF1	45,653	2	2	4	3
Spectrin alpha 2	P16546	284,597	-	3	14	-
Spectrin beta 2 isoform 1 or 2	Q62261	274,223	-	2	5	-
S-phase kinase-associated protein 1A	Q9WTX5	18,672	-	3	3	2
Superoxide dismutase 1, soluble	P08228	15,943	4	4	4	5
Thioredoxin reductase 1	Q8CI31	54,337	3	3	2	-
Transaldolase 1	Q93092	37,387	5	-	3	-
Transgelin	P37804	22,576	3	5	7	5
Transgelin 2	Q91VU2	22,395	2	4	6	6
Transitional endoplasmic reticulum ATPase (valosin-containing protein)	Q01853	89,364	14	23	14	4
Transketolase	P40142	67,630	-	-	3	-
Translin	Q62348	26,201	2	-	4	2
Triosephosphate isomerase 1	P17751	26,713	6	4	4	2
Tropomyosin 1, alpha	P58771	32,681	4	6	4	3
Tropomyosin 4, alpha	Q6IRU2	28,468	5	3	6	2
Tubulin, alpha	P05213	50,152	-	4	5	2
Tubulin, beta	Q9ERD7	50,419	-	5	5	-
Ubiquitin carboxy-terminal hydrolase L1	Q9R0P9	24,838	2	3	3	2
Ubiquitin-activating enzyme E1, Chr X	Q02053	117,809	-	4	3	2
UDP-glucose pyrophosphorylase 2	Q91ZJ5	56,979	3	3	3	-
Villin 2	P26040	69,407	-	-	5	4
Vinculin	Q64727	116,717	11	17	19	6
WD repeat domain 1	Q3TJY2	66,407	4	4	3	-

Proteins are reported with their corresponding accession number, molecular weight (MW), and unique peptides identified for each treatment condition.

[a)]Accession numbers are reported from the Uniprot database (www.uniprot.org) and, when available, refer to the unprocessed precursor protein.

[b)]The average number of unique peptides identified after applying the selection criteria detailed in Materials and Methods. A null value indicates the protein did not meet the minimum criteria for identification.

Table 2-3. Protein Prowler N-terminal signal peptide prediction.

Protein Name (Synonym)	Accession[a]	SP[b]	MTP[c]	Other[d]
Acid ceramidase precursor (Acylsphingosine deacylase)	Q9WV54	0.99	0	0.01
Aminopeptidase (Plasma glutamate carboxypeptidase)	Q9WVJ3	0.99	0	0.01
Carboxypeptidase E precursor	Q00493	0.99	0	0.01
Chemokine (C-X-C motif) ligand 1	P12850	0.99	0	0.01
Collagen alpha-1(XII) chain precursor	Q60847	0.99	0	0.01
Extracellular matrix protein	Q9QX30	0.99	0	0.01
Growth-arrest-specific protein 6 precursor (GAS-6)	Q61362	0.99	0	0.01
Lysosomal-associated membrane glycoprotein 1 (LAMP1)	P11438	0.99	0	0.01
Metalloproteinase inhibitor 2 precursor (TIMP-2)	P25785	0.99	0	0.01
Basement membrane-specific heparan sulfate proteoglycan core protein	Q05793	0.99	0	0.01
SPARC precursor	Q5NBV5	0.99	0	0.01
Plasma protease C1 inhibitor	P97290	0.99	0	0.01
4632419I22Rik protein	Q6GU68	0.98	0	0.02
Alpha-N-acetylglucosaminidase	O88325	0.98	0	0.02
Amyloid beta A4 protein precursor (APP)	P12023	0.98	0	0.02
Astrocytic phosphoprotein PEA-15	Q62000	0.98	0	0.02
Beta-2-microglobulin precursor	P01887	0.98	0	0.02
Beta-glucuronidase precursor	P12265	0.98	0	0.02
Bone morphogenetic protein 1	P09581	0.98	0	0.02
Cadherin-2 precursor (Neural-cadherin)	P15116	0.98	0	0.01
Calreticulin precursor	P14211	0.98	0	0.02
Cathepsin B precursor	P10605	0.98	0	0.02
Cathepsin L precursor	P06797	0.98	0	0.02
CD109 antigen homolog precursor	Q8R422	0.98	0.01	0.02
Chemokine (C-C motif) ligand 7	Q03366	0.98	0	0.02
Chemokine (C-C motif) ligand 8	Q9Z121	0.98	0	0.02
Chemokine (C-X3-C motif) ligand 1	O35188	0.98	0	0.02
Clusterin precursor (Apolipoprotein J)	Q06890	0.98	0	0.02
Collagen alpha-1(I) chain precursor	P11087	0.98	0	0.02
Collagen alpha-1(IV) chain precursor	P02463	0.98	0	0.02
Collagen alpha-1(VI) chain precursor	Q04857	0.98	0	0.02
Collagen alpha-2(I) chain precursor	Q01149	0.98	0	0.02
Macrophage colony-stimulating factor 1 receptor	Q6NXM5	0.98	0	0.02
Complement C1q tumor necrosis factor-related protein 5 precursor	Q8K479	0.98	0	0.02
Complement C1s-A subcomponent	Q8CG14	0.98	0	0.02
Complement factor B precursor	P04186	0.98	0	0.02
Cyclophilin C-associated protein	O35649	0.98	0	0.02
Cystatin-C precursor (Cystatin-3)	P21460	0.98	0	0.02
Dipeptidyl-peptidase 1 precursor (Cathepsin C)	P97821	0.98	0	0.02
Epididymal secretory protein E1 precursor	Q9Z0J0	0.98	0	0.02
Epididymis-specific alpha-mannosidase precursor	O54782	0.98	0	0.02
Fibromodulin precursor (FM)	P50608	0.98	0	0.02
Fibulin-5 precursor (FIBL-5)	Q9WVH9	0.98	0	0.02
Ganglioside GM2 activator precursor	Q60648	0.98	0	0.02
Glypican-4 precursor (K-glypican)	P51655	0.98	0	0.02
H-2 class I histocompatibility antigen, D-B alpha chain precursor	P01899	0.98	0	0.02

H-2 class I histocompatibility antigen, Q8 alpha chain	P14430	0.98	0	0.02
Insulin-like growth factor-binding protein 5	Q07079	0.98	0	0.02
Inter-alpha-trypsin inhibitor heavy chain H3 precursor	Q61704	0.98	0	0.02
Legumain	A2RTI3	0.98	0	0.02
Lipopolysaccharide binding protein	A2AC66	0.98	0	0.02
Low-density lipoprotein receptor-related protein 1 precursor (A2MR)	Q91ZX7	0.98	0	0.02
Lysosomal protective protein precursor	P16675	0.98	0	0.02
Lysozyme C type M precursor	P08905	0.98	0	0.02
Cell adhesion molecule 4 precursor	Q8R464	0.98	0	0.02
mouse fat 1 cadherin	Q9QXA3	0.98	0	0.02
Neutrophil gelatinase-associated lipocalin precursor (Lipocalin 2)	P11672	0.98	0	0.02
Phospholipid transfer protein precursor (Lipid transfer protein II)	P55065	0.98	0	0.02
Platelet-derived growth factor receptor-like protein precursor	Q61147	0.98	0	0.02
Procollagen, type XI, alpha 1	P22777	0.98	0	0.02
Procollagen-lysine, 2-oxoglutarate 5-dioxygenase 1 (Lysyl hydroxylase 1)	Q9R0E2	0.98	0	0.02
protein disulfide isomerase associated 6	Q922R8	0.98	0	0.02
Retinoic acid receptor responder protein 2 precursor	Q9DD06	0.98	0	0.02
Serotransferrin precursor (Transferrin)	Q921I1	0.98	0	0.02
Sulfated glycoprotein 1 precursor (Prosaposin)	Q61207	0.98	0	0.02
Transcobalamin-2 precursor (Transcobalamin II)	O88968	0.98	0	0.02
Acid sphingomyelinase-like phosphodiesterase 3a precursor	P70158	0.97	0	0.03
Apolipoprotein E precursor (Apo-E)	P08226	0.97	0	0.03
Cathepsin D precursor	P18242	0.97	0	0.03
Collagen alpha-2(V) chain precursor	Q3U962	0.97	0	0.03
Complement C1q subcomponent subunit C precursor	Q640N1	0.97	0	0.03
Complement C1r-A subcomponent	Q8CG16	0.97	0	0.03
Fibronectin 1	Q3UGY5	0.97	0.01	0.03
Glia-derived nexin precursor (Serpine 2)	Q07235	0.97	0	0.03
Igfbp3 protein (Insulin-like growth factor binding protein 3)	Q6PE55	0.97	0	0.03
Insulin-like growth factor binding protein 7	Q61581	0.97	0	0.03
Lysyl oxidase-like 3	Q91VN8	0.97	0	0.03
Mini-agrin	Q5EBX5	0.97	0	0.03
Monocyte differentiation antigen CD14 precursor	P10810	0.97	0	0.03
Nidogen 2 protein	Q8R5G0	0.97	0	0.03
Nucleobindin-1 precursor (CALNUC)	Q02819	0.97	0	0.03
Pentraxin-related protein PTX3 precursor	P48759	0.97	0	0.03
Platelet-activating factor acetylhydrolase	Q60963	0.97	0	0.02
protein disulfide isomerase associated 4	P08003	0.97	0	0.03
Renin receptor precursor	Q9CYN9	0.97	0	0.03
Ribonuclease T2 isoform 1	Q9CQ01	0.97	0	0.03
Secretogranin 3	Q8R1D7	0.97	0	0.03
Tenascin precursor (TN-C)	Q80YX1	0.97	0	0.03
Complement C1q subcomponent subunit B precursor	P14106	0.96	0	0.04
Complement C3 precursor	P01027	0.96	0	0.03
Immunoglobulin superfamily containing leucine-rich repeat	Q62356	0.96	0	0.04
Laminin subunit alpha-4 precursor	P97927	0.96	0	0.04
Laminin subunit gamma-1 precursor (Laminin B2 chain)	P02468	0.96	0.01	0.04
Mammalian ependymin related protein-2	Q99M71	0.96	0	0.04

Peptidyl-prolyl cis-trans isomerase B	P24369	0.96	0	0.04
Procollagen-lysine, 2-oxoglutarate 5-dioxygenase 3 (Lysyl hydroxylase 3)	Q9R0E1	0.96	0	0.04
Serine protease inhibitor A3N precursor (Serpin A3N)	Q91WP6	0.96	0	0.04
Superoxide dismutase, extracellular	O09164	0.96	0	0.04
Tenascin-N precursor (TN-N)	Q80Z71	0.96	0	0.04
Alpha-2-macroglobulin-P precursor (Alpha-2-macroglobulin)	Q02105	0.95	0	0.04
Beta-1,3-N-acetylglucosaminyltransferase lunatic fringe	O09010	0.95	0	0.05
Biotinidase precursor	Q8CIF4	0.95	0	0.05
Cathepsin S precursor	O70370	0.95	0.01	0.05
EGF-containing fibulin-like extracellular matrix protein 2	Q9JM06	0.95	0	0.05
Insulin-like growth factor binding protein 2	P47877	0.95	0	0.04
Calsyntenin 1	A2A800	0.94	0.02	0.04
Inter-alpha-trypsin inhibitor heavy chain H5	Q8BJD1	0.94	0	0.06
Ceruloplasmin	Q6NZM2	0.93	0	0.07
Complement C4-B precursor	P01029	0.93	0.01	0.06
Sulfhydryl oxidase 1 precursor (Quiescin Q6)	Q8BND5	0.93	0.01	0.06
Neurocan core protein precursor (Chondroitin sulfate proteoglycan 3)	P55066	0.92	0	0.08
Palmitoyl-protein thioesterase 1 precursor (PPT-1)	O88531	0.92	0.02	0.06
N(4)-(beta-N-acetylglucosaminyl)-L-asparaginase	Q64191	0.91	0.01	0.08
Lysosomal alpha-glucosidase precursor (Acid maltase)	P70699	0.91	0	0.09
Chitinase-3-like protein 1 precursor (Cartilage glycoprotein 39)	Q61292	0.9	0	0.1
Cathepsin Z	Q9ES94	0.89	0.01	0.1
Macrophage colony-stimulating factor 1 precursor (CSF-1)	P07141	0.89	0.02	0.09
Thrombospondin 1	Q8CGB2	0.87	0	0.13
Vacuolar ATP synthase subunit S1 precursor	Q9R1Q9	0.87	0.02	0.11
Laminin subunit beta-2 precursor (S-laminin)	Q61245	0.86	0	0.13
Pigment epithelium-derived factor (PEDF)	P97298	0.84	0.02	0.14
Galactocerebrosidase precursor (GALCERase)	P54818	0.83	0.03	0.14
Vitamin K-dependent protein S precursor	Q08761	0.83	0.02	0.15
Endoplasmin precursor (GRP94)	P08113	0.82	0.03	0.15
Mimecan precursor (Osteoglycin)	Q61592	0.81	0.03	0.16
Follistatin-related protein 1 precursor	Q6GQT1	0.8	0.02	0.17
Putative phospholipase B-like 2 precursor	Q3TCN2	0.8	0.02	0.18
Procollagen-lysine, 2-oxoglutarate 5-dioxygenase 2 (Lysyl hydroxylase 2)	Q9R0B9	0.8	0.01	0.2
Beta-hexosaminidase beta chain precursor (Hexosaminidase B)	P20060	0.77	0.04	0.19
N-acetyllactosaminide beta-1,3-N-acetylglucosaminyltransferase	Q8BWP8	0.77	0.02	0.22
Tripeptidyl-peptidase 1 precursor	O89023	0.77	0.01	0.22
Protein disulfide-isomerase A3 precursor	P27773	0.73	0.03	0.25
Plasminogen activator inhibitor 1	P47878	0.72	0.11	0.17
Gamma-glutamyl hydrolase	Q9Z0L8	0.69	0.06	0.25
Endoplasmic reticulum protein ERp29 precursor	P57759	0.67	0.06	0.28
45 kDa calcium-binding protein precursor (SDF-4)	Q61112	0.66	0.06	0.28
N-acetylglucosamine-6-sulfatase precursor (G6S)	Q8BFR4	0.66	0.06	0.28
Protein disulfide-isomerase precursor (PDI)	P09103	0.66	0.05	0.29
Ptprz1 protein (DSD-1 Proteoglycan)	B2RXS8	0.65	0.06	0.29
Intercellular adhesion molecule	Q922B3	0.65	0.06	0.29
Stromelysin-1 precursor (MMP-3)	P28862	0.63	0.05	0.32
Agrin	A2ASQ0	0.61	0.04	0.35

Exostosin-2	P70428	0.54	0.05	0.41
SPARC-like protein 1 precursor (Matrix glycoprotein Sc1)	P70663	0.54	0.1	0.36
78 kDa glucose-regulated protein precursor	P20029	0.53	0.08	0.39
Beta-hexosaminidase alpha chain precursor (Hexosaminidase A)	P29416	0.53	0.08	0.39
Dipeptidyl-peptidase 2 precursor	Q9ET22	0.52	0.1	0.38
Sortilin-related receptor, LDLR class A repeats-containing	O88307	0.49	0.27	0.24
Bifunctional heparan sulfate N-deacetylase/N-sulfotransferase 1; DAST-1	Q3UHN9	0.48	0.09	0.42
Lysosomal alpha-mannosidase precursor (Mannosidase, alpha B)	O09159	0.44	0.05	0.51
Laminin subunit alpha-5 precursor	Q61001	0.42	0.03	0.55
Vesicular integral-membrane protein VIP36 precursor	Q9DBH5	0.42	0.07	0.51
Adipocyte enhancer-binding protein	Q62165	0.41	0.11	0.48
Meteorin, glial cell differentiation regulator-like	Q8VE43	0.38	0.12	0.5
Plexin domain-containing protein 2 precursor	Q9DC11	0.31	0.07	0.62
Phosphogluconate dehydrogenase	Q91V28	0.29	0.01	0.7
Vascular cell adhesion protein 1 precursor (V-CAM 1)	P29533	0.28	0.13	0.58
Gelsolin precursor (Actin-depolymerizing factor)	P13020	0.27	0.14	0.59
Mannosidase alpha, class 1A, member 1	Q544T7	0.25	0.13	0.62
Glutathione S-transferase, alpha 4	P24472	0.21	0.11	0.68
Galectin-3 (Galactose-specific lectin 3)	P16110	0.19	0.09	0.72
Ferritin light chain 1	P29391	0.17	0.08	0.76
Intermediate filament protein nestin	Q6P5H2	0.16	0.08	0.76
Ca2+-dependent endoplasmic reticulum nucleoside diphosphatase	Q8VCF1	0.15	0.08	0.76
Heat shock protein 90kDa alpha (cytosolic), class B member 1	Q71LX8	0.14	0.09	0.76
Ubiquitin carboxy-terminal hydrolase L1	Q9R0P9	0.14	0.05	0.81
Isocitrate dehydrogenase [NADP] cytoplasmic	O88844	0.11	0.08	0.8
Heat shock protein 4	Q5NCS5	0.11	0.02	0.86
Aminopeptidase puromycin sensitive	Q5PR74	0.1	0.58	0.32
Inositol monophosphatase	O55023	0.1	0.07	0.83
Nit protein 2	Q9JHW2	0.1	0.1	0.8
Vimentin	P20152	0.09	0.38	0.53
Malate dehydrogenase, cytoplasmic	P14152	0.08	0.01	0.91
S-adenosylhomocysteine hydrolase	Q5M9P0	0.07	0.05	0.88
Hypoxanthine guanine phosphoribosyl transferase 1	P00493	0.06	0.05	0.89
Heat shock protein 90kDa alpha (cytosolic), class A member 1	P07901	0.06	0.03	0.91
Superoxide dismutase 1, soluble	P08228	0.06	0.05	0.88
Glutathione S-transferase, mu 5	P48774	0.06	0.06	0.88
Lactate dehydrogenase 1, A chain	P06151	0.04	0.01	0.95
Translin	Q62348	0.04	0.01	0.96
Asparaginase like 1	Q8C0M9	0.03	0.08	0.89
Peroxiredoxin 6 (Acidic calcium-independent phospholipase A2)	O08709	0.02	0.02	0.96
Peptidyl-prolyl cis-trans isomerase A	P17742	0.02	0.02	0.97
Acyl-CoA-binding protein (diazepam-binding inhibitor)	P31786	0.02	0.02	0.96
Phosphatidylethanolamine-binding protein 1 (PEBP-1)	P70296	0.02	0.01	0.96
Profilin 1	P62962	0.02	0.02	0.97
Dystroglycan precursor (Dystrophin-associated glycoprotein 1)	Q62048	0.02	0.02	0.96
Heterogeneous nuclear ribonucleoprotein A2/B1	O88569	0.02	0.02	0.97
Tubulin, alpha	P05213	0.02	0.02	0.97
Annexin A2	P07356	0.02	0.02	0.97

Eukaryotic initiation factor 4AII	P10630	0.02	0.03	0.96
Lactate dehydrogenase 2, B chain	P16125	0.02	0.01	0.96
Spectrin alpha 2	P16546	0.02	0.02	0.96
Fatty acid synthase	P19096	0.02	0.02	0.96
Purine-nucleoside phosphorylase	P23492	0.02	0.02	0.96
Proteasome subunit, beta type 8	P28063	0.02	0.01	0.97
Guanosine diphosphate (GDP) dissociation inhibitor 1	P50396	0.02	0.01	0.97
Actinin, alpha 4	P57780	0.02	0.03	0.96
14-3-3 protein epsilon	P62259	0.02	0.02	0.96
Heat shock 70kDa protein 8 isoform 1	P63017	0.02	0.02	0.96
14-3-3 protein zeta	P63101	0.02	0.02	0.96
14-3-3 protein theta	P68254	0.02	0.02	0.96
Myosin, light polypeptide 6, alkali, smooth muscle and non-muscle	Q60605	0.02	0.02	0.96
Rab GDP dissociation inhibitor beta	Q61598	0.02	0.01	0.97
Vinculin	Q64727	0.02	0.02	0.97
Actinin, alpha 1	Q7TPR4	0.02	0.02	0.96
Filamin-B	Q80X90	0.02	0.02	0.96
Thioredoxin reductase 1	Q8CI31	0.02	0.02	0.96
Aldehyde dehydrogenase 1 family, member L1	Q8R0Y6	0.02	0.01	0.97
Ribonuclease/angiogenesis inhibitor	Q91VI7	0.02	0.02	0.97
Rho GDP dissociation inhibitor (GDI) alpha	Q99PT1	0.02	0.02	0.96
Lactoylglutathione lyase	Q9CPU0	0.02	0.02	0.96
Actin related protein 2/3 complex, subunit 2	Q9CVB6	0.02	0.01	0.97
Tubulin, beta	Q9ERD7	0.02	0.02	0.96
S-phase kinase-associated protein 1A	Q9WTX5	0.02	0.02	0.96
Macrophage migration inhibitory factor (MIF)	P34884	0.01	0.02	0.97
Peroxiredoxin 1	A2AP16	0.01	0.03	0.96
Dihydropyrimidinase-like 2	O08553	0.01	0.03	0.96
Proteasome subunit, beta type 1	O09061	0.01	0.03	0.96
Annexin A3	O35639	0.01	0.03	0.96
Glial fibrillary acidic protein	P03995	0.01	0.39	0.6
Phosphoglycerate kinase 1	P09411	0.01	0.03	0.97
Ferritin heavy chain 1	P09528	0.01	0.03	0.96
Nucleoside-diphosphate kinase 1	P15532	0.01	0.03	0.96
Triosephosphate isomerase 1	P17751	0.01	0.03	0.96
Cofilin 1, non-muscle	P18760	0.01	0.02	0.97
Peroxiredoxin 3	P20108	0.01	0.94	0.05
Villin 2	P26040	0.01	0.02	0.97
Transgelin	P37804	0.01	0.02	0.96
Transketolase	P40142	0.01	0.03	0.96
Glutathione S-transferase, pi 2	P46425	0.01	0.02	0.97
Annexin A5	P48036	0.01	0.03	0.96
Fatty acid binding protein 7, brain	P51880	0.01	0.02	0.97
Pyruvate kinase isozyme M2	P52480	0.01	0.02	0.96
Eukaryotic translation elongation factor 2	P58252	0.01	0.02	0.97
Tropomyosin 1, alpha	P58771	0.01	0.02	0.96
14-3-3 protein gamma	P61982	0.01	0.02	0.96
Cytochrome c	P62897	0.01	0.03	0.96

Eukaryotic translation initiation factor 5A	P63242	0.01	0.03	0.96
14-3-3 protein eta	P68510	0.01	0.02	0.97
Proteasome activator PA28 alpha subunit	P97371	0.01	0.03	0.96
Nucleoside-diphosphate kinase 2	Q01768	0.01	0.03	0.97
Creatine kinase, brain	Q04447	0.01	0.03	0.96
WD repeat domain 1	Q3TJY2	0.01	0.02	0.96
Proteasome subunit, alpha type 5	Q3UPK6	0.01	0.03	0.96
Proteasome subunit, beta type 5	Q3UZI1	0.01	0.03	0.96
Aldolase 1, isoform A	Q5FWB7	0.01	0.02	0.96
Aldolase 3, isoform C	Q5SYM1	0.01	0.02	0.96
Peroxiredoxin 2 (Thioredoxin peroxidase 1)	Q61171	0.01	0.02	0.96
Spectrin beta 2 isoform 1 or 2	Q62261	0.01	0.02	0.96
Clathrin, heavy polypeptide (Hc)	Q68FD5	0.01	0.02	0.97
Tropomyosin 4, alpha	Q6IRU2	0.01	0.02	0.97
Brain glycogen phosphorylase	Q8CI94	0.01	0.03	0.97
Myosin, heavy polypeptide 9, non-muscle isoform 1	Q8VDD5	0.01	0.02	0.96
Filamin-C	Q8VHX6	0.01	0.02	0.97
Transgelin 2	Q91VU2	0.01	0.03	0.96
UDP-glucose pyrophosphorylase 2	Q91ZJ5	0.01	0.03	0.96
Transaldolase 1	Q93092	0.01	0.03	0.97
Phosphoserine aminotransferase 1	Q99K85	0.01	0.02	0.97
Gelsolin-like capping protein	Q99LB4	0.01	0.02	0.96
DJ-1 protein	Q99LX0	0.01	0.02	0.97
14-3-3 protein beta	Q9CQV8	0.01	0.02	0.96
Calponin 3, acidic	Q9DAW9	0.01	0.03	0.96
Phosphoglycerate mutase 1 (brain)	Q9DBJ1	0.01	0.02	0.97
Proteasome subunit, alpha type 3	Q9DCD8	0.01	0.02	0.96
Aldo-keto reductase family 1, member A4	Q9JII6	0.01	0.03	0.96
Plectin 1	Q9QXS1	0.01	0.03	0.96
Proteasome subunit, alpha type 1	Q9R1P4	0.01	0.03	0.96
Proteasome subunit, alpha type 7	Q9Z2U0	0.01	0.02	0.96
Valosin containing protein	Q01853	0.01	0.02	0.96
Glucose-6-phosphate isomerase (GPI)	P06745	0	0.14	0.86
Glutathione S-transferase, mu 1	P10649	0	0.02	0.97
Aspartate aminotransferase	P05202	0	0.95	0.04
Malic enzyme 1, supernatant	P06801	0	0.03	0.97
Malate dehydrogenase 2, NAD (mitochondrial)	P08249	0	0.99	0.01
Glyceraldehyde-3-phosphate dehydrogenase	P16858	0	0.05	0.94
Enolase 1, alpha non-neuron	P17182	0	0.03	0.96
Ornithine aminotransferase	P29758	0	0.98	0.02
Lamin A isoform A	P48678	0	0.04	0.96
Proteasome subunit, alpha type 2	P49722	0	0.04	0.95
H4 histone family, member A	P62806	0	0.03	0.97
Peroxiredoxin 5 precursor	P99029	0	0.96	0.03
Ubiquitin-activating enzyme E1, Chr X	Q02053	0	0.03	0.97
Leukotriene A4 hydrolase	Q3UY71	0	0.08	0.92
Proteasome subunit, beta type 3	Q545G0	0	0.02	0.97
Filamin-A	Q8BTM8	0	0.05	0.95

Glyoxalase domain containing 4	Q9CPV4	0	0.98	0.01
Dimethylarginine dimethylaminohydrolase 1	Q9CWS0	0	0.75	0.24
SH3-binding domain glutamic acid-rich protein like	Q9JJU8	0	0.07	0.93
Proteasome subunit, alpha type 6	Q9QUM9	0	0.04	0.96

Proteins are reported in order of decreasing SP (secretory pathway) score

calculated by Protein Prowler version 1.2 (pprowler.imb.uq.edu.au/index.jsp)

a) Accession numbers are reported from the Uniprot database (www.uniprot.org) and, when available, refer to the unprocessed precursor protein.

b) Secretory pathway targeting score (signal peptide)

c) Mitochondrion targeting score (mitochondrial targeting peptide)

d) Other targeting score (nucleus, cytoplasm, other)

Table 2-4. Redundant peptides from proteins in the astrocyte secretome.

Protein Name (Synonym)	Accession[a]	MW (kDa)	1D Control	1D Cyto	7D Control	7D Cyto
			Redundant Peptides[b]			
Extracellular Matrix and Adhesion						
Agrin	A2ASQ0	205.0	8	46	10	60
Cadherin-2 precursor (Neural-cadherin)	P15116	99.8	19	18	43	35
Calsyntenin 1	A2A800	108.9	18	9	29	15
Collagen alpha-1(I) chain precursor	P11087	138.0	3	7	26	11
Collagen alpha-1(IV) chain precursor	P02463	160.7	-	-	2	4
[d]Collagen alpha-1(VI) chain precursor	Q04857	108.5	-	2	-	5
[c]Collagen alpha-1(XI) chain precursor	Q61245	181.0	-	-	5	-
Collagen alpha-1(XII) chain precursor	Q60847	340.2	4	21	85	52
Collagen alpha-2(I) chain precursor	Q01149	129.6	-	2	10	8
Collagen alpha-2(V) chain precursor	Q3U962	145.0	4	15	24	11
EGF-containing fibulin-like extracellular matrix protein 2	Q9JM06	49.5	4	8	29	8
Extracellular matrix protein	Q9QX30	62.8	-	-	15	8
Fat 1 cadherin	Q9QXA3	506.0	-	-	13	7
Fibromodulin precursor (FM)	P50608	43.1	6	9	21	10
Fibronectin 1	Q3UGY5	262.8	146	238	375	355
Fibulin-5 precursor (FIBL-5)	Q9WVH9	50.2	7	2	25	3
Galectin-3 (Galactose-specific lectin 3)	P16110	27.5	-	2	6	3
Glypican-4 precursor (K-glypican)	P51655	62.6	-	3	11	10
*Intercellular adhesion molecule (Icam1)	Q922B3	58.9	-	-	-	5
*Laminin subunit alpha-4 precursor	P97927	201.8	-	-	-	11
Laminin subunit alpha-5 precursor	Q61001	404.0	-	12	2	46
*Laminin subunit beta-2 precursor (S-laminin)	Q61292	196.4	-	10	-	34
Laminin subunit gamma-1 precursor (Laminin B2 chain)	P02468	177.3	-	20	5	46
Legumain	A2RTI3	49.4	6	18	25	15
Lysyl oxidase-like 3	Q91VN8	83.7	-	-	4	2
Mammalian ependymin related protein-2	Q99M71	25.5	14	21	20	24
Mimecan precursor (Osteoglycin)	Q62000	34.0	-	4	26	6
Mini-agrin	Q5EBX5	103.4	2	4	2	5
Neurocan core protein precursor (Chondroitin sulfate proteoglycan 3)	P55066	137.2	24	27	31	14
Nidogen 2 protein	Q8R5G0	153.9	4	-	13	3
Basement membrane-specific heparan sulfate proteoglycan core protein	Q05793	469.0	3	34	32	117
SPARC-like protein 1 precursor (Matrix glycoprotein Sc1)	P70663	72.3	-	5	13	11
Tenascin precursor (TN-C)	Q80YX1	231.8	8	28	11	73
Tenascin-N precursor (TN-N)	Q80Z71	173.1	-	-	5	29
Thrombospondin 1	Q8CGB2	129.7	-	2	9	21
Vascular cell adhesion protein 1 precursor (CD106 antigen)	P29533	81.3	9	5	34	66
Vitamin K-dependent protein S precursor	Q08761	74.9	-	-	14	10
Protein Processing and Proteolysis						
78 kDa glucose-regulated protein precursor	P20029	72.4	12	14	15	8
Alpha-2-macroglobulin-P precursor (Alpha-2-macroglobulin)	Q6GQT1	164.3	116	204	301	189
Aminopeptidase (Plasma glutamate carboxypeptidase)	Q9WVJ3	51.8	9	11	19	9
Aminopeptidase puromycin sensitive	Q5PR74	103.3	2	9	4	-
Bone morphogenetic protein 1	Q6NZM2	111.7	2	4	5	4

Calreticulin precursor	P14211	48.0	5	3	4	-
Carboxypeptidase E precursor	Q00493	53.3	27	41	90	71
Cathepsin B precursor	P10605	37.3	47	71	131	136
Cathepsin D precursor	P18242	45.0	21	28	79	69
Cathepsin L precursor	P06797	37.5	17	9	28	39
Cathepsin S precursor	O70370	38.4	-	-	26	15
Cathepsin Z precursor	Q9WUU7	34.0	5	6	13	15
Cystatin-C precursor (Cystatin-3)	P21460	15.5	77	109	232	287
Dipeptidyl-peptidase 1 precursor (Cathepsin C)	P97821	52.4	-	4	2	5
Dipeptidyl-peptidase 2 precursor	Q9ET22	56.3	3	6	-	3
dEndoplasmic reticulum protein ERp29 precursor	P57759	28.8	-	-	3	-
Endoplasmin precursor (GRP94)	P08113	92.5	4	3	9	2
Glia-derived nexin precursor (Serpine 2)	Q07235	44.2	-	15	14	29
^Inter-alpha-trypsin inhibitor heavy chain H3	Q61704	99.0	-	-	11	-
Inter-alpha-trypsin inhibitor heavy chain H5	Q8BJD1	106.7	-	-	3	11
Lysosomal protective protein precursor	P16675	53.8	-	8	14	16
Metalloproteinase inhibitor 2 precursor (TIMP-2)	P25785	24.3	9	23	22	19
Peptidyl-prolyl cis-trans isomerase A	P17742	18.0	9	6	15	11
Peptidyl-prolyl cis-trans isomerase B	P24369	22.7	9	14	11	10
Protein disulfide-isomerase A3 precursor	P27773	56.7	14	24	22	9
Protein disulfide-isomerase A4 precursor	P08003	72.0	-	3	10	2
^Protein disulfide-isomerase A6 precursor	Q922R8	48.1	-	-	4	-
Protein disulfide-isomerase precursor (PDI)	P09103	57.1	4	6	7	-
Pigment epithelium-derived factor (PEDF)	P97298	46.2	57	59	61	57
Plasma protease C1 inhibitor	P97290	55.6	7	3	40	73
Plasminogen activator inhibitor 1	P22777	45.0	-	12	5	17
Serine protease inhibitor A3N precursor (Serpin A3N)	Q91WP6	46.7	12	30	43	51
*Stromelysin-1 precursor (MMP-3)	P28862	53.8	-	3	-	14
Sulfhydryl oxidase 1 precursor (Quiescin Q6)	Q8BND5	82.8	-	-	23	7
Tripeptidyl-peptidase 1 precursor	O89023	61.3	-	-	4	7

Metabolism

Acid ceramidase precursor (Acylsphingosine deacylase)	Q9WV54	44.7	-	-	8	15
Alpha-N-acetylglucosaminidase	O88325	82.6	-	-	4	5
Aspartate aminotransferase	P05202	47.4	6	5	5	2
^Beta-1,3-N-acetylglucosaminyltransferase lunatic fringe	O09010	42.0	-	-	7	-
^Beta-glucuronidase precursor	P12265	74.2	-	-	6	-
Beta-hexosaminidase alpha chain precursor (Hexosaminidase A)	P29416	60.6	-	-	6	3
Beta-hexosaminidase beta chain precursor (Hexosaminidase B)	P20060	61.1	8	3	27	6
^Bifunctional heparan sulfate N-deacetylase/N-sulfotransferase 1	Q3UHN9	100.7	-	-	3	-
Chitinase-3-like protein 1 precursor (Cartilage glycoprotein 39)	Q61362	43.0	9	75	42	130
Epididymis-specific alpha-mannosidase precursor	O54782	115.6	2	2	16	9
Exostosin-2	P70428	82.1	-	-	5	2
Galactocerebrosidase precursor (GALCERase)	P54818	75.5	-	-	6	3
Gamma-glutamyl hydrolase	Q9Z0L8	35.4	2	2	8	5
Ganglioside GM2 activator precursor	Q60648	20.8	3	9	12	10
Glucose-6-phosphate isomerase (GPI)	P06745	62.8	18	15	15	6
*Lysosomal alpha-glucosidase precursor (Acid maltase)	P70699	106.2	-	-	-	11
N-acetylglucosamine-6-sulfatase precursor (G6S)	Q8BFR4	61.2	-	7	7	6

^N-acetyllactosaminide beta-1,3-N-acetylglucosaminyltransferase	Q8BWP8	47.4	-	-	7	-
N(4)-(beta-N-acetylglucosaminyl)-L-asparaginase	Q64191	37.0	-	8	5	10
Palmitoyl-protein thioesterase 1 precursor (PPT-1)	O88531	34.5	-	-	11	14
Platelet-activating factor acetylhydrolase	Q60963	49.2	-	2	29	3
Procollagen-lysine, 2-oxoglutarate 5-dioxygenase 1 (Lysyl hydroxylase 1)	Q9R0E2	83.6	4	6	24	10
Procollagen-lysine, 2-oxoglutarate 5-dioxygenase 2 (Lysyl hydroxylase 2)	Q9R0B9	84.5	-	5	8	4
Procollagen-lysine, 2-oxoglutarate 5-dioxygenase 3 (Lysyl hydroxylase 3)	Q9R0E1	84.9	-	-	15	11
Putative phospholipase B-like 2 precursor	Q3TCN2	66.7	-	3	10	2
Ribonuclease T2 isoform 1	Q9CQ01	29.6	2	-	6	9

Immune

Beta-2-microglobulin precursor	P01887	13.8	5	24	24	56
^Cell adhesion molecule 4 precursor	Q8R464	42.7	-	-	6	-
*Chemokine (C-C motif) ligand 7	Q03366	11.0	-	-	-	11
*Chemokine (C-C motif) ligand 8	Q9Z121	11.0	-	-	-	3
*Chemokine (C-X3-C motif) ligand 1 (Fractalkine)	O35188	42.1	-	-	-	9
*Chemokine (C-X-C motif) ligand 1 (Growth-regulated alpha protein)	P12850	10.3	-	6	-	15
Complement C1q subcomponent subunit B precursor	P14106	26.7	-	-	4	5
Complement C1q tumor necrosis factor-related protein 5 precursor	Q8K479	25.4	4	8	7	11
Complement C3 precursor	P01027	186.5	95	575	484	2036
Complement C4-B precursor	P01029	192.9	18	14	156	112
Complement C1q subcomponent subunit C precursor	Q02105	26.0	-	-	7	5
Complement C1r-A subcomponent	Q8CG16	80.1	-	10	23	67
Complement C1s-A subcomponent	Q8CG14	77.4	-	-	18	132
Complement factor B precursor	P04186	85.0	-	-	5	41
Cyclophilin C-associated protein	O35649	64.1	5	-	20	43
H-2 class I histocompatibility antigen, D-B alpha chain precursor	P01899	40.8	-	5	6	13
H-2 class I histocompatibility antigen, Q8 alpha chain	P14430	37.5	-	13	6	22
Immunoglobulin superfamily containing leucine-rich repeat	Q6GU68	45.6	2	7	7	2
Lysozyme C type M precursor	P08905	16.7	-	-	45	66
Macrophage colony-stimulating factor 1 precursor (CSF-1)	P07141	60.6	-	41	39	90
^Macrophage colony-stimulating factor 1 receptor	P09581	109.3	-	-	4	-
Macrophage migration inhibitory factor (MIF)	P34884	12.5	10	8	8	7
Monocyte differentiation antigen CD14 precursor	P10810	39.2	-	2	21	10
Pentraxin-related protein PTX3 precursor	P48759	41.8	6	38	3	34
Platelet-derived growth factor receptor-like protein precursor	Q6PE55	41.9	-	4	4	7

Binding and Transport

45 kDa calcium-binding protein precursor (SDF-4)	Q61112	42.1	2	2	7	6
^Acyl-CoA-binding protein (DBI)	P31786	10.0	-	-	4	-
*Adipocyte enhancer-binding protein	Q640N1	128.4	-	-	-	12
Annexin A2	P07356	38.7	9	2	13	-
Apolipoprotein E precursor (Apo-E)	P08226	35.9	64	7	177	128
^Biotinidase precursor	Q8CIF4	58.6	-	-	4	-
Ceruloplasmin	Q61147	121.2	19	97	64	300
Dystroglycan precursor (Dystrophin-associated glycoprotein 1)	Q62165	96.9	10	7	26	21
Follistatin-related protein 1 precursor	Q62356	34.6	11	29	16	31
Gelsolin precursor (Actin-depolymerizing factor)	P13020	85.9	6	-	18	3
Rab GDP dissociation inhibitor beta	Q61598	50.5	9	11	20	3
Lipopolysaccharide binding protein	A2AC66	53.1	-	10	10	15

Protein	Accession	MW				
*Lysosomal-associated membrane glycoprotein 1 (LAMP1)	P11438	43.9	-	-	-	7
Neutrophil gelatinase-associated lipocalin precursor (Lipocalin 2)	P11672	22.9	-	33	25	283
Nucleobindin-1 precursor (CALNUC)	Q02819	53.4	2	18	8	8
Phosphatidylethanolamine-binding protein 1 (PEBP-1)	P70296	20.8	11	20	17	14
Phospholipid transfer protein precursor (Lipid transfer protein II)	P55065	54.5	4	-	78	31
Renin receptor precursor	Q9CYN9	39.1	-	-	2	6
SPARC precursor	P07214	34.3	126	73	82	61
Serotransferrin precursor (Transferrin)	Q921I1	76.7	-	-	15	3
^Sortilin-related receptor, LDLR class A repeats-containing	O88307	247.1	-	-	3	-
Sulfated glycoprotein 1 precursor (Prosaposin)	Q61207	61.4	2	7	35	48
Superoxide dismutase, extracellular	O09164	27.4	-	-	8	20
Transcobalamin-2 precursor	O88968	47.6	11	11	33	24
Vacuolar ATP synthase subunit S1 precursor	Q9R1Q9	51.0	-	9	9	16
Vesicular integral-membrane protein VIP36 precursor	Q9DBH5	40.4	-	-	4	5

Cell Growth & Maintenance

Protein	Accession	MW				
Epididymal secretory protein E1 precursor	Q9Z0J0	16.4	5	13	14	21
Growth-arrest-specific protein 6 precursor (GAS-6)	Q61592	74.6	-	-	11	7
Insulin-like growth factor binding protein 2	P47877	32.8	32	17	86	98
Insulin-like growth factor binding protein 3	P47878	31.7	-	5	6	5
Insulin-like growth factor binding protein 7	Q61581	28.9	-	7	11	71
Insulin-like growth factor-binding protein 5	Q07079	30.4	8	8	20	21
Prolow-density lipoprotein receptor-related protein 1 precursor (A2MR)	Q91ZX7	504.7	-	-	4	8
^Plexin domain-containing protein 2 precursor	Q9DC11	59.6	-	-	4	-
Ptprz1 protein (DSD-1 Proteoglycan)	B2RXS8	175.2	7	5	33	9

Other

Protein	Accession	MW				
4632419I22Rik protein	Q6NXM5	31.9	-	-	6	3
Acid sphingomyelinase-like phosphodiesterase 3a precursor	P70158	49.9	-	-	4	2
Amyloid beta A4 protein precursor (APP)	P12023	86.7	4	11	25	28
CD109 antigen homolog precursor	Q8R422	161.7	-	5	19	3
Clusterin precursor (Apolipoprotein J)	Q06890	51.7	20	14	119	154
^Meteorin, glial cell differentiation regulator-like	Q8VE43	34.5	-	-	4	-
Peroxiredoxin 3	P20108	28.1	-	-	6	9
Profilin 1	P62962	11.8	16	19	19	14
Retinoic acid receptor responder protein 2 precursor	Q9DD06	18.4	-	-	4	12
Secretogranin 3	P47867	53.3	2	2	32	6
Vimentin	P20152	53.7	77	132	172	108

Proteins are organized by functional category and reported with their corresponding accession number, molecular weight (MW), and redundant peptides identified for each treatment condition.

a) Accession numbers are reported from the Uniprot database (www.uniprot.org) and, when available, refer to the unprocessed precursor protein.

b) The average numbers of redundant peptides identified are reported for protein identifications that passed the selection criteria as detailed in the Experimental Procedures. A null value indicates the protein did not meet the minimum criteria for identification.

c) Protein was exclusively detected under control conditions.

d) Protein was exclusively detected under cytokine-treated conditions.

Table 2-5. Redundant peptides from unclassified proteins.

Protein Name (Synonym)	Accession[a]	MW (kDa)	1D Control	1D Cytokine	7D Control	7D Cytokine
			Redundant Peptides[b]			
14-3-3 protein beta	Q9CQV8	28,086	8	8	13	8
14-3-3 protein epsilon	P62259	29,174	29	39	41	24
14-3-3 protein eta	P68510	28,212	6	5	-	3
14-3-3 protein gamma	P61982	28,303	10	12	14	9
14-3-3 protein theta	P68254	27,778	4	10	14	5
14-3-3 protein zeta	P63101	27,771	16	35	25	19
Actin related protein 2/3 complex, subunit 2	Q9CVB6	34,357	2	4	4	4
Actinin, alpha 1	Q7TPR4	103,068	50	53	104	14
Actinin, alpha 4	P57780	104,977	8	88	29	23
Aldehyde dehydrogenase 1 family, member L1	Q8R0Y6	98,709	-	4	4	-
Aldo-keto reductase family 1, member A4	Q9JII6	36,587	6	6	3	5
Aldolase 1, isoform A	Q5FWB7	39,356	12	17	27	10
Aldolase 3, isoform C	Q5SYM1	39,395	4	24	4	8
Annexin A3	O35639	36,371	3	-	10	-
Annexin A5	P48036	35,752	12	5	12	2
Asparaginase like 1	Q8C0M9	33,950	6	7	5	-
Astrocytic phosphoprotein PEA-15	Q62048	15,054	-	11	5	6
Brain glycogen phosphorylase	Q8CI94	96,730	-	3	5	-
Calponin 3, acidic	Q9DAW9	36,429	-	-	2	2
Clathrin, heavy polypeptide (Hc)	Q68FD5	191,557	4	16	8	4
Cofilin 1, non-muscle	P18760	18,560	-	7	8	7
Creatine kinase, brain	Q04447	42,713	25	44	74	38
Cytochrome c	P62897	11,605	7	4	4	2
Dihydropyrimidinase-like 2	O08553	62,278	23	21	25	8
Dimethylarginine dimethylaminohydrolase 1	Q9CWS0	31,381	6	9	4	2
DJ-1 protein	Q99LX0	20,021	2	5	7	3
Enolase 1, alpha non-neuron	P17182	47,141	11	20	17	11
Eukaryotic initiation factor 4AII	P10630	46,402	-	3	6	4
Eukaryotic translation elongation factor 2	P58252	95,314	4	8	11	4
Eukaryotic translation initiation factor 5A	P63242	16,303	-	2	3	3
Fatty acid binding protein 7, brain	P51880	14,893	6	8	10	5
Fatty acid synthase	P19096	272,428	-	6	4	2
Ferritin heavy chain 1	P09528	21,067	-	6	9	17
Ferritin light chain 1	P29391	20,802	5	2	11	19
Filamin-A	Q8BTM8	281,194	16	67	66	28
Filamin-B	Q80X90	277,753	28	66	86	55
Filamin-C	Q8VHX6	291,119	-	-	11	2
Gelsolin-like capping protein	Q99LB4	38,769	-	-	5	4
Glial fibrillary acidic protein (GFAP)	P03995	46,492	38	40	73	42
Glutathione S-transferase, alpha 4	P24472	25,564	9	4	9	5
Glutathione S-transferase, mu 1	A2AE90	25,970	48	44	61	38
Glutathione S-transferase, mu 5	P48774	26,635	-	3	6	-
Glutathione S-transferase, pi 2	P46425	23,537	-	-	8	7
Glyceraldehyde-3-phosphate dehydrogenase (GAPDH)	P16858	35,810	-	-	2	7

111

Protein	Accession	MW				
Glyoxalase domain containing 4	Q9CPV4	33,317	-	-	9	-
Guanosine diphosphate (GDP) dissociation inhibitor 1	P50396	50,522	2	3	6	-
H4 histone family, member A	P62806	11,367	5	12	5	6
Heat shock 70kDa protein 8 isoform 1	P63017	70,871	10	22	30	8
Heat shock protein 4	Q5NCS5	94,209	6	7	10	-
Heat shock protein 90kDa alpha (cytosolic), class A member 1	P07901	84,788	13	12	30	8
Heat shock protein 90kDa alpha (cytosolic), class B member 1	Q71LX8	83,281	13	34	10	5
Heterogeneous nuclear ribonucleoprotein A2/B1	O88569	37,403	-	7	8	8
Hypoxanthine guanine phosphoribosyl transferase 1	P00493	24,570	-	-	3	-
Inositol monophosphatase	O55023	30,436	4	4	3	-
Isocitrate dehydrogenase [NADP] cytoplasmic	O88844	46,660	3	3	5	-
Lactate dehydrogenase 1, A chain	P06151	36,499	15	11	14	15
Lactate dehydrogenase 2, B chain	P16125	36,572	38	31	34	14
Lactoylglutathione lyase	Q9CPU0	20,810	-	6	2	2
Lamin A isoform A	P48678	74,238	-	-	7	4
Leukotriene A4 hydrolase	Q3UY71	69,051	3	-	7	-
Lysosomal alpha-mannosidase precursor (Mannosidase, alpha B)	O09159	114,604	3	10	26	10
Malate dehydrogenase 2, NAD (mitochondrial)	P08249	35,611	25	24	15	9
Malate dehydrogenase, cytoplasmic	P14152	36,511	14	6	8	5
Malic enzyme 1, supernatant	P06801	63,999	-	-	2	2
Mannosidase alpha, class 1A, member 1	Q544T7	73,276	2	16	16	13
Myosin, heavy polypeptide 9, non-muscle isoform 1	Q8VDD5	226,357	-	-	9	-
Myosin, light polypeptide 6, alkali, smooth muscle and non-muscle	Q60605	16,930	-	5	7	4
Nestin	Q6P5H2	202,011	-	9	5	-
Nit protein 2	Q9JHW2	30,502	-	-	2	-
Nucleoside-diphosphate kinase 1	P15532	17,208	3	-	6	9
Nucleoside-diphosphate kinase 2	Q01768	17,363	3	11	3	4
Ornithine aminotransferase	P29758	48,355	-	-	3	3
Peroxiredoxin 1	A2AP16	22,176	14	20	19	24
Peroxiredoxin 2 (Thioredoxin peroxidase 1)	Q61171	21,779	7	14	14	12
Peroxiredoxin 5 precursor	P99029	21,897	-	9	8	20
Peroxiredoxin 6 (Acidic calcium-independent phospholipase A2)	O08709	24,871	38	48	35	19
Phosphogluconate dehydrogenase	Q91V28	53,261	9	13	10	4
Phosphoglycerate kinase 1	P09411	44,536	22	18	13	12
Phosphoglycerate mutase 1 (brain)	Q9DBJ1	28,832	3	6	12	9
Phosphoserine aminotransferase 1	Q99K85	40,473	8	-	2	-
Plectin 1	Q9QXS1	534,216	-	-	7	-
Proteasome activator PA28 alpha subunit	P97371	28,673	-	-	4	4
Proteasome subunit, alpha type 1	Q9R1P4	29,547	7	4	4	-
Proteasome subunit, alpha type 2	P49722	25,926	-	2	6	-
Proteasome subunit, alpha type 3	Q9DCD8	28,490	9	3	2	-
Proteasome subunit, alpha type 5	Q3UPK6	26,411	4	3	5	-
Proteasome subunit, alpha type 6	Q9QUM9	27,372	4	8	4	4
Proteasome subunit, alpha type 7	Q9Z2U0	27,855	10	8	8	7
Proteasome subunit, beta type 1	O09061	26,372	8	-	7	-
Proteasome subunit, beta type 3	Q545G0	22,965	4	6	7	-

Protein	Accession	MW				
Proteasome subunit, beta type 5	Q3UZI1	28,532	6	11	7	-
Proteasome subunit, beta type 8	P28063	30,260	2	4	5	-
Purine-nucleoside phosphorylase	P23492	32,277	5	-	7	4
Pyruvate kinase isozyme M2	P52480	57,887	4	7	17	12
Rho GDP dissociation inhibitor (GDI) alpha	Q99PT1	23,407	8	8	13	14
Ribonuclease/angiogenesis inhibitor	Q91VI7	49,816	6	-	3	3
S-adenosylhomocysteine hydrolase	Q5M9P0	47,674	3	-	3	-
SH3-binding domain glutamic acid-rich protein like	Q9JJU8	12,811	3	4	5	5
Soluble calcium-activated nucleotidase 1	Q8VCF1	45,653	2	4	5	4
Spectrin alpha 2	P16546	284,597	-	3	18	-
Spectrin beta 2 isoform 1 or 2	Q62261	274,223	-	2	5	-
S-phase kinase-associated protein 1A	Q9WTX5	18,672	-	5	4	3
Superoxide dismutase 1, soluble	P08228	15,943	18	30	15	27
Thioredoxin reductase 1	Q8CI31	54,337	6	5	2	-
Transaldolase 1	Q93092	37,387	6	-	3	-
Transgelin	P37804	22,576	9	15	18	13
Transgelin 2	Q91VU2	22,395	4	11	12	10
Transitional endoplasmic reticulum ATPase (valosin-containing protein)	Q01853	89,364	27	57	31	5
Transketolase	P40142	67,630	-	-	4	-
Translin	Q62348	26,201	3	-	7	3
Triosephosphate isomerase 1	P17751	26,713	9	6	6	3
Tropomyosin 1, alpha	P58771	32,681	7	11	7	4
Tropomyosin 4, alpha	Q6IRU2	28,468	8	4	14	6
Tubulin, alpha	P05213	50,152	-	7	8	2
Tubulin, beta	Q9ERD7	50,419	-	5	7	-
Ubiquitin carboxy-terminal hydrolase L1	Q9R0P9	24,838	2	6	6	2
Ubiquitin-activating enzyme E1, Chr X	Q02053	117,809	-	4	4	2
UDP-glucose pyrophosphorylase 2	Q91ZJ5	56,979	3	4	3	-
Villin 2	P26040	69,407	-	-	8	6
Vinculin	Q64727	116,717	14	30	46	8
WD repeat domain 1	Q3TJY2	66,407	7	6	4	-

Proteins are reported with their corresponding accession number, molecular weight (MW), and redundant peptides identified for each treatment condition.

a) Accession numbers are reported from the Uniprot database (www.uniprot.org) and, when available, refer to the unprocessed precursor protein.

b) The average number of redundant peptides identified after applying the selection criteria detailed in Experimental Procedures. A null value indicates the protein did not meet the minimum criteria for identification.

CHAPTER 3

QUANTITATIVE MASS SPECTROMETRY-BASED PROTEOMICS IDENTIFIES NOVEL, NON-CONVENTIONALLY SECRETED PROTEINS IN MOUSE ASTROCYTES

By

Todd M. Greco[1], Steven H. Seeholzer[1], Adrian Mak[1], Lynn Spruce[1], and Harry Ischiropoulos[1,2]

(manuscript in preparation)

From [1]The Joseph Stokes Jr. Research Institute and Department of [2]Pharmacology, The Children's Hospital of Philadelphia and The University of Pennsylvania Philadelphia, PA, 19104, USA

Running title: Quantitative proteomics of the astrocyte secretome

Address correspondence to: Harry Ischiropoulos, Stokes Research Institute, Children's Hospital of Philadelphia, 416D Abramson Research Center, 3517 Civic Center Boulevard, Philadelphia, Pennsylvania, 19104-4318, USA. Phone: (215) 590-5320; Fax: (215) 590-4267; E-mail: ischirop@mail.med.upenn.edu.

3.1 Abstract

Growing appreciation for astrocytes as active participants in nervous system development, neurovascular metabolic coupling, as well as neurological disease progression has stimulated investigation into specific astrocyte-secreted proteins that mediate these functions. Collections of secreted proteins, known as cellular secretomes, have been investigated by mass spectrometry-based proteomics in diverse organisms, biological fluids, and cell types. While improvements in the depth of the astrocyte secretome have been significant over the last several years, integration of stable isotope dilution mass spectrometric approaches for astrocyte secretome analysis has not been performed. The current work implemented a stable isotope labeling by amino acids in cell culture (SILAC)-based method to quantify relative changes in protein abundance in the astrocyte secretome and intracellular proteome. Paired with multidimensional Gel-LC-MS/MS, SILAC quantitative analysis of astrocyte conditioned media quantified 516 proteins relative to the intracellular proteome. Ninety-two of these proteins were greater than 1.5-fold enriched in ACM, including twelve proteins that lacked N-terminal signal peptides, including vimentin, 2 histones, and ferritin light and heavy chains, suggesting their enrichment was due to secretion through nonconventional pathways. In summary, this work demonstrated the relative quantification of astrocyte-secreted proteins by SILAC quantitative mass spectrometry. This SILAC approach can aid in deciphering the distinct pathways and molecular mechanisms of protein secretion in across different cellular model systems.

3.2 Introduction

For intact tissues and whole organisms, cells rarely operate autonomously, but rather in concert with or in response to the cellular physiology of their neighbors. While these responses can be generated by direct cell-cell coupling, such as the propagation of calcium waves through gap junctions in astrocytic cellular networks (Nedergaard 1994), other responses are elicited as a result of secreted biomolecules. Stimulus-coupled neurotransmitter release is the prototypic intercellular signal in the brain; responsible for initiating activity-dependent synapse formation during development (Zito, Svoboda 2002) as well as synaptic remodeling after learning (De Roo et al. 2008). In addition, there is growing appreciation for the roles secreted proteins play in nervous system function, particularly in distinct developmental stages or disease states (Christopherson et al. 2005, Liauw et al. 2008, Nagai et al. 2007, Park et al. 2008, Krumbholz et al. 2006, Koistinaho et al. 2004, Glabinski et al. 1997). However, the intracellular molecular pathways underlying protein secretion and the subsequent extracellular signaling cascades are not completely understood.

Recent studies suggest that astrocyte protein secretion may subserve a host of critical functions within the nervous system, including synapse formation and trophic support during development (Christopherson et al. 2005), adult neurogenesis (Song, Stevens & Gage 2002) , and immune response (Dong, Benveniste 2001, Babcock et al. 2003). In particular, *in vitro* and *in vivo* synapse formation was promoted by thrombospondins secreted by immature, but not mature astrocytes (Christopherson et al. 2005). While astrocytes provide trophic, pro-survival support to neurons (Banker 1980), under cellular or physiological states associated with disease, astrocytes can shift to a

highly "reactive" phenotype (Pekny, Nilsson 2005). Under these conditions, astrocytes secret pro-inflammatory mediators, such as cytokines and chemokines (Dong, Benveniste 2001, Babcock et al. 2003) and give rise to increased levels of extracellular excitatory amino acids, such as glutamate, which can significantly impair neuronal survival (Abele et al. 1990, Ding et al. 2007). In contrast, the involvement of astrocyte-secreted proteins in these processes has not been extensively investigated.

In efforts to define the potential physiological and pathological implications of astrocyte protein secretion, several studies have begun to characterize the astrocyte secretome using cell culture conditioned medium, identifying classically secreted and nonconventionally secreted proteins as well as cytosolic proteins (Keene et al. 2009, Dowell, Johnson & Li 2009, Moore et al. 2009). Although the identification of classically secreted proteins can be confirmed by signal peptide prediction algorithms, the identification of novel nonconventionally secreted proteins is more difficult, due in part to poorly understood secretion mechanisms and lack of extensive training datasets for prediction algorithms (Bendtsen et al. 2004a). Therefore, a proteome-wide quantitative mass spectrometry-based approach that measures extracellular protein enrichment would accelerate the identification of proteins secreted by these alternative mechanisms.

Although a quantitative MS-based approach was recently applied to study protein secretion in primary astrocytes using isotopic chemical labeling of protein lysates (Delcourt et al. 2005), metabolic stable isotope labeling strategies have not been demonstrated. Metabolic labeling techniques provide accurate quantitation at low signal-to-noise and reduce errors introduced during sample preparation prior to mass spectrometry analysis (Ong, Mann 2005). SILAC has been applied in transformed cell

lines to assess relative changes in protein expression as a function of temporal and stimulus-dependent variables (Ong et al. 2002). More recent work has demonstrated success in application of SILAC to non-transformed cells, such as embryonic stem cells (Graumann et al. 2008) and primary neurons (Spellman et al. 2008). In the current work, SILAC in primary astrocyte cultures achieved at least 98 % incorporation of isotope label into the astrocyte proteome and secretome. These isotope reference proteome standards were used to evaluate astrocytic protein secretory pathways by quantitative analysis of relative protein abundance within and between the astrocyte secretome and intracellular proteome.

3.3 Materials and Methods

Chemicals and Materials. All reagents were purchased from Sigma-Aldrich (St. Louis, MO) unless otherwise stated. Custom Minimal Essential Media (MEM) lacking natural abundance L-leucine and L-lysine was purchased from AthenaES (Baltimore, MD). $^{13}C_6$-$^{15}N_2$-lysine and $^{13}C_6$-$^{15}N_1$-leucine were purchased from Cambridge Isotope Laboratories (Boston, MA).

Astrocyte culture and media conditioning. Cortical astrocyte cultures were prepared from neonatal CD-1 mice (Charles River, Wilmington, MA) on postnatal day 1 as previously described (Chapter 2, section 3) but with minor modifications. Neonatal cortices were triturated in Minimal Essential Media (Invitrogen, Carlsbad, CA) supplemented with 10% fetal bovine serum (Hyclone), sodium pyruvate (1 mM), L-glutamine (2 mM), D-glucose (42 mM), sodium bicarbonate (14 mM), penicillin (100 U/ml), streptomycin (100μg/ml), fungizone (2.5 μg/ml) and plated at 3 cortices per T-75 vent-cap flask (Corning, Corning, NY). Mixed cortical cultures were raised for 10 days in 37°C and 5% CO_2 with media change every 3-4 days. Cultures were then washed with cold EBSS and separated from neurons and microglia by shaking overnight at 37°C. Adherent cells were trypsinized (0.25%) and seeded in 100 mm Petri dishes (Corning) at 5 x 10^6 cells/plate (5 ml). Forty-two hours after plating, cells were washed three times with EBSS and then with serum-free media for 6 hours. Washing media was replaced with fresh serum-free media containing 1 ug/ml of brefeldin A or DMSO vehicle. Cell viability was quantified by trypan blue exclusion. For brefeldin A treatments, astrocyte-conditioned media (ACM) was collected after 24 hours, while all other experiments were conducted for 7 days.

ACM was pooled between three culture dishes (15 mL) and centrifuged at 500 x g for 5 min to remove cell debris. The protein fraction (> 3 kDa) was obtained by 30-fold concentration by ultrafiltration of ACM at 4 °C using CentriPrep Ultracel YM-3 filters (Millipore, Billerica, MA). Filtrates were then adjusted with protease inhibitors, 2ug/ml aprotinin, 3.3 ug/ml bestatin, 3.3 ug/ml E-64, and aliquoted and stored at -80 °C. Cell pellets were lysed by homogenization in 50 mM HEPES-NaOH, pH 7.2, containing 50 mM NaCl, 1 mM EDTA, 1% Triton-X100, and protease inhibitors (as above), incubated on ice for 20 min, and centrifuged at 20,000 x g for 20 min at 4 °C. Protein concentration of conditioned media and soluble lysates was determined by the Bradford method.

Astrocyte Stable Isotope Labeling by Amino Acids in Cell Culture (SILAC). SILAC labeling of primary astrocytes was used to generate isotope reference proteomes for both intracellular and extracellular proteomes. Astrocytes were cultured by the protocol described above, except for the modification of culture medium and culture flasks. MEM devoid of natural abundance lysine and leucine was adjusted to 10% dialyzed FBS and repleted with $^{13}C_6$-$^{15}N_2$-lysine and $^{13}C_6$-$^{15}N_1$-leucine (Cambridge Isotope Laboratories, Boston, MA). In preparation for media conditioning, enriched astrocytes were seeded in T-175 flasks at 12.7 x 10^6 cells/plate (20 mL) in serum-containing heavy medium. Forty-eight hours later, serum was withdrawn as described above, and media conditioning was performed for 7 days. Collection and processing of media and cells was performed as described above, except ACM was concentrated about 300-fold. From this protocol, one can expect about 1.5 mg of heavy labeled ACM and 25 mg of heavy labeled cell lysates. IRPs were spiked into non-labeled (light) samples at a nominal protein ratio of 1:1 or 2:3

(light:heavy). Given a single gel-LC-MS/MS analysis was performed with between 50 and 100 ug of total protein, 1.5 mg of heavy labeled ACM is sufficient for about 25 to 50 experiments.

Gel/LC-MS/MS analysis. The protein fraction obtained from ACM was analyzed by Gel/LC-MS/MS as described previously (Tang et al. 2005) with modification. Concentrated ACM was mixed with 6X LDS sample buffer and equal protein (20 – 50 ug) were loaded per lane on NuPAGE 10% Bis-Tris gels (Invitrogen, Carlsbad, CA) and electrophoresed in MOPS running buffer until the dye front reached either 1.6 or 3.2 cm. Proteins were visualized by Colloidal Blue (Invitrogen, Carlsbad, CA) and each lane was cut into uniform (2 mm) slices using a MEF-1.5 Gel Cutter (The Gel Company, San Francisco, CA). Individual gel slices were cut into 1 x 1 mm cubes and digested in-gel with trypsin as previously described (Speicher et al. 2000). Tryptic digests were analyzed on either an LTQ or hybrid LTQ-Orbitrap mass spectrometer (Thermofisher Scientific, San Jose, CA) coupled with a NanoLC pump (Eksigent Technologies, Livermore, CA) and autosampler. Tryptic peptides were separated by reverse phase (RP)-HPLC on a nanocapillary column, 75 μm id x 20 cm ProteoPep (New Objective, Woburn, MA, USA). Peptides were eluted into the mass spectrometer at 300 nL/min, running a gradient of ACN (solvent B). Each RP-LC run comprised a 15 min sample load at 1 % B and a 90 min total gradient from 5 to 45 % B. The mass spectrometer was set to repetitively scan m/z from 300 to 1700 (R = 30,000 for Orbitrap) followed by data-dependent MS/MS scans on the five most abundant ions, with a minimum signal of 1000, isolation width of 2.0, normalized collision energy of 28, and waveform injection and dynamic exclusion enabled. FTMS full scan AGC target value was 1e6, while MSn AGC

121

was 5e3, respectively. FTMS full scan maximum fill time was 500 ms, while ion trap MSn fill time was 50 ms; microscans were set at one. A hybrid LTQ-Oribtrap was utilized for all SILAC experiments with additional instrument parameters as follows: a reject mass list containing 272 fully tryptic peptide m/z values from bovine serum albumin; a 5 ppm reject mass width; FT preview mode; charge state screening, and monoisotopic precursor selection were all enabled with rejection of unassigned and 1+ charge states.

Protein Identification and Validation. DTA files were generated from MS/MS spectra extracted from the RAW data file (intensity threshold of 1000; minimum ion count 30). DTA files generated from LC-MS/MS runs belonging to the same biological samples were submitted to Sorcrerer-SEQUEST (ver. 4.0.3, rev 11; SagenResearch, San Jose, CA). Database searching was performed against a Uniprot database (Release 14.6) containing *Mus musculus* sequences from SwissProt and TrEMBL plus common contaminants, which were then reversed and appended to the forward sequences (121,248 sequences). The database was indexed with the following parameters: mass range of 600 - 4200, semi-tryptic cleavages with a maximum of 2 missed cleavage sites and static modification of cysteine by S-carbamidomethylation (+57 amu). Database searching was performed with the following parameters: precursor tolerance, 30 ppm; fragment tolerance, 1.0 amu; variable modification of methionine (+16 amu), and for SILAC experiments, variable modification of leucine (+7.017 amu) and lysine (+8.014 amu). The maximum number of variable modifications per instance and per peptide was 3 and 4, respectively. [13]C isotope mass check was enabled. SEQUEST sequence-to-spectrum assignments were analyzed by either Scaffold (Proteome Software, Portland, OR), the

TransProteomic Pipeline (TPP ver. 4.0.2), or DTASelect (ver. 2.0). Reverse database hits were used to control error rate at the peptide and protein level to less than 1 %. The following command-line parameters were used for modeling and filtering of sequence-to-spectrum assignments by DTASelect: -s 100 -d 0.1 -Smn 7 -e CON_ --iso --sp --mass --ionstat --trypstat. Peptides were assembled into protein groups to satisfy rules of parsimony requiring at least two unique peptides.

Census quantitative isotope labeling analysis. The isotope labeling feature of Census (ver. 1.44) was used for automated computation and filtering of extracted ion chromatograms and peptide ratios, respectively. Individual isotope extraction of SILAC pairs was performed with a mass tolerance of 30 ppm and a.p.e of 0.98. Default values for filtering of peptide ratios were used except an outlier p-value of 0.2 was selected. Proteins with 2 or more unique, quantified spectra were retained. Protein ratio calculation was repeated for additional sample sets and normalized ratios were calcaulted between two experimental conditions to obtain relative fold differences in protein abundance. These normalized protein ratios were utilized for downstream functional and statistical analyses.

LC-MRM-MS/MS analysis of SILAC pairs. This approach was used to determine the degree of isotope incorporation into the astrocyte proteome and to validate SILAC ratios obtained by proteome-wide SILAC quantification. Data-independent analysis of light and heavy isotope-labeled peptides was conducted using a "pseudo-MRM" approach on an LTQ instrument (Thermofisher Scientific, San Jose, CA). The RP-LC gradient was identical to the method described above. The mass spectrometer was set to repetitively perform data-independent MS^2 acquisition on specific precursor masses corresponding to

selected light and heavy labeled SILAC pairs identified from data-dependent experiments. Between 4 and 8 precursor masses (2 - 4 SILAC pairs) were monitored in a single segment, with an isolation width of 3.0, normalized collision energy of 28, 2 microscans, and accumulation time and target value of 100 ms and 5e3, respectively. Xcalibur was used to reconstruct precursor-product ion chromatograms. SILAC peptide pair ratios were computed by AUC measurements and the average of four SILAC ratios (two precursors per protein x two product ions per precursor) reflected the final protein ratio. This calculation was repeated for the same protein in the second sample to determine relative protein abundance.

Computational and functional gene ontology analysis. For computational analysis of classically secreted proteins, FASTA sequences were submitted to SignalP (Bendtsen et al. 2004b) to predict proteins containing signal peptides, followed by TargetP (Emanuelsson et al. 2000) to predict the localization (Extracellular, Mitochondria, Other). For prediction of nonconventionally secreted proteins, SecretomeP 2.0 (Bendtsen et al. 2004a) was used. FatiGO (Al-Shahrour, Diaz-Uriarte & Dopazo 2004) and Ingenuity Pathways Analysis software (Ingenuity® Systems, www.ingenuity.com) were used to provide gene ontology annotation and analysis of functional pathways, respectively.

Statistical analysis of normalized protein ratios. Histograms were constructed and statistical analyses were performed using GraphPad Prism 5 (GraphPad Software, Inc., San Diego, CA). For brefeldin A experiments, significantly altered protein ratios were determined from large-scale protein profiling experiments using the complementary error function (erfc) within Microsoft Excel (see Eq. 1), which determines the probability that each individual protein ratio is not significantly different from the average protein ratio

(Li et al. 2003). The average ratio and other parameters (shown below) were calculated

from a Gaussian least-squares nonlinear regression of the distribution of protein ratios.

Gaussian fits were constructed using the normal distribution equation provided in

GraphPad Prism with automatic outlier detection enabled.

$$p = \text{erfc}\left\{ |\log(r_p|r_0)| \middle| \sqrt{2\left((\Delta \log r_p)^2 + (\Delta \log r_0)^2 + \sigma^2\right)} \right\} \quad \text{(Eq. 1);}$$

where $\Delta \log r_p = 0.4343\left(\Delta r_p / r_p\right)$, $\Delta \log(r_0) = 0.4343\left(\Delta r_0 / r_0\right)$, r_p and $\Delta r_p =$
protein abundance ratio and its associated error, r_0 and $\Delta r_0 =$ average curve fit ratio and
its associated error, and $\sigma =$ mean error of the background distribution.

3.3 Results

Work from our lab and others have established astrocytes as a viable model for the study of protein secretion under various cellular conditions (Lafon-Cazal et al. 2003, Keene et al. 2009, Dowell, Johnson & Li 2009, Moore et al. 2009). In an effort to further understand and define the pathways of astrocyte protein secretion, we used SILAC in primary mouse astrocyte cultures. Using this approach, isotope reference proteomes (IRPs) were generated in independent experiments and then spiked into samples collected from natural abundance culture conditions. This strategy has been previously used to uncover novel biomarkers and pharmacological targets for leukemias with MLL translocations (Yocum et al. 2006). Except for the addition of heavy labeled amino acids, $^{13}C_6$-$^{15}N_2$-lysine and $^{13}C_6$-$^{15}N_1$-leucine, to medium that was devoid of their light counterparts, this approach did not require significant changes in preparation of enriched astrocyte cultures as compared to our previous work (Keene et al. 2009). Briefly, mixed glial/neuronal cortical cultures were established from cortices dissected from a total of 20 P1 neonatal CD-1 mice and maintained in heavy labeled medium from *in vitro* day 0 until the end of the experiment at day 20. At 11 days *in vitro*, cells were washed, trypsinized and combined into a single cell stock, which was used to establish enriched cultures (> 95% astrocytes). After 48 hours, astrocytes were switched to serum-free heavy isotope-containing media and remained in culture without media change for additional 7 days. No apparent differences in rate of proliferation, gross morphology (as visualized by light microscopy), or cell viability were observed (data not shown). After collection of both astrocyte-conditioned media (ACM) and cells, ACM was concentrated by 300-fold and

cells were lysed. The heavy labeled ACM IRP yielded about 1.5 mg of protein, while the astrocyte lysate IRP yielded approximately 25 mg of protein.

Data-dependent and –independent mass spectrometric analyses were performed on each IRP to determine atom percent excess of stable isotope incorporation. Protein aliquots (25 ug) from each IRP were in-solution trypsin digested. Tryptic peptides (5 ug) were separated by reverse-phase LC and analyzed by either data-dependent MS/MS conducted on an LTQ-Orbitrap or by a data-independent "pseudo-MRM" approach on an LTQ mass spectrometer. For the former approach, 1085 and 2067 unique peptides were identified from ACM and lysate IRPs, respectively, with less than 1 % of unique peptides containing a light leucine or lysine. Atom percent excess was estimated by Census, a quantitative software tool that provides automated reconstruction of light/heavy (SILAC) extracted ion chromatograms and computation of SILAC peptide ratios (see *Materials and Methods*). For greater than 98% of the leucine and/or lysine-containing peptides, the light component was below the limit of quantification, resulting in a SILAC ratio of zero. In contrast, vimentin was identified with 3 light peptide sequences (30 unique peptides total), which allowed more accurate quantification. Reconstruction of extracted ion chromatograms from two of the SILAC peptide pairs, EEAESTLQSFR and DNLAEDIMR, gave SILAC ratios that were 0.02 (1:50), corresponding to an estimated atom percent excess of about 98% (Figure 3-1A, B).
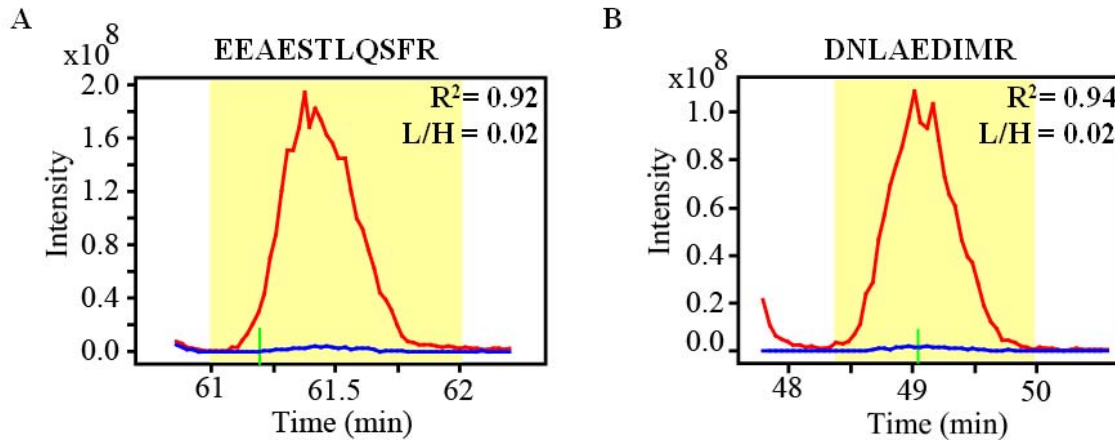
Figure 3-1. Extracted ion chromatograms of vimentin peptides identified from ACM isotope reference proteome. Extracted ion chromatograms were constructed by the Census quantitation tool with automatic thresholds for acceptance of light/heavy extracted ion chromatograms were set at a correlation coefficient of 0.7 and outlier detection value of 0.2. Extracted ion chromatograms shown above are from two peptides from vimentin, (A) EEAESTLQSFR and (B) DNLAEDIMR, which were identified from the ACM isotope reference proteome. Extracted ion chromatograms have excellent correlation coefficients, reflecting a light (*blue trace*) to heavy (*red trace*) ratio of 0.02, which would be the equivalent of 98 % isotopic enrichment.

Data-independent mass spectrometric analysis of IRPs supported the Census analysis. In these experiments, 16 SILAC peptide pairs were selected for MS/MS analysis (2 unique peptides from 4 ACM proteins and from 4 cell lysate proteins). Reconstruction of precursor-product ion chromatograms for peptide pairs from GAPDH showed greater than 98 % incorporation (data not shown). Moreover, for the remaining 14 peptides, the intensity of the light component was undetectable. Collectively, these data demonstrate that culturing primary mouse astrocytes in isotope-containing medium for 20 days in vitro achieved at least 98 % incorporation for the majority of the intracellular and extracellular proteome.

As a proof-of-concept, the IRPs were used to quantify alterations in the astrocyte proteome and secretome following exposure of cells to brefeldin A (BFA), an inhibitor of

vesicular transport between the ER and Golgi compartments. A previous study clearly documented inhibition of classically secreted proteins in astrocytes after treatment with 1 ug/mL of BFA for 24 hours (Lafon-Cazal et al. 2003); and therefore would serve as a useful model to develop SILAC quantitative analysis of the astrocyte secretome and proteome. Consistent with the previous work, BFA exposure did not significantly impair cell viability (data not shown). ACM and soluble intracellular protein lysates were isolated from control and BFA-treated astrocytes, normalized by protein, and mixed in equal amounts with their respective IRP. Samples were separated by SDS-PAGE and in-gel digested with trypsin. Peptides (~2.5 ug) from each gel slice were analyzed by LC-MS/MS using an LTQ-Orbitrap XL.

SEQUEST sequence-to-spectrum assignments were generated and probabilistic validation of peptides was performed by PeptideProphet (Keller et al. 2002a). Peptide assignments were filtered by probability to achieve an error rate of less than 1 % and then analyzed by Census. In total, 231 and 535 normalized protein ratios ($Ratio_{BFA}/Ratio_{Ctl}$) were calculated for proteins in ACM and cellular lysates, respectively. (Figure 3-2A). Large-scale protein expression profiling studies by isotopic labeling have different statistical approaches to classify proteins that exhibit differential expression or abundance (Oda et al. 1999, Li et al. 2003). One approach, implemented by Li and colleagues in the ASAPRatio algorithm (Li et al. 2003), modeled a best-fit Gaussian curve to the distribution of protein ratios, and then computed the complementary error function to test the null hypothesis that each protein ratio was not significantly different from the mean curve fit ratio (see *Materials and Methods*). Using this approach, the distribution of cellular lysate protein ratios showed a good fit to the Gaussian curve and resulted in a

mean curve fit ratio close to the expected 1:1 (1.28 ± 0.01) (Figure 3-2B). Statistical analysis identified 21 out of 535 proteins that were significantly altered due to BFA treatment (p < 0.05) (Figure 3-2C). Proteins such as coatomer subunit beta and gamma as well as RAP guanine nucleotide exchange factor 2 were down-regulated due to BFA treatment (Table 3-1). In contrast, the relative intracellular abundance of several classically secreted proteins were found significantly increased, including cathepsin L1 precursor (9.4-fold), apolipoprotein E precursor (21-fold), and thrombospondin-1 precursor (28-fold). Also, the ATP-binding cassette sub-family A member 1 (ABCA1) was increased five-fold, consistent with its functional relationship between apolipoprotein E lipidation and promotion of mature lipoparticle secretion from astrocytes (Hirsch-Reinshagen et al. 2004) as well as macrophages (Von Eckardstein et al. 2001). Moreover, the glucose-regulated proteins, grp78 and grp94, were 3.4±1.5-fold (p = 0.06) and 2.32±1.05-fold (p = 0.25) increased after BFA treatment, respectively, though these changes did not reach significance. These data support the SILAC methodology as a useful tool in relative quantification of intracellular protein abundance in primary astrocytes.

This analysis was then performed to quantify the concomitant changes in protein abundance in ACM after BFA treatment. In contrast to cellular lysate protein ratios, the distribution of ACM protein ratios deviated from normality (Fig 3-2D), which was not unexpected given that a significant proportion of proteins identified in ACM contain an N-terminal signal peptide and therefore would be potential targets of BFA-mediated inhibition. Although this resulted in curve fit values with a larger standard deviation and a wider distribution (σ) (see Fig 3-2), the strong inhibitory effect of BFA on classical

secretion permitted the identification of 55 proteins that were significantly decreased in ACM after BFA treatment ($p < 0.05$) (Table 3-2 and Figure 3-2E); 51 of which contained an N-terminal signal peptide. Overall, these experiments demonstrated that SILAC-generated IRPs can be employed to identify proteins with relative abundance changes in the astrocyte secretome and intracellular proteome.
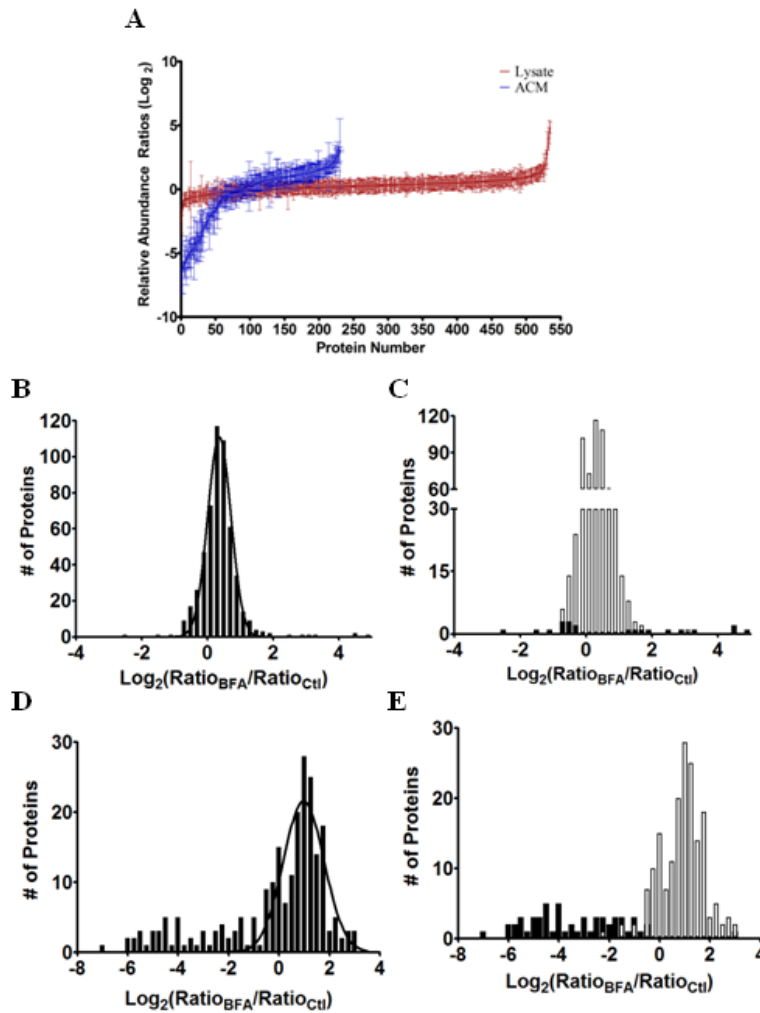
Figure 3-2. Brefeldin A-induced changes in relative protein abundance. Relative protein abundance ratios were calculated by normalizing protein ratios calculated in the BFA-treated astrocyte sample to the corresponding protein ratio from the control sample. Gaussian curve fit parameters; mean ratio (r_0), standard deviation of the mean ratio (SD), and the background distribution (σ) were calculated for protein ratio distributions. (A) Individual $\log_2$ protein ratios from ACM (blue; N = 231) and cell lysates (red; N=535) plotted in order of increasing relative abundance. (B) Histogram of BFA-induced changes in cell lysates as a function of $\log_2$ normalized protein ratio. Protein ratio distribution provided a good fit to the Gaussian curve ($r_0 \pm$ SD = 1.28 ± 0.01, σ = 1.28). (C) Significantly altered cell lysate protein ratios (black) versus non-significant protein ratios (white) calculated using the complementary error function (p < 0.05) and Gaussian curve fit values. (D) Histogram of BFA-induced changes in relative protein abundance of ACM proteins. Curve fit values for ACM protein ratios were $r_0 \pm$ SD = 1.97 ± 0.10, σ = 1.75. (E) Significantly altered cell lysate protein ratios (black) versus non-significant ratios (white) calculated using the complementary error function (p < 0.05) and Gaussian curve fit values.

Next, this SILAC workflow was employed to assemble a quantitative protein enrichment profile of astrocyte conditioned media under basal cell culture conditions. The degree of enrichment for each protein would be calculated by the relative abundance between the extracellular and intracellular compartments, essentially reflecting the extent of protein secretion. For this purpose, a combined "whole cell" IRP was generated that contained reference proteins from both the intracellular and extracellular proteomes. This IRP was then spiked into ACM and cell lysates samples obtained from the same astrocyte culture after 7 days of conditioning in light isotope-containing media. Samples (100 ug) were split between two lanes, resolved by SDS-PAGE and in-gel trypsin digested. Extracted peptides corresponding to gel slices from replicate lanes were pooled and analyzed by LC-MS/MS. SEQUEST sequence-to-spectrum assignments were analyzed by DTASelect and Census, resulting in the relative quantification of 516 proteins. Normalized protein ratios ($Ratio_{ACM}/Ratio_{Lysate}$) represent the fold difference in abundance between the extracellular and intracellular proteomes. The distribution of protein enrichment ratios spanned at least 4 orders of magnitude (Figure 3-3A) and included cytosolic proteins such as filamins and ribosomal subunits that were 20-fold to 50-fold more abundant in cell lysates, as well as known secreted proteins such as SPARC and alpha-2-macroglobulin, which were 20- to 50-fold more abundant in ACM (see Table 3-3). An additional 109 protein ratios were calculated in the ACM sample, but could not be normalized by the respective protein ratio in cellular lysates as the ratio was zero.

As MRM quantitative MS analysis can provide improved selectivity and sensitivity compared to non-targeted, global approaches based on precursor (MS^1) ion abundances, the former approach was used to estimate the linear range of ACM

enrichment ratios calculated by global SILAC analysis. Six proteins were selected, GAPDH, triosphosphate isomerase, glyoxylase domain-containing protein 4, alpha-N-acetylglucosaminidase, histone H4, and SPARC, which ranged in relative enrichment from -6 to +6 ($\log_2$ units), respectively. Light-to-heavy peptide ratios were calculated from data-independent collection of MS/MS spectra and reconstruction of precursor-product ion chromatograms by Xcalibur. MRM protein enrichment ratios were then calculated as the average ratio from two unique peptides and two distinct precursor-product ion transitions per peptide. As shown in figure 3-3B, the global SILAC method yielded enrichment ratios that were in good agreement with targeted MRM ratios between +4 and -4 $\log_2$ units, while for ratios outside this range, enrichment ratios measured by SILAC were systematically greater than those measured by MRM.

Segregation of ACM enrichment ratios by subcellular localization showed a strong clustering as a function of degree of enrichment (Figure 3-3C). A 1.5-fold or greater enrichment ratio cut-off was selected to represent significantly enriched proteins in ACM as this ratio equaled two times the median relative standard deviation of all enrichment ratios (RSD = 25 %; N = 516). As expected, the extracellular/membrane protein group had the largest proportion of significantly enriched ratios (N = 52/62; median = 8.92-fold) (Figure 3-3C). These proteins also showed the widest range of enrichment ratios, consisting of constitutively secreted proteins with large (> 50-fold) enrichment ratios such as extracellular superoxide dismutase and osteopontin, as well as secreted proteins with enrichment ratios less than one, such as mesencephalic astrocyte-derived neurotrophic factor/protein ARMET (0.32-fold) and gelsolin (0.48-fold). Additionally, a majority of proteins localized to the endosomal/lysosomal compartment

were significantly enriched (N = 22/31; median = 1.96-fold). In contrast, median enrichment ratios for proteins localized to the ER/Golgi/mitochondria were not significantly enriched, though six proteins were enriched on an individual basis (Figure 3-3C). The remaining 392 proteins quantified did not contain N-terminal signal peptides, consistent with the observation that the majority (378/390) had enrichment ratios below 1.5-fold (Figure 3-3C). The 12 proteins lacking signal peptides but which were enriched in ACM were analyzed by SecretomeP, a computational prediction algorithm for nonconventional protein secretion (Bendtsen et al. 2004a). Interestingly, 7 of these proteins were predicted as nonconventionally secreted including vimentin (26-fold), ferritin heavy chain (3.6-fold), and histone H2A.x (6.8-fold), while the other 5 proteins included ferritin light chain (3.8-fold), Rho GDP-dissociation inhibitor 2 (4.8-fold), and histone H4 (16.2-fold).
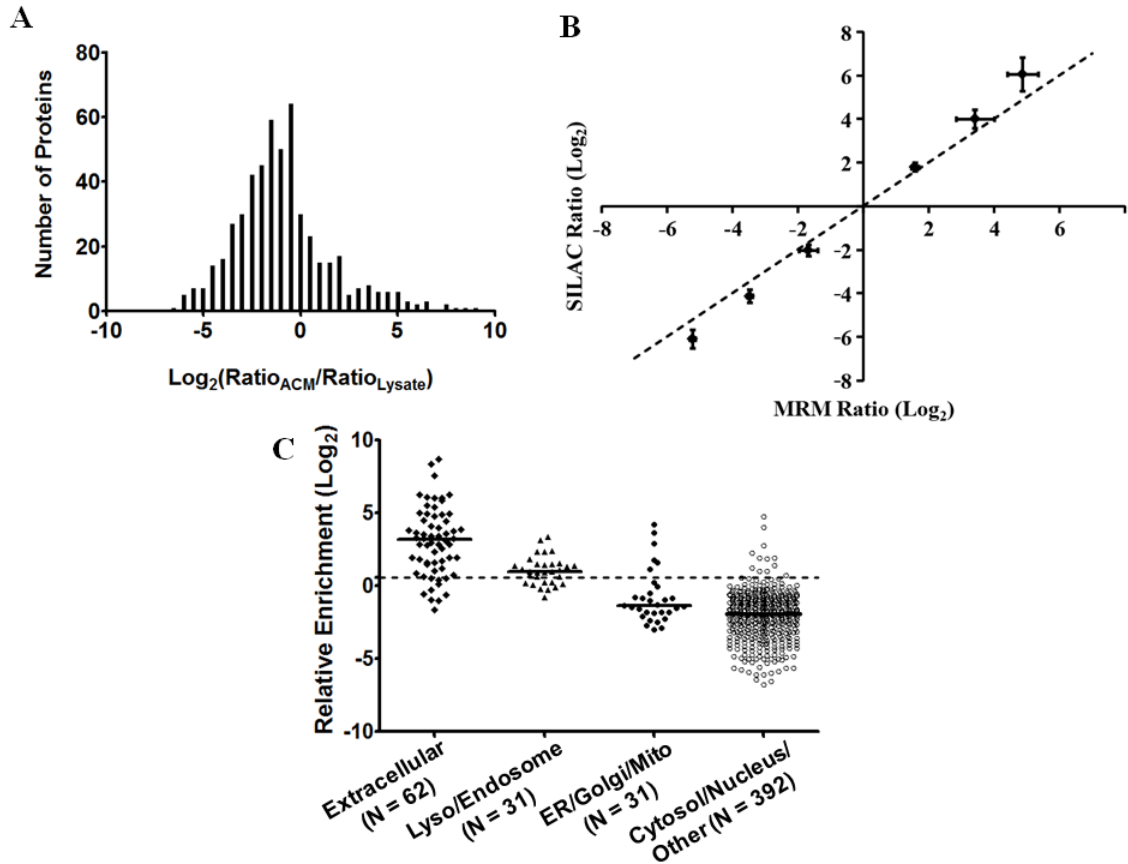
Figure 3-3. Quantification of relative protein enrichment in ACM by SILAC. ACM and cell lysates were collected following 7 days of media conditioning. Equivalent amounts of an isotopic reference proteome were spiked into ACM and cell lysates and analyzed by quantitative mass spectrometry. (A) Histogram of 516 relative enrichment ratios, expressed as normalized $\log_2$ ratios of ACM protein ratios to their corresponding cell lysate protein ratios. Positive values represent proteins that were enriched in ACM, while negative values represent proteins that were enriched in cell lysates. A linear protein ratio of 1.5-fold is depicted by a vertical dashed line. Protein ratios greater than 1.5-fold were considered significantly enriched in ACM.   (B) Comparison of protein abundance ratios obtained by global SILAC MS/MS analysis to abundance ratios for the same proteins calculated by targeted MRM-MS/MS analysis. Six proteins that ranged from -6 to +6 $\log_2$-fold enriched in ACM were selected for MRM-MS/MS analyses. MRM protein ratios were calculated as the average light-to-heavy ratio of at least 2 unique peptides with two different precursor-product ion transitions per peptide. A dashed line representing the ideal 1:1 correlation is plotted for reference. (C) Protein ratios from A were separated by subcellular localization. Subcellular localization prediction was performed using SignalP and TargetP algorithms as well as the Uniprot Knowledgebase. Proteins which did not contain a predicted signal peptide were placed in the "cytosol/nucleus/other" category. A protein ratio of 1.5-fold is indicated by the dashed horizontal line, while solid horizontal lines represent median relative enrichment ratios.

136

Extracted ion chromatograms for these proteins were derived from at least two unique peptides and showed correlation coefficients of greater than 0.7. A representative example is shown for histone H4 in figure 3-4. Reasonable sequence coverage (42 %) was obtained for histone H4 and high quality MS/MS spectra were acquired for both the light (Figure 3-4B, *top*) and heavy (Figure 3-4B, *bottom*) TVTAMDVVYALK peptides. ACM enrichment of H4 was supported by extracted ion chromatograms (XICs) that provided relatively SILAC peptide ratios with a relative standard deviation of 26 % (N = 6). A typical XIC (Figure 3-4C) for the TVTAMDVVYALK SILAC pair quantified in ACM (Figure 3-4C, *top*) and cell lysates (Figure 3-4C, *bottom*) showed identical reference peptide intensities (4.0×10^{6}) for both samples (Figure 3-5C, *red traces*), while only the endogenous intensities were significantly different (Figure 3-5C, *blue traces*).

Finally, SecretomeP was used to evaluate potential proteins that proceed by nonconventional secretion from the group of 378 proteins that were not significantly enriched in ACM. Interestingly, 153 were predicted to be nonconventionally secreted including known nonconventionally secreted proteins such as galectins, macrophage migration inhibitory factor, and acyl-CoA-binding protein (Nickel, Rabouille 2009, Kinseth et al. 2007, Seelenmeyer, Stegmayer & Nickel 2008, Merk et al. 2009).
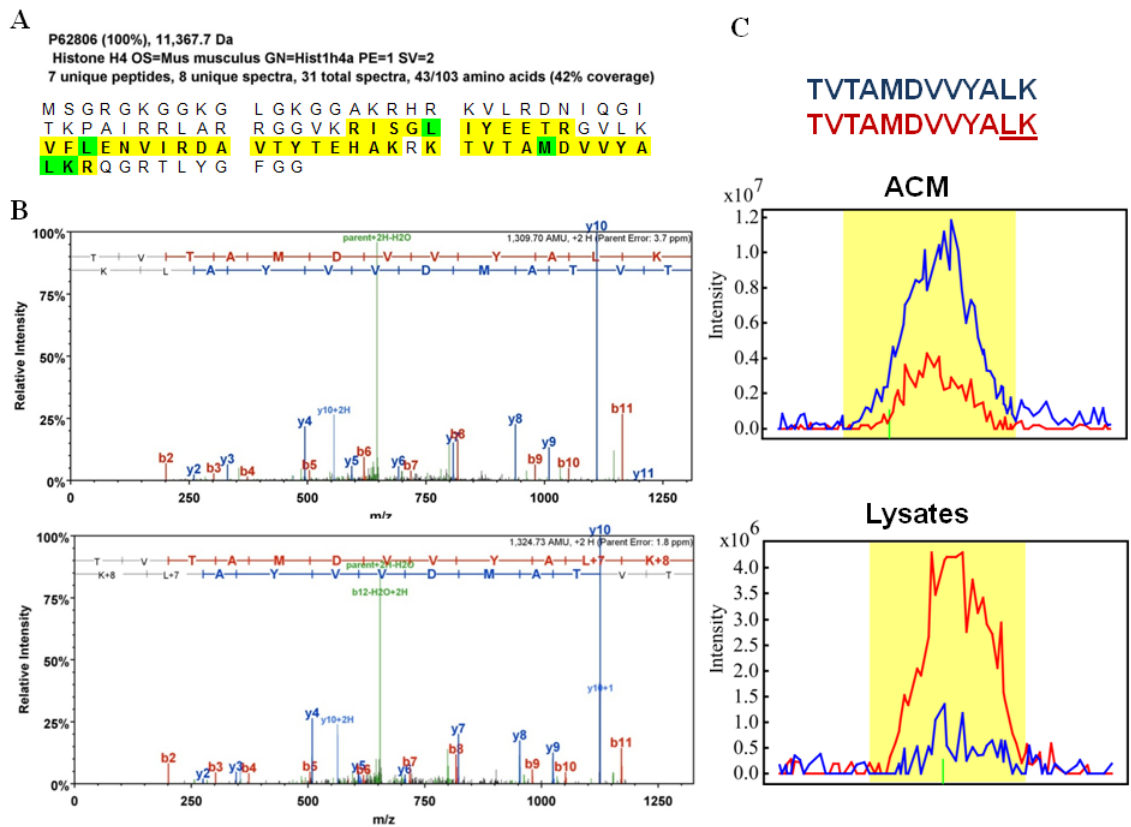
Figure 3-4. Identification and quantification of histone H4. Excellent sequence coverage and high quality MS/MS spectra and extracted ion chromatograms support the identification and relative quantification of histone H4. (A) Amino acid sequence of histone H4. Sequence coverage is highlighted in yellow based on peptides identified; variable modifications are indicated in green. (B) MS/MS spectra corresponding to the light (*top*) and heavy labeled (*bottom*) doubly charged tryptic peptide, TVTAMDVVYALK, identified from ACM sample with less than 5 ppm error. (C) Extracted ion chromatograms constructed by Census, representing light and heavy peptide intensity as a function of time for the same peptide, TVTAMDVVYALK, compared between ACM (*top*) and cell lysates (*bottom*). The yellow highlighted area represents the region used for integration and the green bar indicates the time of MS/MS acquisition.

3.5 Discussion

Cellular and tissue secretomes represent an important, but often overlooked cellular sub-proteome. Recently, the astrocyte secretome has gained greater interest in the neuroscience community as astrocyte-derived protein secretion has recognized roles in nervous system development, neurogenesis, and neurological diseases, such as Alzheimer's, amyotrophic lateral sclerosis (ALS), and multiple sclerosis (Cassina et al. 2005, Seth, Koul 2008, Antony et al. 2004). Also, methodological and technical improvements in mass spectrometry-based proteomics have enabled greater depth of analysis for the astrocyte secretome, allowing comparative analyses of secretomes under different conditions and the identification of novel astrocyte-secreted factors (Keene et al. 2009, Dowell, Johnson & Li 2009, Moore et al. 2009). Yet quantitative analysis of cellular secretomes is necessary to adequately define protein secretion, particularly with respect to distinct secretory pathways and molecular mechanisms. Although global quantitative MS strategies have been developed to study differential protein secretion in primary astrocytes (Delcourt et al. 2005), strategies incorporating stable isotope labeling in primary astrocytes have not been demonstrated. Here, a modified SILAC approach was employed in primary astrocyte cultures, providing a quantitative profile of ACM protein enrichment.

The feasibility of SILAC quantitative MS for primary astrocytes was confirmed with stable isotope incorporation at 98 % or greater at 20 days *in vitro*. Previous SILAC studies conducted in primary neurons demonstrated incorporation to a maximum of 80 % incorporation (Spellman et al. 2008). The difference in isotope incorporation between neurons and astrocytes likely resulted from the ability of P1 astrocytes to maintain their

139

proliferative state when cultured under serum conditions. The generation of isotope reference proteomes (IRPs) made generating a heavy isotope culture unnecessary for each new experiment, which for a primary culture system is particularly useful as their preparation is often more technically challenging and laborious. Also, IRPs provided a reproducible proteome standard, which is sufficient to conduct hundreds of large-scale quantitative experiments. And since the same IRP serves as a reference for all samples, any error introduced due to culturing under heavy-labeled conditions would be normalized in the calculation of the final protein abundance ratio.

These isotope reference proteomes were used to quantify changes in protein abundance within intracellular and extracellular proteomes after brefeldin A treatment. BFA treatment was selected as a proof-of-concept for several reasons: (1) the direct effects of BFA on classical protein secretion have been well-documented (Donaldson, Finazzi & Klausner 1992, Helms, Rothman 1992), (2) predictive capabilities of N-terminal signal peptides for classical protein secretion are specific and sensitive (Bendtsen et al. 2004b, Emanuelsson et al. 2000), and (3) the treatment conditions and effects of BFA on primary astrocyte cultures have been previously documented (Lafon-Cazal et al. 2003). Overall, the proteins identified as differentially expressed in the intracellular proteome due to BFA treatment were consistent with the targeting of the ER-Golgi trafficking system, including downregulation of several vesicular transport proteins as well as increased abundance of classically secreted proteins, which likely resulted from an inhibition of secretion. Grp78 and grp94 were both upregulated, and though their changes did not reach statistical significance ($p > 0.05$), upregulation of glucose-regulated proteins is a known consequence of ER stress and the unfolded protein

response (Price, Mannheim-Rodman & Calderwood 1992). The observation that BFA exposure only induced a modest upregulation of these glucose-regulated proteins, while clearly inhibiting classical proteins secretion, suggested that the concentration and time course of BFA treatment was appropriate. For the extracellular proteome, statistical analysis of SILAC ratios identified classically secreted proteins with greater than 90 % specificity.

On the other hand, quantitative analysis failed to identify 49 signal peptide-containing proteins as significantly inhibited after BFA treatment. Several possibilities could explain this result. For instance, not all luminal or integral membrane proteins (which have a signal peptide) would actively accumulate in conditioned media. Alternatively, some signal peptide-containing proteins, such as CD45 and cystic fibrosis transmembrane conductance regulator (CFTR), can be secreted by Golgi- or COPII-independent mechanisms (Fatal et al. 2004, Baldwin, Ostergaard 2002, Wang et al. 2004) and therefore would be BFA-insensitive. Also, statistical analysis of protein ratios distributions maintained a high specificity, which could lower overall sensitivity for the identification of classically secreted proteins. Also, deviation of the protein ratio distribution from normality was a contributor to reduced sensitivity as the distribution around the mean ratio (σ) was wider than for the cellular lysate distribution. This highlights a challenge for differential quantitative proteomic experiments where a large proportion of the proteome is significantly altered. For these cases, development and validation of more sophisticated statistical analyses will be valuable for improving sensitivity and accuracy while maintaining low error rates.

The primary goal of this work was to utilize SILAC in primary astrocytes to generate a quantitative protein enrichment profile of astrocyte conditioned media under basal culture conditions. For this purpose, a "whole cell" (lysate + secretome) isotope reference proteome was employed to quantify 516 proteins in ACM. An additional 109 proteins had to be excluded as valid ratios were only obtained in the ACM sample, but not in the cellular lysate sample. Yet these proteins were *identified* by reference peptides in the cellular lysate sample. As seventy-five percent of the proteins possessing a signal peptide, this suggests that low intracellular abundance of these proteins precluded their quantification. Also, increased sample complexity in cellular lysates may have impaired the calculation of protein ratios, especially at low signal-to-noise. Therefore, SILAC quantitative MS studies will benefit from advances in instrument sensitivity as well as in quantitative software development. The current Census quantitative analysis tool supports an alternative algorithm to detect and quantify instances where only a single light or heavy peptide is identified, referred to as "singleton" peptide quantification (Park et al. 2008a). Although this feature was available in the current software version, it was not integrated into the automated workflow at the time this study was performed. Further improvements in detection and quantification algorithms will aid in increasing the dynamic range of quantitative MS experiments.

Correlation of relative enrichment ratios with subcellular localization (Figure 3-3C) served not only as validation of the SILAC ACM enrichment analysis, but also facilitated the identification of proteins with enrichment ratios that differed from the mean ratio within each subcellular compartment. For instance, ten extracellularly-localized proteins (containing N-terminal signal peptides) were not found significantly

enriched in ACM (< 1.5-fold), such as thrombospondin 1 (1.42-fold) and angiotensin-converting enzyme (1.30-fold), which were just below the significance threshold. Yet other proteins such as ARMET (0.32-fold) and gelsolin (0.48-fold) had relative enrichment ratios that were more similar to intracellular protein ratios. Interestingly, gelsolin can exist in three different isoforms derived due to alternative mRNA splicing (Kwiatkowski, Mehl & Yin 1988, Vouyiouklis, Brophy 1997). One isoforms lacks a signal peptide and functions predominantly in the cytosol as an actin-binding protein. The other isoforms are identical in sequence except for the addition of an N-terminal signal peptide. Upon secretion, these proteins retain their actin-binding ability and may function extracellularly in actin filament clearance after tissue injury (Kwiatkowski, Mehl & Yin 1988). Given the enrichment ratio of gelsolin was significantly less than one, the steady-state levels of total gelsolin under basal conditions are predominantly cytosol, consistent with the proposal that secreted gelsolins function primarily after injury. These data suggest that secreted proteins with enrichment ratios significantly less than one correspond to proteins that have dual extra/intracellular function or to proteins that enter stimulus-dependent, regulated secretory pathways.

A subset of proteins was identified that traditionally reside in membrane-bound compartments such as lysosomes or ER, but which exhibited ratios with significant enrichment in ACM, suggesting they may be actively secreted products. The most prominent of these proteins included 22 lysosomal proteins such as cathepsin B (2.2-fold), D (5.25-fold), S (10.1-fold), and Z (1.5-fold), alpha-N-acetylglucosaminidase (3.5-fold), and beta-mannosidase (5.0-fold). Cell types from the haematopoietic lineage, such as neutrophils, basophils, and cytotoxic T lymphocytes, possess secretory lysosomes

(Stinchcombe, Bossi & Griffiths 2004, Holt, Gallo & Griffiths 2006), which function primarily in immune defense. Although astrocytes are not derived from this lineage, the role of astrocyte in CNS immune responses has been well studied (Dong, Benveniste 2001) and recent work has shown that cultured astrocytes spontaneously internalize styryl dyes into a lysosomal/endosomal vesicular pool, a subset of which could undergo calcium-depenent exocytosis (Li et al. 2008). Also, ATP release from astrocytes, which subserves vital astrocyte functions including calcium wave propagation (Nedergaard 1994) and modulation of synaptic transmission (Haydon, Carmignoto 2006), was found to occur from a lysosomal vesicular pool (Zhang et al. 2007). While the roles of lysosomal secreted proteins in astrocytes are unclear, one could speculate that lysosomal enzymes may function in the extracellular space for tissue remodeling following cellular injury.

Proteins with typical cytosolic or nuclear subcellular localizations were also identified enriched in ACM, suggesting they proceed by nonconventional secretion. The most prominent of these being vimentin, which has been previously identified in astrocyte conditioned media by mass spectrometry-based proteomics (Keene et al. 2009) and as secreted by a nonconventional mechanism from by activated macrophages (Mor-Vaknin et al. 2003). Moreover, this study identified ferritin light and heavy chains as enriched in ACM. The secretion of ferritin chains has recently been documented in macrophages, which was shown to provide a functional ferritin-iron source for cultured erthyroid precursor (Leimberg et al. 2008). Although glial cells possess abundant ferritin and are able to accumulate iron, they lack transferrin receptors, which are thought to

mediate much of brain-derived cellular import of iron (Dringen et al. 2007). Therefore, the role of astrocytes in brain iron homeostasis is still unclear.

The extracellular enrichment of histone H4 (16-fold) as well as histone H2A (6-fold) was an unexpected finding, though several lines of evidence argue against non-specific release. Histone H4 showed confident MS/MS spectral assignments and quantitative analysis showed a 16-fold ACM enrichment, calculated from 6 unique peptides with a relative standard deviation of 26 % (Figure 3-4). In contrast, other nuclear proteins, exportin-1 and exportin-2, had enrichment ratios of 0.20 and 0.32, respectively. Moreover, the intracellular abundance ratio of GAPDH to histone H4 was nearly 70:1, while the extracellular abundance ratio was 1:15, suggesting that the enrichment of H4 in conditioned media was independent of cell death/lysis. Functionally, histones have been proposed to serve as extracellular messengers stimulating the secretion of growth factors, as demonstrated by the stimulation of prolactin release in rat pituitary cells (Brown et al. 2000). Also, secreted histone H4 was recently found responsible for a majority of the antimicrobial action of human sebocytes (Lee et al. 2009). Also, nuclear proteins HMGB1 and YC-1 have been shown to be nonconventionally secreted, exerting mitogenic extracellular functions such as proliferation and migration (Gardella et al. 2002, Frye et al. 2009). Yet the function(s) that secreted histone H4 may serve in astrocytes is currently unknown and will require further investigation.

Large-scale, proteomic approaches to identify proteins secreted by nonconventional pathways can be of great use as prediction algorithms for non-conventional secretion achieve about half the sensitivity of their classical counterparts (Bendtsen et al. 2004b, Bendtsen et al. 2004a). As this may be due in part to the lack of

robust training datasets, quantitative proteomics studies are a valuable complement to these bioinformatic tools as they do not rely on *a priori* knowledge and may aid in refining predictive algorithms by providing additional nonconventionally secreted proteins for training data sets.

In summary, this work demonstrated a SILAC-based quantitative proteomics method using isotope reference proteomes which were used to quantify relative protein abundance changes within intracellular and extracellular proteomes as demonstrated by brefeldin A treatment of primary astrocyte cultures. A "whole-cell" isotope reference proteome was utilized to assemble a quantitative protein enrichment profile of ACM under basal culture conditions. In combination with computational prediction algorithms and subcellular localization, the ACM enrichment profile revealed a large dynamic range of protein abundance in conditioned media that provided clues as to the potential functional roles of these proteins. For signal peptide-containing proteins, protein enrichment was consistent with the functional difference between constitutively secreted proteins, which are predominantly extracellular, and proteins that undergo regulated release, which largely exist intracellularly in secretory storage vesicles. The enrichment of lysosomal proteins in ACM further supports the capacity of astrocytes to undergo exocytosis of secretory lysosomes, suggesting that in addition to ATP release, secretory lysosomes may release luminal contents as an extracellular signal. More broadly, the comparison of ACM protein enrichment profiles between cellular states where protein secretion has been altered will further advance our understanding of these diverse secretory pathways, encompassing both classical as well as non-conventional secretion.

Table 3-1. BFA-sensitive proteins in cell lysates.

Accession	Protein name	Protein ratio[1]	SD ratio[2]	P-value[3]	CV (%)	SP[4]
P35441	Thrombospondin-1 precursor	28.08	8.50	1.67E-15	30.3	Y
Q61207	Sulfated glycoprotein 1 precursor	21.98	13.81	2.28E-05	62.8	Y
P08226	Apolipoprotein E precursor	21.19	6.10	8.66E-14	28.8	Y
P06797	Cathepsin L1 precursor	9.39	0.81	1.04E-14	8.6	Y
O70310	Glycylpeptide N-tetradecanoyltransferase 1	7.41	0.81	4.20E-11	11.0	N
P41233	ATP-binding cassette sub-family A member 1	5.63	2.15	1.01E-03	38.2	Y
P03995	Glial fibrillary acidic protein	3.31	0.41	4.58E-04	12.4	N
Q8BU30	Isoleucyl-tRNA synthetase, cytoplasmic	2.88	0.65	1.35E-02	22.6	N
P55937	Golgin subfamily A member 3	2.71	0.50	1.31E-02	18.6	N
Q9CZ44	NSFL1 cofactor p47	2.19	0.22	3.85E-02	10.1	N
Q99K01	Pyridoxal-dependent decarboxylase domain-containing protein 1	0.75	0.04	3.68E-02	5.4	N
Q62446	FK506-binding protein 3	0.71	0.08	3.35E-02	12.0	N
P17439	Glucosylceramidase precursor	0.67	0.00	1.01E-02	0.6	Y
Q9JIF7	Coatomer subunit beta	0.66	0.14	4.29E-02	21.4	N
P29758	Ornithine aminotransferase, mitochondrial precursor	0.64	0.10	1.86E-02	15.9	Y
Q61292	Laminin subunit beta-2 precursor	0.58	0.11	1.33E-02	19.7	Y
Q8CHG7	Rap guanine nucleotide exchange factor 2	0.58	0.03	1.73E-03	4.5	N
Q9QZE5	Coatomer subunit gamma	0.56	0.15	2.38E-02	26.8	N
Q8BYM7	Radial spokehead-like protein 3	0.44	0.10	1.54E-03	22.2	N
Q9DB41	Mitochondrial glutamate carrier 2	0.31	0.09	1.71E-04	27.8	N
Q8VDQ8	NAD-dependent deacetylase sirtuin-2	0.17	0.11	2.62E-03	61.6	N

Proteins are sorted in order of decreasing protein ratio.

[1]Calculated from the intensity weighted average of individual peptide ratios. Ratio reflects the relative protein abundance fold change due to BFA treatment.

[2]Standard deviation of the average protein ratio calculated based on variance in peptide ratios.

[3]P-value calculated by the complementary error function (see *Materials and Methods*). $P < 0.05$ was required for significance.

[4]Indicates whether the protein contained a predicted N-terminal signal peptide (SignalP 3.0).

Table 3-2. BFA-sensitive proteins in ACM.

Accession	Protein name	Protein ratio[1]	SD ratio[2]	P-value[3]	CV (%)	SP[4]
Q04857	Collagen alpha-1(VI) chain	0.007	0.005	1.62E-10	68.5	Y
Q6GQT1	Alpha-2-macroglobulin-P	0.014	0.020	1.27E-03	142.9	Y
Q61362	Chitinase-3-like protein 1	0.015	0.004	5.88E-15	28.0	Y
Q60847	Collagen alpha-1(XII) chain	0.016	0.003	1.22E-15	22.0	Y
P70663	SPARC-like protein 1	0.018	0.013	1.70E-07	70.9	Y
P01027	Complement C3	0.019	0.018	1.49E-05	91.3	Y
P07214	SPARC (Secreted protein acidic and rich in cysteine)	0.021	0.028	1.63E-03	133.4	Y
O88968	Transcobalamin-2	0.022	0.004	4.17E-14	19.8	Y
P12023	Amyloid beta A4 protein	0.024	0.014	3.56E-08	57.2	Y
P07141	Macrophage colony-stimulating factor 1	0.028	0.022	1.02E-05	79.2	Y
Q07079	Insulin-like growth factor-binding protein 5	0.028	0.006	1.20E-12	20.7	Y
P11087	Collagen alpha-1(I) chain	0.030	0.023	8.20E-06	75.9	Y
Q00493	Carboxypeptidase E	0.032	0.026	2.38E-05	80.2	Y
P97298	Pigment epithelium-derived factor (PEDF)	0.032	0.044	4.85E-03	135.4	Y
Q61147	Ceruloplasmin	0.035	0.015	1.12E-08	42.8	Y
Q9R0E2	Procollagen-lysine,2-oxoglutarate 5-dioxygenase 1	0.038	0.012	7.26E-10	31.6	Y
O09159	Lysosomal alpha-mannosidase	0.038	0.013	1.62E-09	34.3	Y
Q05895	Thrombospondin-3	0.040	0.021	4.91E-07	54.0	Y
P01029	Complement C4-B	0.040	0.068	2.79E-02	169.2	Y
P06797	Cathepsin L1	0.041	0.025	2.80E-06	60.8	Y
O09164	Extracellular superoxide dismutase [Cu-Zn]	0.049	0.017	2.17E-08	35.1	Y
P08226	Apolipoprotein E	0.057	0.067	6.07E-03	116.9	Y
P11276	Fibronectin	0.059	0.030	2.91E-06	50.3	Y
P47877	Insulin-like growth factor-binding protein 2	0.059	0.061	2.85E-03	104.2	Y
Q06890	Clusterin (Apo-J)	0.059	0.062	3.25E-03	106.0	Y
A2ASQ1	Agrin	0.059	0.025	6.50E-07	43.1	Y
Q02819	Nucleobindin-1	0.063	0.014	1.11E-08	22.0	Y
P08905	Lysozyme C-2	0.076	0.103	2.46E-02	134.3	Y
O89017	Legumain	0.080	0.094	1.31E-02	117.0	Y
P10605	Cathepsin B	0.102	0.115	1.76E-02	112.6	Y
P55066	Neurocan core protein	0.106	0.068	5.58E-04	64.0	Y
Q76KF0	Semaphorin-6D	0.108	0.119	1.77E-02	109.9	Y

		Ratio[1]	SD[2]	P-value[3]		Signal[4]
Q9WVJ3	Plasma glutamate carboxypeptidase	0.112	0.044	2.52E-05	39.0	Y
Q9R0E1	Procollagen-lysine,2-oxoglutarate 5-dioxygenase 3	0.126	0.013	1.34E-06	10.4	Y
Q61508	Extracellular matrix protein 1	0.149	0.018	6.37E-06	11.9	Y
O88531	Palmitoyl-protein thioesterase 1 (PPT-1)	0.163	0.055	1.29E-04	33.6	Y
O88322	Nidogen-2	0.165	0.080	7.84E-04	48.6	Y
O70370	Cathepsin S	0.178	0.080	7.70E-04	44.9	Y
P18242	Cathepsin D	0.179	0.116	4.92E-03	65.1	Y
P01887	Beta-2-microglobulin	0.200	0.060	2.99E-04	30.0	Y
P97290	Plasma protease C1 inhibitor	0.222	0.138	8.49E-03	62.0	Y
Q8K2I4	Beta-mannosidase	0.237	0.006	1.50E-04	2.7	Y
B2RXS8	Ptprz1 protein	0.262	0.177	2.05E-02	67.7	Y
P51655	Glypican-4 (K-glypican)	0.283	0.070	1.45E-03	24.8	Y
P70158	Acid sphingomyelinase-like phosphodiesterase 3a	0.284	0.123	5.84E-03	43.4	Y
Q9Z0J0	Epididymal secretory protein E1	0.308	0.110	4.87E-03	35.7	Y
Q9DBH5	Vesicular integral-membrane protein VIP36	0.313	0.045	1.37E-03	14.3	Y
Q9WTQ5	A-kinase anchor protein 12	0.333	0.187	2.37E-02	56.1	N
Q9QWR8	Alpha-N-acetylgalactosaminidase	0.381	0.100	7.42E-03	26.3	Y
P29416	Beta-hexosaminidase subunit alpha	0.437	0.064	8.67E-03	14.7	Y
A2BFA6	Alpha-N-acetylglucosaminidase	0.480	0.099	1.69E-02	20.7	Y
Q99M71	Mammalian ependymin-related protein 1	0.494	0.134	2.45E-02	27.1	Y
Q6PDJ1	VWFA and cache domain-containing protein 1	0.571	0.120	3.62E-02	21.1	N
P16858	Glyceraldehyde-3-phosphate dehydrogenase	0.628	0.098	4.63E-02	15.7	N
O54990	Prominin-1	0.632	0.095	4.66E-02	15.0	Y
Q9WVA4	Transgelin-2	7.896	0.492	1.64E-02	6.2	N

Proteins are sorted in order of increasing protein ratio.

[1]Calculated from the intensity weighted average of individual peptide ratios. Ratio reflects the relative protein abundance fold change due to BFA treatment.

[2]Standard deviation of the average protein ratio calculated based on variance in peptide ratios.

[3]P-value calculated from the complementary error function (see *Materials and Methods*). $P < 0.05$ was required for significance.

[4]Indicates whether the protein contained a predicted N-terminal signal peptide (SignalP 3.0).

Table 3-3. Quantified ACM proteins from control astrocytes.

Accession	Protein name	Protein ratio[1]	SD ratio[2]	CV (%)
P08226	Apolipoprotein E	414.00	244.00	58.9
O09164	Extracellular superoxide dismutase [Cu-Zn]	327.00	50.00	15.3
P10923	Osteopontin	187.25	93.50	49.9
Q8R422	CD109 antigen	76.00	22.50	29.6
Q00493	Carboxypeptidase E	74.33	26.33	35.4
P07214	SPARC	67.00	35.93	53.6
A2APM1	CD44 antigen	65.33	4.33	6.6
P47867	Secretogranin-3	64.00	16.00	25.0
Q3UGY5	Fibronectin 1	57.67	87.06	151.0
Q6GQT1	Alpha-2-macroglobulin-P	45.60	28.62	62.8
P02463	Collagen alpha-1(IV) chain	41.89	12.13	29.0
O88307	Sortilin-related receptor	31.45	5.76	18.3
P43025	Tetranectin	30.62	5.62	18.4
P29533	Vascular cell adhesion protein 1	30.15	4.23	14.0
Q921T4	Phospholipase A2, group VII (Platelet-activating factor acetylhydrolase, plasma)	29.70	4.80	16.2
P20152	Vimentin	27.43	19.36	70.6
Q80YX1	Tenascin	27.30	10.10	37.0
Q9Z0J0	Epididymal secretory protein E1	22.00	12.65	57.5
Q80W15	Insulin-like growth factor-binding protein-like 1	21.33	2.83	13.3
Q9R0E1	Procollagen-lysine,2-oxoglutarate 5-dioxygenase 3	18.40	3.02	16.4
P51655	Glypican-4	16.91	17.02	100.6
P62806	Histone H4	16.17	4.64	28.7
Q06890	Clusterin	15.71	12.44	79.2
Q61592	Growth arrest-specific protein 6	14.67	2.33	15.9
P21460	Cystatin-C	14.00	2.45	17.5
Q9WTR5	Cadherin-13	13.27	2.27	17.1
Q02819	Nucleobindin-1	12.29	2.22	18.1
Q3UHN9	Bifunctional heparan sulfate N-deacetylase/N-sulfotransferase 1	12.13	2.33	19.2
Q61147	Ceruloplasmin	12.00	14.40	120.0
Q61361	Brevican core protein	11.23	2.39	21.3
Q9WVJ3	Plasma glutamate carboxypeptidase	10.37	1.74	16.8
P30412	Peptidyl-prolyl cis-trans isomerase C	10.36	0.57	5.5
O70370	Cathepsin S	10.09	2.09	20.7
Q80XP1	Complement component 3	9.75	11.25	115.4
Q91ZX7	Prolow-density lipoprotein receptor-related protein	9.48	4.78	50.5

	1			
Q9QXA3	Fat 1 cadherin (Fragment)	9.40	1.52	16.2
Q99LJ1	Tissue alpha-L-fucosidase	8.56	1.73	20.2
P55066	Neurocan core protein	8.47	10.22	120.7
P97298	Pigment epithelium-derived factor	7.65	9.26	121.0
Q9ES89	Exostosin-like 2	7.50	0.38	5.0
Q60847	Collagen alpha-1(XII) chain	7.25	16.12	222.3
Q99M71	Mammalian ependymin-related protein 1	7.00	1.76	25.1
P13595	Neural cell adhesion molecule 1	7.00	1.71	24.4
P27661	Histone H2A.x	6.82	1.93	28.3
Q91VU0	Protein FAM3C	6.81	3.28	48.1
Q8BND5	Sulfhydryl oxidase 1	5.88	1.08	18.3
P18242	Cathepsin D	5.25	8.52	162.3
Q8K2I4	Beta-mannosidase	5.03	1.31	26.0
Q91WP6	Serine protease inhibitor A3N	5.02	2.23	44.4
Q8BFR4	N-acetylglucosamine-6-sulfatase	4.92	1.18	24.0
Q61599	Rho GDP-dissociation inhibitor 2	4.80	2.56	53.2
Q8R464	Cell adhesion molecule 4	3.83	0.50	13.0
B2RXS4	Plexin B2 (MCG140951) (Plxnb2 protein)	3.79	7.13	188.0
Q04857	Collagen alpha-1(VI) chain	3.76	0.68	18.1
Q3UCL5	Ferritin	3.75	0.79	21.0
Q61233	Plastin-2	3.75	1.04	27.8
P09528	Ferritin heavy chain	3.59	1.25	34.9
Q8K479	Complement C1q tumor necrosis factor-related protein 5	3.55	0.35	9.8
O88325	Alpha-N-acetylglucosaminidase (Sanfilippo disease IIIB)	3.50	0.47	13.3
Q9R0B9	Procollagen-lysine,2-oxoglutarate 5-dioxygenase 2	3.44	0.64	18.6
Q9WUT8	DSD-1-proteoglycan	3.22	4.07	126.3
Q61207	Sulfated glycoprotein 1	3.04	0.72	23.5
O88668	Protein CREG1	2.95	0.71	24.0
Q197W7	N-glycan processing alpha-mannosidase IIx	2.94	0.60	20.3
Q64191	N(4)-(beta-N-acetylglucosaminyl)-L-asparaginase	2.88	2.13	74.1
O88531	Palmitoyl-protein thioesterase 1	2.79	0.41	14.9
P20060	Beta-hexosaminidase subunit beta	2.78	1.77	63.8
P70158	Acid sphingomyelinase-like phosphodiesterase 3a	2.77	0.36	13.0
Q9ET22	Dipeptidyl-peptidase 2	2.70	0.66	24.5
P00493	Hypoxanthine-guanine phosphoribosyltransferase	2.63	0.60	23.0
O89017	Legumain	2.60	0.57	21.9
P17047	Lysosome-associated membrane glycoprotein 2	2.55	1.53	60.1
Q3TCN2	Putative phospholipase B-like 2	2.43	0.58	24.1
P80314	T-complex protein 1 subunit beta	2.40	0.39	16.0

A2ARV4	Low-density lipoprotein receptor-related protein 2	2.24	0.62	27.8
Q9EQH2	Endoplasmic reticulum aminopeptidase 1	2.20	0.57	25.8
P10605	Cathepsin B	2.16	1.34	62.0
P50429	Arylsulfatase B	2.12	0.72	34.1
O88569	Heterogeneous nuclear ribonucleoproteins A2/B1	2.06	0.65	31.5
P01029	Complement C4-B	2.03	0.77	38.2
Q8CHQ7	UPF0727 protein C6orf115 homolog	2.01	0.00	0.0
Q9WV54	Acid ceramidase	1.96	0.36	18.2
Q91XG3	Hexosaminidase A	1.93	1.36	70.5
Q60648	Ganglioside GM2 activator	1.87	0.40	21.2
P16675	Lysosomal protective protein	1.87	0.73	39.2
Q07797	Galectin-3-binding protein	1.78	0.22	12.3
O09159	Lysosomal alpha-mannosidase	1.69	0.21	12.6
O54782	Epididymis-specific alpha-mannosidase	1.64	0.89	54.2
Q9CT10	Ran-binding protein 3	1.64	0.00	0.0
P23780	Beta-galactosidase	1.55	0.38	24.5
P97290	Plasma protease C1 inhibitor	1.54	1.53	99.7
Q9WUU7	Cathepsin Z	1.53	0.48	31.5
P10852	4F2 cell-surface antigen heavy chain	1.48	0.34	22.8
Q6P5H2	Nestin	1.44	0.29	19.8
P35441	Thrombospondin-1	1.42	0.50	35.0
Q9CPT4	UPF0556 protein C19orf10 homolog	1.42	0.53	37.8
Q7TPR4	Alpha-actinin-1	1.41	0.37	26.0
P57780	Alpha-actinin-4	1.39	0.33	23.6
P09470	Angiotensin-converting enzyme, somatic isoform	1.30	0.36	27.9
P23492	Purine nucleoside phosphorylase	1.29	0.35	27.4
Q62422	Osteoclast-stimulating factor 1	1.23	0.39	31.4
Q9DBH5	Vesicular integral-membrane protein VIP36	1.23	0.30	24.3
Q9ERR7	15 kDa selenoprotein	1.19	0.03	2.6
P11438	Lysosome-associated membrane glycoprotein 1	1.18	0.38	32.1
P28063	Proteasome subunit beta type-8	1.12	0.94	84.4
P54818	Galactocerebrosidase	1.12	0.15	13.5
Q62426	Cystatin-B	1.10	0.16	14.9
Q80YA8	Crumbs homolog 2	1.10	0.31	28.0
O35955	Proteasome subunit beta type-10	1.07	0.65	60.8
P49935	Cathepsin H	1.07	0.27	24.9
Q9WV32	Actin-related protein 2/3 complex subunit 1B	1.06	0.45	42.8
Q99020	Heterogeneous nuclear ribonucleoprotein A/B	1.06	0.05	4.7
P16110	Galectin-3	1.05	0.22	20.5
Q9D7V9	N-acylethanolamine-hydrolyzing acid amidase	1.04	0.12	11.9
Q921M7	Protein FAM49B	1.02	0.08	7.6

Q9Z1N5	Spliceosome RNA helicase Bat1	1.01	0.60	59.7
P05201	Aspartate aminotransferase, cytoplasmic	0.98	0.18	18.1
P20108	Thioredoxin-dependent peroxide reductase, mitochondrial	0.96	0.31	31.9
P62962	Profilin-1	0.96	0.15	15.5
P26041	Moesin	0.95	0.32	34.3
Q01768	Nucleoside diphosphate kinase B	0.93	0.13	14.5
P70665	Sialate O-acetylesterase	0.92	0.09	10.1
Q93092	Transaldolase	0.91	0.21	22.8
P16045	Galectin-1	0.87	0.13	14.6
P17439	Glucosylceramidase	0.86	0.00	0.0
P14901	Heme oxygenase 1	0.86	0.00	0.0
Q6NXZ0	Dipeptidylpeptidase 3	0.86	0.14	16.6
P06151	L-lactate dehydrogenase A chain	0.85	0.20	23.0
P62991	Ubiquitin	0.85	0.24	28.0
P63028	Translationally-controlled tumor protein	0.85	0.14	16.5
P70699	Lysosomal alpha-glucosidase	0.84	0.33	39.6
Q05816	Fatty acid-binding protein, epidermal	0.83	0.28	33.3
Q06138	Calcium-binding protein 39	0.82	0.82	99.3
Q9QWR8	Alpha-N-acetylgalactosaminidase	0.82	0.16	19.5
Q60709	Amyloid-like protein 2, isoform 751	0.82	0.20	24.3
Q3TW96	UDP-N-acetylhexosamine pyrophosphorylase-like protein 1	0.78	0.00	0.0
P10639	Thioredoxin	0.78	0.37	47.0
P00920	Carbonic anhydrase 2	0.78	0.12	15.8
Q9JII6	Alcohol dehydrogenase [NADP+]	0.78	0.26	33.8
Q920E5	Farnesyl pyrophosphate synthetase	0.78	0.12	15.7
Q9CQF3	Cleavage and polyadenylation specificity factor subunit 5	0.78	0.09	11.0
Q8C845	Efhd2 protein	0.77	0.54	69.9
Q58E70	Putative uncharacterized protein	0.77	0.20	26.3
Q60854	Serpin B6	0.77	0.10	13.5
Q9DCJ9	N-acetylneuraminate lyase	0.77	0.13	16.7
P97822	Acidic leucine-rich nuclear phosphoprotein 32 family member E	0.76	0.23	30.7
P15532	Nucleoside diphosphate kinase A	0.74	0.09	11.7
Q60631	Growth factor receptor-bound protein 2	0.73	0.36	49.4
P08228	Superoxide dismutase [Cu-Zn]	0.72	0.07	9.1
Q9CVB6	Actin-related protein 2/3 complex subunit 2	0.72	0.18	25.5
Q9DCD0	6-phosphogluconate dehydrogenase, decarboxylating	0.72	0.27	37.9
P24369	Peptidyl-prolyl cis-trans isomerase B	0.69	0.15	21.2
P61982	14-3-3 protein gamma	0.69	0.14	20.7

P68510	14-3-3 protein eta	0.68	0.17	25.4
P47791	Glutathione reductase, mitochondrial	0.68	0.13	18.8
Q9Z2U0	Proteasome subunit alpha type-7	0.68	0.18	26.9
Q9JMH6	Thioredoxin reductase 1, cytoplasmic	0.67	0.08	11.3
Q01279	Epidermal growth factor receptor	0.67	0.03	5.2
Q8BHG1	Nardilysin	0.67	0.28	41.8
P05064	Fructose-bisphosphate aldolase A	0.67	0.14	20.8
P63280	SUMO-conjugating enzyme UBC9	0.67	0.00	0.0
Q99LB4	Capping protein (Actin filament), gelsolin-like	0.66	0.55	82.4
P49722	Proteasome subunit alpha type-2	0.66	0.12	19.0
P54923	[Protein ADP-ribosylarginine] hydrolase	0.66	0.24	37.2
Q3U962	Collagen alpha-2(V) chain	0.65	0.31	47.9
Q99K51	Plastin-3	0.64	0.59	92.3
Q3TIH9	Ubiquitin carrier protein	0.64	0.11	17.1
Q9D0B6	UPF0368 protein Cxorf26 homolog	0.63	0.00	0.0
P06745	Glucose-6-phosphate isomerase	0.63	0.11	17.6
O88958	Glucosamine-6-phosphate isomerase 1	0.63	0.25	40.1
O70435	Proteasome subunit alpha type-3	0.62	0.21	34.3
O55135	Eukaryotic translation initiation factor 6	0.62	0.28	45.3
P62897	Cytochrome c, somatic	0.61	0.15	25.1
P17742	Peptidyl-prolyl cis-trans isomerase A	0.61	0.14	22.5
Q3TH46	Putative uncharacterized protein (Fragment)	0.60	0.16	26.9
P59999	Actin-related protein 2/3 complex subunit 4	0.60	0.07	11.1
P51880	Fatty acid-binding protein, brain	0.59	0.60	101.1
Q9Z2W0	Aspartyl aminopeptidase	0.59	0.11	18.0
P14602	Heat shock protein beta-1	0.58	0.03	5.1
Q9JJU8	SH3 domain-binding glutamic acid-rich-like protein	0.58	0.27	46.1
Q9CR09	Ufm1-conjugating enzyme 1	0.58	0.12	21.6
P61161	Actin-related protein 2	0.57	0.23	40.4
P14211	Calreticulin	0.57	0.09	14.9
Q9R1P3	Proteasome subunit beta type-2	0.57	0.09	16.1
P46664	Adenylosuccinate synthetase isozyme 2	0.57	0.06	10.3
O09061	Proteasome subunit beta type-1	0.57	0.17	30.2
O89023	Tripeptidyl-peptidase 1	0.57	0.15	25.8
Q91VI7	Ribonuclease inhibitor	0.57	0.32	56.0
Q61035	Histidyl-tRNA synthetase, cytoplasmic	0.55	0.20	35.7
Q4FJY5	Ltb4dh protein	0.55	0.07	13.5
P27773	Protein disulfide-isomerase A3	0.55	0.11	20.8
P53810	Phosphatidylinositol transfer protein alpha isoform	0.55	0.09	16.9
Q9QUM9	Proteasome subunit alpha type-6	0.55	0.13	23.4

O08795	Glucosidase 2 subunit beta	0.55	0.00	0.0
Q9R1P1	Proteasome subunit beta type-3	0.55	0.13	23.5
P24527	Leukotriene A-4 hydrolase	0.54	0.14	26.1
P63101	14-3-3 protein zeta/delta	0.54	0.12	21.9
P10518	Delta-aminolevulinic acid dehydratase	0.53	0.15	28.6
Q9D8S4	Oligoribonuclease, mitochondrial	0.53	0.11	20.1
Q6WVG3	BTB/POZ domain-containing protein KCTD12	0.53	0.64	121.2
Q64727	Vinculin	0.52	0.18	35.0
P61979	Heterogeneous nuclear ribonucleoprotein K	0.52	0.53	102.3
Q61508	Extracellular matrix protein 1	0.52	0.09	16.4
Q9JHW2	Nitrilase homolog 2	0.52	0.19	36.1
Q3TGE1	Putative uncharacterized protein	0.52	0.11	20.6
Q9R1P0	Proteasome subunit alpha type-4	0.52	0.16	31.4
Q9DBJ1	Phosphoglycerate mutase 1	0.52	0.10	18.5
P62204	Calmodulin	0.51	0.26	50.5
Q9CQV8	14-3-3 protein beta/alpha	0.51	0.15	29.3
Q6IRU2	Tropomyosin alpha-4 chain	0.51	0.10	19.0
Q9R1P4	Proteasome subunit alpha type-1	0.50	0.11	21.6
P57759	Endoplasmic reticulum protein ERp29	0.50	0.05	10.5
Q3U561	Ribosomal protein L1	0.49	0.17	33.6
O54983	Mu-crystallin homolog	0.48	0.24	48.9
P13020	Gelsolin	0.48	0.15	30.3
O35215	D-dopachrome decarboxylase	0.48	0.06	11.7
Q60692	Proteasome subunit beta type-6	0.48	0.25	52.4
Q9D1K7	Uncharacterized protein C20orf27 homolog	0.48	0.51	107.5
Q9CQI6	Coactosin-like protein	0.47	0.11	23.9
P58044	Isopentenyl-diphosphate Delta-isomerase 1	0.47	0.08	16.4
Q3TI11	Putative uncharacterized protein	0.47	0.10	21.8
O55234	Proteasome subunit beta type-5	0.46	0.06	12.9
Q921S3	Malic enzyme	0.46	0.09	20.5
P70195	Proteasome subunit beta type-7	0.46	0.09	20.6
Q9CQ60	6-phosphogluconolactonase	0.45	0.11	24.5
Q9CPY7	Cytosol aminopeptidase	0.45	0.22	48.7
Q07813	Apoptosis regulator BAX	0.45	0.03	7.8
Q9D967	Magnesium-dependent phosphatase 1	0.45	0.14	30.2
O88844	Isocitrate dehydrogenase [NADP] cytoplasmic	0.45	0.02	4.4
Q64010	Proto-oncogene C-crk	0.45	0.14	32.2
Q3U136	Putative uncharacterized protein (Fragment)	0.44	0.18	39.6
P45591	Cofilin-2	0.44	0.03	7.0
O55023	Inositol monophosphatase	0.44	0.14	31.1
Q8BFS6	Uncharacterized metallophosphoesterase CSTP1	0.44	0.12	27.0

Q66JR7	Pgm2 protein (Fragment)	0.43	0.16	38.1
P58252	Elongation factor 2	0.43	0.13	28.9
Q8C0E2	Vacuolar protein sorting-associated protein 26B	0.43	0.00	0.0
O09131	Glutathione S-transferase omega-1	0.43	0.00	0.0
Q3U6V5	Putative uncharacterized protein	0.43	0.02	3.6
Q9Z2U1	Proteasome subunit alpha type-5	0.43	0.18	42.5
Q99KQ4	Nicotinamide phosphoribosyltransferase	0.43	0.11	26.2
Q9WTQ5	A-kinase anchor protein 12	0.42	0.12	28.2
P60843	Eukaryotic initiation factor 4A-I	0.42	0.20	48.5
Q3U449	Putative uncharacterized protein	0.41	0.14	34.2
P09103	Protein disulfide-isomerase	0.41	0.05	12.7
P97371	Proteasome activator complex subunit 1	0.40	0.07	17.5
Q3U1J4	DNA damage-binding protein 1	0.40	0.35	88.0
Q99LS3	Phosphoserine phosphatase	0.40	0.10	26.0
Q99PT1	Rho GDP-dissociation inhibitor 1	0.40	0.13	32.9
Q62348	Translin	0.39	0.09	24.1
P31786	Acyl-CoA-binding protein	0.39	0.29	73.6
P97372	Proteasome activator complex subunit 2	0.39	0.06	14.8
P05202	Aspartate aminotransferase, mitochondrial	0.39	0.11	27.9
Q9CRC9	Glucosamine-6-phosphate isomerase 2	0.39	0.11	28.0
Q8C1A5	Thimet oligopeptidase	0.38	0.08	21.7
Q8BHN3	Neutral alpha-glucosidase AB	0.38	0.16	42.5
P61087	Ubiquitin-conjugating enzyme E2 K	0.38	0.23	61.0
Q9JM76	Actin-related protein 2/3 complex subunit 3	0.37	0.08	21.4
P58389	Serine/threonine-protein phosphatase 2A regulatory subunit B'	0.37	0.15	40.9
Q61598	Rab GDP dissociation inhibitor beta	0.36	0.08	21.7
P20029	78 kDa glucose-regulated protein	0.36	0.13	35.1
P47753	F-actin-capping protein subunit alpha-1	0.36	0.20	56.5
P58771	Tropomyosin alpha-1 chain	0.36	0.05	13.0
P26040	Ezrin	0.36	0.12	32.2
Q8BKC5	Importin-5	0.36	0.09	24.0
P62259	14-3-3 protein epsilon	0.36	0.06	17.7
P34884	Macrophage migration inhibitory factor	0.35	0.05	14.4
Q9DBP5	UMP-CMP kinase	0.35	0.04	12.6
P63242	Eukaryotic translation initiation factor 5A-1	0.34	0.07	19.6
P45376	Aldose reductase	0.34	0.05	14.2
P42932	T-complex protein 1 subunit theta	0.34	0.44	128.5
Q922R8	Protein disulfide-isomerase A6	0.34	0.06	19.0
P05063	Fructose-bisphosphate aldolase C	0.34	0.06	18.1
Q8CDN6	Thioredoxin-like protein 1	0.34	0.14	41.5
Q66JR8	Ptms protein	0.34	0.07	20.6

P24472	Glutathione S-transferase A4	0.34	0.05	14.7
P09671	Superoxide dismutase [Mn], mitochondrial	0.34	0.15	44.2
Q99LP6	GrpE protein homolog 1, mitochondrial	0.33	0.13	38.6
P62257	Ubiquitin-conjugating enzyme E2 H	0.33	0.16	50.6
Q8BHG2	UPF0587 protein C1orf123 homolog	0.33	0.05	15.2
Q8CHP8	Phosphoglycolate phosphatase	0.33	0.36	109.8
Q9ERK4	Exportin-2	0.32	0.30	92.7
B1AXW7	Peroxiredoxin 1	0.32	0.04	13.9
Q99JI4	26S proteasome non-ATPase regulatory subunit 6	0.32	0.12	38.8
O88456	Calpain small subunit 1	0.32	0.17	54.0
Q9JKB1	Ubiquitin carboxyl-terminal hydrolase isozyme L3	0.32	0.41	128.2
Q9CXI5	Protein ARMET	0.32	0.13	41.1
O55013	Trafficking protein particle complex subunit 3	0.31	0.00	0.0
Q61171	Peroxiredoxin-2	0.31	0.07	21.2
Q9DAW9	Calponin-3	0.31	0.38	122.0
P47955	60S acidic ribosomal protein P1	0.30	0.00	0.0
Q9Z2Y8	Proline synthetase co-transcribed bacterial homolog protein	0.30	0.05	16.1
Q9DB16	Calcium-binding protein 39-like	0.30	0.21	68.9
O88851	Retinoblastoma-binding protein 9	0.30	0.02	7.3
P61089	Ubiquitin-conjugating enzyme E2 N	0.30	0.11	37.3
Q9CZY3	Ubiquitin-conjugating enzyme E2 variant 1	0.29	0.00	0.0
Q8BG32	26S proteasome non-ATPase regulatory subunit 11	0.29	0.07	23.2
O88543	COP9 signalosome complex subunit 3	0.29	0.00	0.0
Q9JKR6	Hypoxia up-regulated protein 1	0.29	0.07	24.0
O35381	Acidic leucine-rich nuclear phosphoprotein 32 family member A	0.28	0.10	34.8
O08807	Peroxiredoxin-4	0.28	0.22	76.8
P23506	Protein-L-isoaspartate(D-aspartate) O-methyltransferase	0.28	0.15	53.6
Q9D1Q6	Thioredoxin domain-containing protein 4	0.28	0.00	0.0
P50396	Rab GDP dissociation inhibitor alpha	0.28	0.06	20.9
P29341	Polyadenylate-binding protein 1	0.28	0.02	7.3
Q91W90	Thioredoxin domain-containing protein 5	0.28	0.04	15.2
Q9WVJ2	26S proteasome non-ATPase regulatory subunit 13	0.27	0.25	89.6
Q9QZ88	Vacuolar protein sorting-associated protein 29	0.27	0.06	20.7
Q01730	Ras suppressor protein 1	0.27	0.06	22.1
Q04447	Creatine kinase B-type	0.27	0.07	27.8
Q8C0M9	L-asparaginase	0.27	0.17	62.2
P37804	Transgelin	0.27	0.12	44.6
P68254	14-3-3 protein theta	0.27	0.09	35.6
Q8C1B7	Septin-11	0.27	0.44	164.6

O35593	26S proteasome non-ATPase regulatory subunit 14	0.27	0.22	83.6
Q9WTX5	S-phase kinase-associated protein 1	0.27	0.04	14.1
Q7TQI3	Ubiquitin thioesterase OTUB1	0.26	0.04	16.3
Q01405	Protein transport protein Sec23A	0.26	0.02	6.2
Q3UGR5	Haloacid dehalogenase-like hydrolase domain-containing protein 2	0.26	0.12	45.8
Q99LX0	Protein DJ-1	0.26	0.15	58.5
P14869	60S acidic ribosomal protein P0	0.26	0.17	66.6
P70168	Importin subunit beta-1	0.25	0.07	29.0
Q9DBG3	AP-2 complex subunit beta-1	0.25	0.07	28.0
Q91V76	Ester hydrolase C11orf54 homolog	0.25	0.03	13.4
P70296	Phosphatidylethanolamine-binding protein 1	0.25	0.06	25.9
Q9CPU0	Lactoylglutathione lyase	0.25	0.04	16.8
Q9JI75	Ribosyldihydronicotinamide dehydrogenase [quinone]	0.25	0.00	1.2
Q9CPV4	Glyoxalase domain-containing protein 4	0.25	0.05	18.6
P11499	Heat shock protein HSP 90-beta	0.25	0.10	39.9
Q6P1F6	Serine/threonine-protein phosphatase 2A 55 kDa regulatory subunit B alpha isoform	0.25	0.05	22.2
Q7TMB8	Cytoplasmic FMR1-interacting protein 1	0.24	0.09	35.2
P52480	Pyruvate kinase isozymes M1/M2	0.24	0.08	32.9
Q01853	Transitional endoplasmic reticulum ATPase	0.24	0.07	28.9
Q9CX56	26S proteasome non-ATPase regulatory subunit 8	0.24	0.10	42.6
Q9QYR9	Acyl-coenzyme A thioesterase 2, mitochondrial	0.23	0.07	31.3
Q60605	Myosin light polypeptide 6	0.23	0.04	17.1
O08553	Dihydropyrimidinase-related protein 2	0.23	0.13	56.2
Q6P5E4	UDP-glucose:glycoprotein glucosyltransferase 1	0.23	0.05	20.6
Q8BJY1	26S proteasome non-ATPase regulatory subunit 5	0.23	0.05	20.9
Q8R0Y6	10-formyltetrahydrofolate dehydrogenase	0.23	0.06	24.5
Q9EQH3	Vacuolar protein sorting-associated protein 35	0.23	0.07	29.5
P17156	Heat shock-related 70 kDa protein 2	0.23	0.18	78.9
Q61205	Platelet-activating factor acetylhydrolase IB subunit gamma	0.23	0.00	0.0
P48758	Carbonyl reductase [NADPH] 1	0.23	0.32	140.7
Q61553	Fascin	0.22	0.05	24.7
Q922B2	Aspartyl-tRNA synthetase, cytoplasmic	0.22	0.08	36.0
Q61425	Hydroxyacyl-coenzyme A dehydrogenase, mitochondrial	0.22	0.07	34.7
Q9CZD3	Glycyl-tRNA synthetase	0.21	0.01	6.4
O88545	COP9 signalosome complex subunit 6	0.21	0.05	24.5
Q9D898	Actin-related protein 2/3 complex subunit 5-like protein	0.21	0.00	0.0
P62137	Serine/threonine-protein phosphatase PP1-alpha	0.21	0.15	73.0

	catalytic subunit			
Q9D8N0	Elongation factor 1-gamma	0.21	0.08	36.5
Q6P5F9	Exportin-1	0.20	0.02	11.7
Q6ZQ38	Cullin-associated NEDD8-dissociated protein 1	0.20	0.04	21.8
Q9CQM5	Thioredoxin domain-containing protein 17	0.20	0.00	0.0
P14152	Malate dehydrogenase, cytoplasmic	0.20	0.04	19.2
O55137	Acyl-coenzyme A thioesterase 1	0.20	0.07	34.6
Q9WU78	Programmed cell death 6-interacting protein	0.20	0.05	23.1
Q80Y52	Heat shock protein 90, alpha (Cytosolic), class A member 1	0.19	0.07	38.3
Q9CZ04	COP9 signalosome complex subunit 7a	0.19	0.03	15.1
Q8K4Z3	Apolipoprotein A-I-binding protein	0.19	0.05	27.8
Q9Z1Z2	Serine-threonine kinase receptor-associated protein	0.19	0.04	22.4
Q564P4	Adenine phosphoribosyl transferase	0.19	0.03	14.1
O08749	Dihydrolipoyl dehydrogenase, mitochondrial	0.18	0.05	26.5
Q61206	Platelet-activating factor acetylhydrolase IB subunit beta	0.18	0.03	18.0
Q6ZWX6	Eukaryotic translation initiation factor 2 subunit 1	0.18	0.10	53.8
P60122	RuvB-like 1	0.18	0.01	8.3
P08113	Endoplasmin	0.18	0.07	37.6
O70251	Elongation factor 1-beta	0.17	0.06	33.6
P40142	Transketolase	0.17	0.04	25.5
Q64433	10 kDa heat shock protein, mitochondrial	0.17	0.02	9.3
Q6PJ91	Gstm7 protein	0.17	0.04	21.9
Q99KC8	Loss of heterozygosity 11 chromosomal region 2 gene A protein homolog	0.17	0.09	50.0
Q62048	Astrocytic phosphoprotein PEA-15	0.17	0.04	21.8
P40124	Adenylyl cyclase-associated protein 1	0.17	0.02	13.0
P17710	Hexokinase-1	0.17	0.07	42.1
P68040	Guanine nucleotide-binding protein subunit beta-2-like 1	0.17	0.09	51.9
P47754	F-actin-capping protein subunit alpha-2	0.17	0.07	39.3
P09411	Phosphoglycerate kinase 1	0.17	0.05	28.2
Q8VHX6	Filamin-C	0.17	0.06	33.8
Q9R0Y5	Adenylate kinase isoenzyme 1	0.16	0.08	48.2
Q76MZ3	Serine/threonine-protein phosphatase 2A 65 kDa regulatory subunit A alpha isoform	0.16	0.12	72.2
P26516	26S proteasome non-ATPase regulatory subunit 7	0.16	0.06	36.4
O35643	AP-1 complex subunit beta-1	0.16	0.10	63.5
Q99P72	Reticulon-4	0.16	0.08	47.5
P99029	Peroxiredoxin-5, mitochondrial	0.16	0.04	26.2
Q9R0P9	Ubiquitin carboxyl-terminal hydrolase isozyme L1	0.16	0.04	26.0
P99027	60S acidic ribosomal protein P2	0.16	0.03	21.6

Q91ZJ5	UTP--glucose-1-phosphate uridylyltransferase	0.16	0.20	130.6
P80315	T-complex protein 1 subunit delta	0.16	0.24	151.3
P14685	26S proteasome non-ATPase regulatory subunit 3	0.16	0.07	42.5
Q9Z1Q5	Chloride intracellular channel protein 1	0.15	0.03	18.4
Q80X90	Filamin-B	0.15	0.05	35.8
P61164	Alpha-centractin	0.15	0.00	0.0
P70202	Latexin	0.15	0.04	23.8
P08003	Protein disulfide-isomerase A4	0.15	0.05	31.1
P10649	Glutathione S-transferase Mu 1	0.15	0.03	17.5
P15626	Glutathione S-transferase Mu 2	0.14	0.05	34.6
P97823	Acyl-protein thioesterase 1	0.14	0.00	0.0
P16125	L-lactate dehydrogenase B chain	0.14	0.05	39.5
P60710	Actin, cytoplasmic 1	0.14	0.04	32.5
Q9QXT0	Protein canopy homolog 2	0.13	0.11	81.5
P48774	Glutathione S-transferase Mu 5	0.13	0.02	19.2
Q9WVA4	Transgelin-2	0.13	0.03	25.4
Q9JIF7	Coatomer subunit beta	0.13	0.00	1.5
P18760	Cofilin-1	0.13	0.02	16.3
Q62261	Spectrin beta chain, brain 1	0.13	0.08	60.0
P63017	Heat shock cognate 71 kDa protein	0.13	0.06	45.8
P50247	Adenosylhomocysteinase	0.12	0.05	38.1
Q11011	Puromycin-sensitive aminopeptidase	0.12	0.05	36.5
Q9DBE0	Cysteine sulfinic acid decarboxylase	0.12	0.00	0.0
P34022	Ran-specific GTPase-activating protein	0.12	0.04	34.3
Q68FD5	Clathrin heavy chain 1	0.12	0.03	23.4
P68033	Actin, alpha cardiac muscle 1	0.12	0.05	39.9
P12815	Programmed cell death protein 6	0.12	0.04	34.6
Q6P069	Sorcin	0.12	0.05	40.6
Q99L47	Hsc70-interacting protein	0.12	0.01	10.8
P70670	Nascent polypeptide-associated complex subunit alpha, muscle-specific form	0.12	0.06	48.9
Q91V41	Ras-related protein Rab-14	0.11	0.18	160.1
P62141	Serine/threonine-protein phosphatase PP1-beta catalytic subunit	0.11	0.03	29.6
O70492	Sorting nexin-3	0.11	0.02	14.6
Q9D3D9	ATP synthase subunit delta, mitochondrial	0.11	0.03	27.7
Q61316	Heat shock 70 kDa protein 4	0.11	0.03	25.7
P19096	Fatty acid synthase	0.11	0.03	27.1
Q80UW2	F-box only protein 2	0.11	0.03	29.3
P63085	Mitogen-activated protein kinase 1	0.11	0.05	50.6
Q9QZE5	Coatomer subunit gamma	0.11	0.02	18.5
P42125	3,2-trans-enoyl-CoA isomerase, mitochondrial	0.11	0.03	31.9

P17182	Alpha-enolase	0.11	0.03	30.2
P05213	Tubulin alpha-1B chain	0.10	0.06	53.4
B1ATE2	Ring finger protein 213 (Fragment)	0.10	0.07	68.3
P62737	Actin, aortic smooth muscle	0.10	0.04	37.3
Q9CZC8	Secernin-1	0.10	0.01	12.7
P61082	NEDD8-conjugating enzyme Ubc12	0.09	0.14	151.3
Q9QXS1	Plectin-1	0.09	0.07	82.0
P62827	GTP-binding nuclear protein Ran	0.09	0.03	37.9
P80317	T-complex protein 1 subunit zeta	0.09	0.01	7.4
P68373	Tubulin alpha-1C chain	0.09	0.05	55.6
Q99K85	Phosphoserine aminotransferase	0.09	0.02	25.9
Q8CIE6	Coatomer subunit alpha	0.09	0.05	55.7
Q9DB79	Putative uncharacterized protein	0.09	0.02	27.8
A3QM89	Reticulon 1 (Fragment)	0.09	0.02	25.4
Q9EPQ7	StAR-related lipid transfer protein 5	0.08	0.00	1.5
P14131	40S ribosomal protein S16	0.08	0.02	27.4
Q9JKF1	Ras GTPase-activating-like protein IQGAP1	0.08	0.02	25.6
P35979	60S ribosomal protein L12	0.08	0.02	20.3
Q02053	Ubiquitin-like modifier-activating enzyme 1	0.08	0.02	24.4
Q3THE2	Myosin regulatory light chain MRLC2	0.08	0.05	61.9
Q9D6J6	NADH dehydrogenase [ubiquinone] flavoprotein 2, mitochondrial	0.08	0.02	25.2
P68369	Tubulin alpha-1A chain	0.08	0.04	56.1
P62715	Serine/threonine-protein phosphatase 2A catalytic subunit beta isoform	0.07	0.01	16.8
Q9WUL7	ADP-ribosylation factor-like protein 3	0.07	0.06	76.6
P08249	Malate dehydrogenase, mitochondrial	0.07	0.02	23.4
Q8CI94	Glycogen phosphorylase, brain form	0.07	0.03	38.3
P26039	Talin-1	0.07	0.02	32.6
P62908	40S ribosomal protein S3	0.07	0.03	38.1
P70349	Histidine triad nucleotide-binding protein 1	0.07	0.01	21.1
P28656	Nucleosome assembly protein 1-like 1	0.07	0.01	16.8
Q8VDM4	26S proteasome non-ATPase regulatory subunit 2	0.07	0.01	13.4
P57776	Elongation factor 1-delta	0.07	0.02	29.5
Q6GT24	Peroxiredoxin 6	0.07	0.02	23.8
P47199	Quinone oxidoreductase	0.06	0.01	10.1
Q9CWS0	N(G),N(G)-dimethylarginine dimethylaminohydrolase 1	0.06	0.02	26.2
Q9EQF6	Dihydropyrimidinase-related protein 5	0.06	0.03	41.5
P54071	Isocitrate dehydrogenase [NADP], mitochondrial	0.06	0.06	94.1
Q71LX4	Talin-2	0.06	0.02	29.3
Q8BTM8	Filamin-A	0.06	0.05	80.9

P17751	Triosephosphate isomerase	0.06	0.01	21.4
P63038	60 kDa heat shock protein, mitochondrial	0.06	0.02	32.0
Q9ERD7	Tubulin beta-3 chain	0.05	0.04	74.4
P80318	T-complex protein 1 subunit gamma	0.05	0.01	18.9
P29758	Ornithine aminotransferase, mitochondrial	0.05	0.03	61.9
Q9JHU4	Cytoplasmic dynein 1 heavy chain 1	0.05	0.02	40.0
P19157	Glutathione S-transferase P 1	0.05	0.02	31.7
Q9QUI0	Transforming protein RhoA	0.05	0.04	70.5
Q6ZWZ6	40S ribosomal protein S12	0.05	0.02	33.1
P46638	Ras-related protein Rab-11B	0.05	0.00	1.3
Q9R0P3	S-formylglutathione hydrolase	0.05	0.04	76.2
Q4FE56	Ubiquitin carboxyl-terminal hydrolase	0.05	0.01	20.7
Q9R0Q7	Prostaglandin E synthase 3	0.05	0.01	18.0
Q3UL78	Putative uncharacterized protein	0.05	0.02	37.3
Q3UBK2	Putative uncharacterized protein	0.05	0.02	33.8
A2AN08	E3 ubiquitin-protein ligase UBR4	0.05	0.01	26.6
P62821	Ras-related protein Rab-1A	0.04	0.01	32.4
P56480	ATP synthase subunit beta, mitochondrial	0.04	0.01	16.3
P50518	V-type proton ATPase subunit E 1	0.04	0.00	6.4
P99024	Tubulin beta-5 chain	0.04	0.01	21.0
P62835	Ras-related protein Rap-1A	0.04	0.01	14.5
Q9CRB6	Tubulin polymerization-promoting protein family member 3	0.04	0.00	8.1
P61750	ADP-ribosylation factor 4	0.04	0.01	25.7
P62270	40S ribosomal protein S18	0.04	0.00	13.2
P68372	Tubulin beta-2C chain	0.03	0.01	22.9
P25444	40S ribosomal protein S2	0.03	0.00	11.4
Q922F4	Tubulin beta-6 chain	0.03	0.00	12.5
Q9WTP7	GTP:AMP phosphotransferase mitochondrial	0.03	0.01	24.2
P26443	Glutamate dehydrogenase 1, mitochondrial	0.03	0.02	69.5
Q9WUA3	6-phosphofructokinase type C	0.03	0.02	74.3
Q7TMM9	Tubulin beta-2A chain	0.03	0.01	22.2
P10126	Elongation factor 1-alpha 1	0.03	0.01	27.6
P61027	Ras-related protein Rab-10	0.03	0.02	71.0
P62880	Guanine nucleotide-binding protein G(I)/G(S)/G(T) subunit beta-2	0.03	0.02	86.9
Q6ZWN5	40S ribosomal protein S9	0.03	0.01	25.1
Q8C1X9	Anxa3 protein	0.03	0.01	22.8
P07356	Annexin A2	0.02	0.00	20.5
P62874	Guanine nucleotide-binding protein G(I)/G(S)/G(T) subunit beta-1	0.02	0.01	63.6
O08638	Myosin-11	0.02	0.01	42.7

P97447	Four and a half LIM domains protein 1	0.02	0.00	19.1
Q8VDD5	Myosin-9	0.02	0.01	37.5
P35278	Ras-related protein Rab-5C	0.02	0.00	15.8
P63325	40S ribosomal protein S10	0.02	0.00	0.1
Q91V55	Putative uncharacterized protein	0.02	0.00	3.6
P16858	Glyceraldehyde-3-phosphate dehydrogenase	0.01	0.00	29.6
Q61879	Myosin-10	0.01	0.01	77.5
Q8VDN2	Sodium/potassium-transporting ATPase subunit alpha-1	0.01	0.00	41.9
Q9R0P5	Destrin	0.01	0.00	38.3
P48036	Annexin A5	0.01	0.00	23.8

Proteins are sorted in order of decreasing protein ratio.

[1]Calculated from the intensity weighted average of individual peptide ratios. Ratio reflects the fold difference in protein abundance between ACM and cell lysates.

[2]Standard deviation of the average protein ratio calculated based on variance in peptide ratios. If unique peptides resulted in the same peptide ratio, then the standard deviation was zero.

[3]P-value calculated from the complementary error function (see *Materials and Methods*). P < 0.05 was required for significance.

Table 3-4. ACM proteins with significant enrichment in ACM.

Accession	Protein name	Protein ratio[1]	SD ratio[2]	CV (%)	SP[4]
P20152	Vimentin	27.43	19.36	70.6	N
P62806	Histone H4	16.17	4.64	28.7	N
P27661	Histone H2A.x	6.82	1.93	28.3	N
Q61599	Rho GDP-dissociation inhibitor 2	4.80	2.56	53.2	N
Q3UCL5	Ferritin	3.75	0.79	21.0	N
Q61233	Plastin-2	3.75	1.04	27.8	N
P09528	Ferritin heavy chain	3.59	1.25	34.9	N
P00493	Hypoxanthine-guanine phosphoribosyltransferase	2.63	0.60	23.0	N
P80314	T-complex protein 1 subunit beta	2.40	0.39	16.0	N
O88569	Heterogeneous nuclear ribonucleoproteins A2/B1	2.06	0.65	31.5	N
Q8CHQ7	UPF0727 protein C6orf15 homolog	2.01	0.00	0.0	N
P10852	4F2 cell-surface antigen heavy chain	1.48	0.34	22.8	N
P08226	Apolipoprotein E	414.00	244.00	58.9	Y
O09164	Extracellular superoxide dismutase [Cu-Zn]	327.00	50.00	15.3	Y
P10923	Osteopontin	187.25	93.50	49.9	Y
Q8R422	CD109 antigen	76.00	22.50	29.6	Y
Q00493	Carboxypeptidase E	74.33	26.33	35.4	Y
P07214	SPARC	67.00	35.93	53.6	Y
A2APM1	CD44 antigen	65.33	4.33	6.6	Y
P47867	Secretogranin-3	64.00	16.00	25.0	Y
Q3UGY5	Fibronectin 1	57.67	87.06	151.0	Y
Q6GQT1	Alpha-2-macroglobulin-P	45.60	28.62	62.8	Y
P02463	Collagen alpha-1(IV) chain	41.89	12.13	29.0	Y
O88307	Sortilin-related receptor	31.45	5.76	18.3	Y
P43025	Tetranectin	30.62	5.62	18.4	Y
P29533	Vascular cell adhesion protein 1	30.15	4.23	14.0	Y
Q921T4	Phospholipase A2, group VII (Platelet-activating factor acetylhydrolase, plasma)	29.70	4.80	16.2	Y
Q80YX1	Tenascin	27.30	10.10	37.0	Y
Q9Z0J0	Epididymal secretory protein E1	22.00	12.65	57.5	Y
Q80W15	Insulin-like growth factor-binding protein-like 1	21.33	2.83	13.3	Y
Q9R0E1	Procollagen-lysine,2-oxoglutarate 5-dioxygenase 3	18.40	3.02	16.4	Y
P51655	Glypican-4	16.91	17.02	100.6	Y

164

Q06890	Clusterin	15.71	12.44	79.2	Y
Q61592	Growth arrest-specific protein 6	14.67	2.33	15.9	Y
P21460	Cystatin-C	14.00	2.45	17.5	Y
Q9WTR5	Cadherin-13	13.27	2.27	17.1	Y
Q02819	Nucleobindin-1	12.29	2.22	18.1	Y
Q3UHN9	Bifunctional heparan sulfate N-deacetylase/N-sulfotransferase 1	12.13	2.33	19.2	Y
Q61147	Ceruloplasmin	12.00	14.40	120.0	Y
Q61361	Brevican core protein	11.23	2.39	21.3	Y
Q9WVJ3	Plasma glutamate carboxypeptidase	10.37	1.74	16.8	Y
P30412	Peptidyl-prolyl cis-trans isomerase C	10.36	0.57	5.5	Y
O70370	Cathepsin S	10.09	2.09	20.7	Y
Q80XP1	Complement component 3	9.75	11.25	115.4	Y
Q91ZX7	Prolow-density lipoprotein receptor-related protein 1	9.48	4.78	50.5	Y
Q9QXA3	Fat 1 cadherin (Fragment)	9.40	1.52	16.2	Y
Q99LJ1	Tissue alpha-L-fucosidase	8.56	1.73	20.2	Y
P55066	Neurocan core protein	8.47	10.22	120.7	Y
P97298	Pigment epithelium-derived factor	7.65	9.26	121.0	Y
Q9ES89	Exostosin-like 2	7.50	0.38	5.0	Y
Q60847	Collagen alpha-1(XII) chain	7.25	16.12	222.3	Y
P13595	Neural cell adhesion molecule 1	7.00	1.71	24.4	Y
Q99M71	Mammalian ependymin-related protein 1	7.00	1.76	25.1	Y
Q91VU0	Protein FAM3C	6.81	3.28	48.1	Y
Q8BND5	Sulfhydryl oxidase 1	5.88	1.08	18.3	Y
P18242	Cathepsin D	5.25	8.52	162.3	Y
Q8K2I4	Beta-mannosidase	5.03	1.31	26.0	Y
Q91WP6	Serine protease inhibitor A3N	5.02	2.23	44.4	Y
Q8BFR4	N-acetylglucosamine-6-sulfatase	4.92	1.18	24.0	Y
Q8R464	Cell adhesion molecule 4	3.83	0.50	13.0	Y
B2RXS4	Plexin B2 (MCG140951) (Plxnb2 protein)	3.79	7.13	188.0	Y
Q04857	Collagen alpha-1(VI) chain	3.76	0.68	18.1	Y
Q8K479	Complement C1q tumor necrosis factor-related protein 5	3.55	0.35	9.8	Y
O88325	Alpha-N-acetylglucosaminidase (Sanfilippo disease IIIB)	3.50	0.47	13.3	Y
Q9R0B9	Procollagen-lysine,2-oxoglutarate 5-dioxygenase 2	3.44	0.64	18.6	Y
Q9WUT8	DSD-1-proteoglycan	3.22	4.07	126.3	Y
Q61207	Sulfated glycoprotein 1	3.04	0.72	23.5	Y
O88668	Protein CREG1	2.95	0.71	24.0	Y
Q197W7	N-glycan processing alpha-mannosidase	2.94	0.60	20.3	Y

	IIx				
Q64191	N(4)-(beta-N-acetylglucosaminyl)-L-asparaginase	2.88	2.13	74.1	Y
O88531	Palmitoyl-protein thioesterase 1	2.79	0.41	14.9	Y
P20060	Beta-hexosaminidase subunit beta	2.78	1.77	63.8	Y
P70158	Acid sphingomyelinase-like phosphodiesterase 3a	2.77	0.36	13.0	Y
Q9ET22	Dipeptidyl-peptidase 2	2.70	0.66	24.5	Y
O89017	Legumain	2.60	0.57	21.9	Y
P17047	Lysosome-associated membrane glycoprotein 2	2.55	1.53	60.1	Y
Q3TCN2	Putative phospholipase B-like 2	2.43	0.58	24.1	Y
A2ARV4	Low-density lipoprotein receptor-related protein 2	2.24	0.62	27.8	Y
Q9EQH2	Endoplasmic reticulum aminopeptidase 1	2.20	0.57	25.8	Y
P10605	Cathepsin B	2.16	1.34	62.0	Y
P50429	Arylsulfatase B	2.12	0.72	34.1	Y
P01029	Complement C4-B	2.03	0.77	38.2	Y
Q9WV54	Acid ceramidase	1.96	0.36	18.2	Y
Q91XG3	Hexosaminidase A	1.93	1.36	70.5	Y
Q60648	Ganglioside GM2 activator	1.87	0.40	21.2	Y
P16675	Lysosomal protective protein	1.87	0.73	39.2	Y
Q07797	Galectin-3-binding protein	1.78	0.22	12.3	Y
O54782	Epididymis-specific alpha-mannosidase	1.64	0.89	54.2	Y
P23780	Beta-galactosidase	1.55	0.38	24.5	Y
P97290	Plasma protease C1 inhibitor	1.54	1.53	99.7	Y
Q9WUU7	Cathepsin Z	1.53	0.48	31.5	Y

Proteins are sorted in order of decreasing protein ratio, as well as by predicted classical (SP = Y) and putatively non-conventional section (SP = N). Non-conventional proteins are listed at the top.
[1]Calculated from the correlation-weighted average of individual peptide ratios. Ratio reflects the fold difference in protein abundance between ACM and cellular lysates.
[2]Standard deviation of the average protein ratio calculated based on variance of peptide ratios. Standard deviations of zero occurred when unique peptides had the same peptide ratio.
[3]P-value calculated from the complementary error function (see *Materials and Methods*). P < 0.05 was required for significance.
[4]Indicates whether the protein contained a predicted N-terminal signal peptide (SignalP 3.0) and was secreted (TargetP).

CHAPTER 4

IDENTIFICATION OF S-NITROSYLATION MOTIFS BY SITE-SPECIFIC MAPPING OF THE S-NITROSOCYSTEINE PROTEOME IN HUMAN VASCULAR SMOOTH MUSCLE CELLS

By

Todd M. Greco[1], Roberto Hodara[1], Ioannis Parastatidis[1], Harry F. G. Heijnen[2], Michelle K. Dennehy[3], Daniel C. Liebler[3], and Harry Ischiropoulos[1]

[1]Stokes Research Institute and Departments of Pediatrics and Pharmacology, Children's Hospital of Philadelphia and University of Pennsylvania,
Philadelphia, PA 19104
[2]Thrombosis and Haemostasis Laboratory, Department of Cell Biology, University Medical Center Utrecht, and Institute for Biomembranes, 3584 CH, Utrecht, The Netherlands
[3]Department of Biochemistry and Mass Spectrometry Research Center, Vanderbilt University School of Medicine, Nashville, TN 37232

Running title: Site-specific identification of S-nitrosocysteine

Address correspondence to: Harry Ischiropoulos, Stokes Research Institute, Children's Hospital of Philadelphia, 416D Abramson Research Center, 3517 Civic Center Boulevard, Philadelphia, Pennsylvania, 19104-4318, USA. Phone: (215) 590-5320; Fax: (215) 590-4267; E-mail: ischirop@mail.med.upenn.edu.

4.1 Abstract

S-nitrosylation, the selective modification of cysteine residues in proteins to form S-nitrosocysteine, is a major emerging mechanism by which nitric oxide acts as a signaling molecule. While nitric oxide is intimately involved in the regulation of vascular smooth muscle cell functions, the potential protein targets for nitric oxide modification as well as structural features that underlie the specificity of protein S-nitrosocysteine formation in these cells remain unknown. Therefore, we employed a proteomic approach using selective peptide capturing and site-specific adduct mapping to identify the targets of S-nitrosylation in human aortic smooth muscle cells upon exposure to S-nitrosocysteine and propylamine propylamine NONOate. This strategy identified 20 unique S-nitrosocysteine-containing peptides belonging to 18 proteins including cytoskeletal proteins, chaperones, proteins of the translational machinery, vesicular transport, and signaling. Sequence analysis of the S-nitrosocysteine-containing peptides revealed the presence of acid-base motifs, as well as hydrophobic motifs surrounding the identified cysteine residues. High-resolution immunogold electron microscopy supported the cellular localization of several of these proteins. Interestingly, seven of the 18 proteins identified are localized within the ER/Golgi complex, suggesting a role for S-nitrosylation in membrane trafficking and ER stress response in vascular smooth muscle.

4.2 Introduction

S-Nitrosylation, the formal transfer of nitrosonium to a reduced cysteine, is a reversible and selective post-translational modification, regulating protein activity, localization, and stability, while also functioning as a general sensor for cellular redox balance (Hess et al. 2005, Hara et al. 2005, Rizzo, Piston 2003, Huang et al. 2005, Wang et al. 2006, Matsushita et al. 2003, Morrell et al. 2005). The formation of protein S-nitrosocysteine requires the removal of a single electron, i.e. the conversion of the nitrogen in nitric oxide from an oxidation state of 2 to 3. Several distinct pathways could satisfy the formation of protein S-nitrosocysteine adducts in biological systems, such as auto-oxidation of nitric oxide forming higher oxides of nitrogen, radical recombination of thiyl radical with nitric oxide, catalysis by metal centers, the direct reaction of nitric oxide with a reduced cysteine followed by electron abstraction, and transnitrosation reactions carried out by S-nitrosoglutathione, small molecular mass S-nitrosothiols and more recently by thioredoxin (Gow, Buerk & Ischiropoulos 1997, Mitchell, Marletta 2005, Pawloski, Hess & Stamler 2005).

In vascular smooth muscle cells, nitric oxide derived from endothelium regulates important biological functions beyond relaxation, such as phenotypic changes, proliferation, and commitment to undergo apoptosis (Bennett, Evan & Schwartz 1995, Lincoln et al. 2006). Previous studies have shown that the molecular mechanisms underlying the functions of nitric oxide in vascular smooth muscle are mediated by both soluble guanylate cyclase-dependent and independent mechanisms (Ignarro et al. 1986, Lincoln et al. 2006, Bolotina et al. 1994). It has been suggested that selective S-nitrosylation of protein targets are responsible for the guanylate cyclase-independent regulation of vascular smooth muscle cell biology (Bolotina et al. 1994). Despite these critical roles for nitric oxide, the targets of S-nitrosylation in vascular smooth muscle cells are largely unknown. To that end, proteomic approaches are highly informative in

providing a global assessment of the modified proteins in cells and tissues.

Proteomic approaches based on the biotin-switch method have been employed to identify potential targets of S-nitrosylation in various model systems including murine brain tissue (Jaffrey et al. 2001) and RAW 264.7 cells (Gao et al. 2005), *Mycobacterium tuberculosis* (Rhee et al. 2005), mouse mesangial cells (Kuncewicz et al. 2003), and human aortic endothelial cells (Yang, Loscalzo 2005, Martinez-Ruiz, Lamas 2004), yet the structural features which subserve the specificity of S-nitrosylation remain contentious. Recently, a peptide capture approach simultaneously identified 68 unique S-nitrosocysteine residues belonging to 56 proteins from GSNO-treated rat cerebellar lysates (Hao et al. 2006a). Analysis of the identified peptides by a machine learning approach did not reveal linear sequence motifs under the experimental conditions used (Hao et al. 2006a). However, subsequent inspection of the identified peptides indicated a prevalence of an acid/base motif, suggesting that exploration of additional S-nitrosocysteine proteomes may further clarify the structural motifs that underlie the specificity of S-nitrosylation.

To this end, in intact human aortic smooth muscle cells (HASMC) exposed to S-nitrosocysteine (CysNO) or propylamine propylamine NONOate (PAPANO), we identified potential targets of S-nitrosylation and evaluated S-nitrosylation motifs under conditions that preserve the cellular localization of the proteins as well as endogenous protein-protein interactions. Utilizing a proteomic approach that selectively identified the modified S-nitrosocysteine residues, 18 proteins were identified. The localization of several of these proteins was further supported by high-resolution immunogold electron microscopy. Primary sequence analysis of the S-nitrosocysteine-containing peptides revealed the presence of acid-base motifs as well as the occurrence of cysteine residues within hydrophobic pockets.

4.3 Materials and Methods

Chemicals and Reagents. Unless otherwise indicated, chemicals were purchased from Sigma (St Louis, MO). Kaighn's modification of Ham's F12 medium with 2 mM L-Glutamine (F12K), Earle's Balanced Salt Solution (EBSS), and SDS-PAGE 4-12% Bis-Tris gradient gels were purchased from Invitrogen (Carlsbad, CA). Micro Bio-spin P6 columns were obtained from Biorad (Hercules, CA). Propylamine propylamine NONOate (PAPANO) was purchased from Cayman Chemicals (Ann Arbor, MI). N-[6(Biotinamido)hexyl]-3'-(2'-pyridyldithio) propionamide (biotin-HPDP) and streptavidin-agarose were purchased from Pierce (Rockford, IL). Ultrafree-MC filters, PVDF Immobilon-FL, and ZipTipC$_{18}$ P10 were from Millipore (Billerica, MA). Trypsin Gold, Mass Spectrometry Grade was purchased from Promega (Madison, WI). Mouse monoclonal and rat polyclonal anti-nitrosocysteine antibodies were obtained from A.G. Scientific (San Diego, CA).

S-nitroso-L-cysteine (CysNO) was prepared by mixing equimolar amounts of L-cysteine and NaNO$_2$ under acidic conditions (0.25 M HCl) in the presence of 0.1 mM DTPA. CysNO stock solutions (500 mM) were prepared fresh. The final concentration of CysNO was determined from absorbance at 334 nm using the extinction coefficient 900 M^{-1}cm^{-1}. Immediately before exposure to cell cultures, an intermediate dilution of the stock solution was prepared in HEN buffer (250 mM HEPES, pH 7.7, 1 mM EDTA, 0.1 mM neocuproine). PAPANO was prepared as a concentrated stock in 0.01 M NaOH and the final concentration was determined by absorbance at 250 nm using the extinction coefficient 8050 M^{-1}cm^{-1}. All stock solutions were stored on ice in the dark.

Cell culture and treatment with NO agents. Human Aortic Smooth Muscle Cells (HASMC) were obtained at passage 15 or 16 from American Type Culture Collection (Manassas, VA) and cultured in F12K supplemented with 10 mM HEPES, 10 mM TES, 10% FBS, ITS (0.01 mg/mL insulin, 0.01 mg/mL transferrin, 10 ng/mL sodium selenite),

0.03 mg/mL ECGS, 0.05 mg/mL ascorbic acid. Cells were maintained in a 5% CO_2 incubator at 37 °C in T175 flasks. Experiments were performed between passages 16-21. When intact cells were ready for analysis (~85% confluency) they were washed twice with EBSS and incubated in the dark for 20 min with 100 μM L-cysteine or 100 μM CysNO at 37 °C. For PAPANO treatments, cells were exposed to 2 mM PAPANO for 1 hr at 37 °C in FBS/ITS/Asc-free medium (basal media) or in basal media alone as a control.

Quantitation of protein S-nitrosocysteine. Intracellular S-nitrosoprotein content was determined from HASMC cellular lysates by chemiluminescence using a Sievers 280 nitric oxide analyzer. HASMC were treated with NO agents as described above and cell extracts were obtained as described below. Lysates were then passed over two successive Micro Biospin P6 columns to remove low molecular weight S-nitrosothiols and protein concentration was determined. Lysates were incubated with 0.1% SNA/10% glacial acetic acid for at least 15 min to remove nitrite contamination. Approximately 0.12 mg of cellular lysates were routinely injected into the reaction vessel containing 5 mL of 60 mM potassium iodide (KI) and 10 mM iodine (I_2) in glacial acetic acid at 37 °C. Under these conditions, the lower limit of detection was 0.03 pmol SNO/mg total protein. Equivalent results for S-nitrosoprotein content were also obtained using Cu(I)/ascorbate reduction method. As a negative control for detection of S-nitrosocysteine, lysates were incubated with 3.5 mM $HgCl_2$ for 20 min at 4 °C.

Cell extract preparation and biotin switch assay. Unless otherwise indicated all steps were performed in the dark. After the treatment medium was removed, the cells were quickly trypsinized at 37 °C, inactivated with F12K containing 0.1% FBS, and

centrifuged at 130 x g for 6 min at 4 °C. Cell pellets were washed three times with ice-cold PBS containing 1 mM EDTA and 0.1 mM neocuproine. The biotin-switch assay was performed with between 0.5 and 1 mg of cellular protein as previously described (14) with minor modification. Cell pellets were resuspended in lysis buffer (HEN buffer containing 1% Triton X-100).

Resuspended pellets were then centrifuged at 12, 000 x g, 4 °C for 10 min. The biotin switch assay was performed with between 0.5 and 1 mg of protein. The lysates were adjusted to 0.5 mg/mL containing 2.5% SDS and 200 mM methyl methanethiosulfonate (MMTS) and incubated at 50 °C for 20 min, vortexing every 4 minutes to block free thiols. After blocking, cell extracts were precipitated with 2 volumes of -20 °C acetone, incubated at -20 °C for 20 minutes, centrifuged at 12, 000 x g, 4 °C for 10 min, washed four times with acetone, and resuspended in 0.2 mL of HENS buffer (25 mM HEPES, pH 7.7, 0.1 mM EDTA, 0.01 mM neocuproine, and 1% SDS). To the blocked proteins, 0.4 mM biotin-HPDP and 5 mM ascorbate were added and incubated at 25 °C for 1 hour while rotating. To control for non-specific HPDP labeling of unmodified cysteines, ascorbate was omitted. Following incubation, proteins were precipitated with acetone as described above. Samples in which protein digestion was performed were resuspended in 0.45 mL of 0.1 M ammonium bicarbonate and 0.5% SDS. Protein concentration was checked by the BCA assay (Pierce).

Protein digestion and affinity peptide capture. Biotinylated proteins were incubated with trypsin (1:30 enzyme:protein ratio) at 37 °C for 18-24 hrs in the dark. Samples were then passed through Ultrafree-MC 10 kDa cutoff filters that had been previously rinsed with methanol and washed with H_2O. The filtrate containing the peptides was recovered and

incubated with ~50 uL of dry, washed streptavidin-agarose beads per mg of initial protein for 30 min with gentle mixing. Samples were centrifuged at 5, 000 x g for 5 min and the supernatants were discarded. The beads were washed five times with 10 volumes of 1 M ammonium bicarbonate, followed by five washes with 10 volumes of deionized water. Between washes samples were centrifuged at 1, 000 x g for 1 min. Elution buffer containing 70% formic acid (FA) was incubated with the beads for 30 min with gentle mixing. The captured peptides were recovered by centrifuging beads at 5, 000 x g for 4 min and collecting the supernatant. To ensure complete removal of streptavidin-agarose, the samples were centrifuged again. The captured peptides were evaporated to ~5 uL *in vacuo*, resuspended in 20 uL of 0.1% FA and desalted using Zip-Tips.

Analysis by LC-MS/MS. Desalted samples were analyzed on a Thermo LTQ linear trap instrument equipped with a Thermo micro electrospray source, and a Thermo Surveyor pump and autosampler (Thermo Electron Corporation, San Jose, CA). LC-MS/MS analyses were done by reverse phase chromatography on an 11 cm fused silica capillary column (100 μm ID) packed with Monitor C-18 (5 μm) (Column Engineering, Ontario, CA) with the flow set at 700 nL/min. The mobile phase consisted of 0.1% formic acid in either HPLC grade water A) or acetonitrile (B). Peptides were eluted initially with 99% A, then 95% A from 3-5 min, then a linear gradient to 72% A by 33 min, then to 20% A at 40 min and held to 45 min, then to 99% A at 52 min and held until 60 min. MS/MS spectra were acquired using a full scan which was followed by four data dependent scans on the four most intense precursor ions. Precursors that were detected twice within 15 seconds were put on a dynamic exclusion list for a period of 60 seconds.

Assigning peptide sequences. MS/MS spectra were matched to human NCBI RefSeq database sequences with Sequest (Bioworks Browser 3.1 SR1) (Thermo Electron, San Jose, CA). Cysteine modification by MMTS (+46 amu) and by biotin-HPDP (+428 amu) was specified as variable modifications. MS/MS spectra were extracted from the raw files using Sequest with the following parameters: MW Range, 250-2000; threshold, 1000; precursor mass tolerance, 3; group scan tolerance, 2; minimum group count, 1; minimum number of ions, 26, precursor charge state, auto; MSn level, 2. Sequest output files were created using the following parameters: peptide mass tolerance, 2.5 and fragment ion tolerance, 0.0, as well as the charge state analysis (ZSA) algorithm.

Evaluating Sequest peptide sequence assignments. To efficiently compare Sequest peptide assignments within replicate samples and between experimental conditions Sequest output files were loaded into Scaffold (Proteome Software, Portland, OR). Sequest peptide sequences were accepted for a given sample if it passed the following selection criteria. First, the peptide assignment must contain a biotin-HPDP modified cysteine (+428) included in the *y*- or *b*-ion series were considered. Second, the peptide must be identified in 3 out of the 4 replicate experiments, and it must have the following Sequest scores: $X_C > 2$ for doubly charged and > 2.5 for triply charged ions; $\Delta Cn > 0.1$; RSp < 10; and preliminary score (Sp) >300. Finally, assigned spectra that meet the above criteria were manually reviewed. For peptide assignments to be accepted they must have (i) a continuous *b* or *y*-ion series of at least 5 residues and (ii) the top 3 most intense fragment peaks assigned to either an *a*, *b*, *y*-ion, to an *a*, *b*, *y*-ion resulting from a neutral loss of water or ammonia, or to a multiply protonated fragment ion. In addition, a peptide assignment with below threshold scores and marginal MS/MS spectra was accepted if it

175

showed a similar pattern of ion fragments and relative fragment ion peak intensity as a high scoring assignment present in another replicate. Manual review of MS/MS spectra was performed using Scaffold's built-in MS/MS spectrum view window.

Immunoelectron Microscopy. HASMC cells were treated with CysNO as described above and immediately fixed in 2% paraformaldehyde (PFA) and 0.2% glutaraldehyde in 0.1 M sodium phosphate buffer (pH 7.4) for 2 hours at room temperature. Fixed cells were stored at 4 °C in 1% PFA until cyrosectioning. 50 nm thick cryosections were cut at -120 °C using an Ultracut S ultramicrotome (Leica). The sections were collected on carbon-coated formvar grids using a mixture of 1.8% methylcellulose and 2.3 M sucrose (Liou, Geuze & Slot 1996) and incubated with primary nitrosocysteine antibodies (Gow et al. 2004) and 10 nm protein A–gold (Slot et al. 1991). After labeling, the sections were fixed with 1% glutaraldehyde, counterstained with uranyl acetate, and embedded in methylcellulose–uranyl acetate. The specificity of the labeling was verified in control experiments where sections were treated with 3.5 mM *p*-hydroxymercuricbenzoate (PHMB) for 30 min (3 x 10 min). Immunogold double labeling was performed using 10- and 15 nm protein A gold. After labeling, the sections were fixed with 1% glutaraldehyde, counterstained with uranyl acetate, and embedded in methyl cellulose–uranyl acetate. The sections were viewed in a JEOL 1200CX electron microscope.

4.4 Results and Discussion

The intracellular protein S-nitrosocysteine content was evaluated by reductive chemistries coupled with chemiluminescence detection (Fang et al. 1998). Naïve HASMC in culture had levels of protein S-nitrosocysteine below the lower limits of detection and western blot analysis failed to document expression of nitric oxide synthases in these cells (not shown). Therefore, to generate endogenous S-nitrosylated proteins, intact cells were exposed to either propylamine propylamine NONOate (PAPANO), a nitric oxide donor with defined release kinetics, or S-nitrosocysteine (CysNO), an effective transnitrosating agent. Exposure of HASMC to 100 μM CysNO for 20 min generated 3.0 ± 0.3 nmol of protein S-nitrosocysteine per mg of protein, whereas exposure to 2 mM PAPANO for 1 hour generated 0.40 ± 0.03 nmol protein S-nitrosocysteine per mg of protein (mean ± std, n=4). These two conditions were used to explore the S-nitrosoproteome of HASMC. The difference in the yield of protein S-nitrosocysteine between CysNO and the nitric oxide donor treatment may reflect the higher efficiency of S-nitrosylation by CysNO consistent with previous results (Zhang, Hogg 2004b). Cell culture studies have shown that exogenous CysNO is effectively transported intracellularly via the amino acid transporter system (L-AT) transporter system (Zhang, Hogg 2004b). Consequently, intracellular CysNO may facilitate the formation of protein S-nitrosocysteine adducts primarily by replenishment of endogenous S-nitrosoglutathione or by direct transnitrosation. In contrast, nitric oxide could be consumed by other cellular targets such as soluble guanylate cyclase and thus a smaller fraction may participate in S-nitrosative chemistries. Therefore, the treatment of HASMC with either CysNO or PAPANO, followed by site-specific proteomic analysis of

protein S-nitrosocysteine formation, allowed us to evaluate the potential selectivity of S-nitrosylation.

Due to the selectivity of S-nitrosocysteine modification and the peptide enrichment strategy employed, rigorous selection criteria based on manual inspection of MS/MS spectra was performed to evaluate each sequence-to-spectrum assignment (Figure 4-1). Typical MS/MS spectra that either met (Figure 4-1A) or failed (Figure 4-1B) these criteria are shown. Importantly, the mass shift due to the Cys-HPDP-biotin adduct (+428) was present in either the y- or b-ion series for accepted peptide assignments. While these selection criteria would minimize false peptide identifications resulting from MS/MS sequence-to-spectrum assignments, they would not prevent false positive peptide assignments arising from biotin-HPDP labeling of cysteine residues that were not completely blocked by MMTS. As a control for this non-specific labeling, ascorbate was omitted to largely prevent reduction of S-nitrosocysteine. Although ascorbate-independent biotin-HPDP labeling of S-nitrosocysteine is possible, naïve and cysteine-treated HASMC did not contain significant levels of endogenous S-nitrosoproteins quantified by reductive chemistries coupled to chemiluminescence detection. Therefore, omission of ascorbate from these conditions served as an appropriate false positive control. MS/MS sequence-to-spectrum assignments from these treatments were evaluated by the same criteria as described in Fig. 1 and were used to eliminate peptide identifications if they were also identified in the NO-treated samples. A total of 18 peptides belonging to 16 proteins were identified as possible false positives (Table 4-2), and therefore, were not considered targets of S-nitrosylation under our experimental conditions.
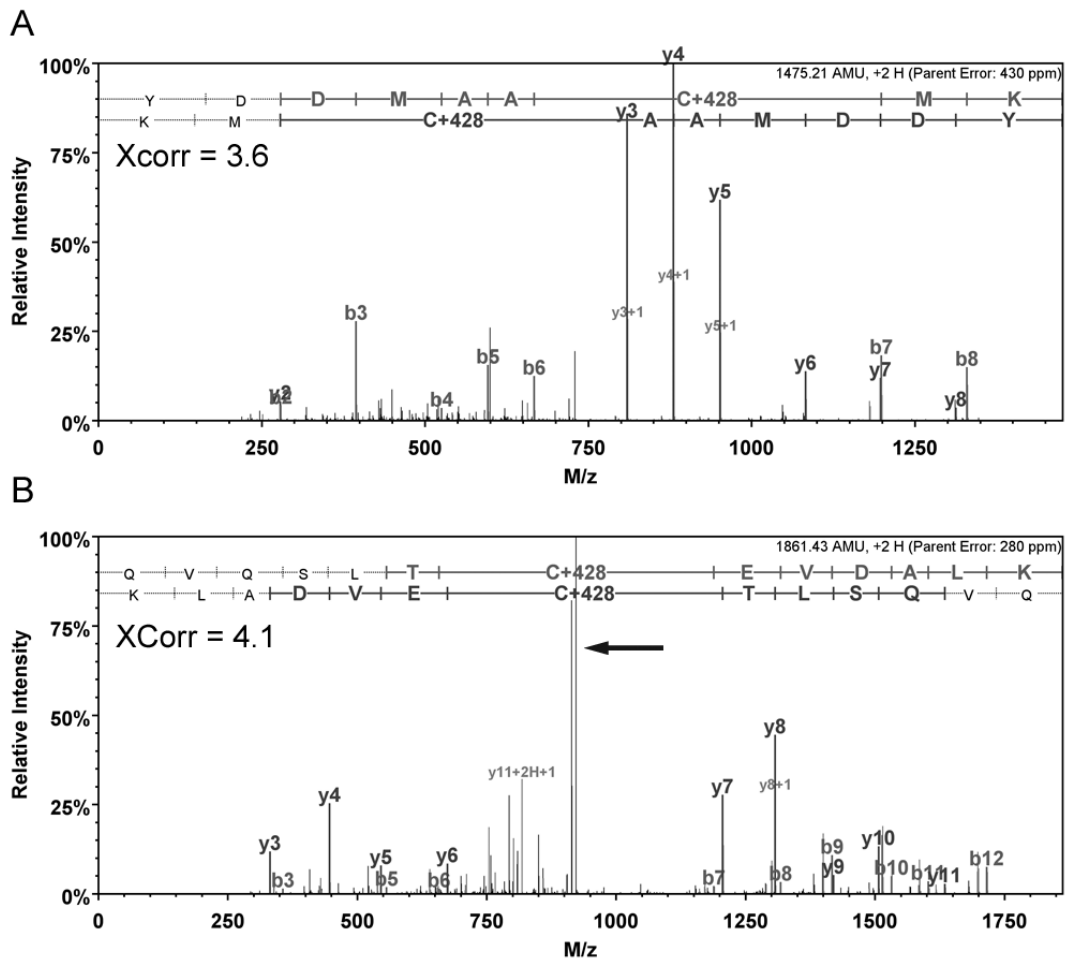
Figure 4-1. Evaluation of Sequest peptide assignments. (A) An MS/MS spectrum (XCorr 3.6) assigned to an S-nitrosocysteine-containing peptide from 14-3-3 protein ζ that met all selection criteria and was accepted. (B) An MS/MS spectrum (Xcorr 4.1) assigned to a peptide from vimentin. Although this assignment passed the initial selection criteria, it was ultimately rejected because the top 3 most intense fragment peaks were not assigned (arrow). The evaluation of Sequest peptide assignments was assessed by multiple selection criteria as follows: 1) Only peptide assignments that identified a biotin-HPDP derivitized cysteine (+428) included in the *y*- or *b*-ion series were considered. 2) Each experimental condition was performed in quadruplicate, with peptide assignments evaluated if they appeared in at least 3 out of the 4 independent replicates. 3) Peptide assignments that passed these two selection filters were then evaluated by output scores assigned by Sequest and were rejected if they did not meet specific threshold values as described in the **Materials and Methods**. 4) If peptide assignments passed this scoring filter, the corresponding MS/MS spectra were manually reviewed. For an assignment to be accepted the MS/MS spectrum must have (i) a continuous *b*-or *y*-ion series of at least 5 residues and (ii) the 3 most intense fragment peaks assigned to either an *a*-, *b*-, or *y*-ion, to an *a*-, *b*-, or *y*-ion resulting from a neutral loss of water or ammonia, or to a multiply protonated fragment ion. All review of peptide assignments and manual interpretation of MS/MS spectra were facilitated by Scaffold, a proteome software package.

179

Employing selective peptide capture followed by LC-MS/MS analysis, 18 S-nitrosocysteine-containing peptides belonging to 16 proteins were identified in HASMC exposed to CysNO (Table 4-1, Figures 4-5 to 4-23). The identification of S-nitrosylated proteins with diverse molecular weights and cellular roles such as cytoskeletal proteins, chaperones, proteins of the translational machinery, calcium-binding proteins and an ion channel protein supported the robustness of this technique.   From the 16 proteins identified as potential targets of S-nitrosylation, 14-3-3 protein θ, 14-3-3 protein ζ, annexin A2, elongation factor 2, and elongation factor 1 A-1 had been previously identified by the biotin switch method in various other systems (Zhang, Hogg 2005, Kuncewicz et al. 2003, Kuncewicz et al. 2003, Gao et al. 2005, Rhee et al. 2005, Rhee et al. 2005, Martinez-Ruiz, Lamas 2004).   In addition, Cys137 of RAB3B has been proposed as susceptible to S-nitrosylation based on a conserved NKCD motif (Lander et al. 1997).   Since these experiments identified S-nitrosocysteine at residue 184, further work will be necessary to examine the site-specificity of S-nitrosylation in RAB3B. Additionally, 4 S-nitrosocysteine-containing peptides belonging to 4 proteins were identified following exposure to a nitric oxide donor (Table 4-1, Figures 4-9, 4-19, 4-22, 4-23). Two of the proteins, 14-3-3 ζ and GRP75, were also identified as S-nitrosylated at the same residue following CysNO treatment, while microtubule-associated protein 4 and myoneurin were exclusive to PAPANO-treated HASMC.

The ability of this method to identify S-nitrosylated proteins from as little as 0.4 nmol of S-nitrosocysteine per mg of protein is an improvement in sensitivity and hence proteome coverage over the traditional biotin-switch approach. For example, exposure of RAW 264.7 cells to 250 μM CysNO generated approximately 5.5 nmol of S-

nitrosocysteine per mg of protein from which the standard biotin-switch assay identified 3 S-nitrosylated proteins (Zhang, Hogg 2005). This increase in sensitivity was likely due to the enrichment of S-nitrosocysteine-containing peptides and subsequent MS/MS analysis using electrospray ionization and linear ion trap detection. Critically, the increase in sensitivity did not sacrifice selectivity as nearly 90% (43 out of 49) of the unique peptides that passed the selection criteria contained a Cys-HPDP-biotin adduct. The capture of 6 nonspecific peptides lacking a biotinylated adduct was likely due to the harsher elution conditions required to denature avidin and release the biotinylated peptides. Overall, the selectivity and increased sensitivity of this method, as well as the ability to identify both the modified proteins and the sites of S-nitrosylation in a single experiment represent a significant advantage for elucidating the S-nitrosoproteome in complex biological mixtures.

The cellular distribution of protein S-nitrosocysteine was explored by high-resolution electron microscopy and immunogold labeling using monoclonal and polyclonal anti-S-nitrosocysteine antibodies. Following treatment of HASMC with 100 μM CysNO, significant immunoreactivity for protein S-nitrosocysteine was observed in distinct cellular compartments such as the endoplasmic reticulum membrane and vesicular membrane structures near the Golgi complex (Figure 4-2B, C), consistent with the proposed subcellular localizations of several of the identified proteins in Table 4-1. Treatment with para-hydroxymercuricbenzoate (PHMB), which displaces S-nitrosocysteine, significantly abolished S-nitrosocysteine immunoreactivity (Figure 4-2A). Of particular interest was the immunogold labeling located in close vicinity to the Golgi complex, which was largely associated with membranes of the endoplasmic

reticulum and on vesicular membrane profiles near the Golgi (Figure 4-2B, C). Based on

the proteomic data and the specific location of these vesicles at lateral rims and cis-Golgi

facing ER exit sites these membranes could represent COP-I-coated vesicles.

Immunogold double labeling against S-nitrosocysteine and COP-I was performed,

revealing low but distinct labeling on ER membranes (Figure 4-2D) as well as occasional

localization on vesicular membranes of the Golgi complex. (Figure 4-2D, arrow). Recent

studies have suggested that besides the COP-I vesicle coat, proteins of the 14-3-3 family

also recognize arginine-based ER localization signals on multimeric membrane proteins

(Yuan, Michelsen & Schwappach 2003). Since this proteomic study identified COP-A,

14-3-3 ζ, RAB3B, cyclophilin B, and chloride intracellular channel protein, which have

proposed roles in ER/Golgi transport and ER protein folding, this suggested a regulatory

role for S-nitrosylation in these cellular processes. Interestingly, recent studies have

revealed a role for S-nitrosylation in the regulation of vesicular trafficking in endothelial

and epithelial cells (Wang et al. 2006, Matsushita et al. 2003), platelets (Morrell et al.

2005), and neurons (Huang et al. 2005). In addition, nitric oxide has been identified as a

proximal mediator of ER stress responses, although the role of S-nitrosylation was not

evaluated (Xu et al. 2004).
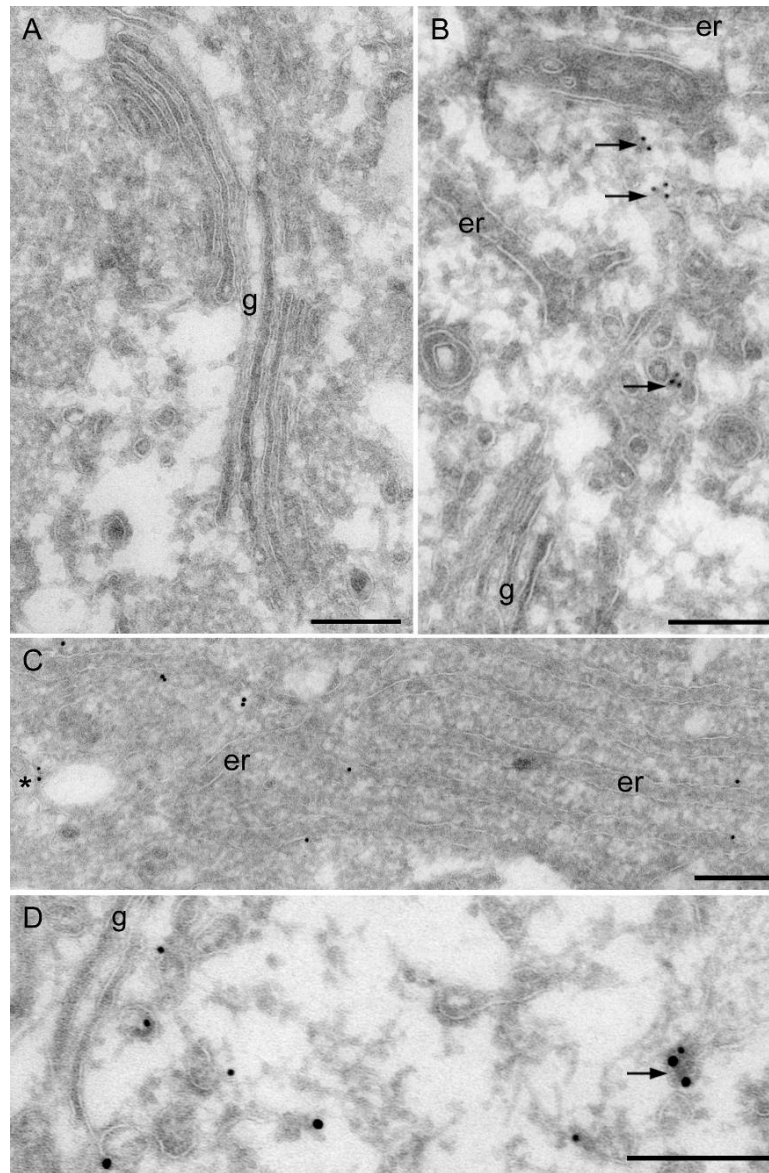
Figure 4-2. High-resolution immunoelectron microscopy. HASMC exposed to 100 μM CysNO for 20 min were fixed and processed for EM. Immunoreactivity for S-nitrosocysteine-containing proteins was visualized by 10-nm protein A gold particles. COP-1 immunoreactivity was visualized by 15-nm protein A gold particles. (A) Sections were treated with para-hydroxymercuricbenzoate (PHMB) to displace the S-nitrosocysteine adducts and then stained with monoclonal anti-S-nitrosocysteine antibody (26). (B) S-nitrosocysteine immunoreactivity (monoclonal antibody) was associated with endoplasmic reticulum, er, and small vesicular structures (arrows) in the vicinity of the Golgi complex, g. (C) A similar pattern of staining obtained with a polyclonal anti-S-nitrosocysteine antibody (asterisk indicates labeling of small vesicle). (D) Double labeling for S-nitrosocysteine (10-nm gold) and COP-1 (15-nm gold) showed localization on vesicular membrane profiles (arrow). Bar 200 nm.

183

The site-specific mapping of S-nitrosocysteine residues allowed direct comparison of primary peptide sequences for motifs that may govern S-nitrosylation specificity. It has been proposed that there is a predisposition towards flanking basic (Lys, Arg, His) and acidic (Asp, Glu) residues (Hess et al. 2005), and if positioned within 6 Å of the modified cysteine, these residues could regulate S-nitrosylation and de-nitrosation by altering thiol nucleophilicity. Sequence alignment of the 18 S-nitrosylated peptides identified from CysNO-treated smooth muscle cells revealed that the highest occurrence of acidic (D, E) residues was about 50% and 40%, at positions –3 and –4, respectively, relative to the modified cysteine. The highest occurrence of basic (K, R, H) residues was approximately 30% at position 2 (Figure 4-3A). Interestingly, there were no basic residues in position –3 and –4, while acidic residues at position 2 only occurred at a 10% frequency. Given the relatively small number of peptides being compared, the differences observed may result by chance; therefore, the same analysis was performed for the 18 false positive peptide identifications (Figure 4-3B). These peptides were excluded as they were not thought to contain S-nitrosocysteine, and therefore they served as an appropriate peptide population for comparison. Sequence alignment of these 18 sequences revealed that at positions –3 and –4 acidic residues occurred at lower frequency, 34% and 17%, compared to 50% and 40% for the S-nitrosocysteine-containing peptides, respectively. Similarly, the frequency of basic residues at position 2 dropped to 6% compared to the S-nitrosocysteine-containing peptides (30%). Given the strong trend for flanking acidic/basic residues revealed by alignment of S-nitrosocysteine-containing peptides, this provides some of the best direct evidence supporting the acid/base motif. Another factor that may govern S-nitrosylation

184

specificity is the occurrence of local hydrophobicity surrounding the cysteine residue (Hess et al. 2005, Hess et al. 2001). Construction of Kyte-Doolittle hydropathy plots revealed that the S-nitrosocysteine residues identified in T-complex protein 1, ζ subunit, annexin A11, and elongation factor 1 A-1 were located in discrete motifs of increased hydrophobicity (Figure 4-3C).
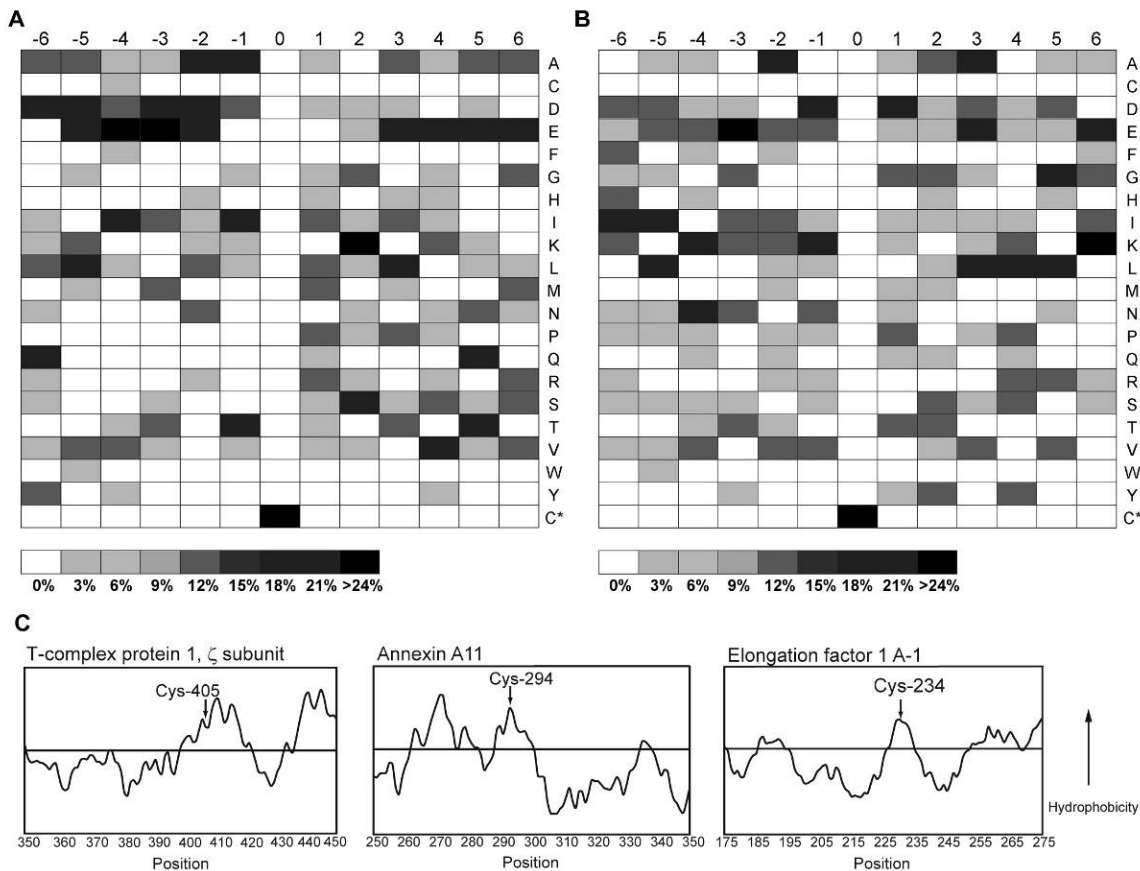
Figure 4-3. S-nitrosylation specificity motifs. (A) Sequence alignments of 18 S-nitrosocysteine-containing peptides identified from CysNO-treated HASMC comparing the occurrence of amino acids at positions flanking the modified cysteine. (B) Sequence alignments of 18 false positive peptides comparing the occurrence of amino acids at positions flanking the cysteine residue. (C) Kyte-Doolittle hydropathy plots from regions flanking the identified S-nitrosocysteine residue (arrow). The identified S-nitrosocysteine residues from T-complex protein 1, ζ subunit, annexin A11, and elongation factor 1 A-1 were located within hydrophobic pockets. Hydropathy plots were constructed using a window of 13 amino acids.

186

Although primary sequence analyses are useful for determining structural features that underlie the specificity of post-translational modifications, they do not reveal motifs that result from three-dimensional protein structure. Therefore, proteins identified in Table 1 and for which the crystal structures (>85% homology to the identified proteins) have been determined were evaluated for acid/base motifs. Four out of the 20 proteins, 14-3-3 ζ, 14-3-3 θ, RAB3B, and chloride intracellular channel 4 met these criteria. Evaluation of the molecular models revealed that for each protein, an acid/base motif opposing the identified cysteine was present within a molecular radius ranging from 2.4 to 7.1 Å (Figure 4-4). Since the proteomic studies identified 14-3-3 ζ and GRP75 as targets of S-nitrosylation in both CysNO and PAPANO-treated HASMC, these agents may share similar molecular specificities with respect to protein S-nitrosocysteine formation. On the other hand, myoneurin and microtubule-associated protein 4, which were identified only from PAPANO-treated HASMC, did not contain acid/base or hydrophobic motifs by primary sequence analysis and the crystal structures have not been determined. Therefore, the presence of common motifs for some but not all proteins identified from CysNO and PAPANO treatments suggests that protein S-nitrosocysteine formation derived from the nitric oxide radical donor include both secondary reactions of nitric oxide to generate transnitrosating species as well as other potential chemistries (8, 9).
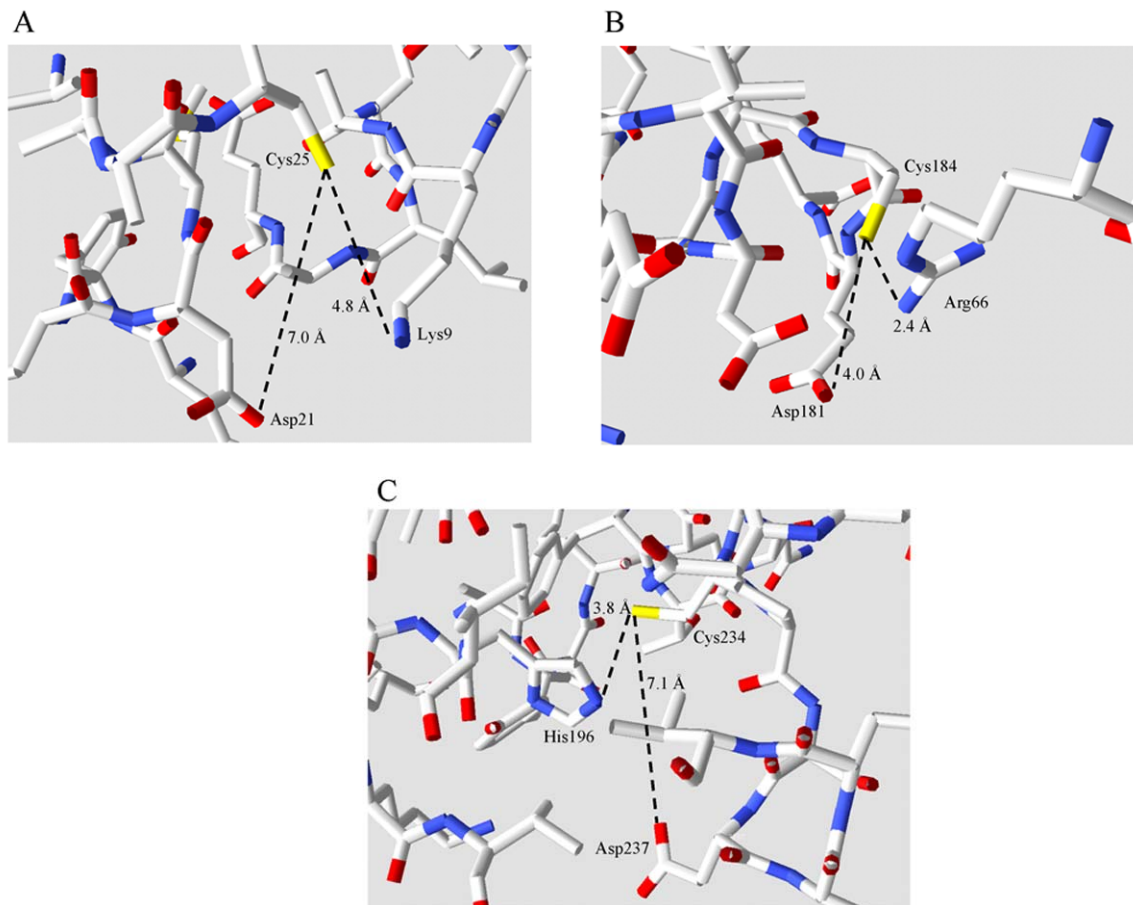
Figure 4-4. Evaluation of acid/base motifs by 3D structure analysis. Three-dimensional structures that had >85% homology to the identified proteins were obtained from the RCSB Protein Data Bank. (A) An acid/base motif was observed in human 14-3-3 ζ, where Cys25 was in close apposition to Asp21 and Lys9. A nearly identical structural arrangement was also observed for 14-3-3 θ (not shown). Similarly apposed acidic and basic residues were observed for Cys184 in rat RAB3B (B) and Cys234 in human chloride intracellular channel 4 (C). Three-dimensional models were loaded into the Swiss-Pdbviewer 3.7 (SP5) and molecular distances were calculated (Å, angstroms).

In summary, the proteomic approach employed permitted not only the evaluation of the S-nitrosoproteome in human aortic smooth muscle cells, but facilitated the elucidation of 2 S-nitrosylation motifs that govern the selectivity of modification. By systematically evaluating potential peptide sequence-to-spectrum assignments and by eliminating false positive S-nitrosocysteine-containing peptide identifications, 20 unique S-nitrosocysteine-containing peptides belonging to 18 proteins were identified. The identification of cytoskeletal, signal transduction, and ER-associated proteins implicates S-nitrosylation in the regulation of smooth muscle cell proliferation, apoptosis, and ER protein folding. The detection of proteins that participate in the ER/Golgi transport system is consistent with previous reports implicating S-nitrosylation in the regulation of vesicular trafficking in other cell types (Huang et al. 2005, Wang et al. 2006, Matsushita et al. 2003, Morrell et al. 2005). Significantly, through regulation of vascular smooth muscle ER/Golgi function, S-nitrosylation may influence vascular wall stress responses.

Table 4-1. Human aortic smooth muscle cell S-nitrosoproteome

Biological Function Protein Name	Acc.	Sequence[a]	AA[b]	Z[c]	XCorr[d]	ΔCn[e]	N[f]
Cell Growth and Maintenance							
Myosin heavy chain 9	P35579	KQELEEIC*HDLEAR	916	3	4.3	0.40	6
		LQLQEQLQAETELC*AEAEELR	895	3	5.8	0.60	5
		VEDMAELTC*LNEASVLHNLK	90	3	3.7	0.44	3
Vinculin	Q5SWX2	VENAC*TK	85	2	2.8	0.23	5
^Microtubule-associated protein 4	P27816	C*SLPAEEDSVLEK	635	3	3.9	0.39	3
Signal Transduction							
14-3-3 protein ζ	P63104	YDDMAAC*MK	25	2	3.6	0.43	8
^14-3-3 protein ζ	P63104	YDDMAAC*MK	25	2	3.7	0.44	4
14-3-3 protein θ	P27348	YDDMATC*MK	25	2	3.5	0.38	5
Annexin A2	Q567R4	GLGTDEDSLIEIIC*SR	133	3	4.2	0.33	5
Annexin A11	P50995	GVGTDEAC*LIEILASR	294	3	3.5	0.31	7
VAV-like protein	Q6TPQ2	C*RSLSQGMELSC#PGSR	33	3	3.0	0.19	4
Protein Metabolism							
Elongation factor 2	P13639	DLEEDHAC*IPIK	567	3	2.9	0.13	3
Elongation factor 1 A-1	P68104	DGNASGTTLLEALDC*ILPPTR	234	3	4.1	0.45	4
Eukaryotic initiation factor 5AII	Q9GZV4	YEDIC*PSTHNMDVPNIK	73	3	4.0	0.52	10
T-complex protein 1, ζ subunit	P40227	NAIDDGC*VVPGAGAVEVAMAEALIK	405	3	5.0	0.50	4
Cyclophilin B	P23284	DVIIADC*GK	194	2	3.1	0.37	3
GRP75	P38646	VC*QGER	487	2	2.4	0.19	4
^GRP75	P38646	VC*QGER	487	2	2.3	0.16	4
Transport							
COP-A	Q8IXZ9	AWEVDTC*R	245	2	2.5	0.31	6
Ras-associated protein 3B	P20337	LVDAIC*DK	184	2	3.1	0.25	8
Chloride intracellular channel 4	Q9Y696	DEFTNTC*PSDK	234	2	3.5	0.34	3
Nucleic Acid Metabolism							
^Myoneurin	Q8WX93	VSSC*EQR	740	2	2.7	0.16	3

^ indicates proteins were identified from PAPANO-treated HASMC; all other identifications were from CysNO-treated HASMC. [a]S-nitrosocysteine-containing tryptic peptide sequences; * specifies biotin-HPDP labeled cysteine, # indicates methyl disulfide. [b]Residue numbers refer to UniRef database sequences (www.uniprot.org). [c]The charge state of the precursor peptide associated with the highest XCorr value. [d]The highest XCorr value obtained for that peptide assignment across four independent experiments. [e]The delta correlation value associated with the highest XCorr value; a measure of similarity between the two best hits matched to the MS-MS spectra. [f]The number of times the assignment was accepted across four independent experiments.

Table 4-2. False positive S-nitrosocysteine-containing peptides

Protein Name	Uniprot Acc	Sequence[a]	AA[b]	Z[c]	XCorr[d]
β-actin	P60709	C*DVDIR	285	2	2.4
		LC*YVALDFEQEMATAASSSSLEK	217	3	6.3
β-tubulin	P07437	TAVC*DIPPR	354	2	2.3
Peroxiredoxin 6	Q5TAH4	DFTPVC*TTELGR	47	2	3.0
Pyruvate kinase M2 isozyme	P14618	AEGSDVANAVLDGADC*IMLSGETAK	357	3	5.8
Plastin 3	Q86YI6	VDLNSNGFIC*DYELHELFK	33	3	3.4
Myosin heavy chain 9	P35579	C*QHLQAEK	930	2	2.8
		KLEEEQIILEDQNC*K	987	3	5.1
Filamin C	Q14315	TPC*EEVYVK	2660	2	3.1
Galectin-1	P09382	FNAHGDANTIVC*NSK	60	3	3.6
Calreticulin precursor	Q6IAT4	HEQNIDC*GGGYVK	105	2	4.4
Protein disulfide isomerase precursor	P07237	KEEC*PAVR	312	3	2.9
Polyposis locus protein 1	Q00765	NC*MTDLLAK	14	2	3.1
Cyclophilin A	P62937	KITIADC*GQLE	160	2	3.9
Alpha-2HS-glycoprotein	P02765	C*DSSPDSAEDVR	132	2	4.4
Thioredoxin domain containing 5	Q5TCQ0	IAEVDC*TAER	381	2	3.3
KDEL ER Receptor 1	P24390	SC*AGISGK	29	2	2.9
Desmoyokin	Q09666	LEGDLTGPSVGVEVPDVELEC*PDAK	1653	3	6.4

[a]False positive tryptic peptide sequences; * indicates biotin-HPDP labeled cysteine. [b]Residue numbers refer to UniRef database sequences (www.uniprot.org). [c]The charge state of the precursor peptide associated with the highest XCorr value. [d]The highest XCorr value obtained for that peptide assignment across four independent experiments.

CHAPTER 5

SUMMARY AND GENERAL DISCUSSION

In the post-genomic era, mass spectrometry-based proteomics has become the tool of choice for global, unbiased investigation of cellular and tissue proteomes. Recent advances in mass spectrometer technology and proteomic methodologies have enabled improved sensitivity and resolution as well as the ability to reduce sample complexity, respectively. Current technology provides the necessary tools to begin defining what could be called a "complete" cellular proteome (Graumann et al. 2008). This increased depth of analysis permits the identification of biologically significant proteins at low abundance, with a depth of seven to eight orders of magnitude lower than the most abundant protein (Tang et al. 2005). The challenge therefore with these tools is to utilize them to answer biologically relevant questions.

This project utilized mass spectrometry-based proteomics to explore two different aspects of cellular signaling. The first aspect focused on the identification and quantification of proteins secreted into the extracellular space (Chapters 2 & 3). Primary postnatal astrocytes in culture were used as a model system to address such fundamental questions as, what proteins are secreted by primary astrocyte cultures under naïve conditions, and how is this secretion altered upon exposure to inflammatory mediators? To answer these questions, comparative proteomics was used to assess changes between proteomes as a function of stimuli and time. An interesting observation from these experiments was the identification of several proteins that lacked an N-terminal signal peptide. This suggested secretory pathway(s) other than the classical ER-Golgi route of

192

export may be functional in astrocytes. To explore this hypothesis, a quantitative strategy was developed using stable isotope labeling by amino acids in culture (SILAC). Using this strategy, proteins from conditioned media were quantified relative to their intracellular abundance. The relative fold increase (or decrease) represented the enrichment of a protein in the extracellular medium. Enrichment values were related to protein subcellular localization and signal peptide status to identify proteins that may be secreted by alternative pathways.

The other focus of this project was to utilize mass spectrometry-based proteomics to address the selectivity of nitric oxide-mediated post translational modification of cysteine residues, termed S-nitrosylation (Chapter 4). This question could not be addressed at the proteome level with existing methodologies as they did not directly identify the site of modification, nor was the sensitivity sufficient to identify an endogenous proteome. Therefore, experiments were designed to reduce the complexity of biological samples by affinity enrichment of cysteinyl-containing peptides that previously contained S-nitrosocysteine residues. A linear ion trap was employed to achieve higher sensitivity compared to previous studies and to enable peptide sequencing by tandem mass spectrometry. With appropriate selection criteria, this enabled both the protein and the site of modification to be identified in a single experiment.

5.1 Characterization of the astrocyte secretome

The astrocyte was chosen as a robust model system for the development of global mass spectrometry-based proteomic approaches for two mains reasons: (1) biologically, growing evidence indicates proteins secreted by astrocytes mediate both physiological

and pathophysiological responses *in vivo*, yet often the proteins that may mediate these effects have not been identified, and (2) the astrocyte can be cultured in serum-free conditions which depletes the most abundant proteins that have a negative impact on depth of analysis for secretome studies (Pellitteri-Hahn et al. 2006). The increase in depth as well as high reproducibility was a direct result of the multidimensional chromatography approach developed by Tang et al., 2005. Even for complex proteomes, technical reproducibility of protein identifications was 80 - 90 % for biological duplicates. This high reproducibility allowed us to make direct comparisons of protein identifications between secretomes generated under control and cytokine-exposed conditions. We identified three chemokines secreted after cytokine exposure, with two not yet described in the literature as being secreted from astrocytes. From these preliminary mass spectrometric finding, it would be possible to develop quantitative assays for these chemokines in other complex biological samples using targeted, MRM-based mass spectrometry.

It was also apparent after conducting the initial mass spectrometry analysis that the increased depth of analysis facilitated the identification of lower abundance intracellular proteins. Initially, classification of *bona fide* secreted proteins was performed by computational prediction algorithms. The sensitivity of prediction for classical secretion by N-terminal signal peptide is at least 90 %, allowing most classically secreted proteins to be identified. Yet this would not be useful to distinguish between non-secreted cytosolic proteins in ACM due to cell death and proteins secreted by nonconventional mechanisms. As nonconventional prediction algorithms have achieved only 40 % sensitivity, a quantitative mass spectrometry approach was developed to assess

194

relative protein enrichment in astrocyte conditioned media compared to the intracellular proteome.

5.2 Quantification of the astrocyte secretome by SILAC

Although it would be possible to quantify putative nonconventionally secreted proteins by Western blot analysis of conditioned media and cell lysates, the efficiency and coverage of the proteome by quantitative mass spectrometry-based strategies would be more economical. For example, from the same amount of protein used for a Western blot of two proteins, one could quantify hundreds of proteins by quantitative mass spectrometry using stable isotope labeling techniques. Stable Isotope Labeling by Amino Acids in Culture (SILAC) was used generate isotope-labeled reference proteomes (IRPs). IRPs generated from primary astrocytes are the ideal proteome standards as they represent the identical protein composition to the model system, except for the incorporation of a stable isotope which alters protein/peptide mass. Moreover, IRPs can be added to the sample immediately after sample collection, greatly reducing variability from sample handling and processing, as well as mass spectrometric analysis. Additionally, SILAC had not yet been applied in primary astrocytes cultures, which could serve as a useful quantitative method for neuroscientists investigating a multitude of cellular states where astrocyte protein expression or secretion is altered.

While SILAC in primary astrocyte cultures achieved greater than 98 % isotope incorporation, an interesting observation was made when examining the isotope profiles of heavy-labeled peptides (containing heavy leucine or lysine amino acids). Specifically, an anomalous shift in ion abundance towards higher m/z was readily apparent from

195

peptides that were derived from the isotope-labeled reference proteome, but not from the proteomes that correspond to natural abundance (light) conditions. Although this degree of isotope shift was variable between different heavy-labeled peptides, the shift was highly reproducible for the same peptide across many reference-spiked samples. The shift towards higher m/z suggests heavy label had been transferred and incorporated into other amino acids. To my knowledge, "back incorporation" from heavy-labeled leucine or lysine has not been reported in other SILAC studies. Fortunately, these anomalous isotope profiles did not impact quantification as (1) the m/z values were identical to the calculated values, (2) the isotope profiles were consistent for the same peptide across multiple samples, and (3) the computation of protein ratios was performed with a ratio of ratios, negating any effect this anomaly would have on the accuracy of peptide ratios. Additional experiments are necessary to determine the source of this phenomenon.

Another interesting observation taken from the ACM enrichment distribution was the wide range of ratios. For instance, proteins containing an N-terminal signal peptide ranged from an enrichment ratio of 0.25-fold (similar to many cytosolic proteins) to ratios well outside the dynamic range of the method (>100-fold). This likely reflects the functional localization of signal peptide-containing proteins into respective cellular compartments, such as endoplasmic reticulum and mitochondria versus secretory proteins stored in storage vesicles versus constitutively secreted proteins in the extracellular space. Interestingly, the sorting of proteins between storage vesicles and constitutive export is not well understood, though the presence of hydrophobic patches in the N-terminal region to divert proteins from bulk flow has been proposed (Gorr, Darling 1995). Based on this, a prediction would be that signal peptide-containing proteins with lower

enrichment ratios would also possess hydrophobic patches, which would be absent in proteins with larger enrichment ratios.

The observation that a majority of lysosomal-localized proteins were significantly enriched in ACM is supported by several publications demonstrating the presence of exocytotic secretory lysosomes in astrocytes (Li et al. 2008). Although these novel vesicular pools were found to release ATP in a calcium-dependent manner (Zhang et al. 2007), the functional consequences of lysosomal proteins/enzymes release were not explored. This quantitative approach would be a useful tool to investigate secretory lysosome function in terms of the stimuli regulating exocytosis as well as the identity and specificity of proteins released under those conditions.

The identification of a 12 proteins with significant enrichment ratios, but which lacked an N-terminal signal peptide suggested these proteins may be nonconventionally secreted under basal conditions. For example, enrichment of histones (H4 and H2a) as well as ferritin light and heavy chain was observed. The quantitative mass spectrometry data clearly supported histone enrichment in ACM. Also, two studies investigating secreted histones have identified functional roles in the extracellular space (Brown et al. 2000, Lee et al. 2009). Clearly, future experiments to explore the functional implications of nonconventional histone secretion in astrocytes are warranted. On the other hand, the observation that the large majority of proteins predicted as nonconventionally secreted were in fact enriched in the intracellular proteome implies that the mechanisms of nonconventional secretion are stimulus-dependent rather than constitutive. The proteome-wide quantitative approach developed in this project would be ideal for comparison of ACM enrichment profiles from astrocytes exposed to different stimuli known to affect

secretory pathways. In this way, novel proteins that proceed by nonconventional secretion could be identified.

5.3 Proteomic identification of S-nitrosylated proteins.

Overall, the goal to develop a complementary approach for identification of S-nitrosylated proteins based on peptide affinity enrichment and tandem mass spectrometry analysis was largely successful. Compared to previous studies examining in vitro S-nitrosylation in cell culture models, a significant increase in sensitivity was achieved with 20 proteins being identified (with sites of modification) from as little as 1 nmol of protein S-nitrosocysteine. However, despite this gain in sensitivity afforded by peptide affinity enrichment and detection by an ion trap mass spectrometer, the current sensitivity still falls short of approaching most endogenous proteomes. Endogenous S-nitrosylation likely occurs 10 to 100-fold less in abundance than what is generated by exposure of cells or tissues to S-nitrosating agents. Given starting material in our experiments was usually between 1-2 mg, 20 to 200 mg of soluble protein would be required to achieve the same depth of analysis in an endogenous S-nitrosoproteome. The most likely weakness in the methodology lies in the ascorbate-mediated reduction of S-nitrosocysteine, which is relatively inefficient.

Development of methods for the identification of endogenous S-nitrosylated proteins will provide tools to address several fundamental questions that remain unanswered in the field of NO-mediated S-nitrosylation. Most notably, what are the *in vivo* mechanism of protein S-nitrosylation and denitrosylation. Current genetics approaches have generated mice which lack an enzyme that breaks down GSNO (Liu et al. 2001), providing an attractive model to test the in vivo mechanisms for regulating protein S-nitrosocysteine levels.

References

Abele, A.E., Scholz, K.P., Scholz, W.K. & Miller, R.J. 1990, "Excitotoxicity induced by enhanced excitatory neurotransmission in cultured hippocampal pyramidal neurons", *Neuron,* vol. 4, no. 3, pp. 413-419.

Al-Shahrour, F., Diaz-Uriarte, R. & Dopazo, J. 2004, "FatiGO: a web tool for finding significant associations of Gene Ontology terms with groups of genes", *Bioinformatics (Oxford, England),* vol. 20, no. 4, pp. 578-580.

Antony, J.M., Ellestad, K.K., Hammond, R., Imaizumi, K., Mallet, F., Warren, K.G. & Power, C. 2007, "The human endogenous retrovirus envelope glycoprotein, syncytin-1, regulates neuroinflammation and its receptor expression in multiple sclerosis: a role for endoplasmic reticulum chaperones in astrocytes", *Journal of immunology (Baltimore, Md.: 1950),* vol. 179, no. 2, pp. 1210-1224.

Antony, J.M., van Marle, G., Opii, W., Butterfield, D.A., Mallet, F., Yong, V.W., Wallace, J.L., Deacon, R.M., Warren, K. & Power, C. 2004, "Human endogenous retrovirus glycoprotein-mediated induction of redox reactants causes oligodendrocyte death and demyelination", *Nature neuroscience,* vol. 7, no. 10, pp. 1088-1095.

Babcock, A.A., Kuziel, W.A., Rivest, S. & Owens, T. 2003, "Chemokine expression by glial cells directs leukocytes to sites of axonal injury in the CNS", *The Journal of neuroscience : the official journal of the Society for Neuroscience,* vol. 23, no. 21, pp. 7922-7930.

Baldwin, T.A. & Ostergaard, H.L. 2002, "The protein-tyrosine phosphatase CD45 reaches the cell surface via golgi-dependent and -independent pathways", *The Journal of biological chemistry,* vol. 277, no. 52, pp. 50333-50340.

Ballanyi, K., Grafe, P. & ten Bruggencate, G. 1987, "Ion activities and potassium uptake mechanisms of glial cells in guinea-pig olfactory cortex slices", *The Journal of physiology,* vol. 382, pp. 159-174.

Banker, G.A. 1980, "Trophic interactions between astroglial cells and hippocampal neurons in culture", *Science (New York, N.Y.),* vol. 209, no. 4458, pp. 809-810.

Bendall, S.C., Hughes, C., Stewart, M.H., Doble, B., Bhatia, M. & Lajoie, G.A. 2008, "Prevention of amino acid conversion in SILAC experiments with embryonic stem cells", *Molecular & cellular proteomics : MCP,* vol. 7, no. 9, pp. 1587-1597.

Bendtsen, J.D., Jensen, L.J., Blom, N., Von Heijne, G. & Brunak, S. 2004a, "Feature-based prediction of non-classical and leaderless protein secretion", *Protein engineering, design & selection : PEDS,* vol. 17, no. 4, pp. 349-356.

Bendtsen, J.D., Nielsen, H., von Heijne, G. & Brunak, S. 2004b, "Improved prediction of signal peptides: SignalP 3.0", *Journal of Molecular Biology,* vol. 340, no. 4, pp. 783-795.

Bennett, M.R., Evan, G.I. & Schwartz, S.M. 1995, "Apoptosis of human vascular smooth muscle cells derived from normal vessels and coronary atherosclerotic plaques", *The Journal of clinical investigation,* vol. 95, no. 5, pp. 2266-2274.

Bernardinelli, Y., Magistretti, P.J. & Chatton, J.Y. 2004, "Astrocytes generate Na+-mediated metabolic waves", *Proceedings of the National Academy of Sciences of the United States of America,* vol. 101, no. 41, pp. 14937-14942.

Bezzi, P., Domercq, M., Brambilla, L., Galli, R., Schols, D., De Clercq, E., Vescovi, A., Bagetta, G., Kollias, G., Meldolesi, J. & Volterra, A. 2001, "CXCR4-activated astrocyte glutamate release via TNFalpha: amplification by microglia triggers neurotoxicity", *Nature neuroscience,* vol. 4, no. 7, pp. 702-710.

Bolotina, V.M., Najibi, S., Palacino, J.J., Pagano, P.J. & Cohen, R.A. 1994, "Nitric oxide directly activates calcium-dependent potassium channels in vascular smooth muscle", *Nature,* vol. 368, no. 6474, pp. 850-853.

Brown, O.A., Sosa, Y.E., Castro, M.G. & Goya, R.G. 2000, "Studies on the prolactin-releasing mechanism of histones H2A and H2B", *Life Sciences,* vol. 66, no. 21, pp. 2081-2089.

Cahoy, J.D., Emery, B., Kaushal, A., Foo, L.C., Zamanian, J.L., Christopherson, K.S., Xing, Y., Lubischer, J.L., Krieg, P.A., Krupenko, S.A., Thompson, W.J. & Barres, B.A. 2008, "A transcriptome database for astrocytes, neurons, and oligodendrocytes: a new resource for understanding brain development and function", *The Journal of neuroscience : the official journal of the Society for Neuroscience,* vol. 28, no. 1, pp. 264-278.

Calegari, F., Coco, S., Taverna, E., Bassetti, M., Verderio, C., Corradi, N., Matteoli, M. & Rosa, P. 1999, "A regulated secretory pathway in cultured hippocampal astrocytes", *The Journal of biological chemistry,* vol. 274, no. 32, pp. 22539-22547.

Carvalho, P.C., Fischer, J.S., Chen, E.I., Yates, J.R.,3rd & Barbosa, V.C. 2008, "PatternLab for proteomics: a tool for differential shotgun proteomics", *BMC bioinformatics,* vol. 9, pp. 316.

Cassina, P., Pehar, M., Vargas, M.R., Castellanos, R., Barbeito, A.G., Estevez, A.G., Thompson, J.A., Beckman, J.S. & Barbeito, L. 2005, "Astrocyte activation by fibroblast growth factor-1 and motor neuron apoptosis: implications for amyotrophic lateral sclerosis", *Journal of neurochemistry,* vol. 93, no. 1, pp. 38-46.

Choi, H., Fermin, D. & Nesvizhskii, A.I. 2008, "Significance analysis of spectral count data in label-free shotgun proteomics", *Molecular & cellular proteomics : MCP,* vol. 7, no. 12, pp. 2373-2385.

Choi, H. & Nesvizhskii, A.I. 2008, "Semisupervised model-based validation of peptide identifications in mass spectrometry-based proteomics", *Journal of proteome research,* vol. 7, no. 1, pp. 254-265.

Choi, Y.B. & Lipton, S.A. 2000, "Redox modulation of the NMDA receptor", *Cellular and molecular life sciences : CMLS,* vol. 57, no. 11, pp. 1535-1541.

Choi, Y.B., Tenneti, L., Le, D.A., Ortiz, J., Bai, G., Chen, H.S. & Lipton, S.A. 2000, "Molecular basis of NMDA receptor-coupled ion channel modulation by S-nitrosylation", *Nature neuroscience,* vol. 3, no. 1, pp. 15-21.

Christopherson, K.S., Ullian, E.M., Stokes, C.C., Mullowney, C.E., Hell, J.W., Agah, A., Lawler, J., Mosher, D.F., Bornstein, P. & Barres, B.A. 2005, "Thrombospondins are astrocyte-secreted proteins that promote CNS synaptogenesis", *Cell,* vol. 120, no. 3, pp. 421-433.

Chukkapalli, G., Guda, C. & Subramaniam, S. 2004, "SledgeHMMER: a web server for batch searching the Pfam database", *Nucleic acids research,* vol. 32, no. Web Server issue, pp. W542-4.

Chung, K.N., Walter, P., Aponte, G.W. & Moore, H.P. 1989, "Molecular sorting in the secretory pathway", *Science (New York, N.Y.),* vol. 243, no. 4888, pp. 192-197.

Ciccarelli, R., Di Iorio, P., Bruno, V., Battaglia, G., D'Alimonte, I., D'Onofrio, M., Nicoletti, F. & Caciagli, F. 1999, "Activation of A(1) adenosine or mGlu3 metabotropic glutamate receptors enhances the release of nerve growth factor and S-100beta protein from cultured astrocytes", *Glia,* vol. 27, no. 3, pp. 275-281.

Cleves, A.E., Cooper, D.N., Barondes, S.H. & Kelly, R.B. 1996, "A new pathway for protein export in Saccharomyces cerevisiae", *The Journal of cell biology,* vol. 133, no. 5, pp. 1017-1026.

Cociorva, D., L Tabb, D. & Yates, J.R. 2007, "Validation of tandem mass spectrometry database search results using DTASelect", *Current protocols in bioinformatics / editoral board, Andreas D.Baxevanis ...[et al.],* vol. Chapter 13, pp. Unit 13.4.

Combrinck, M., Williams, J., De Berardinis, M.A., Warden, D., Puopolo, M., Smith, A.D. & Minghetti, L. 2006, "Levels of CSF prostaglandin E2, cognitive decline, and survival in Alzheimer's disease", *Journal of neurology, neurosurgery, and psychiatry,* vol. 77, no. 1, pp. 85-88.

Cox, J. & Mann, M. 2008, "MaxQuant enables high peptide identification rates, individualized p.p.b.-range mass accuracies and proteome-wide protein quantification", *Nature biotechnology,* vol. 26, no. 12, pp. 1367-1372.

Craig, R. & Beavis, R.C. 2004, "TANDEM: matching proteins with tandem mass spectra", *Bioinformatics (Oxford, England),* vol. 20, no. 9, pp. 1466-1467.

Craig, R., Cortens, J.P. & Beavis, R.C. 2005, "The use of proteotypic peptide libraries for protein identification", *Rapid communications in mass spectrometry : RCM,* vol. 19, no. 13, pp. 1844-1850.

Czapski, G. & Goldstein, S. 1995, "The role of the reactions of .NO with superoxide and oxygen in biological systems: a kinetic approach", *Free radical biology & medicine,* vol. 19, no. 6, pp. 785-794.

Darwin, K.H., Ehrt, S., Gutierrez-Ramos, J.C., Weich, N. & Nathan, C.F. 2003, "The proteasome of Mycobacterium tuberculosis is required for resistance to nitric oxide", *Science (New York, N.Y.),* vol. 302, no. 5652, pp. 1963-1966.

Davis, B.D. & Tai, P.C. 1980, "The mechanism of protein secretion across membranes", *Nature,* vol. 283, no. 5746, pp. 433-438.

de Belder, A.J., MacAllister, R., Radomski, M.W., Moncada, S. & Vallance, P.J. 1994, "Effects of S-nitroso-glutathione in the human forearm circulation: evidence for selective inhibition of platelet activation", *Cardiovascular research,* vol. 28, no. 5, pp. 691-694.

De Roo, M., Klauser, P., Garcia, P.M., Poglia, L. & Muller, D. 2008, "Spine dynamics and synapse remodeling during LTP and memory processes", *Progress in brain research,* vol. 169, pp. 199-207.

Delcourt, N., Jouin, P., Poncet, J., Demey, E., Mauger, E., Bockaert, J., Marin, P. & Galeotti, N. 2005, "Difference in mass analysis using labeled lysines (DIMAL-K): a new, efficient proteomic quantification method applied to the analysis of astrocytic secretomes", *Molecular & cellular proteomics : MCP,* vol. 4, no. 8, pp. 1085-1094.

Dempester, A.J. 1918, "A new Method of Positive Ray Analysis", *Physical Review,* vol. 11, no. 4, pp. 316.

Dennehy, M.K., Richards, K.A., Wernke, G.R., Shyr, Y. & Liebler, D.C. 2006, "Cytosolic and nuclear protein targets of thiol-reactive electrophiles", *Chemical research in toxicology,* vol. 19, no. 1, pp. 20-29.

Denny, C.A., Alroy, J., Pawlyk, B.S., Sandberg, M.A., d'Azzo, A. & Seyfried, T.N. 2007, "Neurochemical, morphological, and neurophysiological abnormalities in retinas of

Sandhoff and GM1 gangliosidosis mice", *Journal of neurochemistry,* vol. 101, no. 5, pp. 1294-1302.

Di Giorgio, F.P., Carrasco, M.A., Siao, M.C., Maniatis, T. & Eggan, K. 2007, "Non-cell autonomous effect of glia on motor neurons in an embryonic stem cell-based ALS model", *Nature neuroscience,* vol. 10, no. 5, pp. 608-614.

Ding, S., Fellin, T., Zhu, Y., Lee, S.Y., Auberson, Y.P., Meaney, D.F., Coulter, D.A., Carmignoto, G. & Haydon, P.G. 2007, "Enhanced astrocytic Ca2+ signals contribute to neuronal excitotoxicity after status epilepticus", *The Journal of neuroscience : the official journal of the Society for Neuroscience,* vol. 27, no. 40, pp. 10674-10684.

Donaldson, J.G., Finazzi, D. & Klausner, R.D. 1992, "Brefeldin A inhibits Golgi membrane-catalysed exchange of guanine nucleotide onto ARF protein", *Nature,* vol. 360, no. 6402, pp. 350-352.

Dong, Y. & Benveniste, E.N. 2001, "Immune function of astrocytes", *Glia,* vol. 36, no. 2, pp. 180-190.

Donsante, A., Levy, B., Vogler, C. & Sands, M.S. 2007, "Clinical response to persistent, low-level beta-glucuronidase expression in the murine model of mucopolysaccharidosis type VII", *Journal of inherited metabolic disease,* vol. 30, no. 2, pp. 227-238.

Dowell, J.A., Johnson, J.A. & Li, L. 2009, "Identification of Astrocyte Secreted Proteins with a Combination of Shotgun Proteomics and Bioinformatics", *Journal of proteome research,* .

Dringen, R., Bishop, G.M., Koeppe, M., Dang, T.N. & Robinson, S.R. 2007, "The pivotal role of astrocytes in the metabolism of iron in the brain", *Neurochemical research,* vol. 32, no. 11, pp. 1884-1890.

Duan, X., Yang, J., Ren, B., Tan, G. & Ding, H. 2009, "Reactivity of nitric oxide with the [4Fe-4S] cluster of dihydroxyacid dehydratase from Escherichia coli", *The Biochemical journal,* vol. 417, no. 3, pp. 783-789.

Ducret, A., Van Oostveen, I., Eng, J.K., Yates, J.R.,3rd & Aebersold, R. 1998, "High throughput protein characterization by automated reverse-phase chromatography/electrospray tandem mass spectrometry", *Protein science : a publication of the Protein Society,* vol. 7, no. 3, pp. 706-719.

Egnaczyk, G.F., Pomonis, J.D., Schmidt, J.A., Rogers, S.D., Peters, C., Ghilardi, J.R., Mantyh, P.W. & Maggio, J.E. 2003, "Proteomic analysis of the reactive phenotype of astrocytes following endothelin-1 exposure", *Proteomics,* vol. 3, no. 5, pp. 689-698.

Emanuelsson, O., Brunak, S., von Heijne, G. & Nielsen, H. 2007, "Locating proteins in the cell using TargetP, SignalP and related tools", *Nature protocols,* vol. 2, no. 4, pp. 953-971.

Emanuelsson, O., Nielsen, H., Brunak, S. & von Heijne, G. 2000, "Predicting subcellular localization of proteins based on their N-terminal amino acid sequence", *Journal of Molecular Biology,* vol. 300, no. 4, pp. 1005-1016.

Eriksson, J. & Fenyo, D. 2007, "Improving the success rate of proteome analysis by modeling protein-abundance distributions and experimental designs", *Nature biotechnology,* vol. 25, no. 6, pp. 651-655.

Escartin, C., Valette, J., Lebon, V. & Bonvento, G. 2006, "Neuron-astrocyte interactions in the regulation of brain energy metabolism: a focus on NMR spectroscopy", *Journal of neurochemistry,* vol. 99, no. 2, pp. 393-401.

Fang, K., Ragsdale, N.V., Carey, R.M., MacDonald, T. & Gaston, B. 1998, "Reductive assays for S-nitrosothiols: implications for measurements in biological systems", *Biochemical and biophysical research communications,* vol. 252, no. 3, pp. 535-540.

Fatal, N., Karhinen, L., Jokitalo, E. & Makarow, M. 2004, "Active and specific recruitment of a soluble cargo protein for endoplasmic reticulum exit in the absence of functional COPII component Sec24p", *Journal of cell science,* vol. 117, no. Pt 9, pp. 1665-1673.

Fenn, J.B., Mann, M., Meng, C.K., Wong, S.F. & Whitehouse, C.M. 1989, "Electrospray ionization for mass spectrometry of large biomolecules", *Science (New York, N.Y.),* vol. 246, no. 4926, pp. 64-71.

Flieger, O., Engling, A., Bucala, R., Lue, H., Nickel, W. & Bernhagen, J. 2003, "Regulated secretion of macrophage migration inhibitory factor is mediated by a non-classical pathway involving an ABC transporter", *FEBS letters,* vol. 551, no. 1-3, pp. 78-86.

Frye, B.C., Halfter, S., Djudjaj, S., Muehlenberg, P., Weber, S., Raffetseder, U., En-Nia, A., Knott, H., Baron, J.M., Dooley, S., Bernhagen, J. & Mertens, P.R. 2009, "Y-box protein-1 is actively secreted through a non-classical pathway and acts as an extracellular mitogen", *EMBO reports,* vol. 10, no. 7, pp. 783-789.

Furchgott, R.F. & Zawadzki, J.V. 1980, "The obligatory role of endothelial cells in the relaxation of arterial smooth muscle by acetylcholine", *Nature,* vol. 288, no. 5789, pp. 373-376.

Gao, C., Guo, H., Wei, J., Mi, Z., Wai, P.Y. & Kuo, P.C. 2005, "Identification of S-nitrosylated proteins in endotoxin-stimulated RAW264.7 murine macrophages", *Nitric*

oxide : biology and chemistry / official journal of the Nitric Oxide Society, vol. 12, no. 2, pp. 121-126.

Garcia, A.D., Doan, N.B., Imura, T., Bush, T.G. & Sofroniew, M.V. 2004, "GFAP-expressing progenitors are the principal source of constitutive neurogenesis in adult mouse forebrain", *Nature neuroscience,* vol. 7, no. 11, pp. 1233-1241.

Gardella, S., Andrei, C., Ferrera, D., Lotti, L.V., Torrisi, M.R., Bianchi, M.E. & Rubartelli, A. 2002, "The nuclear protein HMGB1 is secreted by monocytes via a non-classical, vesicle-mediated secretory pathway", *EMBO reports,* vol. 3, no. 10, pp. 995-1001.

Gilchrist, A., Au, C.E., Hiding, J., Bell, A.W., Fernandez-Rodriguez, J., Lesimple, S., Nagaya, H., Roy, L., Gosline, S.J., Hallett, M., Paiement, J., Kearney, R.E., Nilsson, T. & Bergeron, J.J. 2006, "Quantitative proteomics analysis of the secretory pathway", *Cell,* vol. 127, no. 6, pp. 1265-1281.

Glabinski, A.R., Tani, M., Strieter, R.M., Tuohy, V.K. & Ransohoff, R.M. 1997, "Synchronous synthesis of alpha- and beta-chemokines by cells of diverse lineage in the central nervous system of mice with relapses of chronic experimental autoimmune encephalomyelitis", *The American journal of pathology,* vol. 150, no. 2, pp. 617-630.

Gorr, S.U. & Darling, D.S. 1995, "An N-terminal hydrophobic peak is the sorting signal of regulated secretory proteins", *FEBS letters,* vol. 361, no. 1, pp. 8-12.

Gow, A.J., Buerk, D.G. & Ischiropoulos, H. 1997, "A novel reaction mechanism for the formation of S-nitrosothiol in vivo", *The Journal of biological chemistry,* vol. 272, no. 5, pp. 2841-2845.

Gow, A.J., Davis, C.W., Munson, D. & Ischiropoulos, H. 2004, "Immunohistochemical detection of S-nitrosylated proteins", *Methods in molecular biology (Clifton, N.J.),* vol. 279, pp. 167-172.

Graumann, J., Hubner, N.C., Kim, J.B., Ko, K., Moser, M., Kumar, C., Cox, J., Scholer, H. & Mann, M. 2008, "Stable isotope labeling by amino acids in cell culture (SILAC) and proteome quantitation of mouse embryonic stem cells to a depth of 5,111 proteins", *Molecular & cellular proteomics : MCP,* vol. 7, no. 4, pp. 672-683.

Grimmond, S.M., Miranda, K.C., Yuan, Z., Davis, M.J., Hume, D.A., Yagi, K., Tominaga, N., Bono, H., Hayashizaki, Y., Okazaki, Y., Teasdale, R.D., RIKEN GER Group & GSL Members 2003, "The mouse secretome: functional classification of the proteins secreted into the extracellular environment", *Genome research,* vol. 13, no. 6B, pp. 1350-1359.

Gronborg, M., Kristiansen, T.Z., Iwahori, A., Chang, R., Reddy, R., Sato, N., Molina, H., Jensen, O.N., Hruban, R.H., Goggins, M.G., Maitra, A. & Pandey, A. 2006, "Biomarker discovery from pancreatic cancer secretome using a differential proteomic approach", *Molecular & cellular proteomics : MCP,* vol. 5, no. 1, pp. 157-171.

Guidotti, A., Forchetti, C.M., Corda, M.G., Konkel, D., Bennett, C.D. & Costa, E. 1983, "Isolation, characterization, and purification to homogeneity of an endogenous polypeptide with agonistic action on benzodiazepine receptors", *Proceedings of the National Academy of Sciences of the United States of America,* vol. 80, no. 11, pp. 3531-3535.

Gygi, S.P., Rist, B., Gerber, S.A., Turecek, F., Gelb, M.H. & Aebersold, R. 1999, "Quantitative analysis of complex protein mixtures using isotope-coded affinity tags", *Nature biotechnology,* vol. 17, no. 10, pp. 994-999.

Halassa, M.M., Fellin, T. & Haydon, P.G. 2007, "The tripartite synapse: roles for gliotransmission in health and disease", *Trends in molecular medicine,* vol. 13, no. 2, pp. 54-63.

Hansen, T.J., Croisy, A.F. & Keefer, L.K. 1982, "N-nitrosation of secondary amines by nitric oxide via the 'Drago complex'", *IARC scientific publications,* vol. (41), no. 41, pp. 21-29.

Hao, G., Derakhshan, B., Shi, L., Campagne, F. & Gross, S.S. 2006a, "SNOSID, a proteomic method for identification of cysteine S-nitrosylation sites in complex protein mixtures", *Proceedings of the National Academy of Sciences of the United States of America,* vol. 103, no. 4, pp. 1012-1017.

Hao, G., Derakhshan, B., Shi, L., Campagne, F. & Gross, S.S. 2006b, "SNOSID, a proteomic method for identification of cysteine S-nitrosylation sites in complex protein mixtures", *Proceedings of the National Academy of Sciences of the United States of America,* vol. 103, no. 4, pp. 1012-1017.

Hara, M.R., Agrawal, N., Kim, S.F., Cascio, M.B., Fujimuro, M., Ozeki, Y., Takahashi, M., Cheah, J.H., Tankou, S.K., Hester, L.D., Ferris, C.D., Hayward, S.D., Snyder, S.H. & Sawa, A. 2005, "S-nitrosylated GAPDH initiates apoptotic cell death by nuclear translocation following Siah1 binding", *Nature cell biology,* vol. 7, no. 7, pp. 665-674.

Hawkins, J. & Boden, M. 2006, "Detecting and sorting targeting peptides with neural networks and support vector machines", *Journal of bioinformatics and computational biology,* vol. 4, no. 1, pp. 1-18.

Haydon, P.G. & Carmignoto, G. 2006, "Astrocyte control of synaptic transmission and neurovascular coupling", *Physiological Reviews,* vol. 86, no. 3, pp. 1009-1031.

Helms, J.B. & Rothman, J.E. 1992, "Inhibition by brefeldin A of a Golgi membrane enzyme that catalyses exchange of guanine nucleotide bound to ARF", *Nature,* vol. 360, no. 6402, pp. 352-354.

Hengst, U., Albrecht, H., Hess, D. & Monard, D. 2001, "The phosphatidylethanolamine-binding protein is the prototype of a novel family of serine protease inhibitors", *The Journal of biological chemistry,* vol. 276, no. 1, pp. 535-540.

Heo, J., Prutzman, K.C., Mocanu, V. & Campbell, S.L. 2005, "Mechanism of free radical nitric oxide-mediated Ras guanine nucleotide dissociation", *Journal of Molecular Biology,* vol. 346, no. 5, pp. 1423-1440.

Hess, D.T., Matsumoto, A., Kim, S.O., Marshall, H.E. & Stamler, J.S. 2005, "Protein S-nitrosylation: purview and parameters", *Nature reviews.Molecular cell biology,* vol. 6, no. 2, pp. 150-166.

Hess, D.T., Matsumoto, A., Nudelman, R. & Stamler, J.S. 2001, "S-nitrosylation: spectrum and specificity", *Nature cell biology,* vol. 3, no. 2, pp. E46-9.

Hirsch-Reinshagen, V., Zhou, S., Burgess, B.L., Bernier, L., McIsaac, S.A., Chan, J.Y., Tansley, G.H., Cohn, J.S., Hayden, M.R. & Wellington, C.L. 2004, "Deficiency of ABCA1 impairs apolipoprotein E metabolism in brain", *The Journal of biological chemistry,* vol. 279, no. 39, pp. 41197-41207.

Holt, O.J., Gallo, F. & Griffiths, G.M. 2006, "Regulating secretory lysosomes", *Journal of Biochemistry,* vol. 140, no. 1, pp. 7-12.

Huang, Y., Man, H.Y., Sekine-Aizawa, Y., Han, Y., Juluri, K., Luo, H., Cheah, J., Lowenstein, C., Huganir, R.L. & Snyder, S.H. 2005, "S-nitrosylation of N-ethylmaleimide sensitive factor mediates surface expression of AMPA receptors", *Neuron,* vol. 46, no. 4, pp. 533-540.

Huang, Y., Weisgraber, K.H., Mucke, L. & Mahley, R.W. 2004, "Apolipoprotein E: diversity of cellular origins, structural and biophysical properties, and effects in Alzheimer's disease", *Journal of molecular neuroscience : MN,* vol. 23, no. 3, pp. 189-204.

Ignarro, L.J., Harbison, R.G., Wood, K.S. & Kadowitz, P.J. 1986, "Activation of purified soluble guanylate cyclase by endothelium-derived relaxing factor from intrapulmonary artery and vein: stimulation by acetylcholine, bradykinin and arachidonic acid", *The Journal of pharmacology and experimental therapeutics,* vol. 237, no. 3, pp. 893-900.

Ihrie, R.A. & Alvarez-Buylla, A. 2008, "Cells in the astroglial lineage are neural stem cells", *Cell and tissue research,* vol. 331, no. 1, pp. 179-191.

Imitola, J., Raddassi, K., Park, K.I., Mueller, F.J., Nieto, M., Teng, Y.D., Frenkel, D., Li, J., Sidman, R.L., Walsh, C.A., Snyder, E.Y. & Khoury, S.J. 2004, "Directed migration of neural stem cells to sites of CNS injury by the stromal cell-derived factor 1alpha/CXC chemokine receptor 4 pathway", *Proceedings of the National Academy of Sciences of the United States of America,* vol. 101, no. 52, pp. 18117-18122.

Ischiropoulos, H., Zhu, L., Chen, J., Tsai, M., Martin, J.C., Smith, C.D. & Beckman, J.S. 1992, "Peroxynitrite-mediated tyrosine nitration catalyzed by superoxide dismutase", *Archives of Biochemistry and Biophysics,* vol. 298, no. 2, pp. 431-437.

Ishihama, Y., Oda, Y., Tabata, T., Sato, T., Nagasu, T., Rappsilber, J. & Mann, M. 2005, "Exponentially modified protein abundance index (emPAI) for estimation of absolute protein amount in proteomics by the number of sequenced peptides per protein", *Molecular & cellular proteomics : MCP,* vol. 4, no. 9, pp. 1265-1272.

Jaffrey, S.R., Erdjument-Bromage, H., Ferris, C.D., Tempst, P. & Snyder, S.H. 2001, "Protein S-nitrosylation: a physiological signal for neuronal nitric oxide", *Nature cell biology,* vol. 3, no. 2, pp. 193-197.

Jaffrey, S.R. & Snyder, S.H. 2001, "The biotin switch method for the detection of S-nitrosylated proteins", *Science's STKE : signal transduction knowledge environment,* vol. 2001, no. 86, pp. PL1.

Katsuki, S., Arnold, W., Mittal, C. & Murad, F. 1977, "Stimulation of guanylate cyclase by sodium nitroprusside, nitroglycerin and nitric oxide in various tissue preparations and comparison to the effects of sodium azide and hydroxylamine", *Journal of cyclic nucleotide research,* vol. 3, no. 1, pp. 23-35.

Keene, S.D., Greco, T.M., Parastatidis, I., Lee, S.H., Hughes, E.G., Balice-Gordon, R.J., Speicher, D.W. & Ischiropoulos, H. 2009, "Mass spectrometric and computational analysis of cytokine-induced alterations in the astrocyte secretome", *Proteomics,* vol. 9, no. 3, pp. 768-782.

Keller, A., Nesvizhskii, A.I., Kolker, E. & Aebersold, R. 2002a, "Empirical statistical model to estimate the accuracy of peptide identifications made by MS/MS and database search", *Analytical Chemistry,* vol. 74, no. 20, pp. 5383-5392.

Keller, A., Nesvizhskii, A.I., Kolker, E. & Aebersold, R. 2002b, "Empirical statistical model to estimate the accuracy of peptide identifications made by MS/MS and database search", *Analytical Chemistry,* vol. 74, no. 20, pp. 5383-5392.

Kelly, R.B. 1985, "Pathways of protein secretion in eukaryotes", *Science (New York, N.Y.),* vol. 230, no. 4721, pp. 25-32.

Kim, S.F., Huri, D.A. & Snyder, S.H. 2005, "Inducible nitric oxide synthase binds, S-nitrosylates, and activates cyclooxygenase-2", *Science (New York, N.Y.),* vol. 310, no. 5756, pp. 1966-1970.

Kinseth, M.A., Anjard, C., Fuller, D., Guizzunti, G., Loomis, W.F. & Malhotra, V. 2007, "The Golgi-associated protein GRASP is required for unconventional protein secretion during development", *Cell,* vol. 130, no. 3, pp. 524-534.

Klee, E.W. & Sosa, C.P. 2007, "Computational classification of classically secreted proteins", *Drug discovery today,* vol. 12, no. 5-6, pp. 234-240.

Koistinaho, M., Lin, S., Wu, X., Esterman, M., Koger, D., Hanson, J., Higgs, R., Liu, F., Malkani, S., Bales, K.R. & Paul, S.M. 2004, "Apolipoprotein E promotes astrocyte colocalization and degradation of deposited amyloid-beta peptides", *Nature medicine,* vol. 10, no. 7, pp. 719-726.

Koppenol, W.H., Moreno, J.J., Pryor, W.A., Ischiropoulos, H. & Beckman, J.S. 1992, "Peroxynitrite, a cloaked oxidant formed by nitric oxide and superoxide", *Chemical research in toxicology,* vol. 5, no. 6, pp. 834-842.

Kreft, M., Potokar, M., Stenovec, M., Pangrsic, T. & Zorec, R. 2009, "Regulated exocytosis and vesicle trafficking in astrocytes", *Annals of the New York Academy of Sciences,* vol. 1152, pp. 30-42.

Krumbholz, M., Theil, D., Cepok, S., Hemmer, B., Kivisakk, P., Ransohoff, R.M., Hofbauer, M., Farina, C., Derfuss, T., Hartle, C., Newcombe, J., Hohlfeld, R. & Meinl, E. 2006, "Chemokines in multiple sclerosis: CXCL12 and CXCL13 up-regulation is differentially linked to CNS immune cell recruitment", *Brain : a journal of neurology,* vol. 129, no. Pt 1, pp. 200-211.

Kuncewicz, T., Sheta, E.A., Goldknopf, I.L. & Kone, B.C. 2003, "Proteomic analysis of S-nitrosylated proteins in mesangial cells", *Molecular & cellular proteomics : MCP,* vol. 2, no. 3, pp. 156-163.

Kuster, B., Schirle, M., Mallick, P. & Aebersold, R. 2005, "Scoring proteomes with proteotypic peptide probes", *Nature reviews.Molecular cell biology,* vol. 6, no. 7, pp. 577-583.

Kwiatkowski, D.J., Mehl, R. & Yin, H.L. 1988, "Genomic organization and biosynthesis of secreted and cytoplasmic forms of gelsolin", *The Journal of cell biology,* vol. 106, no. 2, pp. 375-384.

Lafon-Cazal, M., Adjali, O., Galeotti, N., Poncet, J., Jouin, P., Homburger, V., Bockaert, J. & Marin, P. 2003, "Proteomic analysis of astrocytic secretion in the mouse.

209

Comparison with the cerebrospinal fluid proteome", *The Journal of biological chemistry,* vol. 278, no. 27, pp. 24438-24448.

Lander, H.M., Hajjar, D.P., Hempstead, B.L., Mirza, U.A., Chait, B.T., Campbell, S. & Quilliam, L.A. 1997, "A molecular redox switch on p21(ras). Structural basis for the nitric oxide-p21(ras) interaction", *The Journal of biological chemistry,* vol. 272, no. 7, pp. 4323-4326.

Lee, D.Y., Huang, C.M., Nakatsuji, T., Thiboutot, D., Kang, S.A., Monestier, M. & Gallo, R.L. 2009, "Histone H4 Is a Major Component of the Antimicrobial Action of Human Sebocytes", *The Journal of investigative dermatology, .*

Leimberg, M.J., Prus, E., Konijn, A.M. & Fibach, E. 2008, "Macrophages function as a ferritin iron source for cultured human erythroid precursors", *Journal of cellular biochemistry,* vol. 103, no. 4, pp. 1211-1218.

Li, D., Ropert, N., Koulakoff, A., Giaume, C. & Oheim, M. 2008, "Lysosomes are the major vesicular compartment undergoing Ca2+-regulated exocytosis from cortical astrocytes", *The Journal of neuroscience : the official journal of the Society for Neuroscience,* vol. 28, no. 30, pp. 7648-7658.

Li, X.J., Zhang, H., Ranish, J.A. & Aebersold, R. 2003, "Automated statistical analysis of protein abundance ratios from data generated by stable-isotope dilution and tandem mass spectrometry", *Analytical Chemistry,* vol. 75, no. 23, pp. 6648-6657.

Liauw, J., Hoang, S., Choi, M., Eroglu, C., Choi, M., Sun, G.H., Percy, M., Wildman-Tobriner, B., Bliss, T., Guzman, R.G., Barres, B.A. & Steinberg, G.K. 2008, "Thrombospondins 1 and 2 are necessary for synaptic plasticity and functional recovery after stroke", *Journal of cerebral blood flow and metabolism : official journal of the International Society of Cerebral Blood Flow and Metabolism,* vol. 28, no. 10, pp. 1722-1732.

Lincoln, T.M., Wu, X., Sellak, H., Dey, N. & Choi, C.S. 2006, "Regulation of vascular smooth muscle cell phenotype by cyclic GMP and cyclic GMP-dependent protein kinase", *Frontiers in bioscience : a journal and virtual library,* vol. 11, pp. 356-367.

Lingappa, V.R., Chaidez, J., Yost, C.S. & Hedgpeth, J. 1984, "Determinants for protein localization: beta-lactamase signal sequence directs globin across microsomal membranes", *Proceedings of the National Academy of Sciences of the United States of America,* vol. 81, no. 2, pp. 456-460.

Lingappa, V.R., Lingappa, J.R. & Blobel, G. 1980, "Signal sequences for early events in protein secretion and membrane assembly", *Annals of the New York Academy of Sciences,* vol. 343, pp. 356-361.

210

Liou, W., Geuze, H.J. & Slot, J.W. 1996, "Improving structural integrity of cryosections for immunogold labeling", *Histochemistry and cell biology,* vol. 106, no. 1, pp. 41-58.

Liu, H., Sadygov, R.G. & Yates, J.R.,3rd 2004, "A model for random sampling and estimation of relative protein abundance in shotgun proteomics", *Analytical Chemistry,* vol. 76, no. 14, pp. 4193-4201.

Liu, L., Hausladen, A., Zeng, M., Que, L., Heitman, J. & Stamler, J.S. 2001, "A metabolic enzyme for S-nitrosothiol conserved from bacteria to humans", *Nature,* vol. 410, no. 6827, pp. 490-494.

Liu, Q., Tan, G., Levenkova, N., Li, T., Pugh, E.N.,Jr, Rux, J.J., Speicher, D.W. & Pierce, E.A. 2007, "The Proteome of the Mouse Photoreceptor Sensory Cilium Complex", *Mol.Cell.Proteomics,* vol. 6, no. 8, pp. 1299-1317.

Liu, X., Miller, M.J., Joshi, M.S., Thomas, D.D. & Lancaster, J.R.,Jr 1998, "Accelerated reaction of nitric oxide with O2 within the hydrophobic interior of biological membranes", *Proceedings of the National Academy of Sciences of the United States of America,* vol. 95, no. 5, pp. 2175-2179.

Liu, X.Y., Yang, J.L., Chen, L.J., Zhang, Y., Yang, M.L., Wu, Y.Y., Li, F.Q., Tang, M.H., Liang, S.F. & Wei, Y.Q. 2008, "Comparative proteomics and correlated signaling network of rat hippocampus in the pilocarpine model of temporal lobe epilepsy", *Proteomics,* vol. 8, no. 3, pp. 582-603.

Lu, P., Vogel, C., Wang, R., Yao, X. & Marcotte, E.M. 2007, "Absolute protein expression profiling estimates the relative contributions of transcriptional and translational regulation", *Nature biotechnology,* vol. 25, no. 1, pp. 117-124.

Lukes, A., Mun-Bryce, S., Lukes, M. & Rosenberg, G.A. 1999, "Extracellular matrix degradation by metalloproteinases and central nervous system diseases", *Molecular neurobiology,* vol. 19, no. 3, pp. 267-284.

Maere, S., Heymans, K. & Kuiper, M. 2005, "BiNGO: a Cytoscape plugin to assess overrepresentation of gene ontology categories in biological networks", *Bioinformatics (Oxford, England),* vol. 21, no. 16, pp. 3448-3449.

Mallick, P., Schirle, M., Chen, S.S., Flory, M.R., Lee, H., Martin, D., Ranish, J., Raught, B., Schmitt, R., Werner, T., Kuster, B. & Aebersold, R. 2007, "Computational prediction of proteotypic peptides for quantitative proteomics", *Nature biotechnology,* vol. 25, no. 1, pp. 125-131.

Martinez-Ruiz, A. & Lamas, S. 2004, "Detection and proteomic identification of S-nitrosylated proteins in endothelial cells", *Archives of Biochemistry and Biophysics,* vol. 423, no. 1, pp. 192-199.

Matsushita, K., Morrell, C.N., Cambien, B., Yang, S.X., Yamakuchi, M., Bao, C., Hara, M.R., Quick, R.A., Cao, W., O'Rourke, B., Lowenstein, J.M., Pevsner, J., Wagner, D.D. & Lowenstein, C.J. 2003, "Nitric oxide regulates exocytosis by S-nitrosylation of N-ethylmaleimide-sensitive factor", *Cell,* vol. 115, no. 2, pp. 139-150.

Mauch, D.H., Nagler, K., Schumacher, S., Goritz, C., Muller, E.C., Otto, A. & Pfrieger, F.W. 2001, "CNS synaptogenesis promoted by glia-derived cholesterol", *Science (New York, N.Y.),* vol. 294, no. 5545, pp. 1354-1357.

Meda, L., Baron, P. & Scarlato, G. 2001, "Glial activation in Alzheimer's disease: the role of Abeta and its associated proteins", *Neurobiology of aging,* vol. 22, no. 6, pp. 885-893.

Merk, M., Baugh, J., Zierow, S., Leng, L., Pal, U., Lee, S.J., Ebert, A.D., Mizue, Y., Trent, J.O., Mitchell, R., Nickel, W., Kavathas, P.B., Bernhagen, J. & Bucala, R. 2009, "The Golgi-associated protein p115 mediates the secretion of macrophage migration inhibitory factor", *Journal of immunology (Baltimore, Md.: 1950),* vol. 182, no. 11, pp. 6896-6906.

Minagar, A. & Alexander, J.S. 2003, "Blood-brain barrier disruption in multiple sclerosis", *Multiple sclerosis (Houndmills, Basingstoke, England),* vol. 9, no. 6, pp. 540-549.

Mitchell, D.A. & Marletta, M.A. 2005, "Thioredoxin catalyzes the S-nitrosation of the caspase-3 active site cysteine", *Nature chemical biology,* vol. 1, no. 3, pp. 154-158.

Mitchell, D.A., Morton, S.U., Fernhoff, N.B. & Marletta, M.A. 2007, "Thioredoxin is required for S-nitrosation of procaspase-3 and the inhibition of apoptosis in Jurkat cells", *Proceedings of the National Academy of Sciences of the United States of America,* vol. 104, no. 28, pp. 11609-11614.

Moller, M., Botti, H., Batthyany, C., Rubbo, H., Radi, R. & Denicola, A. 2005, "Direct measurement of nitric oxide and oxygen partitioning into liposomes and low density lipoprotein", *The Journal of biological chemistry,* vol. 280, no. 10, pp. 8850-8854.

Moncada, S. & Higgs, A. 1993, "The L-arginine-nitric oxide pathway", *The New England journal of medicine,* vol. 329, no. 27, pp. 2002-2012.

Montana, V., Malarkey, E.B., Verderio, C., Matteoli, M. & Parpura, V. 2006, "Vesicular transmitter release from astrocytes", *Glia,* vol. 54, no. 7, pp. 700-715.

Moore, N.H., Costa, L.G., Shaffer, S.A., Goodlett, D.R. & Guizzetti, M. 2009, "Shotgun proteomics implicates extracellular matrix proteins and protease systems in neuronal development induced by astrocyte cholinergic stimulation", *Journal of neurochemistry,* vol. 108, no. 4, pp. 891-908.

Morrell, C.N., Matsushita, K., Chiles, K., Scharpf, R.B., Yamakuchi, M., Mason, R.J., Bergmeier, W., Mankowski, J.L., Baldwin, W.M.,3rd, Faraday, N. & Lowenstein, C.J. 2005, "Regulation of platelet granule exocytosis by S-nitrosylation", *Proceedings of the National Academy of Sciences of the United States of America,* vol. 102, no. 10, pp. 3782-3787.

Mor-Vaknin, N., Punturieri, A., Sitwala, K. & Markovitz, D.M. 2003, "Vimentin is secreted by activated macrophages", *Nature cell biology,* vol. 5, no. 1, pp. 59-63.

Mulligan, S.J. & MacVicar, B.A. 2004, "Calcium transients in astrocyte endfeet cause cerebrovascular constrictions", *Nature,* vol. 431, no. 7005, pp. 195-199.

Munson, M.S.B and Field, F.H. 1966, "Chemical Ionization Mass Spectrometry. I. General Introduction", [Online], vol. 88, no. 12. Available from: http://proxy.library.upenn.edu:5665/doi/abs/10.1021/ja00964a001. [3/18/2009].

Nagai, M., Re, D.B., Nagata, T., Chalazonitis, A., Jessell, T.M., Wichterle, H. & Przedborski, S. 2007, "Astrocytes expressing ALS-linked mutated SOD1 release factors selectively toxic to motor neurons", *Nature neuroscience,* vol. 10, no. 5, pp. 615-622.

Nair, R. & Rost, B. 2005, "Mimicking cellular sorting improves prediction of subcellular localization", *Journal of Molecular Biology,* vol. 348, no. 1, pp. 85-100.

Nakanishi, T., Okamoto, N., Tanaka, K. & Shimizu, A. 1994, "Laser desorption time-of-flight mass spectrometric analysis of transferrin precipitated with antiserum: a unique simple method to identify molecular weight variants", *Biological mass spectrometry,* vol. 23, no. 4, pp. 230-233.

Nedergaard, M. 1994, "Direct signaling from astrocytes to neurons in cultures of mammalian brain cells", *Science (New York, N.Y.),* vol. 263, no. 5154, pp. 1768-1771.

Nesvizhskii, A.I., Keller, A., Kolker, E. & Aebersold, R. 2003, "A statistical model for identifying proteins by tandem mass spectrometry", *Analytical Chemistry,* vol. 75, no. 17, pp. 4646-4658.

Nickel, W. 2005, "Unconventional secretory routes: direct protein export across the plasma membrane of mammalian cells", *Traffic (Copenhagen, Denmark),* vol. 6, no. 8, pp. 607-614.

Nickel, W. & Rabouille, C. 2009, "Mechanisms of regulated unconventional protein secretion", *Nature reviews.Molecular cell biology,* vol. 10, no. 2, pp. 148-155.

Nickel, W. & Seedorf, M. 2008, "Unconventional mechanisms of protein transport to the cell surface of eukaryotic cells", *Annual Review of Cell and Developmental Biology,* vol. 24, pp. 287-308.

Nishino, J., Yamashita, K., Hashiguchi, H., Fujii, H., Shimazaki, T. & Hamada, H. 2004, "Meteorin: a secreted protein that regulates glial cell differentiation and promotes axonal extension", *The EMBO journal,* vol. 23, no. 9, pp. 1998-2008.

Oda, Y., Huang, K., Cross, F.R., Cowburn, D. & Chait, B.T. 1999, "Accurate quantitation of protein expression and site-specific phosphorylation", *Proceedings of the National Academy of Sciences of the United States of America,* vol. 96, no. 12, pp. 6591-6596.

Old, W.M., Meyer-Arendt, K., Aveline-Wolf, L., Pierce, K.G., Mendoza, A., Sevinsky, J.R., Resing, K.A. & Ahn, N.G. 2005, "Comparison of label-free methods for quantifying human proteins by shotgun proteomics", *Molecular & cellular proteomics : MCP,* vol. 4, no. 10, pp. 1487-1502.

Olsen, J.V., Ong, S.E. & Mann, M. 2004, "Trypsin cleaves exclusively C-terminal to arginine and lysine residues", *Molecular & cellular proteomics : MCP,* vol. 3, no. 6, pp. 608-614.

Ong, S.E., Blagoev, B., Kratchmarova, I., Kristensen, D.B., Steen, H., Pandey, A. & Mann, M. 2002, "Stable isotope labeling by amino acids in cell culture, SILAC, as a simple and accurate approach to expression proteomics", *Molecular & cellular proteomics : MCP,* vol. 1, no. 5, pp. 376-386.

Ong, S.E., Kratchmarova, I. & Mann, M. 2003, "Properties of 13C-substituted arginine in stable isotope labeling by amino acids in cell culture (SILAC)", *Journal of proteome research,* vol. 2, no. 2, pp. 173-181.

Ong, S.E. & Mann, M. 2006, "A practical recipe for stable isotope labeling by amino acids in cell culture (SILAC)", *Nature protocols,* vol. 1, no. 6, pp. 2650-2660.

Ong, S.E. & Mann, M. 2005, "Mass spectrometry-based proteomics turns quantitative", *Nature chemical biology,* vol. 1, no. 5, pp. 252-262.

Padgett, C.M. & Whorton, A.R. 1995, "S-nitrosoglutathione reversibly inhibits GAPDH by S-nitrosylation", *The American Journal of Physiology,* vol. 269, no. 3 Pt 1, pp. C739-49.

Park, J.A., Lee, H.S., Ko, K.J., Park, S.Y., Kim, J.H., Choe, G., Kweon, H.S., Song, H.S., Ahn, J.C., Yu, Y.S. & Kim, K.W. 2008, "Meteorin regulates angiogenesis at the gliovascular interface", *Glia,* vol. 56, no. 3, pp. 247-258.

Park, S.K., Liao, L., Kim, J.Y. & Yates, J.R.,3rd 2009, "A computational approach to correct arginine-to-proline conversion in quantitative proteomics", *Nature methods,* vol. 6, no. 3, pp. 184-185.

Park, S.K., Venable, J.D., Xu, T. & Yates, J.R.,3rd 2008a, "A quantitative analysis software tool for mass spectrometry-based proteomics", *Nature methods,* vol. 5, no. 4, pp. 319-322.

Park, S.K., Venable, J.D., Xu, T. & Yates, J.R.,3rd 2008b, "A quantitative analysis software tool for mass spectrometry-based proteomics", *Nature methods,* vol. 5, no. 4, pp. 319-322.

Pascual, O., Casper, K.B., Kubera, C., Zhang, J., Revilla-Sanchez, R., Sul, J.Y., Takano, H., Moss, S.J., McCarthy, K. & Haydon, P.G. 2005, "Astrocytic purinergic signaling coordinates synaptic networks", *Science (New York, N.Y.),* vol. 310, no. 5745, pp. 113-116.

Pawloski, J.R., Hess, D.T. & Stamler, J.S. 2005, "Impaired vasodilation by red blood cells in sickle cell disease", *Proceedings of the National Academy of Sciences of the United States of America,* vol. 102, no. 7, pp. 2531-2536.

Pearson, R.B. & Kemp, B.E. 1991, "Protein kinase phosphorylation site sequences and consensus specificity motifs: tabulations", *Methods in enzymology,* vol. 200, pp. 62-81.

Pekny, M. & Nilsson, M. 2005, "Astrocyte activation and reactive gliosis", *Glia,* vol. 50, no. 4, pp. 427-434.

Pellitteri-Hahn, M.C., Warren, M.C., Didier, D.N., Winkler, E.L., Mirza, S.P., Greene, A.S. & Olivier, M. 2006, "Improved mass spectrometric proteomic profiling of the secretome of rat vascular endothelial cells", *Journal of proteome research,* vol. 5, no. 10, pp. 2861-2864.

Peng, J., Elias, J.E., Thoreen, C.C., Licklider, L.J. & Gygi, S.P. 2003, "Evaluation of multidimensional chromatography coupled with tandem mass spectrometry (LC/LC-MS/MS) for large-scale protein analysis: the yeast proteome", *Journal of proteome research,* vol. 2, no. 1, pp. 43-50.

Perkins, D.N., Pappin, D.J., Creasy, D.M. & Cottrell, J.S. 1999, "Probability-based protein identification by searching sequence databases using mass spectrometry data", *Electrophoresis,* vol. 20, no. 18, pp. 3551-3567.

Pfeffer, S.R. 1988, "Mannose 6-phosphate receptors and their role in targeting proteins to lysosomes", *The Journal of membrane biology,* vol. 103, no. 1, pp. 7-16.

Pfeffer, S.R. & Rothman, J.E. 1987, "Biosynthetic protein transport and sorting by the endoplasmic reticulum and Golgi", *Annual Review of Biochemistry,* vol. 56, pp. 829-852.

Pickart, M.A., Klee, E.W., Nielsen, A.L., Sivasubbu, S., Mendenhall, E.M., Bill, B.R., Chen, E., Eckfeldt, C.E., Knowlton, M., Robu, M.E., Larson, J.D., Deng, Y.,

Schimmenti, L.A., Ellis, L.B., Verfaillie, C.M., Hammerschmidt, M., Farber, S.A. & Ekker, S.C. 2006, "Genome-wide reverse genetics framework to identify novel functions of the vertebrate secretome", *PLoS ONE,* vol. 1, pp. e104.

Price, B.D., Mannheim-Rodman, L.A. & Calderwood, S.K. 1992, "Brefeldin A, thapsigargin, and AIF4- stimulate the accumulation of GRP78 mRNA in a cycloheximide dependent manner, whilst induction by hypoxia is independent of protein synthesis", *Journal of cellular physiology,* vol. 152, no. 3, pp. 545-552.

Radi, R. 2004, "Nitric oxide, oxidants, and protein tyrosine nitration", *Proceedings of the National Academy of Sciences of the United States of America,* vol. 101, no. 12, pp. 4003-4008.

Radomski, M.W., Rees, D.D., Dutra, A. & Moncada, S. 1992, "S-nitroso-glutathione inhibits platelet activation in vitro and in vivo", *British journal of pharmacology,* vol. 107, no. 3, pp. 745-749.

Ramamoorthy, P. & Whim, M.D. 2008, "Trafficking and fusion of neuropeptide Y-containing dense-core granules in astrocytes", *The Journal of neuroscience : the official journal of the Society for Neuroscience,* vol. 28, no. 51, pp. 13815-13827.

Rappsilber, J., Ryder, U., Lamond, A.I. & Mann, M. 2002, "Large-scale proteomic analysis of the human spliceosome", *Genome research,* vol. 12, no. 8, pp. 1231-1245.

Rhee, K.Y., Erdjument-Bromage, H., Tempst, P. & Nathan, C.F. 2005, "S-nitroso proteome of Mycobacterium tuberculosis: Enzymes of intermediary metabolism and antioxidant defense", *Proceedings of the National Academy of Sciences of the United States of America,* vol. 102, no. 2, pp. 467-472.

Rizzo, M.A. & Piston, D.W. 2003, "Regulation of beta cell glucokinase by S-nitrosylation and association with nitric oxide synthase", *The Journal of cell biology,* vol. 161, no. 2, pp. 243-248.

Saha, R.N. & Pahan, K. 2006, "Signals for the induction of nitric oxide synthase in astrocytes", *Neurochemistry international,* vol. 49, no. 2, pp. 154-163.

Sampson, J.B., Ye, Y., Rosen, H. & Beckman, J.S. 1998, "Myeloperoxidase and horseradish peroxidase catalyze tyrosine nitration in proteins from nitrite and hydrogen peroxide", *Archives of Biochemistry and Biophysics,* vol. 356, no. 2, pp. 207-213.

Sariola, H. & Saarma, M. 2003, "Novel functions and signalling pathways for GDNF", *Journal of cell science,* vol. 116, no. Pt 19, pp. 3855-3862.

Schmidt, A., Kellermann, J. & Lottspeich, F. 2005, "A novel strategy for quantitative proteomics using isotope-coded protein labels", *Proteomics,* vol. 5, no. 1, pp. 4-15.

Schmidt, M.W., Houseman, A., Ivanov, A.R. & Wolf, D.A. 2007, "Comparative proteomic and transcriptomic profiling of the fission yeast Schizosaccharomyces pombe", *Molecular systems biology,* vol. 3, pp. 79.

Searle, B.C., Turner, M. & Nesvizhskii, A.I. 2008, "Improving sensitivity by probabilistically combining results from multiple MS/MS search methodologies", *Journal of proteome research,* vol. 7, no. 1, pp. 245-253.

Seelenmeyer, C., Stegmayer, C. & Nickel, W. 2008, "Unconventional secretion of fibroblast growth factor 2 and galectin-1 does not require shedding of plasma membrane-derived vesicles", *FEBS letters,* vol. 582, no. 9, pp. 1362-1368.

Seth, P. & Koul, N. 2008, "Astrocyte, the star avatar: redefined", *Journal of Biosciences,* vol. 33, no. 3, pp. 405-421.

Shevchenko, A., Chernushevich, I., Ens, W., Standing, K.G., Thomson, B., Wilm, M. & Mann, M. 1997, "Rapid 'de novo' peptide sequencing by a combination of nanoelectrospray, isotopic labeling and a quadrupole/time-of-flight mass spectrometer", *Rapid communications in mass spectrometry : RCM,* vol. 11, no. 9, pp. 1015-1024.

Slot, J.W., Geuze, H.J., Gigengack, S., Lienhard, G.E. & James, D.E. 1991, "Immuno-localization of the insulin regulatable glucose transporter in brown adipose tissue of the rat", *The Journal of cell biology,* vol. 113, no. 1, pp. 123-135.

Song, H., Stevens, C.F. & Gage, F.H. 2002, "Astroglia induce neurogenesis from adult neural stem cells", *Nature,* vol. 417, no. 6884, pp. 39-44.

Sontheimer, H., Fernandez-Marques, E., Ullrich, N., Pappas, C.A. & Waxman, S.G. 1994, "Astrocyte Na+ channels are required for maintenance of Na+/K(+)-ATPase activity", *The Journal of neuroscience : the official journal of the Society for Neuroscience,* vol. 14, no. 5 Pt 1, pp. 2464-2475.

Speicher, K., Kolbas, O., Harper, S. & Speicher, D. 2000, "Systematic analysis of peptide recoveries from in-gel digestions for protein identifications in proteome studies", *Journal of Biomolecular Techniques,* vol. 11, no. 2, pp. 74-86.

Spellman, D.S., Deinhardt, K., Darie, C.C., Chao, M.V. & Neubert, T.A. 2008, "Stable isotopic labeling by amino acids in cultured primary neurons: application to brain-derived neurotrophic factor-dependent phosphotyrosine-associated signaling", *Molecular & cellular proteomics : MCP,* vol. 7, no. 6, pp. 1067-1076.

Stamler, J.S., Toone, E.J., Lipton, S.A. & Sucher, N.J. 1997, "(S)NO signals: translocation, regulation, and a consensus motif", *Neuron,* vol. 18, no. 5, pp. 691-696.

Stella, N., Estelles, A., Siciliano, J., Tence, M., Desagher, S., Piomelli, D., Glowinski, J. & Premont, J. 1997, "Interleukin-1 enhances the ATP-evoked release of arachidonic acid from mouse astrocytes", *The Journal of neuroscience : the official journal of the Society for Neuroscience,* vol. 17, no. 9, pp. 2939-2946.

Stinchcombe, J., Bossi, G. & Griffiths, G.M. 2004, "Linking albinism and immunity: the secrets of secretory lysosomes", *Science (New York, N.Y.),* vol. 305, no. 5680, pp. 55-59.

Stone, J.R. & Marletta, M.A. 1996, "Spectral and kinetic studies on the activation of soluble guanylate cyclase by nitric oxide", *Biochemistry,* vol. 35, no. 4, pp. 1093-1099.

Sun, J., Xin, C., Eu, J.P., Stamler, J.S. & Meissner, G. 2001, "Cysteine-3635 is responsible for skeletal muscle ryanodine receptor modulation by NO", *Proceedings of the National Academy of Sciences of the United States of America,* vol. 98, no. 20, pp. 11158-11162.

Suzuki, J., Jin, Z.G., Meoli, D.F., Matoba, T. & Berk, B.C. 2006, "Cyclophilin A is secreted by a vesicular pathway in vascular smooth muscle cells", *Circulation research,* vol. 98, no. 6, pp. 811-817.

Tang, H.Y., Ali-Khan, N., Echan, L.A., Levenkova, N., Rux, J.J. & Speicher, D.W. 2005, "A novel four-dimensional strategy combining protein and peptide separation methods enables detection of low-abundance proteins in human plasma and serum proteomes", *Proteomics,* vol. 5, no. 13, pp. 3329-3342.

Tannenbaum, S.R. & White, F.M. 2006, "Regulation and specificity of S-nitrosylation and denitrosylation", *ACS chemical biology,* vol. 1, no. 10, pp. 615-618.

Tsai, H.H., Frost, E., To, V., Robinson, S., Ffrench-Constant, C., Geertman, R., Ransohoff, R.M. & Miller, R.H. 2002, "The chemokine receptor CXCR2 controls positioning of oligodendrocyte precursors in developing spinal cord by arresting their migration", *Cell,* vol. 110, no. 3, pp. 373-383.

Ullian, E.M., Christopherson, K.S. & Barres, B.A. 2004, "Role for glia in synaptogenesis", *Glia,* vol. 47, no. 3, pp. 209-216.

Vargas, M.R., Pehar, M., Cassina, P., Martinez-Palma, L., Thompson, J.A., Beckman, J.S. & Barbeito, L. 2005, "Fibroblast growth factor-1 induces heme oxygenase-1 via nuclear factor erythroid 2-related factor 2 (Nrf2) in spinal cord astrocytes: consequences for motor neuron survival", *The Journal of biological chemistry,* vol. 280, no. 27, pp. 25571-25579.

Villoslada, P. & Genain, C.P. 2004, "Role of nerve growth factor and other trophic factors in brain inflammation", *Progress in brain research,* vol. 146, pp. 403-414.

Volterra, A. & Meldolesi, J. 2005, "Astrocytes, from brain glue to communication elements: the revolution continues", *Nature reviews.Neuroscience,* vol. 6, no. 8, pp. 626-640.

Von Eckardstein, A., Langer, C., Engel, T., Schaukal, I., Cignarella, A., Reinhardt, J., Lorkowski, S., Li, Z., Zhou, X., Cullen, P. & Assmann, G. 2001, "ATP binding cassette transporter ABCA1 modulates the secretion of apolipoprotein E from human monocyte-derived macrophages", *The FASEB journal : official publication of the Federation of American Societies for Experimental Biology,* vol. 15, no. 9, pp. 1555-1561.

von Heijne, G. 1985, "Signal sequences. The limits of variation", *Journal of Molecular Biology,* vol. 184, no. 1, pp. 99-105.

Vouyiouklis, D.A. & Brophy, P.J. 1997, "A novel gelsolin isoform expressed by oligodendrocytes in the central nervous system", *Journal of neurochemistry,* vol. 69, no. 3, pp. 995-1005.

Wang, G., Moniri, N.H., Ozawa, K., Stamler, J.S. & Daaka, Y. 2006, "Nitric oxide regulates endocytosis by S-nitrosylation of dynamin", *Proceedings of the National Academy of Sciences of the United States of America,* vol. 103, no. 5, pp. 1295-1300.

Wang, X., Matteson, J., An, Y., Moyer, B., Yoo, J.S., Bannykh, S., Wilson, I.A., Riordan, J.R. & Balch, W.E. 2004, "COPII-dependent export of cystic fibrosis transmembrane conductance regulator from the ER uses a di-acidic exit code", *The Journal of cell biology,* vol. 167, no. 1, pp. 65-74.

Washburn, M.P., Ulaszek, R., Deciu, C., Schieltz, D.M. & Yates, J.R.,3rd 2002, "Analysis of quantitative proteomic data generated via multidimensional protein identification technology", *Analytical Chemistry,* vol. 74, no. 7, pp. 1650-1657.

Washburn, M.P., Wolters, D. & Yates, J.R.,3rd 2001, "Large-scale analysis of the yeast proteome by multidimensional protein identification technology", *Nature biotechnology,* vol. 19, no. 3, pp. 242-247.

Whalen, E.J., Foster, M.W., Matsumoto, A., Ozawa, K., Violin, J.D., Que, L.G., Nelson, C.D., Benhar, M., Keys, J.R., Rockman, H.A., Koch, W.J., Daaka, Y., Lefkowitz, R.J. & Stamler, J.S. 2007, "Regulation of beta-adrenergic receptor signaling by S-nitrosylation of G-protein-coupled receptor kinase 2", *Cell,* vol. 129, no. 3, pp. 511-522.

Wolters, D.A., Washburn, M.P. & Yates, J.R.,3rd 2001, "An automated multidimensional protein identification technology for shotgun proteomics", *Analytical Chemistry,* vol. 73, no. 23, pp. 5683-5690.

Xu, W., Liu, L., Charles, I.G. & Moncada, S. 2004, "Nitric oxide induces coupling of mitochondrial signalling with the endoplasmic reticulum stress response", *Nature cell biology,* vol. 6, no. 11, pp. 1129-1134.

Yang, J.W., Rodrigo, R., Felipo, V. & Lubec, G. 2005, "Proteome analysis of primary neurons and astrocytes from rat cerebellum", *Journal of proteome research,* vol. 4, no. 3, pp. 768-788.

Yang, Y. & Loscalzo, J. 2005, "S-nitrosoprotein formation and localization in endothelial cells", *Proceedings of the National Academy of Sciences of the United States of America,* vol. 102, no. 1, pp. 117-122.

Yao, X., Freas, A., Ramirez, J., Demirev, P.A. & Fenselau, C. 2001, "Proteolytic 18O labeling for comparative proteomics: model studies with two serotypes of adenovirus", *Analytical Chemistry,* vol. 73, no. 13, pp. 2836-2842.

Yocum, A.K., Busch, C.M., Felix, C.A. & Blair, I.A. 2006, "Proteomics-based strategy to identify biomarkers and pharmacological targets in leukemias with t(4;11) translocations", *Journal of proteome research,* vol. 5, no. 10, pp. 2743-2753.

Yuan, H., Michelsen, K. & Schwappach, B. 2003, "14-3-3 Dimers Probe the Assembly Status of Multimeric Membrane Proteins", *Current biology : CB,* vol. 13, no. 8, pp. 638-646.

Zafra, F., Lindholm, D., Castren, E., Hartikka, J. & Thoenen, H. 1992, "Regulation of brain-derived neurotrophic factor and nerve growth factor mRNA in primary cultures of hippocampal neurons and astrocytes", *The Journal of neuroscience : the official journal of the Society for Neuroscience,* vol. 12, no. 12, pp. 4793-4799.

Zhang, Y. & Hogg, N. 2005, "S-Nitrosothiols: cellular formation and transport", *Free radical biology & medicine,* vol. 38, no. 7, pp. 831-838.

Zhang, Y. & Hogg, N. 2004a, "Formation and stability of S-nitrosothiols in RAW 264.7 cells", *American journal of physiology.Lung cellular and molecular physiology,* vol. 287, no. 3, pp. L467-74.

Zhang, Y. & Hogg, N. 2004b, "The mechanism of transmembrane S-nitrosothiol transport", *Proceedings of the National Academy of Sciences of the United States of America,* vol. 101, no. 21, pp. 7891-7896.

Zhang, Z., Chen, G., Zhou, W., Song, A., Xu, T., Luo, Q., Wang, W., Gu, X.S. & Duan, S. 2007, "Regulated ATP release from astrocytes through lysosome exocytosis", *Nature cell biology,* vol. 9, no. 8, pp. 945-953.

Zhao, W.Q., Chen, G.H., Chen, H., Pascale, A., Ravindranath, L., Quon, M.J. & Alkon, D.L. 2003, "Secretion of Annexin II via activation of insulin receptor and insulin-like growth factor receptor", *The Journal of biological chemistry,* vol. 278, no. 6, pp. 4205-4215.

Zito, K. & Svoboda, K. 2002, "Activity-dependent synaptogenesis in the adult Mammalian cortex", *Neuron,* vol. 35, no. 6, pp. 1015-1017.

Zonta, M., Angulo, M.C., Gobbo, S., Rosengarten, B., Hossmann, K.A., Pozzan, T. & Carmignoto, G. 2003, "Neuron-to-astrocyte signaling is central to the dynamic control of brain microcirculation", *Nature neuroscience,* vol. 6, no. 1, pp. 43-50.

Zybailov, B.L., Florens, L. & Washburn, M.P. 2007, "Quantitative shotgun proteomics using a protease with broad specificity and normalized spectral abundance factors", *Molecular bioSystems,* vol. 3, no. 5, pp. 354-360.